Chemogenetic silencing of sensory neuron populations to uncover their role in touch and pain

Steven James Middleton

Harris Manchester College

University of Oxford

A thesis submitted for the degree of

Doctor of Philosophy

in Ion Channels in Health and Disease

Michaelmas Term 2020

Acknowledgements

I would like to thank my supervisor Professor David Bennett for welcoming me into his lab four years ago. I am very thankful for his mentorship, continuous encouragement, optimism and support. I couldn't have wished for a better supervisor to lead me through my DPhil studies. I would also like to thank Dr Greg Weir for his mentorship and for taking me under his wing at the very beginning of my DPhil journey. Without his guidance, I would not be in the position I am today. I am extremely thankful to both of you for everything you have taught and shown me, you have truly shaped the scientist I am today.

I would like to thank all the members of the Bennett lab (past and present), you been fantastic colleagues and amazing friends, you are all so generous, accepting and positive. I have had some truly excellent times with you over the last four years. Thank you all for being so great, you've definitely helped me to enjoy my DPhil experience.

I would like to thank the directors of the OXION programme, for accepting me onto this prestigious DPhil studentship, and the Wellcome Trust for generously funding my research.

My biggest thanks go to all my family and friends that have supported me throughout this journey. Thank you for all the love and support you have shown me, not just over the last four years but every day prior and every day since.

I have thoroughly enjoyed my DPhil and look forward to the next chapter of my career.

Declaration

I declare that the work within this thesis is my own unless otherwise stated. Acknowledgements are found at the end of each data chapter.

Key contributions were made by:

- Dr Greg Weir from the University of Oxford, UK (currently at the University of Glasgow, UK). All rodent surgeries and behaviour in **Chapters 3** and **4** were performed together and/or equally split between Dr Weir and myself.

- Dr Andreas Themistocleous from the University of Oxford, UK and Dr Irene Perini from Linkoping University, Sweden (together with their collaborators), collected all of the human data in **Chapter 5**.

Table of Contents

Word count: 40,094 (excluding figure legends, references and appendix). Page count: 257.

Abstract

The ability of humans to experience touch and pain sensation is critical for our survival. The experience of pain is typically a protective mechanism, and ensures we avoid dangerous environmental cues. However, following incidences of genetic mutations, injury or disease of the somatosensory nervous system, protective pain can become pathological. Indeed, neuropathic pain affects seven to ten percent of the general population, and our current treatment strategies show poor efficacy and tolerability.

Currently, mechanisms surrounding neuropathic pain involve both peripheral and central sensitisation. However, there is an incomplete understanding of the functional roles of different sensory neuron populations, the sensory modalities they encode, and how they change under neuropathic conditions. Therefore, it is unclear which primary afferent subpopulations contribute to the induction and maintenance of neuropathic pain and which should be therapeutically targeted. This is largely due to the fact that peripheral sensory neurons within dorsal root ganglia (DRG) are highly heterogeneous and are thought to contain up to 17 different subpopulations.

A key aim of this work is to ascribe roles to primary afferent subpopulations in naïve rodents and those that have undergone traumatic nerve injury. Therefore, I have developed a novel chemogenetic toolbox to facilitate selective, reversible and repeatable neuronal silencing of defined sensory neuron populations. I have employed AAV9-GluClv2.0 to broadly silence all DRG neurons and observed functional recovery from neuropathic pain *in vivo*. Subsequently, I used AAV9-GluCl.Cre^{ON} to target two populations of sensory neurons: the Nav1.8 positive (largely nociceptive) population, and the tyrosine hydroxylase positive C-low threshold mechanoreceptor (C-LTMR) population. Silencing each of these populations resulted in population-specific sensory phenotypes, with subtle or no changes in neuropathic mechanical hypersensitivity. Finally, using a molecule to man approach, the role of the voltage-gated sodium channel Nav1.7 was investigated in C-LTMRs and pleasant touch sensation. In humans and mice

either genetic or pharmacological disruption of Nav1.7 resulted in deficits in C-LTMR function. This work challenges the current dogma that therapeutically targeting Nav1.7 will only effect the nociceptive system. Together, this work illustrates the need to better understand the roles of different primary afferent subpopulations and provides chemogenetic tools to achieve this. Ultimately, this work will facilitate the development of therapeutics which are better targeted towards the appropriate sensory neuron populations.

Chapter 1: General Introduction

1. The somatosensory system

Throughout human evolution, the ability to experience pain has been a protective phenomenon vital for our survival. Equally, our ability to process touch sensation allows us to detect and discriminate our environment. However, these essential and protective systems can become pathological, either through injury, disease or because of genetic mutations (Colloca *et al.* 2017). There are still a lot of questions about the mechanisms behind different touch modalities and pain-states, but it is well established that the dorsal root ganglion (DRG) is critical for both touch and pain. DRG neurons are pseudo-unipolar neurons which have peripheral terminals innervating sensory targets such as muscle, bone, viscera and skin (the skin will be a major focus of this thesis). The sensory endings of these DRG neurons form morphologically distinct structures, particularly apparent in the skin. DRG neurons also project centrally where they terminate in the dorsal horn (DH) of the spinal cord, forming synapses with distinct DH neurons in specific lamina organisations. Here, the signal is gated and modified in complex dorsal horn circuits of interneurons before being transmitted via projection neurons to the brain, where sensory perception is generated.

DRG populations are classically characterised by soma size (small, medium, large), histological protein/peptide expression and electrophysiological properties (largely dependent on their degree of myelination). Classically, there are two major primary afferent populations: A-fibre mechanoreceptors which code touch sensation, and C-fibre nociceptors which signal and transmit pain. However, these populations are perhaps too simplistic. Indeed, A-fibres can be subdivided into thickly myelinated Aβ fibres and thinly myelinated Aδ fibres, while unmyelinated C-fibres can be subdivided into populations based on the sensory modalities which they detect. For instance, mechanical pain, pleasant touch, thermal detection and pain and those which are silent under normal conditions. The role of each population is a topic of large debate,

particularly when conditions become pathological. In addition, recent studies based on gene expression profiling show that DRG neurons can subdivide further and are more heterogeneous; a fact underappreciated in historical literature.

2. The heterogeneity of the DRG

DRG heterogeneity can, in part, be resolved by assessing the morphological features and protein expression of groups of neurons. On this basis A- and C-fibres are distinct and can subdivided into subpopulations (Fig. 1). This thesis will mostly focus on the characterisation of mouse DRG neurons, which are thought to show broad similarity to human DRG neurons. However, there are likely some differences as not all populations have been resolved in humans, such as D-hairs.

2.1. A-fibres: structural and molecular features

A-fibres can be subdivided in two populations based on structural and molecular features. Aβ-SA (slowly adapting) mechanoreceptors are large neurons with myelinated axons which innervate cutaneous merkel cells and wrap around hair follicles as circumferential endings (pilo-Ruffini) (Li *et al.*, 2011; Bai *et al.*, 2015). Aβ-SA neurons specifically co-express the receptor tyrosine kinase (Ret) and tyrosine receptor kinase C (TrkC) (Li *et al.*, 2011; Bai *et al.*, 2015). Aβ-RA (rapidly adapting) mechanoreceptors are large neurons with myelinated axons which form cutaneous meissener corpuscles, hair follicle longitudinal lanceolate endings and pacinian corpuscles (not present in rodent skin). Aβ-RA mechanoreceptors express Calbindin (Calb), split and low levels of the tyrosine receptor kinase B (TrkB) (Rutlin *et al.*, 2014; Dhandapani *et al.*, 2018; Zheng *et al.*, 2019). Aδ fibres can subdivided into thinly myelinated Aδ low-threshold mechanoreceptors (LTMRs), also known as D-hairs, and Aδ-nociceptors. D-hairs are medium sized neurons which form longitudinal lanceolate endings around hair follicles and express the voltage-gated calcium channel 3.2 (Cav3.2) and high levels of TrkB (Shin *et al.*, 2003; Li *et al.*,

2011; Bernal Sierra *et al.*, 2017; Dhandapani *et al.*, 2018). A second Aδ subpopulation is the thinly myelinated Aδ-nociceptors (A-mechanonocieptors). Aδ-nociceptors are medium sized neurons that innervate skin as free nerve endings and express nociceptive markers such as the tyrosine receptor kinase A (TrkA), the voltage-gated sodium channel 1.8 (Nav1.8) and the myelination markers Neurofilament 200 (NF200) and S100β. Some Aδ nociceptors also express calcitonin gene-related peptide (CGRP) and Neuropeptide Y receptor type 2 (Npy2r) (Arcourt *et al.*, 2016).

2.2. C-fibres: structural and molecular features

C-fibre nociceptors that respond to noxious stimuli are small sized neurons and all innervate the skin as free nerve endings, that are closely associated with specialised Schwann cells (Abdo *et al.*, 2019). All C-fibre nociceptors express TrkA and Nav1.8 and are classically split into two groups: those which are peptidergic and express neuropeptides such as CGRP and substance P (Peptidergic nociceptors), and those which are non-peptidergic, which bind isolectin-B4 and express MrgD (non-peptidergic nociceptors) (Le Pichon and Chesler, 2014). There is a third population of C-fibre nociceptors which do not innervate the skin but instead target deeper structures such as muscle and viscera. These fibres are termed silent nociceptors and express TrkA, Nav1.8 and the Cholinergic Receptor Nicotinic Alpha 3 Subunit (CHRNA3) (Prato *et al.*, 2017). Another population of C-fibres, which are also small in size and unmyelinated, instead innervate hair follicles as longitudinal lanceolate endings and are termed C-low threshold mechanoreceptors (C-LTMRs). C-LTMRs express the voltage-gate calcium channels Cav3.2 and Cav3.3, vesicular glutamate transporter 3 (VGLUT3), TAFA chemokine like family member 4 (TAFA4) and tyrosine hydroxylase (TH) (Seal *et al.*, 2009; Li *et al.*, 2011; Delfini *et al.*, 2013; François *et al.*, 2015; Reynders *et al.*, 2015).

However, in addition to structural and molecular features a large degree of the heterogeneity and classification of DRG neurons is determined by their electrophysiological properties. In this vein, the described populations above have distinct electrophysiological characteristics (Fig. 1).

2.3. A-Fibres: electrophysiological characteristics

Populations of sensory neurons can be classified due to their electrical features. A-fibre afferents can be defined due to their electrophysiological characteristics at both the level of the cell soma and the primary afferent terminal (Koltzenburg *et al.*, 1997; Hu and Lewin, 2006; Zheng *et al.*, 2019) (fig 1). Due to identification of specific molecular markers studies have used genetic labelling to define populations and characterise them using *in vivo* or *in vitro* patch-clamp recordings. For instance the genetic labelling of Aβ-SAMs, Aβ-RAM and Aδ-LTMRs led researchers to conclude that, in response to depolarising current injections and recordings from the cell soma, these three populations have narrow action potential widths, do not repetitively fire and do not have a delay in AP firing (Zheng *et al.*, 2019). The fourth population of myelinated afferents, Aδ-nociceptors, have been less well characterised at the level of the DRG due to a lack of a single molecular marker.

However, much more information can be gained at the single fibre level. This is frequently assayed for using the *ex vivo* skin nerve preparation (Zimmermann *et al.*, 2009). Using the skin-nerve preparation A-fibres can be distinguished as Aβ-SAMs Aβ-RAM, Aδ-LTMRs and Aδ-nociceptors based on their conduction velocities and stimulus response functions at the single fibre level (Fig.1). For instance, Aβ and Aδ fibres can be divided due to their conduction velocities (Aβ > 10 m/s, Aδ 1.2-10 m/s), then further divided based on their coding of different mechanical and thermal stimuli (Fig 1) (Koltzenburg *et al.*, 1997; Li *et al.*, 2011; Lechner and Lewin, 2013) .

2.4. C-Fibres: electrophysiological characteristics

Different populations of C-fibres can be classified due to their electrophysiological features (Koerber, Druzinsky and Mendell, 1988; Lewin and Moshourab, 2004; Fang *et al.*, 2005; Zheng *et al.*, 2019). For instance at the level of the DRG cell body, peptidergic, non-peptidergic and low threshold mechano-receptive C-fibres have wide action potential widths, all repetitively fire to extended membrane depolarisation, and peptidergic and C-LTMRs exhibit AP delays (Koerber, Druzinsky and Mendell, 1988; Fang *et al.*, 2005; Zheng *et al.*, 2019) (Fig. 1).

Investigating C-fibre heterogeneity at the single fibre level can be achieved using the *ex vivo* skin nerve preparation. C-fibres are first distinguished by their conduction velocities (< 1.2 m/s), followed by their mechanical thresholds, and responsiveness to mechanical, and thermal stimuli as well as algogens such as capsaicin and acid (Koltzenburg, Stucky and Lewin, 1997; Lewin and Moshourab, 2004) (Fig. 1).

However, with the recent development and use of single cell sequencing technologies it is becoming clearer that the classically described primary afferent populations are perhaps too broad and the field is missing a large number of novel discrete populations (Usoskin *et al.*, 2015; Li *et al.*, 2016; Zeisel *et al.*, 2018). Fig 1C illustrates the most recent populations of sensory neurons revealed though the clustering of single cell RNA sequencing data (Zeisel *et al.*, 2018).

A) Cell body characteristics

Fibre Class	Aβ Fibres		Aδ Fibres		C Fibres	
Sub-Class	SA-LTMRs	RA-LTMRs	D-Hairs	Aδ-Nociceptors	C-LTMRs	C-Nociceptors
Soma size (Diameter)	Large (>35µm)		Medium (35>25µm)		Small (<25µm)	
Soma AP width	Narrow	Narrow	Narrow	Wide	Wide	Wide
Supra-stimuli	Few APs	Repetitive APs	Few APs	Repetitive APs	Repetitive APs	Repetitive APs
AP delay?	No	No	No	No	Yes	Yes/No

B) Terminal characteristics and population markers

Fibre Class	Aβ Fibres		Aδ Fibres		C Fibres		
Sub-Class	SA-LTMRs	RA-LTMRs	D-Hairs	Aδ-Nociceptors	C-LTMRs	C-Nociceptors	
Sensory Ending	Circumferential Ending, Merkel Cell Afferents	Meissener Corpuscles, Lanceolate Endings	Lanceolate Endings	Free nerve endings	Lanceolate Endings	Mechano/thermo: Free nerve endings; "Silent": Free nerve endings	
Markers	S100β; TrkC(P5); MafA; Ret(P5); TrkC(E12.5); Ret(E12.5)	MafA; S100β; TrkB; Calbindin	MafA; S100β; TrkB; Cav3.2	Nav1.8; S100β; CGRP*; Npy2r*	Nav1.8; TH; GINIP; VGLUT3; Cav3.3; Cav3.2; TAFA4	Nav1.8; MrgprD*; CGRP*; P2RX3; SubP*; TRPV1/A1/M8*	TrkA; CHRNA3; CGRP
Skin-nerve responses: C/V	>10m/s	>10m/s	10>1.2m/s	10>1.2m/s	<1.2m/s	<1.2m/s	
Skin-nerve responses: Thresold	Low	Low	Low	High	Low	High	
Skin-nerve responses: Force	Yes	No	No	Yes	Yes	Yes	
Skin-nerve responses: Velocity	Yes	Yes	Yes	No	Yes	No	
Skin-nerve responses: Vibration	Yes	Yes	Yes	No	No	No	
Skin-nerve responses: Heat	No	No	No	Sub-pop	No	Sub-pop	
Skin-nerve responses: Cold	No	No	No	No	Sub-pop	Sub-pop	
Skin-nerve responses: Algogens	No	No	No	Sub-pop	No	Sub-pop	
Modality							

* Denotes further subpopulations.

C) Populations defined through single cell sequencing

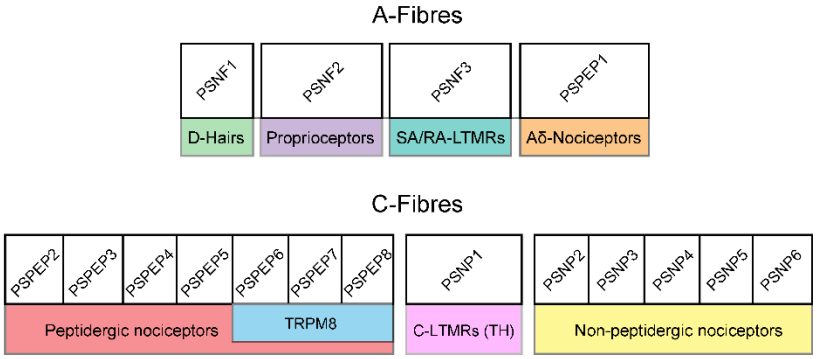

Figure 1: Characteristics of sensory neuron populations at the cell soma and peripheral terminals. **A**) Characteristic of mouse DRG neuron cell bodies. **B**) Characterisation of mouse primary afferent cutaneous terminals and popualtion molecular markers. **C**) The most recent 17 DRG populations revealed through single cell RNA sequencing. (Koerber, Druzinsky and Mendell, 1988; Koltzenburg *et al.*, 1997; Koltzenburg, Stucky and Lewin, 1997; Shin *et al.*, 2003; Lewin and Moshourab, 2004; Fang *et al.*, 2005; Hu and Lewin, 2006; Seal *et al.*, 2009; Li *et al.*, 2011; Delfini *et al.*, 2013; Lechner and Lewin, 2013; Le Pichon and Chesler, 2014; Rutlin *et al.*, 2014; Bai *et al.*, 2015; François *et al.*, 2015; Reynders *et al.*, 2015; Usoskin *et al.*, 2015; Arcourt *et al.*, 2016; Bernal Sierra *et al.*, 2017; Prato *et al.*, 2017; Dhandapani *et al.*, 2018; Zeisel *et al.*, 2018; Zheng *et al.*, 2019)

3. Neuro-modulatory tools

One way to understand neuron heterogeneity as described above, is to activate or silence defined populations of cells in order to ascribe function. Some of the tools used to achieve this are introduced below (their use in the sensory system are described in detail a later chapter)

3.1. Diphtheria toxin/receptor mediated cell ablation

The most popular ablation technique is the use of the diphtheria toxin (DTX) and its receptor (DTR) to induce apoptosis in defined cellular populations. Indeed, this tool has been employed in the pain field to selectively ablate non-peptidgergic and peptidergic nociceptors and a population of LTMRs (Cavanaugh *et al.*, 2009; McCoy *et al.*, 2013; Dhandapani *et al.*, 2018)

In the early 2000s two independent research groups established the technique to ablate cells (Saito *et al.*, 2001; Jung *et al.*, 2002). DTX is a heterodimeric toxin formed of DTX-A and DTX-B that is cytotoxic, but only when it binds to its receptor, the heparin-binding EGF like growth factor precursor (proHB-EGF or DTR) (Holmes, 2000). Endocytosis of DTX is facilitated by DTX-B binding to proHB-EGF. Following cell entry, the DTX-A subunit inactivates eukaryotic elongation factor 2 (EEF2), which is an essential factor for protein synthesis. Inactivating EEF2 results in cell apoptosis (Pappenheimer *et al.*, 1982; Ruedl and Jung, 2018) (Fig. 2). This system is extremely powerful as a single active DTX-A molecule can cause cell apoptosis (Yamaizumi *et al.*, 1978).

This tool requires the use of targeted mouse transgenics for successful use. Firstly, the mouse DTR contains mutations which render it insensitive to DTX. Therefore there is a requirement to genetically introduce a DTX sensitive receptor cloned from other species, such a humans or primates (Naglich *et al.*, 1992). Secondly, although local administration of DTX can provide spatially limited ablation,

transgenic techniques using cell-type specific promotors are required to specify DTR expression to discrete cell types (Saito *et al.*, 2001; Jung *et al.*, 2002). Alternatively, a Cre recombinase dependent inducible DTR (iDTR) is available that, in conjunction with cell-type specific Cre driver lines, can target defined populations of cells (Buch *et al.*, 2005).

Like many technologies there are pitfalls in using the DTX/DTR system. A major challenge using most technologies is ensuring the specificity of the effector molecule. Although using Cre driver lines can aid this challenge, some proteins of interest are expressed in other locations. An example would be using the $TrkB^{CreERT2}$ line, while it is a marker of a defined population of sensory neurons it is also highly expressed in other CNS regions (Gupta *et al.*, 2013). This has led researchers to develop an intersectional approach to specify DTR within the DRG, using a DRG specific promotor to harbour iDTR (Stantcheva *et al.*, 2016) (The use of this tool will be discussed in a later chapter). A second pitfall with using the DTX/DTR system is that it is not suited for repeated ablation, which might be desired when ablating mitotic cells. Post a single DTX injection mice develop antibodies against DTX reducing its ablation efficacy (Hochweller *et al.*, 2008). However, this is not an issue when ablating post-mitotic neurons. Other drawbacks include lack of reversibility and potential apoptosis related effects such as immune reactions and synaptic plasticity.

3.2. Light-gated proteins for neuronal activation/inactivation

An alternative to using ablation techniques is activating or inactivating cell populations using light-gated microbial opsins. In the pain field opsins have mostly been used to interrogate the function of different populations of nociceptors (Daou *et al.*, 2016; Iyer *et al.*, 2016; Beaudry *et al.*, 2017; Samineni *et al.*, 2017; Cowie *et al.*, 2018; Mickle and Gereau, 2018).

There are three families of opsins: archaer/bacteriorhodopsins (inhibitory proton pumps), halorhodopsins (inhibitory chloride pumps) and channelrhodopsin (excitatory cation channels) that are all activated by different wavelengths of light to inhibit or increase excitable cell function (Fig. 2) (Boyden, 2011). The discovery of optogenetics came through the efforts of multiple groups. The first paper to demonstrate that neurons could be artificially activated by light sensitive proteins and photostimulation, was when a trio of drosophila genes termed “chARGe" were co expressed in rat hippocampal neurons (Zemelman *et al.*, 2002). However, due to the relatively slow (seconds) temporal resolution of this tool and the discovery of channelrhodopsin-2 (ChR2) (Nagel *et al.*, 2003) soon after, chARGe was not readily adopted. ChR2 is activated by blue light (470 nM) and lets positively charged ions enter the membrane of cells (Nagel *et al.*, 2003). ChR2 was first used in mammalian neurons in 2005 and it was extremely effective at controlling neural activity at millisecond resolution (Boyden *et al.*, 2005). After ChR2’s first use in mammalian neurons, ChR2 transgenic mouse lines were soon generated (Arenkiel *et al.*, 2007; Wang *et al.*, 2007; Madisen *et al.*, 2012) and enabled the transgenic expression of ChR2 in defined cell populations in order to better understand CNS and PNS circuits.

Inhibitory optogenetic tools allow light-activated shutdown of neuronal activity (Han and Boyden, 2007; Zhang *et al.*, 2007). These studies used the tool Halorhodopsin (Halo/NpHR), activated by yellow light (580 nM) to mediate a chloride conductance to supress neuronal activity at millisecond resolution (Han and Boyden, 2007; Zhang *et al.*, 2007). However, Halo/NpHR was not the ideal tool due to low current magnitude, prolonged stimulation inactivation and slow recovery (Hegemann, Oesterhelt and Steiner, 1985; Bamberg, Tittor and Oesterhelt, 1993; Chow *et al.*, 2010). Consequently, a new and more effective optogenetic silencing tool was generated, Archaerhodopsin-3 (Arch). Arch is activated by yellow light and

is an outward proton pump that can induce robust and repeatable neuronal silencing, which quickly recovers from light dependent inactivation (Chow *et al.*, 2010).

Since the discovery of these major three optogenetic tools the technique has soared in popularity, and is commonly used throughout neuroscience to understand neuronal circuits in both the CNS and PNS. Furthermore, groups are continuously looking for the next generation of optogenetic activators, silencers and implantable stimulators (Berndt *et al.*, 2009, 2014; Lin *et al.*, 2009; Kleinlogel *et al.*, 2011; Park *et al.*, 2015; Samineni *et al.*, 2017; Shin *et al.*, 2017; Alberio *et al.*, 2018; Mickle *et al.*, 2019; Zhang *et al.*, 2019). However, optogenetics also has technical drawbacks, such as the requirement of a light source, light source penetration difficulties and the need for implants to stimulate deep tissues, the heat generated from light sources and the challenges with maintaining long term neuronal control.

3.3. Chemogenetic tools to modulate neuronal activity

Chemogenetics tools also offers the ability to activate or inactivate neurons of interest in order to interrogate the role of neuronal populations and associated circuits. Chemogenetic approaches require the expression of an engineered non-native receptor or ion channel that is exclusively activated by an exogenous agonist.

Historically, early chemogenetic tools were receptors activated solely by synthetic ligands (RASSLs) used to modulate specific cells (Coward *et al.*, 1998; Zhao *et al.*, 2003; Conklin *et al.*, 2008). However a major pitfall with RASSLs was that their synthetic ligands were able to activate endogenous targets, leading to systematic administration being highly confounded.

At present, the most widely used chemogenetic tools employed in neuroscience are the designer receptors exclusively activated by designer drugs (DREADDs). The main DREADDs are engineered human muscarinic G-protein coupled receptors that are activated by clozapine-N-oxide (CNO) and Clozapine

(Armbruster *et al.*, 2007; Gomez *et al.*, 2017). The main excitatory DREADD is hM3Dq (M1 and M5 variants also exist) (Armbruster *et al.*, 2007). hM3Dq, when activated by CNO or clozapine, initiates the PLC/PIP_2/DAG/IP_3 signalling cascade, where IP_3 binds to the IP_3 receptor on the endoplasmic reticulum (ER) resulting in release of calcium from ER stores. The increase in intracellular calcium concentrations depolarises neurons and increases neuronal excitability (Armbruster *et al.*, 2007; Roth, 2016).

The main inhibitory DREADD tools are the hM2Di, hM4Di and KORD (kappa-opioid receptor D138N mutant) (Fig. 2) (Armbruster *et al.*, 2007; Vardy *et al.*, 2015; Roth, 2016). When these tools are activated by their agonist (CNO, clozapine or salvinorin-B), two mechanisms occur that lead to neuronal silencing. Gi/Gβ/γ activation of GIRK (G-protein coupled inwardly rectifying potassium) channels results in neuronal hyperpolarisation and prevention of presynaptic neurotransmitter release (Armbruster *et al.*, 2007; Stachniak, Ghosh and Sternson, 2014; Vardy *et al.*, 2015). The temporal resolution of activatory and inhibitory DREADDs is in the range of minutes to hours. For a review of their use in the brain see (Sternson and Roth, 2014). In the pain field DREADDs been employed to inactivate large populations of nociceptors (Saloman *et al.*, 2016; Miller *et al.*, 2017; Jayaraj *et al.*, 2018).

Since the discovery and application of DREADDs, others have created novel chemogenetic ion channels to modulate neuronal activity. These include the ivermectin (IVM) sensitive, engineered glutamate-gate chloride channel (GluCl) (Fig. 2) (Slimko *et al.*, 2002; Lerchner *et al.*, 2007). GluCl will be discussed in detail in the next chapter, but briefly, it has been modified so that it is no longer sensitive to glutamate but highly sensitive to low doses of the safe non-toxic agonist ivermectin (IVM). When activated, this channel facilitates a chloride conductance to hyperpolarise CNS neurons and was used to silence striatal neurons and reduce amphetamine induced behaviour (Lerchner *et al.*, 2007). However, due to problems

with IVM crossing the blood-brain barrier this tool may not be the best suited to studies of the CNS. Hence, this tool is a key candidate for the modulation of the PNS.

The final family of chemogenetic silencing tools are the pharmacologically selective actuator modules (PSAMs) and, pharmacologically selective effector molecules (PSEMs) (Fig 2). These tools were designed though the generation of chimeric cys-loop ion channels. Chimeric ion channels were created by combining the ligand binding domain (LBD) of the α7 nicotinic acetylcholine receptor (nAChR) fused to the ion pore domain (IPD) of either the, nAChR, the $5HT_3$ receptor or the $GABA_C$ or Glycine receptor (GlyR) (Magnus *et al.*, 2011). The α7-nAChR LBD underwent mutagenesis to reduce ACh potency and identify novel binding sites and partners not present in wild type α7-nAChRs. This modified α7-nAChR-LBD can be attached to the IPD of the modified $5HT_3$ receptor and activated by synthetic PSEMs to induce large depolarising currents to activate neurons (Magnus *et al.*, 2011). PSEM. activation of α7-nAChR(LBD) and a modified nAChR (IPD) resulted in a desensitisation free, calcium conductance (Magnus *et al.*, 2011). Finally, PSEM. activation of α7-nAChR(LBD) and a modified GlyR/$GABA_C$ (IPD) resulted in a chloride conductance which reduced the membrane input resistance and dramatically silenced neuronal activity (Magnus *et al.*, 2011). The toolbox of PSAM/PSEMs allows a powerful, flexible and interchangeable means to modulate neuronal activity. For a review of their use in the CNS, see (Atasoy and Sternson, 2018). However, challenges with the PSAM/PSEM. system were the low micromolar potency and the relatively quick clearance of PSEM.s (*in vivo* use issues), and there are no identified clinically applicable drugs that can activate PSAMs (translational issue) (Magnus *et al.*, 2011). This led to the recent development of ultrapotent chemogenetic tools termed $PSAM^4$-GlyR, $PSAM^4$-$5HT_3$, sensitive to $uPSEM^{792}$ and the clinically approved drug varenicline (Fig. 2) (Magnus *et al.*, 2019).

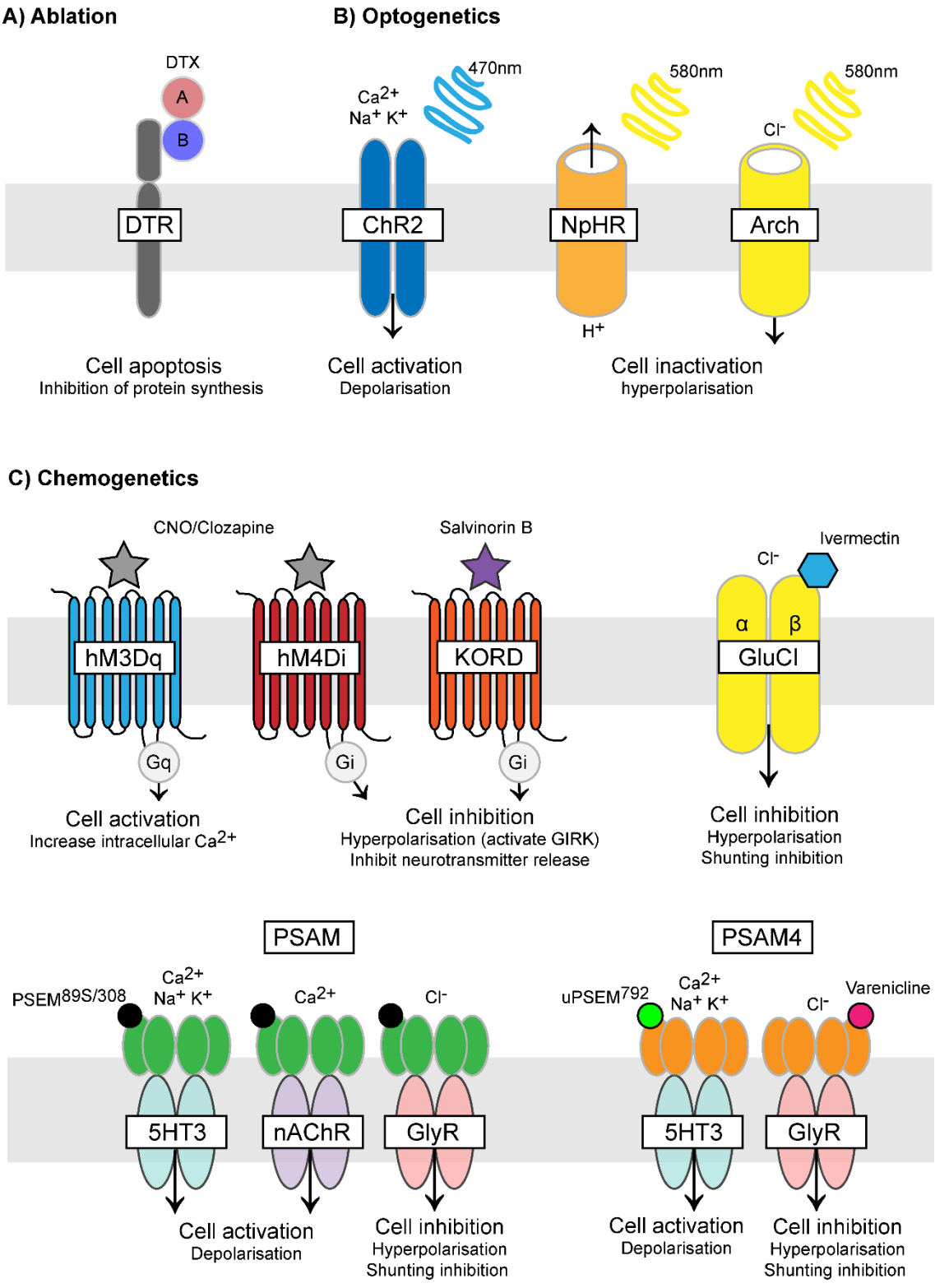

Figure 2: Examples of different neuromodulators. A) The DTX/DTR system for cell ablation. **B)** The common three optogenetic tools used for neuronal excitation (Chr2) and inhibition (NpHR proton pump and Arch chloride pump). **C)** Chemogenetic tools available for neuronal activation or inhibition, DREADDs, GluCl and PSAM/PSEMs and PSAM4/uPSEMs.

4. Nerve injury and neuropathic pain

Neuropathic pain occurs due to injury or disease of the somatosensory nervous system, affecting 7-10% of the population (Jensen *et al.*, 2011; Van Hecke *et al.*, 2014), though this figure is predicated to rise due to the increased prevalence of diabetes and use of chemotherapy (Van Hecke *et al.*, 2014). Chronic pain is a large socioeconomic burden and ranks third in the important causes of disability-adjusted life years worldwide (Rice, Smith and Blyth, 2016; James *et al.*, 2018). Effective treatments of neuropathic pain are lacking (Finnerup *et al.*, 2015). In order to develop new treatments for neuropathic pain, many researchers use rodents (and other organisms) to model neuropathic pain.

4.1. Rodent models of neuropathic pain

The most common rodent models of neuropathic pain are the traumatic nerve injuries achieved through surgical procedures. In order of discovery, complete transection of the sciatic nerve is the oldest model and results in limb autotomy, and can reflect symptoms of phantom limb pain in humans (Wall *et al.*, 1979). The introduction of loosely constrictive ligatures around the sciatic nerve is termed chronic constriction injury and models nerve compression (Bennett and Xie, 1988) and the ligatures themselves initiate an immune-response component to the model (Maves *et al.*, 1993). The partial ligation of one- to two-thirds of the sciatic nerve is ligated modelling nerve contusion (Seltzer, Dubner and Shir, 1990). The tight ligation of (L5 and L6 but not L4) spinal nerves is termed spinal nerve ligation (SNL) and offers the ability to study both injured and uninjured afferents from the same peripheral nerve (Kim and Chung, 1992). The transection of one of the three sciatic nerve branches is termed sciatic nerve injury (SNI) and results in a mix of injured and uninjured neurons from the respective afferents (Decosterd and Woolf, 2000).

While traumatic nerve injury induced neuropathic pain is a popular model there are other models of neuropathic pain that are clinically relevant. Chemotherapy induced neuropathy can be modelled in rodents through administration of chemotherapeutic agents such as platinum compounds (Cisplatin, Carboplatin and Oxaliplatin), taxanes (Docetaxel and Paclitaxel)**,** vinca alkaloids (Vincristine), and proteasome inhibitors (Bortezomib and Carfilzomib). All of these compounds are commonly used in animal models of chemotherapy-induced peripheral neuropathy (Höke and Ray, 2014).

Other models of peripheral neuropathic pain include diabetic neuropathy which has been historically modelled in rodents using Streptozotocin (STZ) which destroys pancreatic β-cells (Jakobsen and LundbæK, 1976; Islam, 2013). STZ is neurotoxic and activates TRPA1 on sensory neurons complicating the interpretation of STZ induced diabetic neuropathy (Andersson *et al.*, 2015). However, other models (such as transgenic ob/ob and Akita mice) are available and may offer possibilities moving forward (Islam, 2013). Another clinically relevant models of neuropathic pain include, HIV-associated neuropathies (Keswani *et al.*, 2002; Huang *et al.*, 2013) and passive transfer of human auto-antibodies to rodents, from patients with neuropathic pain (Dawes *et al.*, 2018).

4.2. Measuring pain in rodent models of neuropathic pain

In many rodent models of neuropathic pain both hypo- and hypersensitivity to different stimuli occurs. As an example, the SNI model results in hyposensitivity to sensory stimuli in the hind paw region that is normally innervated by the severed nerves (tibial and common peroneal) through loss of innervation. However, adjacent regions such as the sural territory become hypersensitive to mechanical and thermal stimuli (Decosterd and Woolf, 2000). This hypersensitivity can be measured by researchers by looking at reflex withdrawals thresholds, latencies and the number or type of responses evoked to various stimuli. For

instance following SNI, rodents show robust and reliable hypersensitivity to punctate (von Frey) and dynamic (brush) stimuli (Decosterd and Woolf, 2000; Cheng *et al.*, 2017). These assays are thought to resemble the mechanical allodynia (normally innocuous stimuli experienced as noxious) in neuropathic pain patients. Rodents can also develop cold and heat hypersensitivity, measured using hot/cold plates, radiant heat sources and in some cases acetone (Deuis, Dvorakova and Vetter, 2017). These outcome measures are thought to resemble the thermal allodynia and hyperalgesia (increased sensitivity to thermal pain) experienced by neuropathic pain patients. These techniques are being regularly refined and updated, the most recent example being a sub-second mouse pain scale using behavioural mapping and statistical modelling (Abdus-Saboor *et al.*, 2019).

These outcome measures are frequently used to measure outcomes of neuropathic pain in the different rodent models. This is often due to the ease and reproducibility available to researchers. However, although a proportion of patients do experience gain of function symptoms, the major clinical complaint is non-evoked spontaneous pain (Backonja and Stacey, 2004; Colloca *et al.*, 2017; Rice *et al.*, 2018). Which poses the question, are we overlooking an important component of neuropathic pain in our rodent models? This question has led to researchers to look for other outcomes to measure non-evoked neuropathic pain in rodent models. One method of analysing spontaneous pain is quantifying spontaneous foot lifting (Djouhri *et al.*, 2006). One group developed methods to assess facial grimace in rodents as an observational outcome of pain, however facial grimace scores were not associated with neuropathic pain models (Langford *et al.*, 2010; Sotocinal *et al.*, 2011). Other groups have adopted ethological assays such as the quantification of burrowing behaviour. This assay is self-motivated with injured or unwell mice burrowing less than non-injured or healthy mice (Deacon, 2006; Jirkof *et al.*, 2010; Andrews *et al.*, 2012). Other studies have used weight bearing as a measure of

neuropathic pain (Tétreault *et al.*, 2011; Buys and Alphonso, 2014). These assays may serve as surrogates for non-evoked pain and are ethologically relevant. However, spontaneous foot lifting is an extreme measure of spontaneous pain and an absence of foot lifting does not necessarily equate to an absence of on-going pain. Unfortunately, the other methods have not been reproduced or readily taken up by the pain field.

Hence, other than observational and etiological assays, methods have been developed to assess spontaneous non-evoked neuropathic pain using conditioned place preference paradigms (King *et al.*, 2009). This assay uses context dependent conditioning to an inert and non-addictive analgesic after injury. Following conditioning, mice are tested for their chamber preference, and neuropathic mice spend longer in chambers previously paired with non-addictive analgesics such as Clonidine (King *et al.*, 2009). Researchers can assess the analgesic properties of novel analgesics or other interventions and their effects on non-evoked spontaneous pain.

4.3. Mechanisms of Neuropathic pain

A key pathophysiological driver of neuropathic pain is the increased spontaneous activity of primary afferents (cell bodies and terminals) following nerve injury. This post injury ectopia initially begins in A-fibre afferents and then later in C-fibres (Wall and Gutnick, 1974; Boucher *et al.*, 2000; Liu *et al.*, 2000; Wu *et al.*, 2001, 2002). This phenomenon is thought to be true for injured and uninjured afferents (Liu *et al.*, 2000; Wu *et al.*, 2001). This ongoing activity is required to maintain neuropathic pain in patients (Haroutounian *et al.*, 2014). Neuropathic insult results in maladaptive changes, such as peripheral and central sensitisation, that are thought to give rise to and maintain neuropathic pain (Devor, 2009; Harriott and Gold, 2009; Latremoliere and Woolf, 2009; Meacham *et al.*, 2017).

The changes in aberrant activity and peripheral sensitisation that occur following nerve injury are thought to be a consequence of a multitude of changes in the expression and function of growth factors, neurotransmitters, and ion channels within the DRG. In particular, ion channels undergo changes in their expression, their biophysical properties, and localisation within primary afferents (Harriott and Gold, 2009; Calvo *et al.*, 2016; Bennett *et al.*, 2019). There is evidence of increased localisation/activity of transducers at the primary afferent terminals, a reduction in potassium channel localisation/activity and an increase in VGSC and HCN localisation/activity at the axon and soma following nerve injury (Harriott and Gold, 2009; Tsantoulas and McMahon, 2014; Mickle, Shepherd and Mohapatra, 2016; Bennett *et al.*, 2019). All of which promote signal transduction, action potential initiation, propagation and neurotransmission, contributing to on-going aberrant activity and hyperexcitable sensory neurons.

In addition to peripheral sensitisation, following nerve injury there is a large body of evidence to support central sensitisation as a mechanism that maintains neuropathic pain. The spinal cord cannot be ignored when interrogating the sensory system as this is the first synaptic contact of the circuit. Central sensitisation is a phenomenon where spinal circuits become more excitable, enhancing the response to noxious stimuli and facilitating the engagement of innocuous stimuli and nociceptive pathways (Woolf, 2011). Following neuropathic injury there is evidence that the dorsal horn of the spinal cord undergoes structural changes, synaptic plasticity, glial and immune cell infiltration, chloride dysregulation (which largely results in increased neuronal excitability or circuit disinhibition) and alterations in GABAergic and Glycinergic inhibitory tone (Latremoliere and Woolf, 2009; Woolf, 2011). However, there is also evidence that higher centres and brain regions may contribute to neuropathic pain following peripheral injury. There is evidence that wide dynamic range neurons in the ventral posterior thalamus become hyperexcitable,

upregulation of T-Type calcium channels in the anterior cingulate cortex, glial-dependent synaptic plasticity of the somatosensory cortex and changes in descending modulation (Ossipov, Dussor and Porreca, 2010; Meacham *et al.*, 2017).

While central changes post injury are important, arguably, changes in the periphery are translationally more attractive loci for drug intervention. However, due to the vast roles of primary afferents (as described above), non-selective targeting or blockade may not be ideal and lead to undesired side effects such insensitivity to pain (i.e. loss of protective pain). Therefore, targeted therapeutics is a major future goal and hence I have the following aims.

5. Aims

The understanding of the mechanisms that drive and maintain different forms of neuropathic pain are incomplete. In particular, it is unclear and debated as to which population or populations of sensory neurons are key drivers of neuropathic pain pathophysiology. However, there is now a plethora of preclinical tools available to interrogate sensory neuron populations, their circuitry and their function. The aim of this work is to develop and validate the engineered GluCl channel, creating a chemogenetic tool box to silence sensory neurons. First, I aim to employ GluCl in an unbiased manner to silence all DRG neurons and second in a Cre dependent manner to silence two sensory neuron populations, the Nav1.8+ population and the TH+ (C-LTMRs) population. I aim to assess the sensory function of these two populations with a particular focus on neuropathic pain. Finally, using what I have learnt from the chemogenetic silencing of C-LTMRs, I aim investigate the role of the VGSC Nav1.7 in C-LTMRs in humans and mice.

6. References

Abdo, H. *et al.* (2019) ‘Specialized cutaneous schwann cells initiate pain sensation’, *Science*. American Association for the Advancement of Science, 365(6454), pp. 695–699. doi: 10.1126/science.aax6452.

Abdus-Saboor, I. *et al.* (2019) ‘Development of a Mouse Pain Scale Using Sub-second Behavioral Mapping and Statistical Modeling’, *CellReports*, 28, pp. 1623-1634.e4. doi: 10.1016/j.celrep.2019.07.017.

Alberio, L. *et al.* (2018) ‘A light-gated potassium channel for sustained neuronal inhibition’, *Nature Methods*. Nature Publishing Group, 15(11), pp. 969–976. doi: 10.1038/s41592-018-0186-9.

Andersson, D. A. *et al.* (2015) ‘Streptozotocin stimulates the ion channel TRPA1 directly: Involvement of peroxynitrite’, *Journal of Biological Chemistry*. American Society for Biochemistry and Molecular Biology Inc., 290(24), pp. 15185–15196. doi: 10.1074/jbc.M115.644476.

Andrews, N. *et al.* (2012) ‘Spontaneous burrowing behaviour in the rat is reduced by peripheral nerve injury or inflammation associated pain’, *European Journal of Pain*. Wiley, 16(4), pp. 485–495. doi: 10.1016/j.ejpain.2011.07.012.

Arcourt, A. *et al.* (2016) ‘Touch Receptor-Derived Sensory Information Alleviates Acute Pain Signaling and Fine-Tunes Nociceptive Reflex Coordination’, *Neuron*. Elsevier Inc., 93(1), pp. 179–193. doi: 10.1016/j.neuron.2016.11.027.

Arenkiel, B. R. *et al.* (2007) ‘In Vivo Light-Induced Activation of Neural Circuitry in Transgenic Mice Expressing Channelrhodopsin-2’, *Neuron*, 54(2), pp. 205–218. doi: 10.1016/j.neuron.2007.03.005.

Armbruster, B. N. *et al.* (2007) ‘Evolving the lock to fit the key to create a family of G protein-coupled receptors potently activated by an inert ligand’, *Proceedings of the*

National Academy of Sciences of the United States of America, 104(12), pp. 5163–5168. doi: 10.1073/pnas.0700293104.

Atasoy, D. and Sternson, S. M. (2018) ‘Chemogenetic tools for causal cellular and neuronal biology’, *Physiological Reviews*. American Physiological Society, 98(1), pp. 391–418. doi: 10.1152/physrev.00009.2017.

Backonja, M.-M. and Stacey, B. (2004) ‘Neuropathic pain symptoms relative to overall pain rating’, *The Journal of Pain*. Churchill Livingstone, 5(9), pp. 491–497. doi: 10.1016/J.JPAIN.2004.09.001.

Bai, L. *et al.* (2015) ‘Genetic Identification of an Expansive Mechanoreceptor Sensitive to Skin Stroking’, *Cell*. Cell Press, 163(7), pp. 1783–1795. doi: 10.1016/j.cell.2015.11.060.

Bamberg, E., Tittor, J. and Oesterhelt, D. (1993) ‘Light-driven proton or chloride pumping by halorhodopsin’, *Proceedings of the National Academy of Sciences of the United States of America*. National Academy of Sciences, 90(2), pp. 639–643. doi: 10.1073/pnas.90.2.639.

Beaudry, H. *et al.* (2017) ‘Distinct behavioral responses evoked by selective optogenetic stimulation of the major TRPV1+ and MrgD+ subsets of C-fibers’, *Pain*. Lippincott Williams and Wilkins, 158(12), pp. 2329–2339. doi: 10.1097/j.pain.0000000000001016.

Bennett, D. L. *et al.* (2019) ‘The Role of Voltage-Gated Sodium Channels in Pain Signaling’, *Physiological Reviews*. American Physiological Society Bethesda, MD , 99(2), pp. 1079–1151. doi: 10.1152/physrev.00052.2017.

Bennett, G. J. and Xie, Y. K. (1988) ‘A peripheral mononeuropathy in rat that produces disorders of pain sensation like those seen in man’, *Pain*, 33(1), pp. 87–107. doi: 10.1016/0304-3959(88)90209-6.

Bernal Sierra, Y. A. *et al.* (2017) 'Genetic Tracing of Cav3.2 T-Type Calcium Channel Expression in the Peripheral Nervous System', *Frontiers in Molecular Neuroscience*, 10. doi: 10.3389/fnmol.2017.00070.

Berndt, A. *et al.* (2009) 'Bi-stable neural state switches', *Nature Neuroscience*, 12(2), pp. 229–234. doi: 10.1038/nn.2247.

Berndt, A. *et al.* (2014) 'Structure-guided transformation of channelrhodopsin into a light-activated chloride channel', *Science*. American Association for the Advancement of Science, 344(6182), pp. 420–424. doi: 10.1126/science.1252367.

Boucher, T. J. *et al.* (2000) 'Potent analgesic effects of GDNF in neuropathic pain states', *Science*, 290(5489), pp. 124–127. doi: 10.1126/science.290.5489.124.

Boyden, E. S. *et al.* (2005) 'Millisecond-timescale, genetically targeted optical control of neural activity', *Nature Neuroscience*. Nature Publishing Group, 8(9), pp. 1263–1268. doi: 10.1038/nn1525.

Boyden, E. S. (2011) 'A history of optogenetics: The development of tools for controlling brain circuits with light', *F1000 Biology Reports*. doi: 10.3410/B3-11.

Buch, T. *et al.* (2005) 'A Cre-inducible diphtheria toxin receptor mediates cell lineage ablation after toxin administration', *Nature Methods*, 2(6), pp. 419–426. doi: 10.1038/nmeth762.

Buys, M. J. and Alphonso, C. (2014) 'Novel use of perineural pregabalin infusion for analgesia in a rat neuropathic pain model', in *Anesthesia and Analgesia*. Lippincott Williams and Wilkins, pp. 481–488. doi: 10.1213/ANE.0000000000000291.

Calvo, M. *et al.* (2016) 'Altered potassium channel distribution and composition in myelinated axons suppresses hyperexcitability following injury', *eLife*. eLife Sciences Publications Ltd, 5(APRIL2016). doi: 10.7554/eLife.12661.

Cavanaugh, D. J. *et al.* (2009) 'Distinct subsets of unmyelinated primary sensory fibers

mediate behavioral responses to noxious thermal and mechanical stimuli', *Proceedings of the National Academy of Sciences of the United States of America*. National Academy of Sciences, 106(22), pp. 9075–9080. doi: 10.1073/pnas.0901507106.

Cheng, L. *et al.* (2017) 'Identification of spinal circuits involved in touch-evoked dynamic mechanical pain', *Nature Neuroscience*. Nature Publishing Group, 20(6), pp. 804–814. doi: 10.1038/nn.4549.

Chow, B. Y. *et al.* (2010) 'High-performance genetically targetable optical neural silencing by light-driven proton pumps', *Nature*. Nature Publishing Group, 463(7277), pp. 98–102. doi: 10.1038/nature08652.

Colloca, L. *et al.* (2017) 'Neuropathic pain', *Nature Reviews Disease Primers*. Macmillan Publishers Limited, 3, pp. 1–20. doi: 10.1038/nrdp.2017.2.

Conklin, B. R. *et al.* (2008) 'Engineering GPCR signaling pathways with RASSLs', *Nature Methods*, 5(8), pp. 673–678. doi: 10.1038/nmeth.1232.

Coward, P. *et al.* (1998) 'Controlling signaling with a specifically designed G i -coupled receptor', *Proceedings of the National Academy of Sciences of the United States of America*. National Academy of Sciences, 95(1), pp. 352–357. doi: 10.1073/pnas.95.1.352.

Cowie, A. M. *et al.* (2018) 'Optogenetic Inhibition of CGRPα Sensory Neurons Reveals Their Distinct Roles in Neuropathic and Incisional Pain.', *The Journal of neuroscience*. Society for Neuroscience, 38(25), pp. 5807–5825. doi: 10.1523/JNEUROSCI.3565-17.2018.

Daou, I. *et al.* (2016) 'Optogenetic silencing of Nav1.8-positive afferents alleviates inflammatory and neuropathic pain', *eNeuro*. Society for Neuroscience, 3(1), pp. 702–705. doi: 10.1523/ENEURO.0140-15.2016.

Dawes, J. M. *et al.* (2018) 'Immune or Genetic-Mediated Disruption of CASPR2

Causes Pain Hypersensitivity Due to Enhanced Primary Afferent Excitability', *Neuron*, 97(4), pp. 806-822.e10. doi: 10.1016/j.neuron.2018.01.033.

Deacon, R. M. J. (2006) 'Burrowing in rodents: A sensitive method for detecting behavioral dysfunction', *Nature Protocols*, 1(1), pp. 118–121. doi: 10.1038/nprot.2006.19.

Decosterd, I. and Woolf, C. J. (2000) 'Spared nerve injury: An animal model of persistent peripheral neuropathic pain', *Pain*, 87(2), pp. 149–158. doi: 10.1016/S0304-3959(00)00276-1.

Delfini, M.-C. *et al.* (2013) 'TAFA4, a Chemokine-like Protein, Modulates Injury-Induced Mechanical and Chemical Pain Hypersensitivity in Mice', *Cell Reports*. Cell Press, 5(2), pp. 378–388. doi: 10.1016/J.CELREP.2013.09.013.

Deuis, J. R., Dvorakova, L. S. and Vetter, I. (2017) 'Methods used to evaluate pain behaviors in rodents', *Frontiers in Molecular Neuroscience*. Frontiers Media S.A. doi: 10.3389/fnmol.2017.00284.

Devor, M. (2009) 'Ectopic discharge in Aβ afferents as a source of neuropathic pain', *Experimental Brain Research*, pp. 115–128. doi: 10.1007/s00221-009-1724-6.

Dhandapani, R. *et al.* (2018) 'Control of mechanical pain hypersensitivity in mice through ligand-targeted photoablation of TrkB-positive sensory neurons', *Nature Communications*. Nature Publishing Group, 9(1), p. 1640. doi: 10.1038/s41467-018-04049-3.

Djouhri, L. *et al.* (2006) 'Spontaneous pain, both neuropathic and inflammatory, is related to frequency of spontaneous firing in intact C-fiber nociceptors', *Journal of Neuroscience*, 26(4), pp. 1281–1292. doi: 10.1523/JNEUROSCI.3388-05.2006.

Fang, X. *et al.* (2005) 'Electrophysiological differences between nociceptive and non-nociceptive dorsal root ganglion neurones in the rat in vivo', *Journal of Physiology*,

565(3), pp. 927–943. doi: 10.1113/jphysiol.2005.086199.

Finnerup, N. B. *et al.* (2015) ‘Pharmacotherapy for neuropathic pain in adults: A systematic review and meta-analysis’, *The Lancet Neurology*. Lancet Publishing Group, 14(2), pp. 162–173. doi: 10.1016/S1474-4422(14)70251-0.

François, A. *et al.* (2015) ‘The Low-Threshold Calcium Channel Cav3.2 Determines Low-Threshold Mechanoreceptor Function’, *Cell Reports*. Cell Press, 10(3), pp. 370–382. doi: 10.1016/J.CELREP.2014.12.042.

Gomez, J. L. *et al.* (2017) ‘Chemogenetics revealed: DREADD occupancy and activation via converted clozapine’, *Science*. American Association for the Advancement of Science, 357(6350), pp. 503–507. doi: 10.1126/science.aan2475.

Gupta, V. K. *et al.* (2013) ‘TrkB receptor signalling: Implications in neurodegenerative, psychiatric and proliferative disorders’, *International Journal of Molecular Sciences*. MDPI AG, pp. 10122–10142. doi: 10.3390/ijms140510122.

Han, X. and Boyden, E. S. (2007) ‘Multilpe-color optical activation, silencing, and desynchronization of neural activity, with single-spike temporal resolution’, *PLoS ONE*, 2(3). doi: 10.1371/journal.pone.0000299.

Haroutounian, S. *et al.* (2014) ‘Primary afferent input critical for maintaining spontaneous pain in peripheral neuropathy’, *Pain*. Elsevier B.V., 155(7), pp. 1272–1279. doi: 10.1016/j.pain.2014.03.022.

Harriott, A. M. and Gold, M. S. (2009) ‘Contribution of primary afferent channels to neuropathic pain’, *Current Pain and Headache Reports*, pp. 197–207. doi: 10.1007/s11916-009-0034-9.

Van Hecke, O. *et al.* (2014) ‘Neuropathic pain in the general population: A systematic review of epidemiological studies’, *Pain*. Elsevier B.V., pp. 654–662. doi: 10.1016/j.pain.2013.11.013.

Hegemann, P., Oesterhelt, D. and Steiner, M. (1985) ‘The photocycle of the chloride pump halorhodopsin. I: Azidecatalyzed deprotonation of the chromophore is a side reaction of photocycle intermediates inactivating the pump’, *The EMBO Journal*. Wiley, 4(9), pp. 2347–2350. doi: 10.1002/j.1460-2075.1985.tb03937.x.

Hochweller, K. *et al.* (2008) ‘A novel CD11c.DTR transgenic mouse for depletion of dendritic cells reveals their requirement for homeostatic proliferation of natural killer cells’, *European Journal of Immunology*, 38(10), pp. 2776–2783. doi: 10.1002/eji.200838659.

Höke, A. and Ray, M. (2014) ‘Rodent models of chemotherapy-induced peripheral neuropathy’, *ILAR Journal*, 54(3), pp. 273–281. doi: 10.1093/ilar/ilt053.

Holmes, R. K. (2000) ‘ Biology and Molecular Epidemiology of Diphtheria Toxin and the tox Gene ’, *The Journal of Infectious Diseases*. Oxford University Press (OUP), 181(s1), pp. S156–S167. doi: 10.1086/315554.

Hu, J. and Lewin, G. R. (2006) ‘Mechanosensitive currents in the neurites of cultured mouse sensory neurones’, *Journal of Physiology*, 577(3), pp. 815–828. doi: 10.1113/jphysiol.2006.117648.

Huang, W. *et al.* (2013) ‘A clinically relevant rodent model of the HIV antiretroviral drug stavudine induced painful peripheral neuropathy’, *Pain*. Elsevier B.V., 154(4), pp. 560–575. doi: 10.1016/j.pain.2012.12.023.

Islam, M. S. (2013) ‘Animal models of diabetic neuropathy: Progress since 1960s’, *Journal of Diabetes Research*. doi: 10.1155/2013/149452.

Iyer, S. M. *et al.* (2016) ‘Optogenetic and chemogenetic strategies for sustained inhibition of pain’, *Scientific Reports*. Nature Publishing Group, 6. doi: 10.1038/srep30570.

Jakobsen, J. and LundbæK, K. (1976) ‘Neuropathy in experimental diabetes: An

animal model', *British Medical Journal*, 2(6030), pp. 278–279. doi: 10.1136/bmj.2.6030.278.

James, S. L. *et al.* (2018) 'Global, regional, and national incidence, prevalence, and years lived with disability for 354 Diseases and Injuries for 195 countries and territories, 1990-2017: A systematic analysis for the Global Burden of Disease Study 2017', *The Lancet*. Lancet Publishing Group, 392(10159), pp. 1789–1858. doi: 10.1016/S0140-6736(18)32279-7.

Jayaraj, N. D. *et al.* (2018) 'Reducing CXCR4-mediated nociceptor hyperexcitability reverses painful diabetic neuropathy', *Journal of Clinical Investigation*. American Society for Clinical Investigation, 128(6), pp. 2205–2225. doi: 10.1172/JCI92117.

Jensen, T. S. *et al.* (2011) 'A new definition of neuropathic pain', *Pain*. Elsevier B.V., pp. 2204–2205. doi: 10.1016/j.pain.2011.06.017.

Jirkof, P. *et al.* (2010) 'Burrowing behavior as an indicator of post-laparotomy pain in mice', *Frontiers in Behavioral Neuroscience*, 4(OCT). doi: 10.3389/fnbeh.2010.00165.

Jung, S. *et al.* (2002) 'In vivo depletion of CD11c+ dendritic cells abrogates priming of CD8+ T cells by exogenous cell-associated antigens', *Immunity*. Cell Press, 17(2), pp. 211–220. doi: 10.1016/S1074-7613(02)00365-5.

Keswani, S. C. *et al.* (2002) 'HIV-associated sensory neuropathies.', *AIDS (London, England)*, 16(16), pp. 2105–17. doi: 10.1097/00002030-200211080-00002.

Kim, S. H. and Chung, J. M. (1992) 'An experimental model for peripheral neuropathy produced by segmental spinal nerve ligation in the rat.', *Pain*, 50(3), pp. 355–63. Available at: http://www.ncbi.nlm.nih.gov/pubmed/1333581 (Accessed: 4 January 2020).

King, T. *et al.* (2009) 'Unmasking the tonic-aversive state in neuropathic pain', *Nature Neuroscience*, 12(11), pp. 1364–1366. doi: 10.1038/nn.2407.

Kleinlogel, S. *et al.* (2011) ‘Ultra light-sensitive and fast neuronal activation with the Ca 2+-permeable channelrhodopsin CatCh’, *Nature Neuroscience*, 14(4), pp. 513–518. doi: 10.1038/nn.2776.

Koerber, H. R., Druzinsky, R. E. and Mendell, L. M. (1988) ‘Properties of somata of spinal dorsal root ganglion cells differ according to peripheral receptor innervated’, *Journal of Neurophysiology*, 60(5), pp. 1584–1596. doi: 10.1152/jn.1988.60.5.1584.

Koltzenburg, M. *et al.* (1997) ‘Receptive Properties of Mouse Sensory Neurons Innervating Hairy Skin Receptive Properties of Mouse Sensory Neurons Innervating Hairy Skin’, *Journal of Neurophysiology*, 78, pp. 1841–1850.

Koltzenburg, M., Stucky, C. L. and Lewin, G. R. (1997) ‘Receptive Properties of Mouse Sensory Neurons Innervating Hairy Skin’, *Journal of Neurophysiology*, 78(4), pp. 1841–1850. doi: 10.1152/jn.1997.78.4.1841.

Langford, D. J. *et al.* (2010) ‘Coding of facial expressions of pain in the laboratory mouse.’, *Nature Methods*, 7(6), pp. 447–449. doi: 10.1038/NMETH.14.

Latremoliere, A. and Woolf, C. J. (2009) ‘Central Sensitization: A Generator of Pain Hypersensitivity by Central Neural Plasticity’, *Journal of Pain*, pp. 895–926. doi: 10.1016/j.jpain.2009.06.012.

Lechner, S. G. and Lewin, G. R. (2013) ‘Hairy sensation’, *Physiology (Bethesda, Md.)*, 28(3), pp. 142–150. doi: 10.1152/physiol.00059.2012.

Lerchner, W. *et al.* (2007) ‘Reversible silencing of neuronal excitability in behaving mice by a genetically targeted, ivermectin-gated Cl- channel.’, *Neuron*, 54(1), pp. 35–49. doi: 10.1016/j.neuron.2007.02.030.

Lewin, G. R. and Moshourab, R. (2004) ‘Mechanosensation and pain’, *Journal of Neurobiology*, 61(1), pp. 30–44. doi: 10.1002/neu.20078.

Li, C. L. *et al.* (2016) ‘Somatosensory neuron types identified by high-coverage single-

cell RNA-sequencing and functional heterogeneity', *Cell Research*. Nature Publishing Group, 26(1), pp. 83–102. doi: 10.1038/cr.2015.149.

Li, L. *et al.* (2011) 'The Functional Organization of Cutaneous Low-Threshold Mechanosensory Neurons', *Cell*. Cell Press, 147(7), pp. 1615–1627. doi: 10.1016/J.CELL.2011.11.027.

Lin, J. Y. *et al.* (2009) 'Characterization of engineered channelrhodopsin variants with improved properties and kinetics', *Biophysical Journal*. Biophysical Society, 96(5), pp. 1803–1814. doi: 10.1016/j.bpj.2008.11.034.

Liu, C. N. *et al.* (2000) 'Tactile allodynia in the absence of C-fiber activation: Altered firing properties of DRG neurons following spinal nerve injury', *Pain*. Elsevier, 85(3), pp. 503–521. doi: 10.1016/S0304-3959(00)00251-7.

Madisen, L. *et al.* (2012) 'A toolbox of Cre-dependent optogenetic transgenic mice for light-induced activation and silencing', *Nature Neuroscience*, 15(5), pp. 793–802. doi: 10.1038/nn.3078.

Magnus, C. J. *et al.* (2011) 'Chemical and genetic engineering of selective ion channel-ligand interactions', *Science*, 333(6047), pp. 1292–1296. doi: 10.1126/science.1206606.

Magnus, C. J. *et al.* (2019) 'Ultrapotent chemogenetics for research and potential clinical applications', *Science*. American Association for the Advancement of Science, 364(6436). doi: 10.1126/science.aav5282.

Maves, T. J. *et al.* (1993) 'Possible chemical contribution from chromic gut sutures produces disorders of pain sensation like those seen in man', *Pain*, 54(1), pp. 57–69. doi: 10.1016/0304-3959(93)90100-4.

McCoy, E. S. *et al.* (2013) 'Peptidergic CGRPα Primary Sensory Neurons Encode Heat and Itch and Tonically Suppress Sensitivity to Cold', *Neuron*. Cell Press, 78(1), pp.

138–151. doi: 10.1016/J.NEURON.2013.01.030.

Meacham, K. *et al.* (2017) ‘Neuropathic Pain: Central vs. Peripheral Mechanisms’, *Current Pain and Headache Reports*. Current Medicine Group LLC 1. doi: 10.1007/s11916-017-0629-5.

Mickle, A. D. *et al.* (2019) ‘A wireless closed-loop system for optogenetic peripheral neuromodulation’, *Nature*. Nature Publishing Group, pp. 361–365. doi: 10.1038/s41586-018-0823-6.

Mickle, A. D. and Gereau, R. W. (2018) ‘A bright future? Optogenetics in the periphery for pain research and therapy’, *Pain*. NLM (Medline), pp. S65–S73. doi: 10.1097/j.pain.0000000000001329.

Mickle, A. D., Shepherd, A. J. and Mohapatra, D. P. (2016) ‘Nociceptive TRP channels: Sensory detectors and transducers in multiple pain pathologies’, *Pharmaceuticals*. MDPI AG. doi: 10.3390/ph9040072.

Miller, R. E. *et al.* (2017) ‘Chemogenetic Inhibition of Pain Neurons in a Mouse Model of Osteoarthritis’, *Arthritis & Rheumatology*, 69(7), pp. 1429–1439. doi: 10.1002/art.40118.

Nagel, G. *et al.* (2003) ‘Channelrhodopsin-2, a directly light-gated cation-selective membrane channel’, *Proceedings of the National Academy of Sciences of the United States of America*, 100(SUPPL. 2), pp. 13940–13945. doi: 10.1073/pnas.1936192100.

Naglich, J. G. *et al.* (1992) ‘Expression cloning of a diphtheria toxin receptor: Identity with a heparin-binding EGF-like growth factor precursor’, *Cell*, 69(6), pp. 1051–1061. doi: 10.1016/0092-8674(92)90623-K.

Ossipov, M. H., Dussor, G. O. and Porreca, F. (2010) ‘Central modulation of pain’, *Journal of Clinical Investigation*, pp. 3779–3787. doi: 10.1172/JCI43766.

Pappenheimer, A. M. *et al.* (1982) ‘Diphtheria toxin and related proteins: Effect of route

of injection on toxicity and the determination of cytotoxicity for various cultured cells', *Journal of Infectious Diseases*, 145(1), pp. 94–102. doi: 10.1093/infdis/145.1.94.

Park, S. Il *et al.* (2015) 'Soft, stretchable, fully implantable miniaturized optoelectronic systems for wireless optogenetics', *Nature Biotechnology*. Nature Publishing Group, 33(12), pp. 1280–1286. doi: 10.1038/nbt.3415.

Le Pichon, C. E. and Chesler, A. T. (2014) 'The functional and anatomical dissection of somatosensory subpopulations using mouse genetics', *Frontiers in Neuroanatomy*. Frontiers Research Foundation. doi: 10.3389/fnana.2014.00021.

Prato, V. *et al.* (2017) 'Functional and Molecular Characterization of Mechanoinsensitive "Silent" Nociceptors', *Cell Reports*. Elsevier B.V., 21(11), pp. 3102–3115. doi: 10.1016/j.celrep.2017.11.066.

Reynders, A. *et al.* (2015) 'Transcriptional Profiling of Cutaneous MRGPRD Free Nerve Endings and C-LTMRs', *Cell Reports*. Cell Press, 10(6), pp. 1007–1019. doi: 10.1016/J.CELREP.2015.01.022.

Rice, A. S. C. *et al.* (2018) 'Sensory profiling in animal models of neuropathic pain: a call for back-translation', *Pain*. NLM (Medline), pp. 819–824. doi: 10.1097/j.pain.0000000000001138.

Rice, A. S. C., Smith, B. H. and Blyth, F. M. (2016) 'Pain and the global burden of disease', *Pain*. Lippincott Williams and Wilkins, 157(4), pp. 791–796. doi: 10.1097/j.pain.0000000000000454.

Roth, B. L. (2016) 'DREADDs for Neuroscientists', *Neuron*. Cell Press, pp. 683–694. doi: 10.1016/j.neuron.2016.01.040.

Ruedl, C. and Jung, S. (2018) 'DTR-mediated conditional cell ablation—Progress and challenges', *European Journal of Immunology*, 48(7), pp. 1114–1119. doi: 10.1002/eji.201847527.

Rutlin, M. *et al.* (2014) ‘The cellular and molecular basis of direction selectivity of Aδ-LTMRs’, *Cell*. Cell Press, 159(7), pp. 1640–1651. doi: 10.1016/j.cell.2014.11.038.

Saito, M. *et al.* (2001) ‘Diphtheria toxin receptor-mediated conditional and targeted cell ablation in transgenic mice’, *Nature Biotechnology*, 19(8), pp. 746–750. doi: 10.1038/90795.

Saloman, J. L. *et al.* (2016) ‘Gi-DREADD expression in peripheral nerves produces ligand-dependent analgesia, as well as ligand-independent functional changes in sensory neurons’, *Journal of Neuroscience*. Society for Neuroscience, 36(42), pp. 10769–10781. doi: 10.1523/JNEUROSCI.3480-15.2016.

Samineni, V. K. *et al.* (2017) ‘Optogenetic silencing of nociceptive primary afferents reduces evoked and ongoing bladder pain’, *Scientific Reports*. Nature Publishing Group, 7(1). doi: 10.1038/s41598-017-16129-3.

Seal, R. P. *et al.* (2009) ‘Injury-induced mechanical hypersensitivity requires C-low threshold mechanoreceptors’, *Nature*. Nature Publishing Group, 462(7273), pp. 651–655. doi: 10.1038/nature08505.

Seltzer, Z., Dubner, R. and Shir, Y. (1990) ‘A novel behavioral model of neuropathic pain disorders produced in rats by partial sciatic nerve injury’, *Pain*, 43(2), pp. 205–218. doi: 10.1016/0304-3959(90)91074-S.

Shin, G. *et al.* (2017) ‘Flexible Near-Field Wireless Optoelectronics as Subdermal Implants for Broad Applications in Optogenetics In Brief’, *Neuron*, 93, pp. 509–521. doi: 10.1016/j.neuron.2016.12.031.

Shin, J. B. *et al.* (2003) ‘A T-type calcium channel required for normal function of a mammalian mechanoreceptor’, *Nature Neuroscience*, 6(7), pp. 724–730. doi: 10.1038/nn1076.

Slimko, E. M. *et al.* (2002) ‘Selective electrical silencing of mammalian neurons in vitro

by the use of invertebrate ligand-gated chloride channels.', *The Journal of neuroscience : the official journal of the Society for Neuroscience*, 22(17), pp. 7373–7379. doi: 20026775.

Sotocinal, S. G. *et al.* (2011) 'The Rat Grimace Scale: A partially automated method for quantifying pain in the laboratory rat via facial expressions', *Molecular Pain*, 7. doi: 10.1186/1744-8069-7-55.

Stachniak, T. J., Ghosh, A. and Sternson, S. M. (2014) 'Chemogenetic Synaptic Silencing of Neural Circuits Localizes a Hypothalamus→Midbrain Pathway for Feeding Behavior', *Neuron*. Cell Press, 82(4), pp. 797–808. doi: 10.1016/j.neuron.2014.04.008.

Stantcheva, K. K. *et al.* (2016) 'A subpopulation of itch-sensing neurons marked by Ret and somatostatin expression', *EMBO reports*. EMBO, 17(4), pp. 585–600. doi: 10.15252/embr.201540983.

Sternson, S. M. and Roth, B. L. (2014) 'Chemogenetic Tools to Interrogate Brain Functions', *Annual Review of Neuroscience*. Annual Reviews, 37(1), pp. 387–407. doi: 10.1146/annurev-neuro-071013-014048.

Tétreault, P. *et al.* (2011) 'Weight bearing evaluation in inflammatory, neuropathic and cancer chronic pain in freely moving rats', *Physiology and Behavior*. Elsevier Inc., 104(3), pp. 495–502. doi: 10.1016/j.physbeh.2011.05.015.

Tsantoulas, C. and McMahon, S. B. (2014) 'Opening paths to novel analgesics: The role of potassium channels in chronic pain', *Trends in Neurosciences*, pp. 146–158. doi: 10.1016/j.tins.2013.12.002.

Usoskin, D. *et al.* (2015) 'Unbiased classification of sensory neuron types by large-scale single-cell RNA sequencing', *Nature Neuroscience*. Nature Publishing Group, 18(1), pp. 145–153. doi: 10.1038/nn.3881.

Vardy, E. *et al.* (2015) 'A New DREADD Facilitates the Multiplexed Chemogenetic

Interrogation of Behavior', *Neuron*. Cell Press, 86(4), pp. 936–946. doi: 10.1016/j.neuron.2015.03.065.

Wall, P. D. *et al.* (1979) 'Autotomy following peripheral nerve lesions: experimental anesthesia dolorosa', *Pain*, 7(2), pp. 103–113. doi: 10.1016/0304-3959(79)90002-2.

Wall, P. D. and Gutnick, M. (1974) 'Properties of afferent nerve impulses originating from a neuroma', *Nature*, 248(5451), pp. 740–743. doi: 10.1038/248740a0.

Wang, H. *et al.* (2007) 'High-speed mapping of synaptic connectivity using photostimulation in Channelrhodopsin-2 transgenic mice', *Proceedings of the National Academy of Sciences of the United States of America*, 104(19), pp. 8143–8148. doi: 10.1073/pnas.0700384104.

Woolf, C. J. (2011) 'Central sensitization: Implications for the diagnosis and treatment of pain', *Pain*. doi: 10.1016/j.pain.2010.09.030.

Wu, G. *et al.* (2001) 'Early onset of spontaneous activity in uninjured C-fiber nociceptors after injury to neighboring nerve fibers.', *The Journal of neuroscience : the official journal of the Society for Neuroscience*, 21(8). doi: 10.1523/jneurosci.21-08-j0002.2001.

Wu, G. *et al.* (2002) 'Degeneration of myelinated efferent fibers induces spontaneous activity in uninjured C-fiber afferents', *Journal of Neuroscience*, 22(17), pp. 7746–7753. doi: 10.1523/jneurosci.22-17-07746.2002.

Yamaizumi, M. *et al.* (1978) 'One molecule of diphtheria toxin fragment a introduced into a cell can kill the cell', *Cell*, 15(1), pp. 245–250. doi: 10.1016/0092-8674(78)90099-5.

Zeisel, A. *et al.* (2018) 'Molecular Architecture of the Mouse Nervous System', *Cell*. Cell Press, 174(4), pp. 999-1014.e22. doi: 10.1016/J.CELL.2018.06.021.

Zemelman, B. V. *et al.* (2002) 'Selective photostimulation of genetically chARGed

neurons', *Neuron*. Cell Press, 33(1), pp. 15–22. doi: 10.1016/S0896-6273(01)00574-8.

Zhang, F. *et al.* (2007) 'Multimodal fast optical interrogation of neural circuitry', *Nature*. Nature Publishing Group, 446(7136), pp. 633–639. doi: 10.1038/nature05744.

Zhang, Y. *et al.* (2019) 'Battery-free, fully implantable optofluidic cuff system for wireless optogenetic and pharmacological neuromodulation of peripheral nerves', *Science Advances*. American Association for the Advancement of Science, 5(7). doi: 10.1126/sciadv.aaw5296.

Zhao, G. Q. *et al.* (2003) 'The receptors for mammalian sweet and umami taste', *Cell*. Cell Press, 115(3), pp. 255–266. doi: 10.1016/S0092-8674(03)00844-4.

Zheng, Y. *et al.* (2019) 'Deep Sequencing of Somatosensory Neurons Reveals Molecular Determinants of Intrinsic Physiological Properties', *Neuron*. Cell Press. doi: 10.1016/J.NEURON.2019.05.039.

Zimmermann, K. *et al.* (2009) 'Phenotyping sensory nerve endings in vitro in the mouse', *Nature Protocols*, 4(2), pp. 174–196. doi: 10.1038/nprot.2008.223.

Chapter 2: An engineered chemogenetic tool box to silence peripheral sensory neurons

1. Introduction

The overarching aim of this work is to investigate sensory neuron diversity and heterogeneity, with a focus on population function pre and post neuropathic injury. In order to interrogate the roles of different populations, there is a requirement to selectively modulate sensory neuron function. The controlled silencing of select sensory neuron populations will allow us to ascribe function and inform future therapeutics. As described in detail previously (see chapter 1), chemogenetics can be employed to modulate neuronal activity. The rationale for our investigation was that selective expression of a non-native ion channel activated by an exogenous compound to supress sensory neuron excitability had not been successfully employed. Therefore, there is an unmet need for the development of an effective chemogenetic silencer that can be used in the somatosensory nervous system. Utilising the glutamate-gated chloride channel to develop an engineered chemogenetic tool box provides an opportunity to address this requirement.

1.1. The Glutamate-gated chloride channel

The cysteine (cys) loop receptor superfamily are ion-gated receptors involved in fast neurotransmission in both vertebrates and invertebrates. The most common cys loop superfamily receptors are divided into the cation selective; nicotinic acetylcholine (nAChR), and 5-HT receptors (Changeux, 2012; Lummis, 2012), and the anion selective $GABA_A$ and Glycine receptors (Dutertre, Becker and Betz, 2012; Sigel and Steinmann, 2012). Due to their roles in fast neuronal signalling, disorders in cys loop superfamily receptors lead to many neurological disorders such as; schizophrenia, depression, epilepsy and myasthenic syndromes (Yakel, 2010). The fifth member of the cys loop receptor superfamily is the glutamate-gated chloride

channel (GluCl). GluCl is unique as it is exclusively expressed in invertebrate species such as locusts, crustacea, molluscs, flatworms, nematodes and ticks (Wolstenholme, 2012). GluCl is anion selective and part of the invertebrate cys loop ligand-gated chloride channel (cysLGCC) sub-family (Wolstenholme, 2012). As inhibitory channels, invertebrate cysLGCCs have been exploited and targeted in agriculture and veterinary medicine for the eradication of pests and pathogens. Invertebrate cysLGCCs, are activated by the macrocyclic lactone group of anthelmintics and insecticides. The family of anthelmintics which act on invertebrate cysLGCCs are the avermectins, which includes the derivative ivermectin (Wolstenholme, 2012).

In 2015, Youyou Tu, William C. Campbell and Satoshi Ōmura shared the Nobel Prize in Physiology and Medicine. Youyou Tu discovered novel therapies targeting malaria, and William C. Campbell and Satoshi Ōmura discovered that the avermectin derivatives, particularly ivermectin, can eradicate round worm infections, which untreated can lead to river blindness and lymphatic filariasis (elephantitis) (Tambo *et al.*, 2015). Studies identified that ivermectin is a safe and well tolerated member of the avermectin family and as a consequence ivermectin use in developing countries lowered the incidence of roundworn infections and the associated compilations (Tambo *et al.*, 2015). Since then, ivermectin has been used to treat other parasites and conditions such as loa loa filariasis, threadworm, whipworm, scabies, lice, some malaria bearing mosquitos and rosacea. (Victoria and Trujillo, 2001; Strycharz, Yoon and Clark, 2008; Henriquez-Camacho *et al.*, 2016; Siddiqui, Gold and Gill, 2016; Palmeirim *et al.*, 2018; Tizifa *et al.*, 2018; Pion *et al.*, 2019)

The discovery that GluCl was sensitive to IVM in *C.elegans* led to studies identifying that functional GluCl was encoded by two subunits GluClα and GluClβ (GLC-1 and GLC-2) (Cully *et al.*, 1994; Cleland, 1996). It was confirmed that GluClα

and GluClβ belonged to the cysLGCC family due to the glutamate sensitive chloride conductance, which could be blocked by a selective chloride channel toxin (Cully *et al.*, 1994; Cleland, 1996). Later, the GluCl gene family was found to include four more members, *avr-14*, *avr-15*, *glc-3* and *glc-4* (Cully *et al.*, 1996; Dent, Davis and Avery, 1997; Vassilatis *et al.*, 1997; Dent *et al.*, 2000; Horoszok *et al.*, 2001). Functionally, GluCl has pivotal roles in invertebrate nervous systems regulating sensory inputs, feeding, and locomotion (Wolstenholme, 2012). Structurally, GluCl is pentameric and it is between the M1 and M3 membrane-spanning domains of adjacent subunits where IVM binds (Hibbs and Gouaux, 2011). It its predicted that IVM binding results in a conformational change in the GluCl structure and the subsequent long-lasting open configuration (Hibbs and Gouaux, 2011). The structural insights drawn from GluCl have aided the prediction of drug binding sites in mammalian cys loop superfamily members such as GABA and Glycine receptors (Lynagh *et al.*, 2011).

1.2. Exploiting the Glutamate-gated Chloride channel

GABA and Glycine receptors are involved in inhibitory neurotransmission and previous studies have sought to take advantage of these two neurotransmitters to interrogate brain circuitry and function. Focal injections of the GABA agonist muscimol into the amygdala of rodents, activated GABA receptors in order to promote an inhibitory drive in this region (Maren, Yap and Goosens, 2001). These experiments identified this structure as critical for fear conditionings (Maren, Yap and Goosens, 2001). However, these attempts to modulate cellular activity are confounded and limited by the inability to know which neurons are being inhibited (regional or projecting neurons, excitatory or inhibitory neurons), and not being able to target specific populations of neurons. Equally, GABA and Glycine receptors are widely expressed in the CNS making them difficult to selectively modulate.

Chemogenetics offers a powerful solution to selectively modulate neuronal activity. Previous groups have exploited the fact that GluCl is an invertebrate inhibitory channel that is not expressed in mammals and can therefore confer selective neuronal silencing. This makes GluCl an attractive and tangible option to manipulate neuronal function. Indeed, GluCl was expressed in cultured rodent hippocampal neurons and IVM application rendered them electrically silent (Slimko *et al.*, 2002). New versions of GluCl (termed GluClv1.0) were generated to visualise GluCl expression through the introduction of florescent proteins (Table 1) (Slimko *et al.*, 2002) and the glutamate sensitivity was removed (Table 1) (Li, Slimko and Lester, 2002). GluClv1.0/IVM mediated silencing was used *in vivo* to reversibly silence striatal neuron excitability to reduce amphetamine induced behaviour (Lerchner *et al.*, 2007) and to silence hypothalamic activity and aggression (Lin *et al.*, 2011). However, the utility of the GluClv1.0 system was limited by poor blood brain barrier penetration and the variability in silencing efficacy likely due to suboptimal subunit membrane expression. To address these issues, GluClv1.0-α was modified to enhance IVM sensitivity and β-subunit incorporation, via the gain-of-function mutation L9'F introduced into the second transmembrane domain (Table 1) (Frazier, Cohen and Lester, 2013). Additionally, mutating the intracellular loop of the β-subunit to remove an arginine-based endoplasmic reticulum retention motif (RSR to AAA), enhanced β subunit trafficking to the plasma membrane (Table 1) (Frazier, Cohen and Lester, 2013). This was thought to prevent endoplasmic reticulum retention and degradation of the β-subunit (Frazier, Cohen and Lester, 2013). Finally, both subunit reporters were replaced with monomeric florescent proteins to prevent reporter dimerization, which negatively altered channel function (Table 1) (Frazier, Cohen and Lester, 2013). This optimised tool now termed GluClv2.0 had not yet been employed *in vivo* in a mammalian system.

Most recently GluCl was exploited to silence excitatory neurons in the primary motor cortex and reduced pilocarpine induced seizures. GluCl was modified to enhance glutamate sensitivity (Table 1: eGluCl), pathological increases in glutamate levels activated GluCl and silenced pilocarpine induced excitability and epileptic behaviours (Lieb *et al.*, 2018). This was designed as an autoregulatory silencer proposing a possible gene therapy for the treatment of epilepsy (Lieb *et al.*, 2018).

GluCl subunit	Mutation	Consequence	Ref.
GluClβ	Y182F	Glutamate insensitivity	Li *et al* 2002
GluClα + β	XFP	Reporter	Slimko *et al* 2002
GluClα	L9'F	Increased IVM sensitivity	Frazier *et al* 2013
GluClβ	RSR to AAA	Improved β-subunit trafficking	Frazier *et al* 2013
GluClα + β	mXFP	Monomeric reporter	Frazier *et al* 2013
GluCl tools			
GluCl v2.0 - α-mXFP L9'F, β-mXFP Y182F RSR_AAA			
eGluCl - α- mXFP L9'F, P2A, β-mXFP			

Table 1: GluCl subunit mutations, their consequences and the combinations of mutations that underpin different GluCl tools.

1.3. Cell type specificity of viral vectors

Many of the studies using GluCl as a silencer rely on focal viral delivery of GluCl and ubiquitous expression in the target region (Lerchner *et al.*, 2007; Lieb *et al.*, 2018). There are methods available to specify which cell type/s viral vectors are expressed, such as viral tropism (discussed in detail in a later chapter), promoters with activity restricted to selective cell populations, and Cre/LoxP technology. Promoters are enhancer sequences that drive gene expression of a particular gene. Using specific promoters enables viral vectors to be selectively expressed in restricted populations. Examples of ubiquitous promoters include cytomegalovirus (CMV), elongation factor-1 alpha (EF1A), and the synthetic promoter built from CMV fused to the chicken β-actin promoter (CAG). Neuronal specific promoters include

Synapsin (Syn) and α-Calcium/calmodulin-dependent kinase II (CaMKII), an excitatory neuron promoter. However, the largest challenge with using specific promoters to specify viral vector expression is promoter size. Endogeneous promoters are often 10-100kb in size and viral packaging is limited across virus types, particularly in Adeno-associated viruses (~4.7 kb) (Dong, Fan and Frizzell, 1996). This has led to researchers looking for shortened version of promoters, indeed a short tyrosine hydroxylase promoter fragment has been identified and used to target neuroblastoma cells, and dopaminergic neurons *in vivo* (Steffens *et al.*, 2004; Rolland *et al.*, 2017). Additionally, a shortened melatonin-concentrating hormone (MCH) promoter was generated to study the sparse MCH positive hypothalamic population (Van Den Pol *et al.*, 2004). However, until more and more short versions are discovered, the use of specific promoters is limited, and as a result cell specific promoters are not currently available to distinguish between sensory neuron populations.

An alternate way to specify transgene expression is by using the Cre/LoxP system (Tsien *et al.*, 1996). Typically this system relies on the generation and availability of transgenetic mice which express Cre recombinase in defined cell types. In neuroscience, particularly in the sensory field, such driver lines are becoming increasingly available. Cre recombination can achieve two scenarios, the excision of a loxP site flanked region or inversion of a loxP site flanked region, both of which are highly depend on the loxP sites used (Tsien *et al.*, 1996; Schnütgen *et al.*, 2003; Atasoy *et al.*, 2008). One method would be the introduction of a stop cassette flanked by homotypic Lox P sites prior to the transgene. The stop cassette would be excised in the presence of Cre (Fig. 1), however, problems with this method include the large size of stop cassettes and transgene ‘read-through’ i.e. expression prior to stop cassette removal (Kuhlman and Huang, 2008). The second option is more popular, reliable, minimally impacts plasmid size/space and offers the

opportunity to design Cre^{ON} and Cre^{OFF} vectors (Atasoy *et al.*, 2008; Saunders, Johnson and Sabatini, 2012). A Cre^{ON} viral vector is designed so that the transgene of interest is in the reverse orientation flanked by two pairs of heterotypic LoxP sites. In the presence of Cre the transgene undergoes flip excision, into the correct open reading frame (ORF) (Fig. 1). This technology is termed flip excision (FLEx) switch, or double-floxed inverted orientation (DIO) (Schnütgen *et al.*, 2003; Atasoy *et al.*, 2008). Equally, for Double-floxed orientations (DO) Cre^{OFF} systems, everything remains similar except the transgene is originally placed in the ORF and undergoes flip excision in the presence of Cre, turning off transgene expression (Fig. 1) (Saunders, Johnson and Sabatini, 2012). The Cre/LoxP system could also be used to generate a Cre dependent transgenic mouse line that would overexpress an effector (i.e. GluCl) in the presence of Cre. This approach would be a valuable research tool, however it would limit the spatial and temporal control over the transgene expression, which viruses offer. In addition, using viruses would allow assessment of chemogenetic silencing as a potential gene therapy.

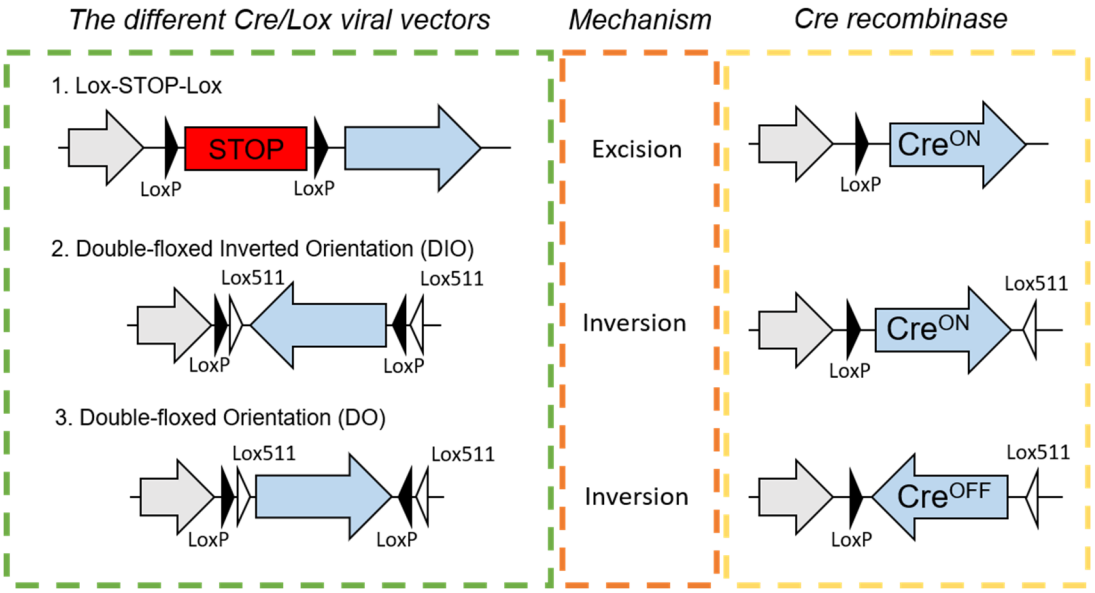

Fig. 1: A schematic outlining the different Cre/Lox construct possibilities, the mechanism of recombination and the resultant construct after Cre recombinase exposure.

GluClv2.0 has never been employed in the sensory system and given that the DRG neurons handle chloride differently to CNS neurons (Sung *et al.*, 2000; Jin *et al.*, 2013), there was a necessity to validate this tool *in vitro*. In addition, I aim to optimise GluClv2.0 further by exchanging the reporter from one subunit to allow subunit identification. Ultimately, the aim is to selectively silence different sensory neuron populations. I will use the techniques discussed above to generate and functionally validate novel GluCl constructs which are Cre recombinase dependent. The assembly of this chemogenetic tool box will provide the means to interrogate sensory neuron heterogeneity, function and circuitry.

2. Methods

2.1. Plasmid Cloning

2.1.1. GluClα reporter exchange: Constructs for GluCl v2.0 (Opt α-GluClv2.0 and Opt β-GluClv2.0) were a gift from Henry Lester (Addgene plasmids 47387 and 47542) (Frazier, Cohen and Lester, 2013). The yellow fluorescent protein (YFP) sequence of α-GluClv2.0 was replaced by the sequence for monomeric Cerulean (mCerulean;(Rizzo *et al.*, 2004)) (gift from Dave Piston, Addgene plasmid 15214). This was achieved by using EcoRI restriction sites. The YFP sequence was excised from the vector using the EcoRI restriction enzyme (New England BioLabs - NEB) in Cut smart buffer (NEB) for overnight (O/N) at 37^{o}C. The vector (GluClα minus YFP) was gel extracted using a commercially available gel extraction kit (Quiagen). The sequence for mCerulean was also flanked by EcoRI sites. mCerulean was digested out from its vector backbone sequence using the EcoRI restriction enzyme and Cut smart buffer for O/N at 37^{o}C. Cerulean was gel extracted and ligated with the GluClα (minus YFP) vector using T4 DNA ligase (NEB), 37^{o}C overnight. Plasmid DNA was transformed into competent E.coli bacteria using a standard protocol (NEB). Transformed bacteria were plated onto ampicillin (100 µg/ml) agar plates, and incubated over night at 37^{o}C. Ampicillin resistant single colonies were picked and grown up in 4 ml LB broth (Sigma-aldrich) overnight. Plasmid DNA was harvested using a commercially available Miniprep kit (Quiagen). Each plasmid was run on an agarose gel to analyse plasmid size to ensure ligation of 1 cerulean sequence. (No insertion size α-6953 bp, double insertion size 8375 bp). Those which matched α-7644 bp were selected to be sequenced. Sanger sequencing was used to confirm that the cerulean was inserted in the correct orientation. Samples which passed both

screening methods were sequenced in full to ensure no base pair mutations had occurred during PCR amplification.

2.1.2. Generation of GluClα.Cre^{ON} and GluClβ.Cre^{ON}: The same procedure was carried out for GluClα and GluClβ. GluCl v2.0 was PCR amplified using primers designed with over hanging enzyme restrictions sites:

GluClα-NheI forward: 5' CTAGTTGCTAGCATGGCCACGTGGATCGTG 3'
GluClα-AscI reverse:
5' TTGACTGGCGCGCCCTAGCTCAGAACAGAACGTTCTGC 3'
GluClβ-NheI forward: 5' CTAGAGGCTAGCCCACCATGGCCACCCCCT 3'
GluClβ-AscI reverse:
5' TGGATTGGCGCGCCCTACACCAGGGACTCGGGGGT 3'

The GluCl insert was PCR amplified and the product was digested in NheI and AscI restriction enzymes (NEB) in Cut smart buffer, 37^{o}C 1 hr. The vector plasmid which contained a shortened CAG promoter with RFP in the reverse orientation flanked by NheI and AscI cut sites and heterotypic lox sites, as well as AAV2 ITR sites. The RFP sequence was removed using NheI and AscI restriction enzymes, 37^{o}C 1hr. The vector was gel extracted and ligated with the new GluCl insert using DNA ligase, 37^{o}C overnight. The new plasmid was transformed into competent Ecoli bacteria and plated onto ampicillin agar plates. Ampicillin resistant single colonies were picked, grown up, and screened for successful plasmid generation. Initial screening was for plasmid size α-7057 bp, β-6973 bp, followed by sequencing to confirm.

2.1.3. Generation of GluClα.Cre^{OFF} and GluClβ.Cre^{OFF}: The same procedure was carried out for GluClα and GluClβ. GluCl v2.0 was PCR amplified using primers designed with over hanging enzyme restrictions sites:

GluClα-AscI forward: 5' TTGACTGGCGCGCCCATGGCCACGTGGATCGTG 3'

GluClα-NheI reverse: 5' CTAGTTGCTAGCTAGCTCAGAACAGAACGTTCTGC 3'

GluClβ-AscI forward: 5' TGGATTGGCGCGCCATGGCCACCCCCT 3'

GluClβ-NheI reverse: 5' CTAGAGGCTAGCCCACCCTACACCAGGGACTCGGGGGT 3'

A similar procedure as above (2.1.2) was carried out. The GluCl insert was PCR amplified and the product was digested with NheI and AscI restriction enzymes in Cut smart buffer, 37^{o}C O/N. The vector plasmid contained a shortened CAG promoter with RFP in the reverse orientation flanked by NheI and Asc1 cut sites and heterotypic loxP sites, as well as AAV2 ITR sites. The RFP sequence was removed using NheI and Asc1 restriction enzymes, 37^{o}C O/N. The vector was gel extracted and ligated with the new GluCl insert using T4 DNA ligase, 37^{o}C overnight. The new plasmid was transformed into competent E.coli bacteria and plated onto ampicillin agar plates. Ampicillin resistant single colonies were picked, grown up, and screened for successful plasmid generation. Initial screening was for plasmid size α-7057bp, β-6973bp, followed by sequencing to confirm.

2.2. Animal use

All mice were group-housed in individually ventilated cages with free access to food and water, in humidity and temperature controlled rooms with a 12 hr light-dark cycle, in a pathogen free facility. All animal procedures adhered to the UK Home Office (Scientific Procedures) Act (1986) and performed under a UK Home Office Project Licence. All animal experiments were carried out in accordance with

University of Oxford Policy on the Use of Animals in Scientific Research. The work within this study also conforms to the ARRIVE guidelines (Kilkenny *et al.*, 2010).

Nav1.8^{Cre} mice were a kind gift from John Wood (UCL, UK) and have been previously described (Nassar *et al.*, 2004). The Nav1.8^{Cre} line largely targets nociceptors, the efficacy of the Cre line and details of how it was generated will be discussed in chapter 4. The Nav1.8^{Cre} line was crossed with a Cre dependent reporter line, Rosa26-Flox-Stop-Flox-TdTomato (Ai14, JAX). C57BL/6 wild type mice were purchased form the Oxford University Breeding Unit. All experiments were carried out on adult male and female mice. All experiments were conducted blind to genotype or treatment group until post analysis.

2.3. Cell culture

2.3.1. Dorsal root ganglion neuronal culture: Mice were sacrificed and spinal columns removed. Dorsal root ganglia were rapidly dissected (Sleigh, Weir and Schiavo, 2016) and enzymatically digested at 37°C for 80 mins in dispase type II (4.7 mg/ml) and collagenase type II (4 mg/ml). Cells were centrifuged for 6 mins at 400 g and HBSS/CollagenaseDispase removed. Pre-warmed culture media (Neurobasal, 2% B-27 supplement, 1% Penicillin streptomyocin) was added and cells were mechanically dissociated using fire-polished pipettes. Cells were plated on Poly-D-lysine/Laminin coated cover slips with the addition of growth factors (Mouse nerve growth factor (50 ng/ml; NGF, PeproTech) and 10 ng/ml glial-derived neurotrophic factor (GDNF, PeproTech)).

2.3.2. Electroporation*:* Neurons were transfected via electroporation using the Neon system (Life technologies). Dissociated cells were re-suspended in 10 µl of Buffer R plus 1 µg of total plasmid DNA per 50-100,000 cells. The electrical protocol applied was three 1500-V pulses of 10 ms duration. Cells

were plated as stated above and used 48-72 hrs later when plasmid DNA expression was maximal.

2.3.3. Human embryonic kidney 293t cells and transfection: HEK293t cell were routinely cultured in Dulbecco's modified Eagle Medium (DMEM, Thermofisher scientific) and 10% foetal calf serum. Cells were periodically split using Varracine and mechanical dissociation. Dissociated cells were seeded into 6 well plates and when cells reached 70% confluency, transfected using JetPEI following the manufacturers protocol (PolyPlus transfection). A total of 3 µg of DNA/per 35 cm well was combined with NaCl and JetPEI and after 20 mins added to HEK cells. The next day transfected cells were re-plated onto cover slips and used 24 hrs later.

2.4. Electrophysiology

2.4.1. Whole-cell patch clamp: Voltage-clamp recordings using an Axopatch 200B amplifier and Digidata 1550 acquisition system (Molecular Devices) were performed at room temperature (21°C – the standard for the field when not directly assessing temperature sensitivity). Data were sampled at 20 kHz and low-pass filtered at 5 kHz. Series resistance was compensated 60% –80% to reduce voltage errors. All data were analyzed by Clampfit 10 software (Molecular Devices). GFP/XFP+ DRG neurons and HEK cells were detected with an Olympus microscope with an inbuilt GFP filter set (470/40x excitation filter, dichroic LP 495 mirror and 525/50 emission filter). Filamental borosilicate glass capillaries (1.5 mm OD, 0.84 mm ID; World Precision Instruments) were pulled to form patch pipettes of 2–4 MΩ tip resistance and filled with an internal solution containing (mM): 100 K-gluconate, 28 KCl, 1 $MgCl_2$, 5 MgATP, 10 HEPES, and 0.5 EGTA; pH was adjusted to 7.3 with KOH and osmolarity set at 305 mOsm (by adding glucose). Cells were maintained in a chamber constantly perfused with a

physiological extracellular buffer containing (mM): 140 NaCl, 4.7 KCl, 2.5 $CaCl_2$, 1.2 $MgCl_2$, 10 HEPES and 10 glucose; pH was adjusted to 7.4 with NaOH and osmolarity set at 315 mOsm (by adding glucose). Ivermectin (Sigma Aldrich) was prepared in DMSO (fresh daily), diluted in extracellular buffer to a final concentration of 20 nM and was delivered to the cells via the perfusion system. All post IVM recordings were made 15 mins post IVM application. Membrane conductance was measured in voltage clamp with a 100ms voltage ramp from -90 mV to +40 mV every 10 s. The resultant linear current gradient was used to calculate membrane conductance using the rearranged Ohm's law equation where V = voltage, I = current, R = resistance, C = conductance.

$$\left[V = IR, C = \frac{1}{R}\right] \qquad \therefore \quad C = \frac{I}{V}$$

In current clamp mode DRGs were held at -60 mV. Input resistance (R_{input}) was derived by measuring the membrane deflection caused by a 20 pA current step. Rheobase was determined by applying 50 ms depolarising currents of increasing steps of 25 pA until action potential (AP) generation. AP firing in response to 10 s of 1 μM capsaicin was assessed in bridge mode while recording from small diameter DRGs (<25μm).

2.5. Immunohistochemistry (IHC)

2.5.1. Cultured cells: Coverslips containing cultured cells were fixed with 4% PFA (Paraformaldehyde) for 10 mins and washed in PBS. Cells were blocked for 1 hr in a blocking solution (PBS, 10% normal goat serum, 0.3% TX-100) at RT (room temperature) followed by primary antibody (appendix table 1) incubation in blocking solution for 2 hrs RT. Cells were washed in

wash solution (PBS, 0.3% Tx-100) prior to secondary antibody (appendix table 1) incubation in PBS overnight at 4^{o}C. Cells were washed and coverslips mounted onto microscope slides using Vectorsheild mounting medium and nail varnish. Samples were imaged on a confocal microscope (Zeiss LSM-710). Images were analysed using Fuji/ImageJ (NIH).

2.6. Statistical analysis

All data was tested for normality using the D'Agostino-Pearson normality test and the appropriate parametric or non-parametric statistical tests used accordingly. All statistical tests used were two-tailed. Statistical comparisons were made using a Student's t-test or Mann Whitney U-test. In experimental groups in which multiple comparisons were made, one way or two-way analysis of variance (ANOVA) tests with appropriate *post-hoc* tests were performed. All ANOVA results, details and tables can be found in the appendix. All data is represented as mean ± the standard error of the mean (S.E.M.) unless otherwise stated. Statistical significance is indicated as follows * $P < 0.05$, ** $P < 0.01$, *** $P < 0.001$, **** $P < 0.0001$. The statistical test used is reported in the appropriate figure legend. Graph Pad prism 6 was used to perform statistical tests and graph data. Adobe illustrator CS5 was used to create schematics.

3. Results

3.1. IVM activation of GluCl can successfully silence cells *in vitro*.

It was important to first assess if IVM application could activate GluCl *in vitro* using voltage clamp analysis on transfected cultured dorsal root ganglia neurons (Fig. 2A). Cells either expressed both the αβ or β-only GluCl subunits. β-only expression was used as a control as the β-only subunit does not form functional IVM-sensitive homomers (Frazier *et al.* 2013). Upon 20 nM IVM application, those cells which express both α and β GluCl subunits showed a significant and large induced conductance which is absent in the β-only control neurons (Fig. 2B-C). The time scale of the IVM-sensitive GluCl conductance was assessed (Fig. 2D) and took approximately 10 minutes for cells to achieve the maximal IVM induced GluCl conductance following IVM application (Fig. 2D).

To interrogate the effect of the IVM induced GluCl conductance on DRG neuronal excitability, current clamp recordings were made pre and post IVM application using an intracellular solution which mimicked likely chloride concentrations (Jin *et al.*, 2013). Using a hyperpolarising current step, the change in membrane potential was used to determine the input resistance of each neuron. The input resistance of neurons expressing the β-only subunit did not change following IVM application (Fig. 2E-F). However, αβ expressing neurons showed a significant reduction in the membrane input resistance after IVM treatment (Fig. 2E), a decrease of 81.2 ± 2.95% (Fig. 2F). Neurons from each group next received incremental current injections in order to assess excitability pre and post IVM. 22/23 of neurons expressing GluClαβ were electrically silent post IVM (>10x rheobase) (Fig. 2G-H) compared to β-only expressing control neurons, 15/15 remained fully excitable (Fig. 2H). The question remained if GluCl mediated silencing is efficacious in reducing sensory neuron excitability in response to natural stimuli, such as capsaicin (an algogen found in chilli peppers), the natural agonist of the non-selective cation

channel TRPV1 (Caterina *et al.*, 1997). Current clamp recordings were carried out on small sized DRG neurons expressing either GluClαβ or β-only subunits. Focal capsaicin was applied to selected neurons pre and post 20 nM IVM and the number of elicited action potentials recorded (Fig. 2I). There was complete abolishment of capsaicin evoked action potentials in neurons expressing both GluClα and β subunits and no changes observed in neurons only expressing the β-only subunit (Fig. 2J-K). Taken together, the GluCl system is a powerful tool and effectively silences DRG neurons to electrical and natural stimuli.

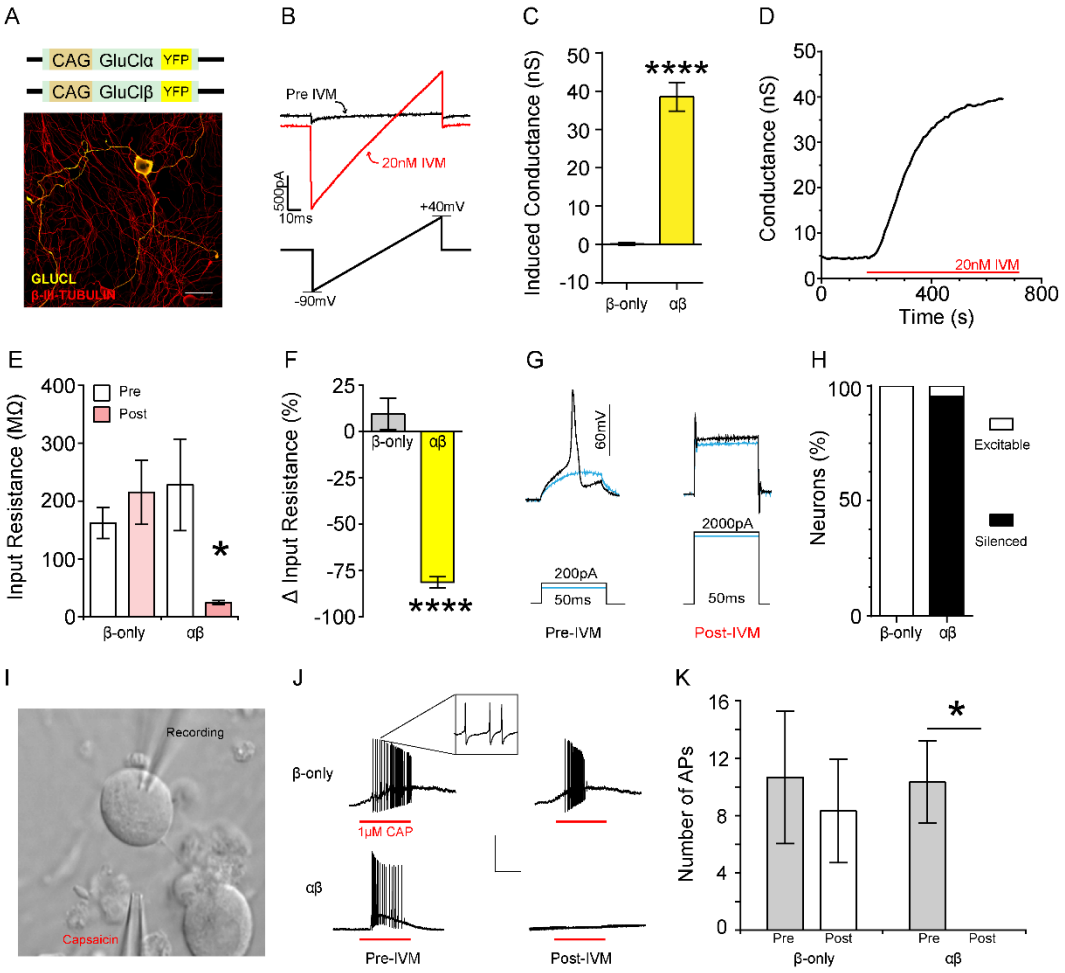

Figure 2: GluCl mediated silencing of DRG neurons i*n vitro*.

A) An example of a DRG neuron transfected with both GluClα and β subunits, scale bar 30 μm. **B)** The voltage clamp protocol used to measure the GluCl conductance pre (black) and post (red) IVM. **C)** The induced membrane conductance following IVM activation of GluClαβ is significantly increased in αβ transfected DRG neurons compared to β-only controls. (n= αβ 16 cells, β-only 24 cells. Mann-Whitney U-test, U = 13, P <0.0001, ****). **D)** Representative trace of conductance

change over time in the presence of 20 nM IVM. **E)** The input resistance of recorded DRG neurons pre and post 20 nM IVM in GluClαβ^{+} neurons and β-only controls (n= αβ 11 cells, β-only 7 cells., RM two-way ANOVA, with *post hoc* Bonferroni test, β-only: t = 2.931, df = 32 P = >0.999, n.s. αβ: t = 0.6097, df = 32, P = 0.012, *) **F)** The percentage change in input resistance in GluClβ-only and GluClαβ+ neurons following 20 nM IVM. (n = αβ 11 cells, β-only 7 cells. Two-tailed unpaired t-test, t = 9.573, df = 16, P < 0.0001, ****). **G)** Example current clamp recordings of action potential rheobase pre and post IVM from a GluClαβ transfected DRG neuron. **H)** The percentage of neurons which were excitable (White) or silenced (>10x rheobase - black) in both β-only and αβ transfected neurons. (n = αβ 23 cells, β-only 15 cells, two-tailed chi-squared test, X^2 = 34.08, df = 1, P < 0.0001, ****). **I)** An example image showing the experimental setup - a small DRG neuron, recording pipette and a capsaicin filled pipette positioned close. **J)** GluCl silencing abolishes DRG responses to algogens. Capsaicin evoked action potential responses, 10 s puff of 1 μm capsaicin pre and post IVM in both β-only and αβ transfected neurons. **K)** Quantification of capsaicin evoked action potentials in (J) pre and post IVM. (n= αβ 6 cells, β-only 6 cells, two-tailed Wilcoxon matched-pairs signed rank test, comparing pre vs post. β-only: W = -12, *no. pairs* = 6, P = 0.187, n.s. αβ: W = -21, *no. pairs* = 6, P = 0.0313, *). All data are mean ± S.E.M..

Although the GluCl system is extremely efficacious, the system relies on co-expression of two subunits to form a functional channel. The reporter for each subunit was monomeric YFP but in order for subunit co-expression to be assessed in future *in vivo* studies, differential reporters were required. YFP reporter of the GluClα subunit was removed and replaced with a monomeric Cerulean reporter (Fig. 3A) using restriction enzyme cloning. The optimised GluClα (Cerulean) and the GluClβ (YFP) constructs were transfected into cultured dissociated DRG neurons (Fig. 3B). Successful co-expression of both subunits was observed. To ensure that changing the fluorophore did not impact channel function, dose response curves were generated from voltage clamp recordings of transfected HEK293t cells. Switching the reporter did not affect the dose response of curves of GluClα-mCerulean/β-mYFP (EC50 = 2 ± 0.3 nM) compared to GluClα-mYFP/β-mYFP (EC50 = 2.6 ± 0.2 nM) (Fig. 3C). To make sure GluClα optimisation did not impact silencing efficacy, patch clamp analysis was conducted on transfected dissociated DRG neurons (Fig. 3D). Optimised GluClαβ exhibited significantly larger IVM induced conductance

compared to β-only expressing neurons (Fig. 3E). This was accompanied by a large decrease in membrane input resistance (Fig. 3F) and neuronal silencing (Fig. 3G) following 20 nM IVM in neurons that expressed optimised GluClαβ compared to β-only controls. Results mirrored those seen with GluClα-mYFP.

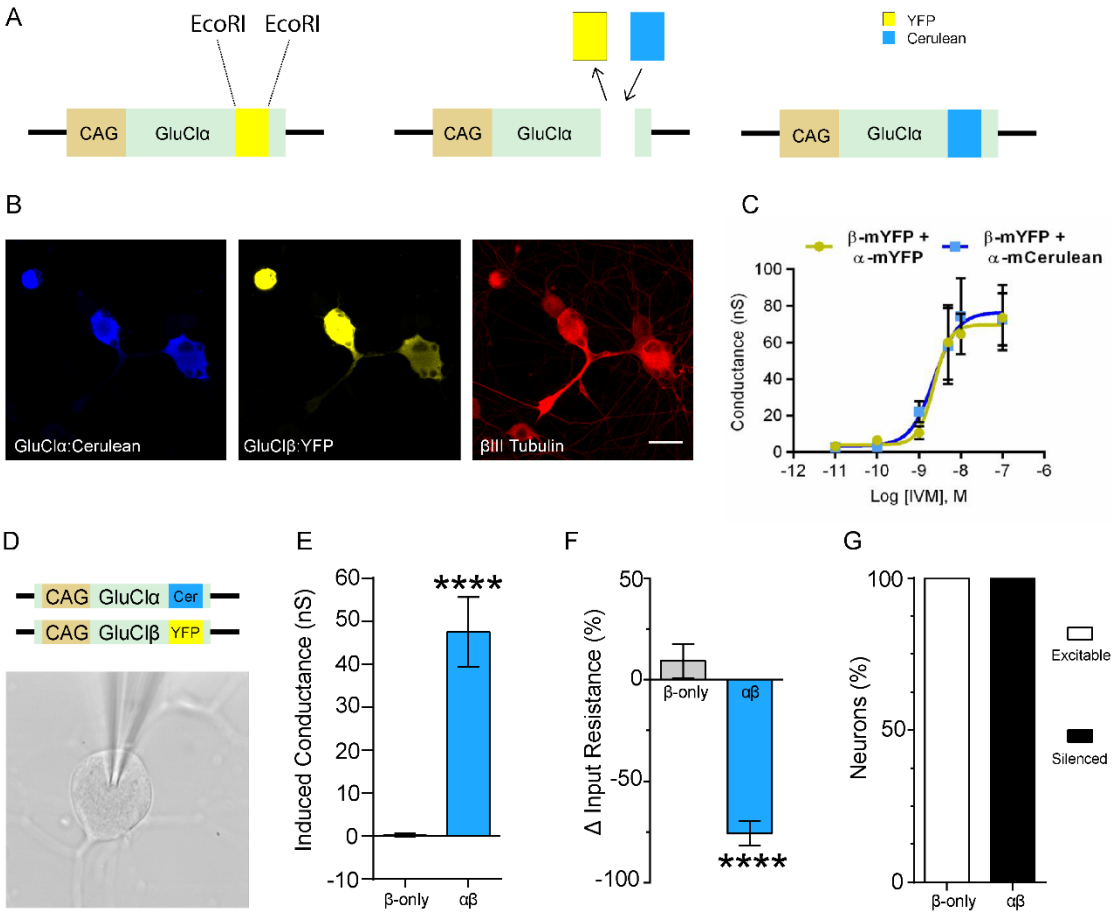

Figure 3: Optimisation of GluClα-YFP, the generation of GluClα-Cerulean.

A) Schematic of the restriction digest cloning strategy. Removal of YFP via EcoRI restriction sites and inclusion of mCerulean. **B)** Confirmation of the successful generation of GluClα-Cerulean in transfected DRG neurons. Scale bar 30 µm. **C)** The IVM dose response of curves for GluClβ-YFP co-transfected with GluClα-YFP or GluClα-Cerulean in HEK293t cells, measured by conductance. (m-denotes monomeric). β-mYFP + α-mYFP EC50 = 2.6 ± 0.2 nM, β-mYFP + α-mCerulean EC50 = 2 ± 0.3 nM (n=5 cells per concentration, two-tailed unpaired t-test (EC50), t = 1.664, df = 8, P = 0.134, n.s.). **D)** Example of a DRG neuron used for patch clamp analysis of GluClα-Cerulean GluClβ-YFP. **E)** The induced membrane conductance following IVM activation of optimised GluClαβ is significantly increased in αβ transfected DRG neurons compared to β-only controls. (n= αβ 6 cells, β-only 16 cells, two-tailed Mann-Whitney U test, U = 0, P <0.0001, ****). **F)** The percentage change in input resistance in GluClβ-only and optimised GluClαβ positive neurons following 20 nM IVM. (n = αβ 5 cells, β-only 11 cells. Two-tailed unpaired t-test, t = 12.92,

df = 14, *P* < 0.0001, ****). **G)** The percentage of neurons that were excitable (White) or silenced (>10x rheobase – black) post IVM in both β-only and optimised-αβ transfected neurons (n= αβ 6 cells, β-only 16 cells, two-tailed chi-squared test, X^2 = 200, *df* = 1, *P* < 0.0001, ****). All data are mean ±S.E.M..

Collectively, these data suggest that GluCl combined with IVM is an effective tool for sensory neuron silencing and that optimisation of GluClα did not alter channel function.

3.2. Generation and Validation of GluCl.Cre^{ON}

In order to specifically express GluCl in defined neuronal populations it was necessary to generate novel versions of the GluCl subunits. These novel constructs were designed such that they would undergo Cre-mediated recombination to invert the orientation of the transgene (which is originally in the reverse orientation), allowing selective expression only in Cre expressing cells. The following cloning strategy was carried out for each subunit to achieve Cre dependent GluCl expression. The GluCl transgene was PCR amplified using primers which were designed with NheI and AscI restriction sites at either end (5'NheI and 3'AscI) (Fig. 4A). The PCR product was PCR purified (Fig 4B). An AAV plasmid vector was sourced which contained shortened CAG promoter and a red fluorescent protein (RFP) in the reverse orientation flanked by heterotypic LoxP sites. The RFP sequence was flanked by AscI and NheI restriction sites (Fig. 4C). RFP was digested out of the vector and the 'empty' vector was gel extracted and purified. The generated GluCl insert and backbone vector were ligated and transformed into competent bacteria. Ampicillin resistant colonies were picked and screened for successful candidates (initially plasmid size, confirmed by Sanger sequencing) (Fig. 4D).

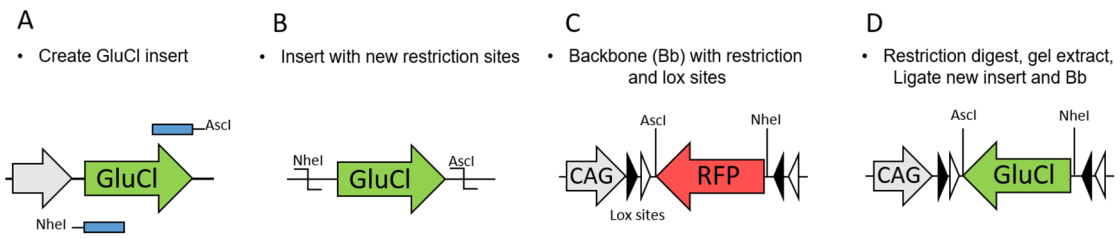

Figure 4: Generation of GluCl.Cre^{ON}. An illustrative schematic outlining the cloning strategy used to generate GluCl.Cre^{ON}

It was necessary to validate the Cre dependency of the generated GluCl.Cre^{ON} constructs (Fig. 5A). GluClα.Cre^{ON} and β.Cre^{ON} were co-transfected with a plasmid which constitutively expresses Cre into HEK293t cells. In the presence of Cre both GluClα.Cre^{ON} and β.Cre^{ON} were expressed and present on the plasma membrane (Fig. 5B). It was next important to assess GluCl.Cre^{ON} expression in the absence as well as the presence of Cre. To increase the sensitivity of GluCl detection, antibodies against GFP (cross-reacts with YFP and Cerulean) were used. GluCl was not detected in HEK293t cells in the absence of Cre but was detected in cells in the presence of Cre (Fig. 5C). To ensure GluCl.Cre^{ON} functions in a neuronal system, and in particular sensory neurons, DRG neurons from the voltage-gated sodium channel Nav1.8^{Cre} tdTomato reporter line, (Nav1.8^{Cre} targets all nociceptors and is discussed in greater detail in a later chapter), were electroporated with GluClαβ.Cre^{ON}. GluCl expression was only detected in tdTomato (Cre+) neurons (Fig. 5D).

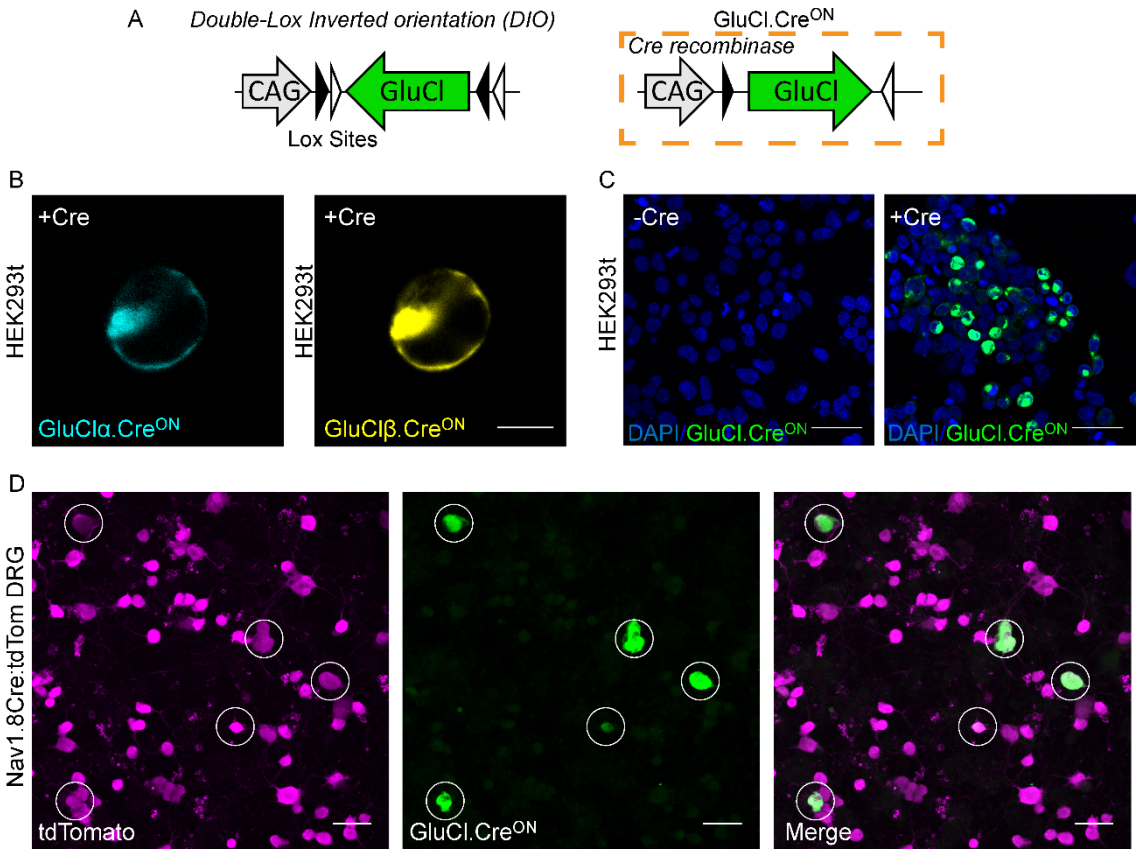

Figure 5: Using Cre recombinase to express GluCl.Cre^{ON} *in vitro.*

A) A diagram outlining the recombination of the GluCl transgene in the presence of Cre recombinase, GluCl is inverted and expression turned on in the presence of Cre. **B)** GluClα.Cre^{ON} and GluClβ.Cre^{ON} co-transfected with a Cre recombinase in HEK293t cells. GluClα.Cre^{ON} and β.Cre^{ON} both localise to the cell membrane. Scale bar 10 µm. **C)** High sensitivity detection of GluCl.Cre^{ON} using a GFP antibody following GluClαβ.Cre^{ON} transfection in HEK293t cells, in the absence or presence of Cre. GluCl.Cre^{ON} expression is only detected when Cre is present. Scale bar 50 µm. **D)** GluClαβ.Cre^{ON} transfected into DRG neurons from Nav1.8^{Cre}tdTomato mice. GluCl.Cre^{ON} is only expressed in Nav1.8^{Cre} positive neurons (white circles). Scale bar 50 µm.

It was critical to validate the function of the generated GluCl.Cre^{ON}. Initially, GluClαβ.Cre^{ON} was co-transfected with Cre recombinase into HEK293t cells and using voltage-clamp recordings the chloride conductance assessed pre and post IVM. GluCl positive HEK cells showed a significant and large conductance post 20 nM IVM compared to pre-treatment (Fig. 6A). Next, GluCl.Cre^{ON} was co-transfected

with Cre recombinase into wild type DRG neurons and following IVM treatment GluCl positive cells exhibited a large and significant increase in conductance compare to pre-treatment (Fig. 6A). Finally, the system was validated in a neuronal system which constitutively expressed Cre. Dissociated DRG neurons from Nav1.8^{Cre} mice were transfected with GluCl.Cre^{ON} and GluCl conductance measured pre and post 20 nM IVM. There was also a large and significant increase in the observed conductance post IVM compared to pre IVM in this system (Fig. 6A). To ensure that the GluCl.Cre^{ON} chloride conductance was enough to supress neuronal activity current clamp recordings were employed. GluClαβ.Cre^{ON} positive DRG neurons exhibited a large decrease in the membrane input resistance following IVM, both when Cre was delivered through transfection and transgenics (Fig. 6B). The percentage change decrease in the membrane input resistance was similar for both conditions, a decrease of 78.8 ± 2.74% and 81.2 ± 2.19% (Fig. 6C). Finally, the ability to fire an action potential was assessed for all GluCl.Cre^{ON} positive DRG neurons from both groups (Cre co-transfect, or Nav1.8^{Cre}). Post IVM, wild type DRG + Cre, 4/6 neurons were fully silent (no AP in response to current injection or 10x pre-treatment rheobase) and 2/6 neurons partially silent (3-10x original rheobase) and Nav1.8^{Cre} DRG 6/6 neurons were fully silent (Fig. 6D-E).

Collectively, these results demonstrate the functional validity of a Cre dependent (Cre^{ON}) GluCl viral vector. This tool will facilitate the selective targeting and silencing of sensory neuron populations using Cre driver lines for desired populations.

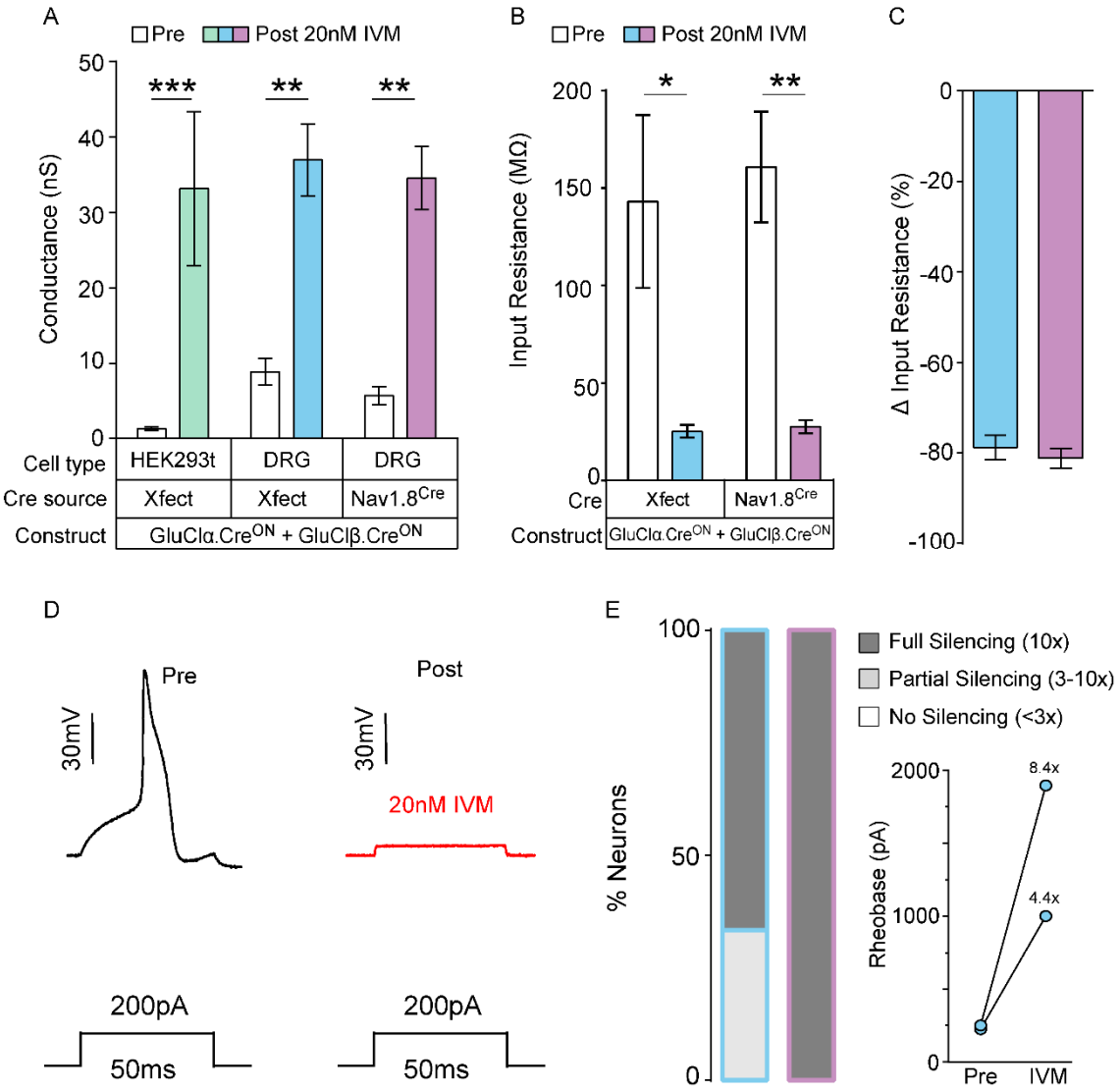

Figure 6: Functional analysis of GluCl.Cre^{ON} in multiple *in vitro* systems.

A) Conductance of GluCl.Cre^{ON} transfected HEK293t cells (green) and DRG neurons (blue/purple) pre and post IVM . Cre was delivered through co-transfection (Xfect) or present constitutively (Nav1.8^{Cre} - purple). Both HEK293t and DRG neurons expressing GluCl.Cre^{ON} showed significant increases in the observed membrane conductance post IVM. (n= HEK239t 6 cells, wild type DRG 6 cells, Nav1.8^{Cre} DRG 6 cells, two way RM ANOVA with *post hoc* Bonferroni test, HEK239t: $t = 4.813$, $df = 15$, $P = 0.0007$, ***. Wild type DRG: $t = 4.245$, $df = 15$, $P = 0.0021$, **. Nav1.8^{Cre} DRG: $t = 4.359$, $df = 15$, $P = 0.0017$, **). **B-C)** The input resistance of DRG neurons expressing GluCl.Cre^{ON} is significantly reduced post IVM. (n = wild type DRG 6 cells, Nav1.8^{Cre} DRG 6 cells two way RM ANOVA with *post hoc* Bonferroni test, wild type DRG: $t = 3.416$, $df = 10$, $P = 0.0131$, *. Nav1.8^{Cre} DRG: $t = 3.857$, $df = 10$, $P = 0.0063$, **). **D)** Example action potential recordings from a GluCl.Cre^{ON} positive DRG neuron pre and post IVM. **E)** Quantification of GluCl.Cre^{ON} silencing post IVM. DRG neurons transfected with Cre (blue) and Nav1.8^{Cre} DRG (purple) neurons show substantial silencing when GluCl.Cre^{ON} is expressed and IVM given. Wild

type DRG + Cre = 4/6 cells fully silent, 2/6 partially silent cells (inset – the two partially silent cells), Nav1.8^{Cre} DRG = 6/6 cells fully silent. All data are mean ±S.E.M..

3.3. Generation and Validation of GluCl.Cre^{OFF}

An alternative way to understand neuron populations, their circuitry, and function, is to target and silence all neurons that do not express Cre recombinase. To achieve this I created a novel GluCl construct which is only expressed in the absence of Cre recombinase. This construct was created in a similar fashion to GluCl.Cre^{ON} except the initial primers used to amplify the GluCl transgene had alternative restrictions site on either end (i.e. 5'AscI and 3'NheI) (Fig. 7A). The same procedure described above was used to generate GluCl.Cre^{OFF} (Fig. 7B-D). The final plasmid sequence contained GluCl in the correct orientation flanked by heterotypic lox sites, driven by a shortened CAG promoter (Fig. 7D).

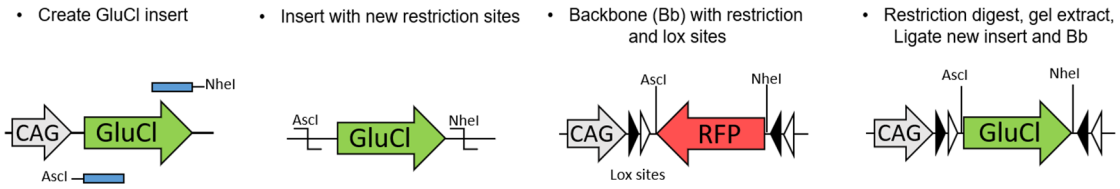

Figure 7: Generation of GluCl.Cre^{OFF} An illustrative schematic outlining the cloning strategy used to generate GluCl.Cre^{OFF}.

It was important to next validate the ability of GluCl.Cre^{OFF} to retain function in the absence of Cre and turn off GluCl expression in the presence of Cre (Fig. 8A). HEK293t cells were co-transfected with GluCl.Cre^{OFF} with or without Cre. Using high sensitivity detection, GluCl expression was only detected in conditions where Cre was absent, and expression was turned off in conditions were Cre was present (Fig. 8B). To ensure that this system was functional in sensory neurons, DRG neurons from the Nav1.8^{Cre}tdTomato reporter line were transfected with GluCl.Cre^{OFF} constructs. As identified by the white circles, only cells that do not express Cre

(tdTomato negative) show positive GluCl expression (Fig. 8C). Function of GluCl.Cre^{OFF} was assessed in transfected HEK293t cells in the presence and absence of Cre. Due to the issue that successful recombination in the presence of Cre would turn off the florescent reporter, all cells were co-transfected with normal GFP in order to identify the transfected cells in both conditions. HEK293t cells transfected with GluClαβ.Cre^{OFF} and GFP without Cre displayed a significant and large GluCl conductance post IVM (Fig. 8D). However cells which also expressed Cre recombinase lost the IVM sensitive GluCl currents after 5 days *in vitro* (time given to allow expression to turn off) (Fig. 8D).

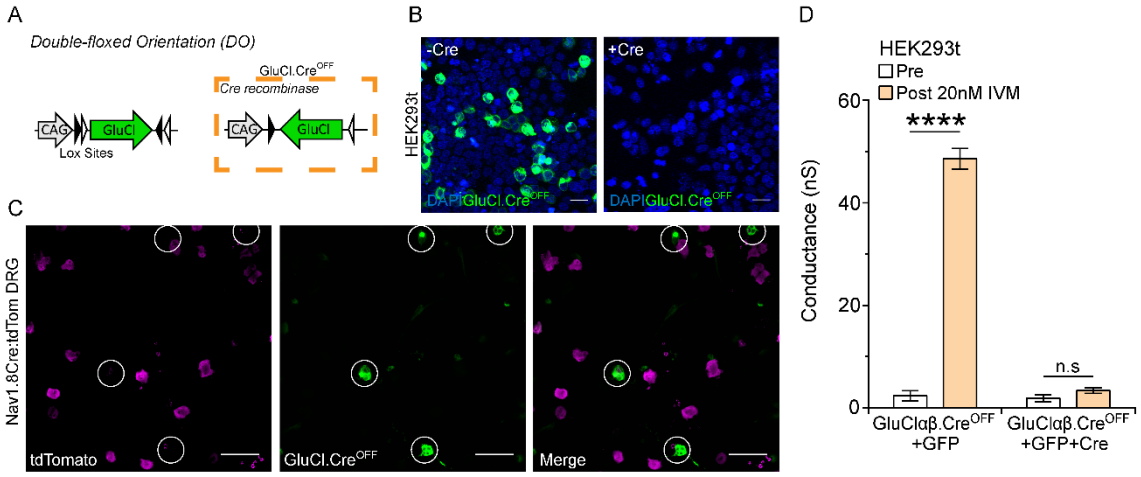

Figure 8: Validation of the GluCl.Cre^{OFF} construct.

A) A diagram outlining the recombination of the GluCl transgene in the presence of Cre recombinase, GluCl is inverted and expression turned off in the presence of Cre. **B)** High sensitivity detection of GluCl.Cre^{OFF} using a GFP antibody when GluClαβ.Cre^{OFF} is transfected into HEK293t cells in the absence or presence of Cre. GluCl.Cre^{OFF} expression is only detected when Cre is absent. Scale bar 25µm. **C)** GluClαβ.Cre^{OFF} transfected into DRG neurons from Nav1.8^{Cre}tdTomato mice. GluCl.Cre^{OFF} is only expressed in Nav1.8^{Cre} negative neurons (white circles). Scale bar 50 µm. **D)** Functional validation of GluCl.Cre^{OFF} co-transfected with either GFP or GFP and Cre into HEK293t cells. GluCl.Cre^{OFF} in the absence of Cre is functional and cells exhibit a large IVM induced conductance. Cells co-transfected with Cre recombinase do not show a functional GluCl conductance post IVM (n = -Cre 3 cells, +Cre 3 cells, two-way RM ANOVA with *post hoc* Bonferroni test, -Cre, t = 27.18, df = 8, P = <0.0001, ****. +Cre, t =0.881, df = 8, P = 0.8077, n.s). All data are mean ±S.E.M..

Together I have demonstrated the design and validation of another GluCl chemogenetic tool. GluCl.Cre^{OFF} is a tool which in the presence of Cre recombinase can turn off GluCl expression, but expression and function will remain in Cre negative neurons. This tool will be extremely useful for future studies of the somatosensory system, but henceforth will not be a main focus of my thesis.

4. Discussion

The central aim of this work is to develop our understanding of DRG neuron heterogeneity and primary afferent contributions to sensory behaviour. Herein, I have developed a chemogenetic tool box to enable the silencing of different and distinct sensory neuron populations allowing us to better understand sensory neuron function in naïve and painful states.

Initially, I considered using the popular tool designer receptors exclusively activated by designer drugs (DREADDs) (Roth, 2016). There is some evidence that the inhibitory G-protein coupled receptor hM4Di in primary afferents can alter acute pain thresholds (Iyer *et al.*, 2016; Saloman *et al.*, 2016). However, while widely used in CNS neurons, its applicability in peripheral sensory neurons can be questioned. Less than 50% of the mouse DRG cells that express hM4Di saw changes in excitability when assessed *in vitro* (Saloman *et al.*, 2016). Previous work in our lab also failed to observe significant silencing efficacy in mouse DRG. Findings suggested that this was due to a lack of endogenous GIRK channel expression (which hM4Di is proposed to act through) in mouse sensory neurons (Nockemann *et al.*, 2013). Saloman *et al.* (2016) also suggested hM4Di expression in primary afferents alters Na^{+} and Ca^{2+} currents in the absence of the ligand, (Clozapine-N-Oxide, CNO), and inhibits the analgesic effect of endogenous inhibitory G-protein-coupled receptors (Saloman *et al.*, 2016). Additionally, there are concerns with using CNO the agonist. CNO is the metabolite of the antipsychotic drug Clozapine. Literature suggests that CNO can revert back to Clozapine (Jann, Lam and Chang, 1994; Chang *et al.*, 1998; Raper *et al.*, 2017) and a compelling study proposes that it is Clozapine which is the major DREADD agonist, suggesting CNO conversion to Clozapine is necessary (Gomez *et al.*, 2017). It is important to recognise that assessing animal behaviour in the presence of an antipsychotic requires careful consideration and rigorous controls. This is particularly true in the pain field where psychological comorbidities accompany painful conditions in both humans and rodents (Dellarole *et*

al., 2014; Yalcin, Barthas and Barrot, 2014; Sieberg *et al.*, 2018). Alternative chemogenetics tools were considered such as PSAMs and KORDs, but the slow kinetics of GluCl was considered an advantage over others and therefore the engineered GluCl channel was a credible candidate going forward (Slimko *et al.*, 2002; Lerchner *et al.*, 2007; Frazier, Cohen and Lester, 2013). Future work, should investigate the over expression of GluCl and any potential consequences on other native ion channels.

GluCl's function as chemogenetic silencer was investigated *in vitro* in DRG neurons. Low doses of IVM results in a large chloride conductance in transfected DRG neurons, which is mirrored by a large decrease in the membrane input resistance. Typically, CNS neurons have a hyperpolarised Chloride Nernst potential, hence previous studies using GluCl describe a hyperpolarising silencing mechanism (Slimko *et al.*, 2002; Lerchner *et al.*, 2007). However, due to DRG neurons having high intracellular chloride (30mM) (Sung *et al.*, 2000), membrane hyperpolarisation (or depolarisation) was not observed. It is highly likely that GluCl activation by IVM is causing prolonged membrane leak and subsequent shunting inhibition (Segev, 1990; Borg-Graham, Monier and Fregnac, 1998). This membrane shunting mechanism leads to silencing of sensory neurons to both suprathreshold depolarising current injections and natural algogens such as capsaicin.

Future studies could use perforated patch-clamp recordings instead of whole cell patch clamp recordings to circumvent the need to control intracellular chloride in our solutions. This would also elucidate if GluCl alters chloride homeostasis. Currently there is no evidence that GluCl disrupts chloride homeostasis. Changes in chloride homeostasis could lead to cell swelling, however this was not observed here. In addition, work by another lab member has shown GluCl silencing efficacy using DRG calcium imagining (data not shown), a method that does not disturb native intracellular chloride. It is also possible that DRG neurons express a chloride transporter that removes the chloride that rapidly enters via GluCl activation in order to maintain chloride homeostasis.

Together, this could speak towards the unique chloride handling previously seen in DRG neurons, a mechanism that is not fully resolved (Sung *et al*., 2000).

This chemogenetic system allows reversible silencing of neuronal activity, a critical advantage over ablation techniques. Using GluCl/IVM we observed slow onset of the chloride conductance, likely due to the IVM binding sites located in the membrane region of GluCl and the requirement of IVM accumulation in the lipid bilayer. However, we were not able to observe a reversal of our IVM induced chloride conductance *in vitro* (data not shown). Previous studies demonstrate that cells require 8 hours of wash off before GluClv1.0 activation fully diminishes (Slimko *et al.*, 2002). This is likely due to a few major technical challenges; firstly GluClv2.0 contains a gain-of-function mutation (L'9F) to enhance IVM sensitivity, and second, IVM is thought to be retained in tissues and lipid bilayers which could facilitate re-binding and re-activation (Martin and Kusel, 1992; Lerchner *et al.*, 2007). I also observed that IVM is 'sticky' molecule particularly apparent when using plastic culture ware and perfusion systems. Without using 70% ethanol to wash IVM away it is difficult to ensure IVM is absent in recording conditions. Despite the difficulties experienced here, I was confident the system was reversible due to previous studies (Lerchner *et al.*, 2007) and perhaps something best assayed for in *in vivo* conditions where appropriate molecular clearance is present, and indeed I have discussed this in later chapters.

In order to better distinguish between GluClα and GluClβ expression, one of the subunits was optimised by replacing the reporter with an alternative fluorophore. It has been reported in the literature (Slimko *et al.*, 2002) that, on occasion, only one subunit is transfected into dissociated neurons and this would be difficult to determine, in our system with all reporters being YFP. The GluClα subunit was chosen to undergo reporter exchange, as GluClα was considered to be the more stable of the two subunits. Previous literature suggested that the GluClv1.0-β had difficulties in reaching the plasma

membrane, which was rectified by generation of GluClv2.0 and introducing the RSR-AAA mutation. To avoid further GluClβ manipulation GluClα was chosen. Cloning methods were used to switch mYFP for mCerulean and subsequently the optimised GluClα-mCerluean and GluClβ-mYFP constructs were functionally characterised to ensure introducing a new reporter had not adversely effected the GluCl system. In particular, optimised GluCl activation via IVM could induce a large chloride conductance in both transfected HEK293t and DRG neurons without changes in efficacy. Indeed, optimised GluCl was able to silence the evoked firing properties of DRG neurons to current injections that were suprathreshold, following IVM treatment. The optimisation of the GluCl reporters has other key benefits. The different subunit reporters will facilitate future studies allowing the use of FRET imaging to investigate subunit expression and subunit association, and ratio metric imaging to use the change in YFP fluorescence as a direct chloride sensor (Batti *et al.*, 2013). GluCl can therefore be considered as an effective and powerful tool for silencing DRG neurons and optimising the reporter of the alpha subunit had no negative effects on our silencing system and provides new avenues for GluCl as a versatile tool.

There was still a need to generate new versions of GluCl to enable restricted expression in select sensory neuron populations. There are generally two ways to achieve this, selecting a specific promoter to drive transgene expression, or by taking advantage of Cre/Lox technology (Tsien *et al.*, 1996). The former method comes with significant challenges such a promoter strength and size. Particularly important, due to the limited packaging space in viral vectors such Adeno-associated viruses, using large promoters is not possible. Cre/Lox technology overcomes these two issues, one can drive transgene expression in desired populations using a short ubiquitous promoter. However, the Cre/LoxP system greatly depends on the availability of Cre expressing mouse driver lines, which in the sensory biology field are becoming more readily available.

The aim was to take advantage of the Cre/Lox system and generate novel GluCl constructs which depend on Cre recombinase for expression (Schnütgen *et al.*, 2003; Atasoy *et al.*, 2008). GluCl.Cre^{ON} was created, where GluCl was cloned the reverse orientation flanked heterotypic Lox P sites. In the presence of Cre recombinase this results in flipping inversion of the GluCl transgene to the correct reading frame and selective GluCl expression. This method was chosen over the method of integrating a Lox STOP Lox coding region prior to the GluCl transgene as the latter approach was not possible due to packaging limits. The generated GluCl.Cre^{ON} construct was validated *in vitro* both using high sensitivity immunohistology as well as patch-clamp analysis. GluCl.Cre^{ON} showed selective expression only in cells co-expressing Cre and was functionally validated in three systems, i) HEK293t cells co-transfected with Cre, ii) wild type DRG neurons co-transfected with Cre, and iii) DRG neurons cultured from Nav1.8^{Cre} mice which constitutively express Cre in the Nav1.8 positive nociceptor population. In all cases GluCl, when activated by low doses of IVM, was able to induce a large Chloride conductance and silence neuronal activity. This addition to the chemogenetic tool box will allow selective expression in cell populations which are driving Cre recombinase expression. Future work with use this tool to selectively silence discrete primary afferent populations.

The final addition to the chemogenetic tool box was the GluCl.Cre^{OFF} construct. Although less frequently used in transgene targeting the Cre^{OFF} system allows the targeting and manipulation of only those cells that do not express cre recombinase (Saunders, Johnson and Sabatini, 2012). This method would spare the selected population and provide an alternate method to interrogate Cre negative DRG populations, their circuitry and function. Here in, I have developed GluClCre^{OFF} through molecular cloning techniques such that GluCl is correctly orientated and flanked by heterotypic Lox sites. In the presence of Cre the GluCl sequence inverts, resulting in the transgene being orientated in reverse, switching off GluCl expression. I have functionally

validated this plasmid in HEK293t cells. Expression and function is only observed when Cre is absent. Future work will validate this construct in the sensory system *in vivo*. However, throughout this thesis GluClCre^{OFF} will not be used or discussed further.

To summarise, a chemogenetic tool box was generated and validated i*n vitro* using both heterologous and primary culture systems. The generation of the optimised GluCl construct will enable unbiased GluCl expression in the DRG for non-selective silencing, in addition the visualisation of the independent GluCl subunits is now possible. Two Cre dependent constructs were also generated, GluCl.Cre^{ON} and GluCl.Cre^{OFF}. These constructs will facilitate the interrogation of sensory neuron heterogeneity and subpopulation function in both naïve and painful conditions. These powerful tools will enable effective chemogenetic neuronal manipulation of DRG sensory neurons, which until now has been unavailable. Finally, this tool box can be widely employed in other neuronal systems where selective neuronal silencing is desired, both outside and within the sensory biology field.

5. Acknowledgements

The data in Figures 2 and 3 is my work and has been published in a peer reviewed journal. I have permission from the senior author to include my published work in this thesis.

6. References

Atasoy, D. *et al.* (2008) 'A FLEX switch targets channelrhodopsin-2 to multiple cell types for imaging and long-range circuit mapping', *Journal of Neuroscience*, 28(28), pp. 7025–7030. doi: 10.1523/JNEUROSCI.1954-08.2008.

Batti, L. *et al.* (2013) 'Transgenic mouse lines for non-invasive ratiometric monitoring of intracellular chloride', *Frontiers in Molecular Neuroscience*. Frontiers, 6(MAY), p. 11. doi: 10.3389/fnmol.2013.00011.

Borg-Graham, L. J., Monier, C. and Fregnac, Y. (1998) 'Visual input evokes transient and strong shunting inhibition in visual cortical neurons', *Nature*, 393(6683), pp. 369–373. doi: 10.1038/30735.

Caterina, M. J. *et al.* (1997) 'The capsaicin receptor: A heat-activated ion channel in the pain pathway', *Nature*, 389(6653), pp. 816–824. doi: 10.1038/39807.

Chang, W. H. *et al.* (1998) 'Reversible metabolism of clozapine and clozapine N-oxide in schizophrenic patients', *Progress in Neuro-Psychopharmacology and Biological Psychiatry*, 22(5), pp. 723–739. doi: 10.1016/S0278-5846(98)00035-9.

Changeux, J. P. (2012) 'The nicotinic acetylcholine receptor: The founding father of the pentameric ligand-gated ion channel superfamily', *Journal of Biological Chemistry*, pp. 40207–40215. doi: 10.1074/jbc.R112.407668.

Cleland, T. A. (1996) 'Inhibitory glutamate receptor channels', *Molecular Neurobiology*. Humana Press, 13(2), pp. 97–136. doi: 10.1007/BF02740637.

Cully, D. F. *et al.* (1994) 'Cloning of an avermectin-sensitive glutamate-gated chloride channel from Caenorhabditis elegans', *Nature*, 371(6499), pp. 707–711. doi: 10.1038/371707a0.

Cully, D. F. *et al.* (1996) 'Molecular biology and electrophysiology of glutamate-gated chloride channels of invertebrates.', *Parasitology*, 113 Suppl, pp. S191-200. doi:

10.1017/s0031182000077970.

Dellarole, A. *et al.* (2014) ‘Neuropathic pain-induced depressive-like behavior and hippocampal neurogenesis and plasticity are dependent on TNFR1 signaling’, *Brain, Behavior, and Immunity*. Academic Press Inc., 41(1), pp. 65–81. doi: 10.1016/j.bbi.2014.04.003.

Dent, J. A. *et al.* (2000) ‘The genetics of ivermectin resistance in Caenorhabditis elegans’, *Proceedings of the National Academy of Sciences of the United States of America*, 97(6), pp. 2674–2679. doi: 10.1073/pnas.97.6.2674.

Dent, J. A., Davis, M. W. and Avery, L. (1997) ‘avr-15 encodes a chloride channel subunit that mediates inhibitory glutamatergic neurotransmission and ivermectin sensitivity in Caenorhabditis elegans’, *EMBO Journal*, 16(19), pp. 5867–5879. doi: 10.1093/emboj/16.19.5867.

Dong, J. Y., Fan, P. D. and Frizzell, R. A. (1996) ‘Quantitative analysis of the packaging capacity of recombinant adeno-associated virus’, *Human Gene Therapy*. Mary Ann Liebert Inc., 7(17), pp. 2101–2112. doi: 10.1089/hum.1996.7.17-2101.

Dutertre, S., Becker, C. M. and Betz, H. (2012) ‘Inhibitory glycine receptors: An update’, *Journal of Biological Chemistry*, pp. 40216–40223. doi: 10.1074/jbc.R112.408229.

Frazier, S. J., Cohen, B. N. and Lester, H. a. (2013) ‘An engineered glutamate-gated chloride (GLUCL) channel for sensitive, consistent neuronal silencing by ivermectin’, *Journal of Biological Chemistry*, 288(29), pp. 21029–21042. doi: 10.1074/jbc.M112.423921.

Gomez, J. L. *et al.* (2017) ‘Chemogenetics revealed: DREADD occupancy and activation via converted clozapine’, *Science*. American Association for the Advancement of Science, 357(6350), pp. 503–507. doi: 10.1126/science.aan2475.

Henriquez-Camacho, C. *et al.* (2016) 'Ivermectin versus albendazole or thiabendazole for Strongyloides stercoralis infection', *Cochrane Database of Systematic Reviews*. John Wiley and Sons Ltd. doi: 10.1002/14651858.CD007745.pub3.

Hibbs, R. E. and Gouaux, E. (2011) 'Principles of activation and permeation in an anion-selective Cys-loop receptor', *Nature*, 474(7349), pp. 54–60. doi: 10.1038/nature10139.

Horoszok, L. *et al.* (2001) 'GLC-3: A novel fipronil and BIDN-sensitive, but picrotoxinin-insensitive, L-glutamate-gated chloride channel subunit from Caenorhabditis elegans', *British Journal of Pharmacology*. John Wiley and Sons Inc., 132(6), pp. 1247–1254. doi: 10.1038/sj.bjp.0703937.

Iyer, S. M. *et al.* (2016) 'Optogenetic and chemogenetic strategies for sustained inhibition of pain', *Scientific Reports*. Nature Publishing Group, 6. doi: 10.1038/srep30570.

Jann, M. W., Lam, Y. W. F. and Chang, W. H. (1994) 'Rapid formation of clozapine in guinea-pigs and man following clozapine-N-oxide administration', *Archives Internationales de Pharmacodynamie et de Therapie*, 328(2), pp. 243–250.

Jin, X. *et al.* (2013) 'Activation of the Cl- Channel ANO1 by localized calcium signals in nociceptive sensory neurons requires coupling with the IP3 receptor', *Science Signaling*, 6(290). doi: 10.1126/scisignal.2004184.

Kilkenny, C. *et al.* (2010) 'Improving Bioscience Research Reporting: The ARRIVE Guidelines for Reporting Animal Research', *PLoS Biology*, 8(6), p. e1000412. doi: 10.1371/journal.pbio.1000412.

Kuhlman, S. J. and Huang, Z. J. (2008) 'High-Resolution Labeling and Functional Manipulation of Specific Neuron Types in Mouse Brain by Cre-Activated Viral Gene Expression', *PLoS ONE*. Edited by R. O. L. Wong, 3(4), p. e2005. doi:

10.1371/journal.pone.0002005.

Lerchner, W. *et al.* (2007) ‘Reversible silencing of neuronal excitability in behaving mice by a genetically targeted, ivermectin-gated Cl- channel.’, *Neuron*, 54(1), pp. 35–49. doi: 10.1016/j.neuron.2007.02.030.

Li, P., Slimko, E. M. and Lester, H. A. (2002) ‘Selective elimination of glutamate activation and introduction of fluorescent proteins into a *Caenorhabditis elegans* chloride channel’, *FEBS Letters*, 528(1–3), pp. 77–82. doi: 10.1016/S0014-5793(02)03245-3.

Lieb, A. *et al.* (2018) ‘Biochemical autoregulatory gene therapy for focal epilepsy’, *Nature Medicine*. Nature Publishing Group, pp. 1324–1329. doi: 10.1038/s41591-018-0103-x.

Lin, D. *et al.* (2011) ‘Functional identification of an aggression locus in the mouse hypothalamus’, *Nature*, 470(7333), pp. 221–227. doi: 10.1038/nature09736.

Lummis, S. C. R. (2012) ‘5-HT3 receptors’, *Journal of Biological Chemistry*, pp. 40239–40245. doi: 10.1074/jbc.R112.406496.

Lynagh, T. *et al.* (2011) ‘Molecular determinants of ivermectin sensitivity at the glycine receptor chloride channel’, *Journal of Biological Chemistry*, 286(51), pp. 43913–43924. doi: 10.1074/jbc.M111.262634.

Maren, S., Yap, S. A. and Goosens, K. A. (2001) ‘The amygdala is essential for the development of neuronal plasticity in the medial geniculate nucleus during auditory fear conditioning in rats.’, *The Journal of neuroscience : the official journal of the Society for Neuroscience*, 21(6). doi: 10.1523/jneurosci.21-06-j0001.2001.

Martin, R. J. and Kusel, J. R. (1992) ‘On the distribution of a fluorescent ivermectin probe (4“ 5, 7 dimethyl-bodipy proprionylivermectin) in Ascaris membranes’, *Parasitology*, 104(3), pp. 549–555. doi: 10.1017/S0031182000063812.

Nassar, M. A. *et al.* (2004) 'Nociceptor-specific gene deletion reveals a major role for Nav1.7 (PN1) in acute and inflammatory pain', *Proceedings of the National Academy of Sciences*, 101(34), pp. 12706–12711. doi: 10.1073/pnas.0404915101.

Nockemann, D. *et al.* (2013) 'The K^+ channel GIRK2 is both necessary and sufficient for peripheral opioid-mediated analgesia', *EMBO Molecular Medicine*, 5(8), pp. 1263–1277. doi: 10.1002/emmm.201201980.

Palmeirim, M. S. *et al.* (2018) 'Efficacy and safety of co-administered ivermectin plus albendazole for treating soil-transmitted helminths: A systematic review meta-analysis and individual patient data analysis', *PLoS Neglected Tropical Diseases*. Public Library of Science, 12(4). doi: 10.1371/journal.pntd.0006458.

Pion, S. D. *et al.* (2019) 'Effect of a single standard dose (150-200 µg/kg) of ivermectin on loa loa microfilaremia: Systematic Review and Meta-analysis', *Open Forum Infectious Diseases*. Oxford University Press, 6(4). doi: 10.1093/ofid/ofz019.

Van Den Pol, A. N. *et al.* (2004) 'Physiological properties of hypothalamic MCH neurons identified with selective expression of reporter gene after recombinant virus infection', *Neuron*, 42(4), pp. 635–652. doi: 10.1016/S0896-6273(04)00251-X.

Raper, J. *et al.* (2017) 'Metabolism and Distribution of Clozapine-N-oxide: Implications for Nonhuman Primate Chemogenetics', *ACS Chemical Neuroscience*. American Chemical Society, 8(7), pp. 1570–1576. doi: 10.1021/acschemneuro.7b00079.

Rizzo, M. A. *et al.* (2004) 'An improved cyan fluorescent protein variant useful for FRET', *Nature Biotechnology*, 22(4), pp. 445–449. doi: 10.1038/nbt945.

Rolland, A. S. *et al.* (2017) 'A quantitative evaluation of a 2.5-kb rat tyrosine hydroxylase promoter to target expression in ventral mesencephalic dopamine neurons in vivo', *Neuroscience*. Elsevier Ltd, 346, pp. 126–134. doi: 10.1016/j.neuroscience.2017.01.014.

Roth, B. L. (2016) ‘DREADDs for Neuroscientists’, *Neuron*. Cell Press, pp. 683–694. doi: 10.1016/j.neuron.2016.01.040.

Saloman, J. L. *et al.* (2016) ‘Gi-DREADD expression in peripheral nerves produces ligand-dependent analgesia, as well as ligand-independent functional changes in sensory neurons’, *Journal of Neuroscience*. Society for Neuroscience, 36(42), pp. 10769–10781. doi: 10.1523/JNEUROSCI.3480-15.2016.

Saunders, A., Johnson, C. A. and Sabatini, B. L. (2012) ‘Novel recombinant adeno-associated viruses for Cre activated and inactivated transgene expression in neurons’, *Frontiers in Neural Circuits*, (JULY 2012). doi: 10.3389/fncir.2012.00047.

Schnütgen, F. *et al.* (2003) ‘A directional strategy for monitoring Cre-mediated recombination at the cellular level in the mouse’, *Nature Biotechnology*, 21(5), pp. 562–565. doi: 10.1038/nbt811.

Segev, I. (1990) ‘Computer study of presynaptic inhibition controlling the spread of action potentials into axonal terminals’, *Journal of Neurophysiology*, 63(5), pp. 987–998. doi: 10.1152/jn.1990.63.5.987.

Siddiqui, K., Gold, L. S. and Gill, J. (2016) ‘The efficacy, safety, and tolerability of ivermectin compared with current topical treatments for the inflammatory lesions of rosacea: a network meta-analysis’, *SpringerPlus*, 5(1), p. 1151. doi: 10.1186/s40064-016-2819-8.

Sieberg, C. B. *et al.* (2018) ‘Neuropathic pain drives anxiety behavior in mice, results consistent with anxiety levels in diabetic neuropathy patients’, *PAIN Reports*, 3(3), p. e651. doi: 10.1097/PR9.0000000000000651.

Sigel, E. and Steinmann, M. E. (2012) ‘Structure, function, and modulation of GABAA receptors’, *Journal of Biological Chemistry*, pp. 40224–40231. doi: 10.1074/jbc.R112.386664.

Sleigh, J. N., Weir, G. A. and Schiavo, G. (2016) ‘A simple, step-by-step dissection protocol for the rapid isolation of mouse dorsal root ganglia’, *BMC Research Notes*, 9(1), p. 82. doi: 10.1186/s13104-016-1915-8.

Slimko, E. M. *et al.* (2002) ‘Selective electrical silencing of mammalian neurons in vitro by the use of invertebrate ligand-gated chloride channels.’, *The Journal of neuroscience : the official journal of the Society for Neuroscience*, 22(17), pp. 7373–7379. doi: 20026775.

Steffens, S. *et al.* (2004) ‘A neuroblastoma-selective suicide gene therapy approach using the tyrosine hydroxylase promoter’, *Pediatric Research*, 56(2), pp. 268–277. doi: 10.1203/01.PDR.0000132666.23103.EF.

Strycharz, J. P., Yoon, K. S. and Clark, J. M. (2008) ‘A New Ivermectin Formulation Topically Kills Permethrin-Resistant Human Head Lice (Anoplura: Pediculidae)’, *Journal of Medical Entomology*, 45(1), pp. 75–81. doi: 10.1093/jmedent/45.1.75.

Sung, K. W. *et al.* (2000) ‘Abnormal GABA(A) receptor-mediated currents in dorsal root ganglion neurons isolated from Na-K-2Cl cotransporter null mice’, *Journal of Neuroscience*, 20(20), pp. 7531–7538. doi: 10.1523/jneurosci.20-20-07531.2000.

Tambo, E. *et al.* (2015) ‘Nobel prize for the artemisinin and ivermectin discoveries: A great boost towards elimination of the global infectious diseases of poverty’, *Infectious Diseases of Poverty*. BioMed Central Ltd. doi: 10.1186/s40249-015-0091-8.

Tizifa, T. A. *et al.* (2018) ‘Prevention Efforts for Malaria’, *Current Tropical Medicine Reports*. Springer Verlag, pp. 41–50. doi: 10.1007/s40475-018-0133-y.

Tsien, J. Z. *et al.* (1996) ‘Subregion- and cell type-restricted gene knockout in mouse brain’, *Cell*. Cell Press, 87(7), pp. 1317–1326. doi: 10.1016/S0092-8674(00)81826-7.

Vassilatis, D. K. *et al.* (1997) ‘Genetic and biochemical evidence for a novel avermectin-sensitive chloride channel in Caenorhabditis elegans. Isolation and

characterization', *Journal of Biological Chemistry*, 272(52), pp. 33167–33174. doi: 10.1074/jbc.272.52.33167.

Victoria, J. and Trujillo, R. (2001) 'Topical Ivermectin: A New Successful Treatment for Scabies', *Pediatric Dermatology*, 18(1), pp. 63–65. doi: 10.1046/j.1525-1470.2001.018001063.x.

Wolstenholme, A. J. (2012) 'Glutamate-gated Chloride Channels', *Journal of Biological Chemistry*, 287(48), pp. 40232–40238. doi: 10.1074/jbc.R112.406280.

Yakel, J. (2010) 'Advances and hold-ups in the study of structure, function and regulation of Cys-loop ligand-gated ion channels and receptors', *Journal of Physiology*, February, pp. 555–556. doi: 10.1113/jphysiol.2009.185488.

Yalcin, I., Barthas, F. and Barrot, M. (2014) 'Emotional consequences of neuropathic pain: Insight from preclinical studies', *Neuroscience and Biobehavioral Reviews*. Elsevier Ltd, pp. 154–164. doi: 10.1016/j.neubiorev.2014.08.002.

Chapter 3: Using optimised GluClv2.0 to silence dorsal root ganglion neurons *in vivo*

1. Introduction

The development of different GluCl chemogenetic tools in chapter 2 enabled great efficacy in silencing sensory neurons *in vitro*. The rationale for the investigations detailed in this chapter was that GluClv2.0 had not yet been employed in the somatosensory system *in vivo*. Using GluCl we will be able to explore the idea that primary afferent activity is critical for the maintenance and development of neuropathic pain. Indeed, this might be driven by defined sensory neuron population(s). Identification of key population(s) will inform therapeutics for the treatment of neuropathic pain. However, there is the need to first carry out a proof of principle study to validate GluCl mediated chemogenetic silencing *in vivo*, and to address whether GluClv2.0 silencing can alleviate neuropathic pain related behaviours. To tackle these questions, GluCl will be expressed in primary afferents of mice using adeno-associated viruses.

1.1. Viruses and viral tropism

Targeting neuronal populations using viruses provides the ability to alter gene expression *in vivo*. Viral vectors can be designed to overexpress, knockdown, or introduce an exogenous gene/s of interest. Using viruses to deliver transgenes requires careful consideration of which virus best suits the experimental question being addressed. Many viruses used for delivering transgenes have multiple benefits and drawbacks, especially capsid capacity, tropism, immunogenicity and cytotoxicity. The major viruses used to deliver transgene payloads are herpes simplex viruses, lentiviruses, adenoviruses and adeno-associated viruses (AAVs). All of these have been used to target the sensory system to address various questions (Glatzel *et al.*, 2000; Glorioso and Fink, 2009; Yu *et al.*, 2011). However, this body of work will focus on the use of AAVs.

1.2. Adeno-associated viruses

AAVs were first discovered in the 1960s and the first 20 years of AAV research was dedicated to their full and detailed characterisation (Atchison, Casto and Hammon, 1965; Wang, Tai and Gao, 2019). Subsequently, this led to the whole AAV2 genome being sequenced, which facilitated the development of AAVs for gene delivery (Srivastava, Lusby and Berns, 1983). AAVs are small viruses approximately 26 nm in diameter, icosahedral in shape and contain a single stranded genome around 4.7kb in size (Dong, Fan and Frizzell, 1996; Wang, Tai and Gao, 2019). The AAV genome contains many features important for proper function. For instance, the whole AAV genome is flanked by inverted terminal repeats (ITRs), the *cap* gene encodes the three capsid subunits (VP1-3) and the *rep* gene encode proteins which are vital for viral replication (Sonntag, Schmidt and Kleinschmidt, 2010; Wang, Tai and Gao, 2019). With the aid of *rep* proteins, wild type AAV ITR sites are able to integrate the viral genome into the genome of host cells, to establish viral latency (Wang, Tai and Gao, 2019). This phenomenon can occur in human cells due to the AAVS1 locus which has a high degree or similarity to ITR sites (Samulski *et al.*, 1991; Philpott *et al.*, 2002). However, despite this observation the current opinion is that AAVs do not cause human disease (Wang, Tai and Gao, 2019).

Since these discoveries recombinant AAVs (rAAVs) have been developed for genetic tools and gene therapies. rAAVs contain the same capsid encoding genes but lack all other protein coding elements. The removal of native AAV protein coding sequences reduces immunogenicity, genome integration and provides the capacity to introduce desired transgenes (Dong, Fan and Frizzell, 1996; Wang, Tai and Gao, 2019). Indeed, researchers can integrate desired genes between the two AAV ITR sites, readily achievable using standard cloning techniques.

It was initially thought, AAVs infect cells solely via the binding of capsid regions to cell surface receptors on host cells, such as Heparan sulphate proteoglycan, O/N

linked sialic acids, FGFR1, integrins, laminin receptors and galactose (Agbandje-McKenna and Kleinschmidt, 2011). However, it was the recently discovered AAV receptor (AAVR) that is now thought to be the major facilitator of cell entry of multiple AAV serotypes (Pillay *et al.*, 2016; Summerford and Samulski, 2016). The binding of AAVs to monomers, dimers, heterodimers or multicomplexes of AAVRs and other co-receptors and glycan attachment factors, induces capsid internalisation, via endocytosis (Nonnenmacher and Weber, 2011; Summerford and Samulski, 2016; Pillay and Carette, 2017). However, other work suggests alternative AAVR independent AAV cell entry are also key (Dudek *et al.*, 2018). After cell entry, the capsid is trafficked to the Golgi and then to the nucleus and enters via the nuclear pore (Nonnenmacher and Weber, 2012; Xiao and Samulski, 2012; Nicolson and Samulski, 2014). The capsid is subsequently uncoated and single stranded DNA converted to double stranded DNA ready for transcription (Ferrari *et al.*, 1996; Fisher *et al.*, 1996).

A major advance in using rAAVs has been the discovery of novel capsid variants which alter or determine viral tropism. Methods used to identify novel AAV serotypes include the identification of naturally occurring AAVs, mutagenesis and receptor/ligand host designs (Wang, Tai and Gao, 2019). Looking for naturally occurring AAVs has led to the identification of human AAV1, AAV2, AAV3, AAV5, AAV6, AAV7, AAV8 and AAV9. Indeed, all of these AAV serotypes are commonly found in humans (Calcedo *et al.*, 2009; Boutin *et al.*, 2010). Other capsids have been identified in non-human primates and in pigs, such as AAVrh.7, AAVrh.8, AAVrh.10, and AAVpo2.1, AAVpo4, AAVpo5, AAVpo6, respectively (Gao *et al.*, 2002; Bello *et al.*, 2009; Tanguy *et al.*, 2015). A powerful method of generating AAV variants is through using Cre recombination-based AAV targeted evolution (CREATE) technology; the selective recovery of capsids that are able to target defined (Cre+)

cell populations. This method resulted in the generation of AAV-PHP.A, AAV-PHP.B, AAV-PHP.eB, and AAV-PHP.S (Deverman *et al.*, 2016; Chan *et al.*, 2017).

Many of the rAAVs discussed above have been investigated for their ability to transduce DRG neurons. In particular AAV1, AAV2, AAV5, AAV6, AAV7 and AAV8 all containing a reporter transgene were injected directly into the DRG and transduction efficiency assessed (Mason *et al.*, 2010; Yu, Fischer and Hogan, 2016). It was shown that AAV5, AAV6 and AAV1 showed good transduction abilities (Mason *et al.*, 2010). AAV6 also transduced satellite glia and all other serotypes had poor efficacy (Mason *et al.*, 2010). Further studies have shown that AAV6 preferentially targeted small diameter neurons while AAV5 and AAV8 had tropism for larger diameter neurons (Towne *et al.*, 2009; Vulchanova *et al.*, 2010; Jacques *et al.*, 2012). However, the efficacy of AAV9 was addressed in a separate study and was given either intravenously or intrathecally in adult mice. AAV9 showed great tropism for peripheral sensory neurons and CNS structures (Schuster *et al.*, 2014). It was also praised for its ability to cross the blood-brain barrier, which many other viruses have struggled to do (Schuster *et al.*, 2014). The AAV-PHP variants have also been trialled *in vivo* with PHP.S showing the highest tropism for peripheral neurons (Chan *et al.*, 2017). The development of rAAVs for their utility in neuronal transduction has been extremely valuable in the progression of both biomedical research and medical gene therapies.

1.3. Modulating the dorsal root ganglia

Many researchers hypothesise that the DRG hyperexcitability drives many painful conditions (Wall and Gutnick, 1974; Wall and Devor, 1983; Kajander and Bennett, 1992; Boucher *et al.*, 2000; Wu *et al.*, 2001; Smith, O'Hara and Stucky, 2013; Haroutounian *et al.*, 2014; Dawes *et al.*, 2018), giving the rationale to modulate or silence DRG neurons to reduce pain following injury or disease. Several means to achieve this have been trialled, some of which are listed below.

1.3.1. Local anaesthetics

Pharmacological blockade of DRG activity, through blocking voltage-gated sodium channels using local anaesthetics, has shown efficacy in alleviating acute pain (Borgeat and Aguirre, 2010). Furthermore, peripheral blockade using the local anaesthetic lidocaine improved spontaneous non-evoked neuropathic pain (Haroutounian *et al.*, 2014) and phantom limb pain (Vaso *et al.*, 2014). There is also evidence in rodents that administration of lidocaine can block the spontaneous discharge observed following sciatic neuroma (Chabal, Russell and Burchiel, 1989; Devor, Wall and Catalan, 1992). Behavioural studies have since shown that intrathecal lidocaine can alleviate non-evoked ongoing pain in neuropathic mice (He *et al.*, 2012). However, there are major concerns with using local anaesthetics to treat neuropathic pain, particularly in terms of cardiac and CNS side effects. Although, these studies do provide evidence that the DRG is critical for the maintenance of neuropathic pain.

1.3.2. Direct DRG stimulation

In addition to the pharmacological blockage of DRG neuron activity rodent and human studies have investigated the efficacy of DRG stimulation and pain relief (Esposito *et al.*, 2019). The mechanisms of DRG stimulation and pain relief are not fully understood but there is some evidence that it leads to conduction blockade of DRG signalling, therefore preventing transmission (Pan *et al.*, 2018). Computational simulations have proposed that it is the T-junction of DRG neurons that is responsible for the stimulation blockade (Kent *et al.*, 2018). DRG T-junctions allow activity coming from the periphery to be blocked, filtered or bypassed by the DRG (Gemes *et al.*, 2013). Simulations suggest that DRG stimulation enhances the T-junction's band-pass filtering properties, resulting in the block of transmission to the CNS (Kent *et al.*, 2018; Pan *et al.*, 2018). An important study, which provided further evidence that the DRG was critical in

maintaining pain-states, used direct DRG stimulation to alleviate pain associated with complex regional pain syndrome (CRPS) and causalgia (Deer *et al.*, 2017).

1.3.3. Virally delivered chemo- and opto-genetics

With the advancement of genetic tools, pre-clinical studies have made attempts to modulate DRG activity through the viral delivery and expression of chemo- and opto-genetic transgenes in primary afferents (transgenic dependent expression of these tools will be discussed in a later chapter). Iyer *et al.* (2016) used AAV6 viral vectors to express either the optogenetic inhibitory tool SwiChR, or the inhibitory DREADD, hM4Di predominantly in small DRG neurons, achieved using the small cell tropism of AAV6. These tools were used to silence DRG neurons following application of blue light or administration of the hM4Di agonist CNO (Iyer *et al.*, 2016). In the presence of blue light or CNO, SwiChR or hM4Di expressing mice were hyposensitive to mechanical and thermal stimuli (Iyer *et al.*, 2016). In addition, AAV1 was used to deliver an optogenetic tool termed BLINK2 into primary afferents of rats. This optically activated potassium channel reversed the mechanical hypersensitivity associated with chemotherapy-induced neuropathy (Alberio *et al.*, 2018). However, no study has demonstrated efficacy of virally delivered chemogenetics in alleviating traumatic nerve injury induced neuropathic pain, or assayed for the recovery of spontaneous non-evoked pain.

Given the powerful silencing capabilities of GluClv2.0 observed *in vitro*, the aim was to validate the system in the context of touch and pain, *in vivo*. In addition, the delivery of GluClv2.0 using AAV9 and intrathecal injections required detailed characterisation and validation. The viral delivery of GluClv2.0 specifically to primary afferents to broadly silence DRG neurons while interrogating sensory function will be addressed. I intend to extend this to the context of neuropathic pain and investigate the chemogenetic silencing of DRG

neurons on evoked and non-evoked pain. This work will facilitate future strategies for the targeted silencing of defined sensory neuron populations.

2. Methods

2.1. Animals

All mice were group-housed in individually ventilated cages with free access to food and water, in humidity and temperature controlled rooms with a 12 hr light-dark cycle, in a pathogen free facility. All animal procedures adhered to the UK Home Office (Scientific Procedures) Act (1986) and were performed under a UK Home Office Project Licence. All animal experiments were carried out in accordance with University of Oxford Policy on the Use of Animals in Scientific Research. The work within this study also conforms to the ARRIVE guidelines (Kilkenny *et al.*, 2010). C57BL/6 wild type mice were purchased form the Oxford University Breeding Unit. All experiments were carried out on adult male and female mice.

2.2. Surgery

2.2.1. Intrathecal injection

C57BL/6 mice, 6-8 weeks old (18-25 g) and of mixed genders, were used for intrathecal (i.t.) injection surgery. Each animal was anesthetised using 2% isoflurane and prepared for surgery by shaving a region over the thoracic vertebrae. Following incision site sterilisation (Iodine, alcohol wipe) a 1-2 cm incision was made to the back (rostral to caudal) above the spine. T-10 and T-11 vertebrae were located, soft tissue was carefully and sparingly removed lateral to the midline to expose the dura and spinal cord. A drop of lidocaine was applied to the dura for approximately 1-2 mins then removed. Using a 30 gauge needle the dura was carefully punctured (CSF leak at this point suggested a successful puncture). An ‘in house’ developed cannula system was designed by connecting tubing of decreasing size until the final cannula tip measured 0.008 in (O.D) x 0.004 in (I.D). The end of the cannula was inserted approximately 1 cm caudal into the subdural space. Using a syringe pump driver, 8 µl of AAV (AAV9-GFP or AAV9-GluClα and/or AAV9-GluClβ) was injected into the subdural space at a

rate of 1 µl/min. Following injection, the cannula was allowed to rest in position for 2 min to avoid back flow and then slowly removed. The dura was coated with a single drop of dura gel (Cambridge NeuroCare) to seal the dura and prevent further CSF leak. Finally, the incision site was sutured closed and appropriate post-operative care and analgesics given (local 2 mg/kg Marcain, AstraZeneca and systemic 5 mg/kg Rimadyl, Pfizer). Animals were used for behaviour or histology at least 3 weeks post-surgery.

2.2.2. Spared nerve injury (SNI)

Mice were anaesthetised using 2% isoflurane and prepared for surgery by shaving and sterilising the leg. A small incision was made to the thigh skin parallel to the thigh bone. The sciatic nerve was identified through separation of muscle and connective tissue. The sciatic nerve branches into three nerves, the common peroneal, tibial and sural. The branching points were identified and a non-absorbable suture was used to tie the common perineal and tibial nerves prior to nerve transection. The sural nerve was untouched and left intact. The site was closed and appropriate post-operative care given (local 2 mg/kg Marcain, AstraZeneca and systemic 5 mg/kg Rimadyl, Pfizer).

2.3. Virus production

Optimised GluClv2.0-αβ transgenes were excised and inserted into separate AAV packaging plasmids using BamHI/NotI (β) and HindIII/NotI (α) restriction enzymes and standard ligation protocols. The AAV plasmid contained a 1.8 kb CAG promoter. AAV serotype 9 viral particles containing GluClα or GluClβ were made commercially by Penn Vector Core in the Gene Therapy Program of the University of Pennsylvania to a final titre of $2.4x10^{13}$ gene copies (GC)/ml (AAV9-GluClα) and $1.5x10^{13}$ GC/ml (AAV9-GluClβ). AAV9-GFP was purchased as a stock virus from Penn Vector Core ($1.2x10^{13}$ GC/ml).

2.4. Ivermectin

Sterile ivermectin (Noromectin®, Norbrook Laboratories) was diluted 1:1 in sterile propylene glycol and administered via intraperitoneal injection (i.p.) at 1 µl/g of body weight.

2.5. Immunohistochemistry (IHC)

2.5.1. DRG, SCG, Nodose ganglia and lumbar sympathetic chain.

Animals were deeply anesthetised with pentobarbital, and the blood cleared from all tissues by perfusing saline through the vascular system. Mice were then perfuse-fixed using 4% paraformaldehyde (PFA). Tissues were then collected and post-fixed in 4% PFA for 1-2 hrs. All tissues were cryoprotected in 30% sucrose for a minimum of 48 hrs followed by embedding the tissue and sectioning on a cryostat (12 µm). Samples were washed in PBS and blocked in a blocking solution (5% normal donkey serum, 0.3% TritonX-100, PBS) for 1 hr at room temperature (RT). Primary antibodies (appendix Table 1) were diluted in blocking solution and applied to tissue overnight at RT. The next day samples were washed in a wash solution (0.3% TritonX-100, PBS) followed by a 2 hr incubation with secondary antibodies (appendix table 1) diluted in wash solution at RT. Samples were mounted using Vectorshield and imaged.

2.5.2. Brain, Spinal cord and Skin

Animals were perfused and tissue dissected as is detailed above. Brain, spinal cord and hind paw skin were post fixed for 24 hr, 24 hr and 2 hr respectively, cryoprotected and embedded in OCT as mentioned previously. Using a cryostat, brain (30 µm), spinal cord (30 µm) and skin (14 µm) were sectioned. All tissue sections were either frozen at -80^{o}C or immediately used for IHC. Brain, spinal cord and skin sections were stained in the same manner as stated previously.

2.6. Imaging and analysis

All IHC experiments were analysed using a Lecia LSM 710 confocal microscope in conjunction with 20X (air) and 40X (oil) objectives and Zeiss 2012 imaging software. Images were analysed using Fuji/ImageJ (NIH). For quantification at least three sections per animal were used, with at least 3 animals per group.

2.7. Behaviour

Both male and female mice were used in this study and mice were tested at a consistent time of day, in the same environment. Mice were habituated to their testing environment and equipment prior to behavioural test days. The experimenter was blind to animal genotype prior to testing and until after behavioural analysis was complete. All tests were conducted to achieve a baseline then repeated once 24 hrs post IVM administration, unless other wise stated.

2.7.1. von Frey: Mice were randomly assigned a test box (5 x 5 x 10 cm) which was elevated on a wire mesh base and were acclimatised to the equipment for 30-60 mins. Mice were then tested on their plantar hind paws using calibrated von Frey hairs (Linton Instrumentation) using the 'up-down' method (Dixon, 1980) to evaluate their 50% paw withdrawal thresholds. Responses from left and right paws were averaged on three different days to obtain an average baseline value, except for post SNI testing.

2.7.2. Hargreaves: Mice were randomly assigned a test box (5 x 5 x 10 cm) which was elevated on a glass base and were acclimatised to the equipment for 30-60 mins. Mice were then tested on their plantar hind paws using Hargreaves apparatus which provides a radiant laser heat source. The latency for mice to withdraw their hind paws was assessed, three times per paw, on three different days to obtain a baseline value. Mice were re-

tested post 24 hrs post IVM and another cohort over a time course 4 hr, 1 d, 3 d, 6 d, 10 d, post IVM.

2.7.3. Pinprick: Mice were randomly assigned a test box (5 x 5 x 10 cm) which was elevated on a wire mesh base and were acclimatised to the equipment for 30-60 mins. Mice were then tested on their plantar hind paws using a pin attached to a 1 g calibrated von Frey filament (Arcourt *et al.*, 2016). Mice were video recorded using a Sony Xperia phone at 120 fps (8.33 ms per frame) and the latency to withdraw from the pinprick analysed, three times per paw, on three different days.

2.7.4. Rotarod: All mice were briefly acclimatised to the rotarod apparatus (Ugo Basile, 47600) and the order that mice were tested was randomised. Mice were placed onto the rotarod equipment while the central rod rotated at a speed of 32 rpm. The latency to fall was recorded on two different days to achieve a baseline.

2.7.5. Beam walk: All mice were briefly acclimatised to the beam walk test (Carter, Morton and Dunnett, 2001) and the order that mice were tested was randomised. The beam walk consisted of a 1 m horizontal elevated beam (width 12 mm), light source at the start site and darkened box at the finish site. Mice were assessed for the number of mistakes/slips made while walking from start to finish. Mice were tested on two different days to generate a baseline.

2.7.6. Cold place preference: Mice were briefly acclimatised to the cold place preference apparatus (temperature not set, equipment at RT) and the order that mice were tested was randomised. Mice were placed in a two chamber paradigm consisting of two chambers, divided by a small corridor, where one base was set to room temperature 22^{o}C and the other set to 16^{o}C. To avoid learning, chamber temperature was randomised. Mice were allowed to freely explore over a 10 min period and time in each chamber live scored.

Mice were assayed on two different days to achieve a pre injury baseline value, and on day 7 for a post injury baseline value and on day 8 (24 hrs post IVM).

2.7.7. Conditioned place preference (CPP): Mice were not acclimatised to the CPP apparatus (76-0278, Harvard apparatus) as it is a paradigm that heavily relies on novelty and exploration. The CPP apparatus consisted of two large chambers and a small connecting chamber. The two large chambers had distinguishing features, spots or stripes and distinguishing scents, vanilla or strawberry (a small amount of scented lip balm applied to the top of the chamber). The cohort was assigned a random order for testing. On day 1 nerve-injured mice were allowed to freely explore the CPP apparatus for 15 min and were live tracked using ANYMaze software (Stoelting Co.), mice were excluded if they had a strong initial preference for a chamber (>720 secs or <180 secs). At the end of day 1 all mice received I.P IVM. On day 2 mice were conditioned for 30 min in the morning to a chamber following a 5 µl saline injection i.t. (lumbar puncture style). 4 hours later mice were i.t. injected with 5 µl clonidine (10 µg) and conditioned to the alternate chamber for 30 min. Chamber assignments were randomised and balanced. On day 3 mice were allowed to freely explore all chambers for 15 min, video tracked and were assessed for chamber preference compared to day 1 tracking values.

2.8. Statistical analysis

All data was tested for normality using the D'Agostino-Pearson normality test and the appropriate parametric or non-parametric statistical tests used accordingly. All statistical tests used were two-tailed. Statistical comparisons were made using a Student's t-test or Mann Whitney U-test. In experimental groups in which multiple comparisons were made one way or two-way analysis of variance (ANOVA) tests with appropriate *post-hoc* tests were performed. All ANOVA results, details and

tables can be found in the appendix. All data is represented as mean ± the standard error of the mean (S.E.M.) unless otherwise stated. Statistical significance is indicated as follows * $P < 0.05$, ** $P < 0.01$, *** $P < 0.001$, **** $P < 0.0001$. The statistical test used is reported in the appropriate figure legend. Graph Pad prism 6 was used to perform statistical tests and graph data. Adobe Illustrator CS5 was used to create schematics.

3. Results

3.1. Intrathecal AAV9.GluClα/β specifically transduces dorsal root ganglia neurons

To take the GluCl silencing system *in vivo*, the generation of viruses were required to target DRG neurons. We tested AAV9 as it previously showed good tropism for DRG neurons (Schuster *et al.*, 2014). While direct lumbar puncture style i.t. injection showed expression in CNS structures, the profile of expression following our surgical approach had not been tested. To optimise delivery and understand transduction efficiency of AAV9 in my hands, mice were first i.t injected with AAV9.GFP and 4 weeks later assessed for GFP expression (Fig. 1A). DRGs taken from the lumbar (L4/L5) levels showed successful GFP expression (Fig. 1B) and in a range of classic DRG subpopulations (Fig. 1C).

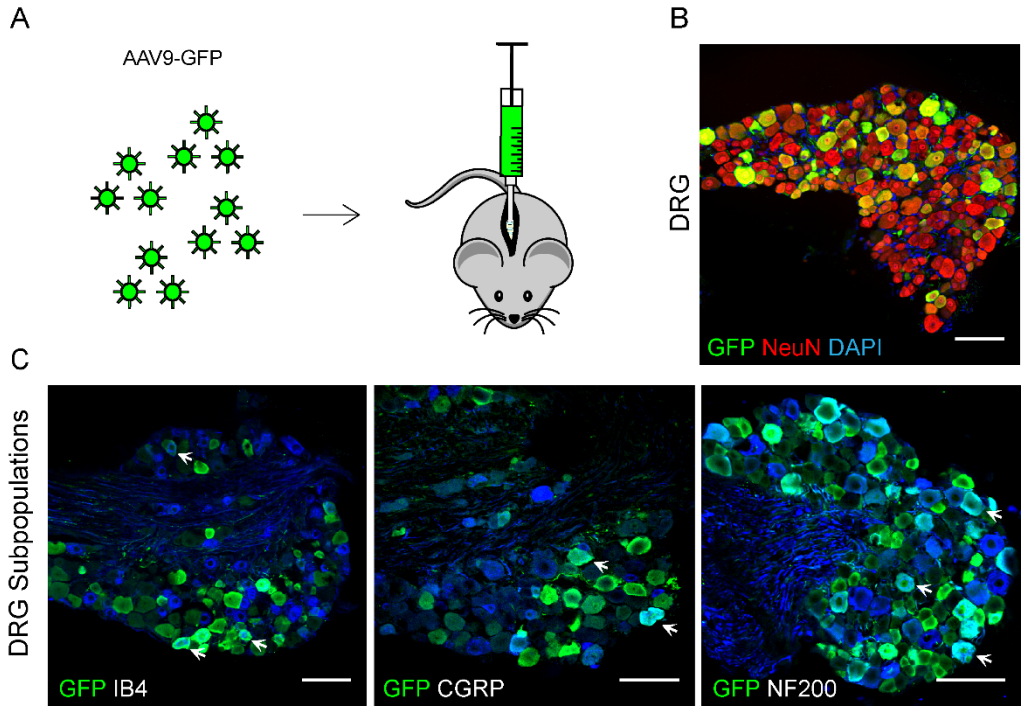

Figure 1: AAV9-GFP effectively transduces DRG neurons *in vivo*.

A) A diagram outlining the intrathecal injection of AAV9-GFP into C57BL/6 mice. **B)** Lumbar DRG neurons which are GFP+ following a single AAV9-GFP injection. Scale bar 100 μm. **C)** GFP expression is seen in the three major subpopulations of DRG neurons. Co-localisation (white arrows) of GFP with IB4, CGRP and NF200 respectively. Scale bar 100 μm.

This pilot experiment provided confidence that AAV9 was appropriate and the intrathecal delivery system was effective. The optimised GluClv2.0 constructs were commercially packaged into two individual AAV9 viruses. Wild type mice were i.t. injected with a cocktail of AAV9.GluClα (4 µl) and AAV9.GluClβ (4 µl) (Fig. 2A) and four weeks post injection tissue was assessed for GluCl expression. Lumbar DRG collected from injected mice demonstrated high levels of GluCl expression (66.02 ± 0.16%) (Fig. 2B-C) which targeted a range of DRG neurons of different sizes (Fig. 2D). GluCl expression was unbiased and non-preferential for any of the classical DRG subpopulations such as those expressing, CGRP, IB4, NF200 or parvalbumin (Fig. 2E-F). Importantly, it was possible to see that GluCl expression was not restricted to DRG cell bodies. It was possible to visualise GluCl positive projection terminals in the dorsal horn of the spinal cord (Fig. 2G) and in PGP9.5 positive fibres of hind paw skin (Fig. 2H).

Finally, it was important to ensure that there was no undesired expression of GluCl following our i.t. injections. Motor neurons (Fig. 2G), brain (Fig. 3A), the nodose sensory ganglia (Fig. 3B), the sympathetic superior cervical ganglia (Fig. 3C) and the lumbar sympathetic chain (Fig. 3D) were all assessed for off target GluCl expression. GluCl expression was absent in all of these structures.

Taken together, AAV9.GluClv2.0 effectively transduces DRG neurons and equally targets different DRG subpopulations without bias for a particular population. The combination of the delivery method and viral serotype resulted in no off-target GluCl expression.

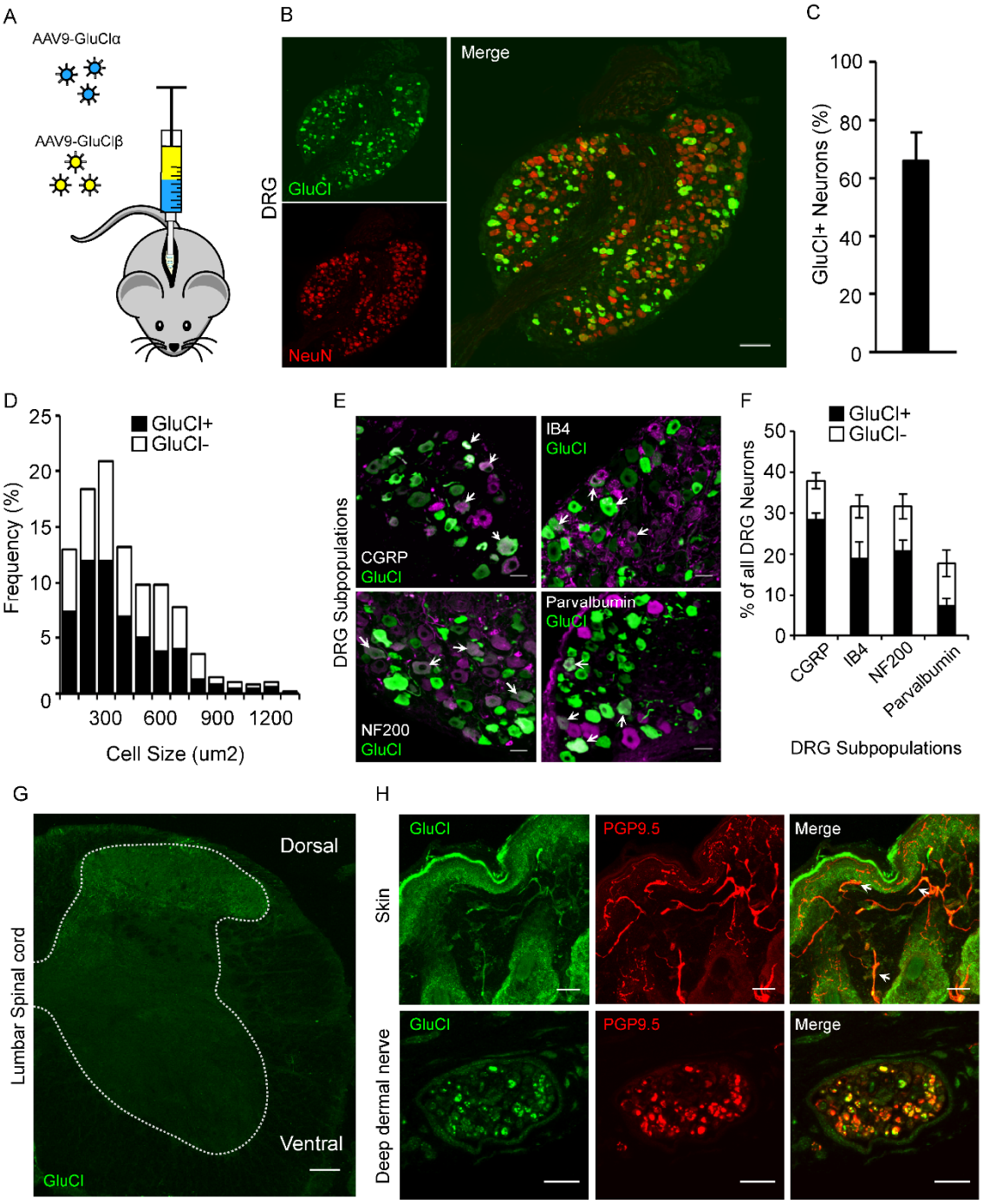

Figure 2: AAV9-GluClαβ can successfully transduce DRG neurons *in vivo*.

A) A diagram outlining the intrathecal injection of AAV9-GluClαβ. **B)** GluCl expression in L4 DRG following in a single injection. GluCl/YFP-Green, Neuronal marker/NeuN- Red. Scale bar 100 µm. **C)** Quantification of GluCl positive neurons as a proportion of total neurons. Data from 3 animals and a total of 912 neurons. **D)** Size frequency of GluCl+ (black) and GluCl- (white) neurons. Data from 3 animals and a total of 379 neurons. **E)** GluCl expression and co-localization with subpopulation markers (magenta). Arrows indicate overlapping neurons. Scale bar 30 µm. **F)** Quantification of GluCl positive neurons in each subpopulation. Data from 3 animals and > 600 neurons per subpopulation. **G)** Example lumbar spinal cord section showing GluCl expression in

primary afferents entering the dorsal horn and no signal observed in ventral motor neurons. Scale bar 100 µm. **H)** GluCl expression in cutaneous primary afferents. Top: skin, Bottom: deep dermal nerve. Scale bar 20 µm. All data is mean ± S.E.M.

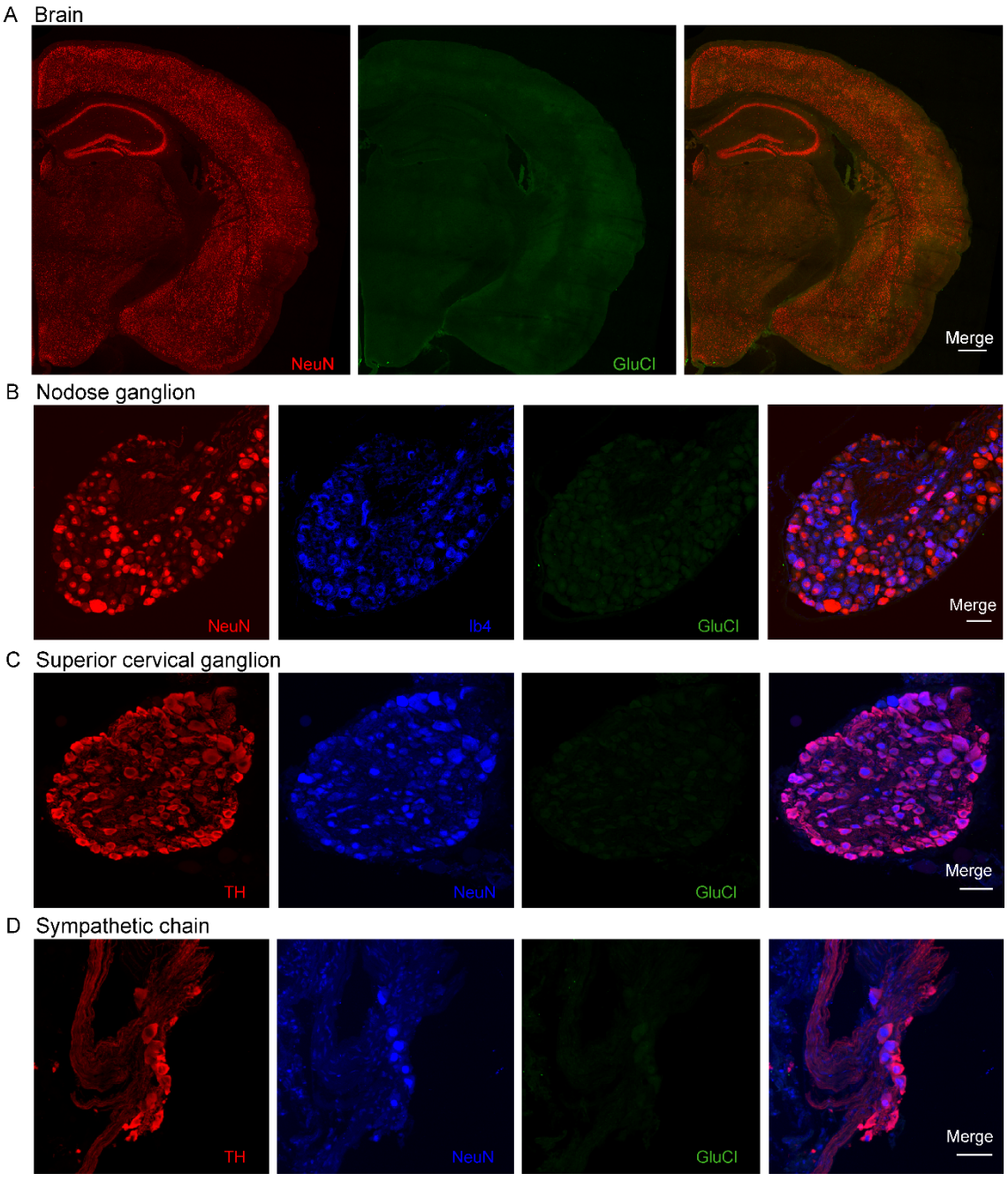

Figure 3: GluCl expression is absent in the brain, sympathetic ganglia and other sensory ganglia. Whole brains and a range of ganglia were assessed from GluCl+ animals following i.t. delivery of AAV9-GluClαβ (n = 3 animals). No GluCl expression was observed in (**A**) brain (scale bar 500 µm), (**B**) nodose ganglion (sensory), (**C**) Superior cervical ganglion (sympathetic), or (**D**) lumbar sympathetic chain neurons. Scale bar represents 50 µm unless stated otherwise. *TH-tyrosine hydroxylase*

3.2. Long-term GluCl expression does not cause overt cellular injury or peripheral neuropathy

Introducing and expressing a transgene can be transient and has the potential in itself to cause injury or damage to the peripheral nervous system. For instance, AAV6 transduction rates decreased over time (Mason *et al.*, 2010). Therefore, a small cohort of animals were maintained for 7 months to address these points. GluCl expression was observed in 36.86 ± 2.1% of L4 DRG neurons 7 months post a single i.t injection (Fig. 4a). To determine any evidence of cellular injury DRG sections were stained for the well-established injury marker, activating transcription factor 3 (ATF3) (Tsujino *et al.*, 2000). In β-only and αβ animals there was low level expression of ATF3, similar to naïve animals (Fig. 4b). For all *in vivo* studies we used β-only as our control to ensure that phenotypes observed in our test group were not due to viral delivery. In contrast, and as a positive control, ATF3 expression in animals subjected to the spared nerve injury (SNI) model of neuropathic pain was quantified. Neuropathic animals had a significantly higher percentage of ATF3 positive neurons compared to all other groups (Fig. 4b). Equally, a well-established method to assess peripheral neuropathy is calculating intra-epidermal nerve fibre density (IENFD). All three groups of animals: naïve, β-only and αβ, had normal and comparable IENFDs with no sign of peripheral neuropathy (Fig. 4c). Therefore, a single i.t. injection of AAV9.GluCl leads to long-lasting expression and does not result in cellular injury or neuropathy.

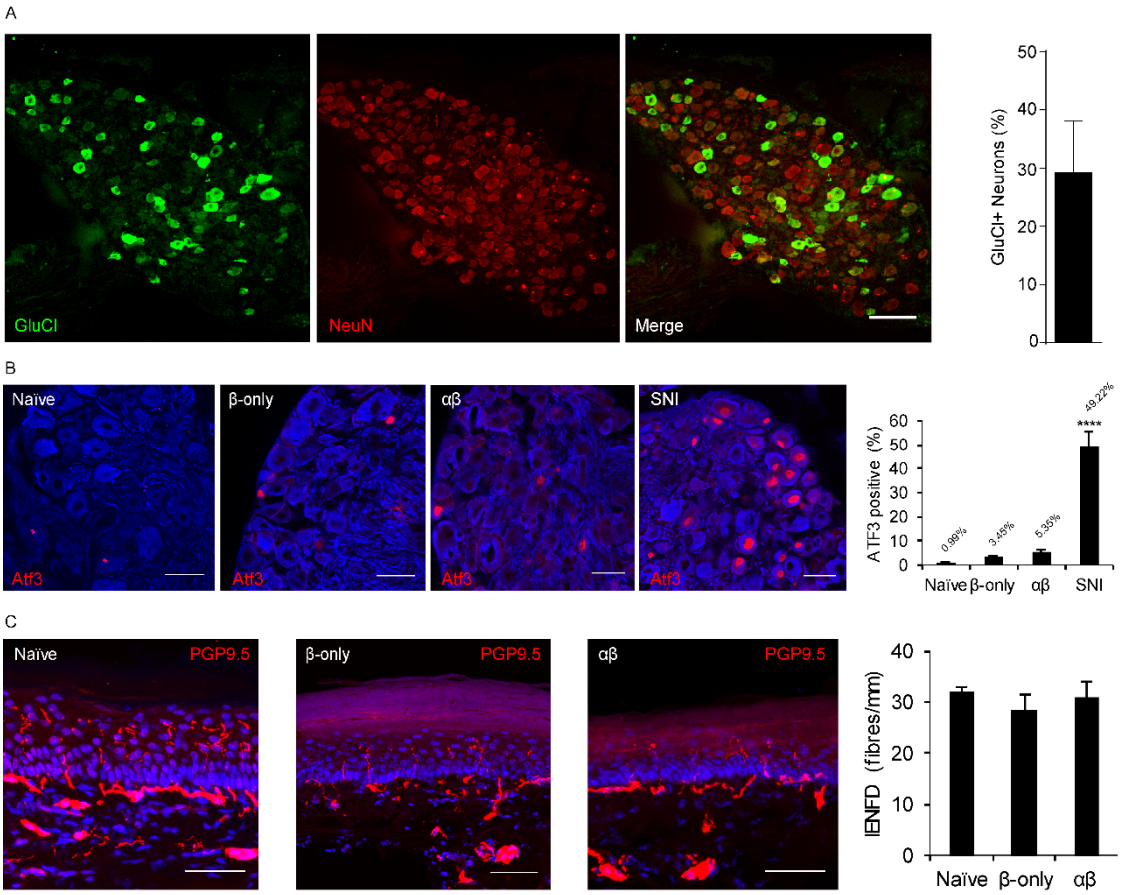

Figure 4: GluCl expression, ATF3 injury marker expression and intra-epidermal nerve fibre densities in aged GluCl+ animals. Tissue derived from animals 7-months following i.t. delivery of AAV9-GluClαβ. **A)** Left: L4 DRG immunostained for GluCl (green) and NeuN (red). Scale bar, 100 µm. Right: Total neurons that were GluCl+ from four animals and a total of 1762 cells. **B)** Left, Representative images of β-III tubulin (blue) and ATF3 (red) staining of L4 DRG sections. Naïve group represents age matched animals that did not undergo i.t. surgery and SNI group represents animals 4-weeks post SNI as a positive control for nerve injury. Right, Quantification of ATF3 expression as a percentage of total neurons. (n = Naïve 3 animals, β-only 3 animals, αβ 4 animals, SNI 4 animals. One-way ANOVA followed by *post-hoc* Bonferroni test, naïve vs β-only; t = 0.414, df = 10, P = >0.99. Naïve vs αβ; t = 0.785, df = 10, P = >0.99. Naïve vs SNI, t = 8.66, df = 10, P < 0.0001, ****). **C)** Left, representative images of DAPI (blue) and PGP9.5 (red) staining of hind paw glabrous skin of aged cohorts. Right, Quantification of intra-epidermal nerve fibre density (IENFD). (n = Naïve 3 animals, β-only 3 animals, αβ 4 animals, one-way ANOVA followed by *post-hoc* Bonferroni test, Naïve vs β-only; t = 0.89, df = 7, P = 0.80. Naïve vs αβ; t = 0.327, df = 7, P >0.99). All data is mean ± S.E.M.

3.3. Silencing DRG neurons can increase acute pain withdrawal thresholds *in vivo*.

As a proof of principle and to test the efficacy of optimised GluClv2.0 silencing *in vivo*, acute pain withdrawal thresholds were assessed following AAV9.GluCl and ivermectin treatment. C57BL/6 mice were i.t. injected with AAV9.GluClαβ or AAV9.GluClβ-only and 4 weeks later, behaviourally phenotyped pre and 24 hr post 5 mg/kg i.p. IVM. Mice were assayed for the mechanical detection thresholds (von Frey), latency to withdraw from a noxious radiant heat source (Hargreaves), latency to withdraw from a noxious mechanical stimulus (pin prick), as well as motor and proprioceptive tasks (rota rod and beam walk respectively). Compared to the β-only control group, GluClαβ^{+} mice dosed with IVM displayed hyposensitivity to von Frey and increased latencies to withdraw from Hargreaves and pinprick (Fig. 5A-C). However, both αβ and β-only mice performed similarly on the rota rod and beam walk tasks following IVM treatment (Fig. 5D-E). To interrogate the reversibility of the GluCl/IVM mediated silencing of sensory function, a cohort of mice were tracked over time following a single dose of IVM. Using the Hargreaves assay, the latency to withdraw following 5 mg/kg IVM did not change after 4 hours in both groups. However, the withdrawal latencies were significantly increased at 1 day and 3 days post IVM in αβ mice compared to β-only mice (Fig. 5F). This was recovered by 6 days post IVM (Fig. 5F). To examine whether GluCl/IVM mediated silencing was repeatable, GluClαβ expressing mice were given one dose of IVM and displayed thermal hyposensitivity (Fig. 5G) and seven days later, when baseline thermal sensitivity returned to normal, the same cohort was given a second IVM. One day after the second dose of IVM, mice displayed thermal hyposensitivity and increased latencies to withdraw from the Hargreaves apparatus (Fig. 5G). Together, these results demonstrate that GluClv2.0 can effectively silence DRG neurons *in vivo* and

increase mechanical and thermal pain thresholds in a robust, reversible and repeatable manner.

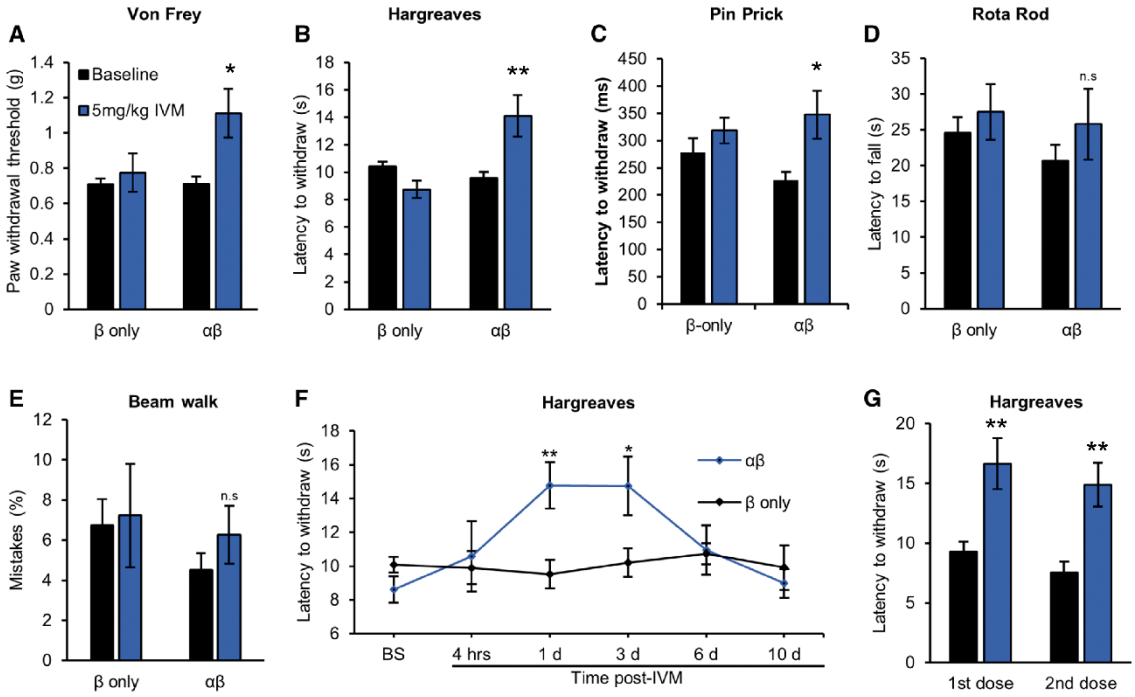

Figure 5: GluCl activation *in vivo* increases acute pain withdrawal thresholds.

Mice expressing GluCl were subject to mechanical, thermal and motor function assays pre (baseline) and 24 hrs post 5 mg/kg IVM. **A)** von Frey for mechanical detection (n = β-only 14 mice, αβ = 13 mice, RM two-way ANOVA with *post hoc* Bonferroni, pre vs post IVM. β-only; t = 0.313, df = 25, P > 0.99. αβ; t = 3.050, df = 25, P = 0.0107, *). **B)** Hargreaves assay for heat pain thresholds (n = β-only 14 mice, αβ = 13 mice, RM two-way ANOVA with *post hoc* Bonferroni test, pre vs post IVM, β-only; t = 1.502, df = 25, P = 0.291. αβ; t = 3.96, df = 25, P = 0.0011, **). **C)** Pin prick assay for noxious mechanosensation (n = β-only 11 mice, αβ = 10 mice, RM two-way ANOVA with *post hoc* Bonferroni test, pre vs post IVM, β-only; t = 1.05, df = 19, P = 0.609, αβ; t = 3.026, df = 19, P = 0.0139, *). **D)** Rotarod motor function test (n = β-only 14 mice, αβ = 13 mice, RM two-way ANOVA with *post hoc* Bonferroni test, pre vs post IVM, β-only; t = 0.684, df = 25, P > 0.99, αβ; t = 1.17, df = 25, P = 0.506). **E)** Beam walk, a proprioceptive task (n = β-only 8 mice, αβ = 9 mice, RM two-way ANOVA with *post hoc* Bonferroni test, pre vs post IVM, β-only; t = 1.24, df = 15, P = 0.462, αβ; t = 0.22, df = 15, P > 0.99). **F)** Time course analysis of GluCl activation and silencing of heat pain following a single dose of IVM (n = β-only 12 mice, αβ = 10 mice, RM two-way ANOVA and *post hoc* Bonferroni test β-only vs αβ, 1d: t = 3.646 , df = 132, P = 0.0023, **. 3d: t = 2.785, df = 132, P = 0.0363, *). **G)** Silencing thermal sensitivity following two doses of IVM given three weeks apart (n = αβ 6 mice, RM two-way ANOVA with *post hoc* Bonferroni test pre vs post IVM. 1st dose: t = 3.388, df = 20 , P = 0.058, **. 2nd dose: t = 3.402, df = 20, P = 0.0057 **). All data mean ± S.E.M. BS = Baseline.

The long-lasting action of GluCl/IVM silencing makes it an ideal system to study neuropathic pain. Neuropathic pain arises and is maintained due to hyperexcitability of primary afferents, where ectopic DRG activity (Wall and Gutnick, 1974; Wall and Devor, 1983; Kajander and Bennett, 1992; Boucher *et al.*, 2000; Wu *et al.*, 2001) and afferent sensitisation occurs (Shim *et al.*, 2005; Smith, O'Hara and Stucky, 2013). The SNI model of neuropathic pain was used to address the ability of GluCl/IVM to silence neuropathic pain at its source. Mice were i.t. injected with AAV9.GluClαβ or β-only, and 3 weeks later underwent SNI. Animals were subsequently behaviourally tracked for 21 days. Robust mechanical hypersensitivity was observed in both αβ and β-only mice. However, αβ mice partially recovered following a single dose of IVM and repeated dosing resulted in repeated recovery (Fig. 6B). Neuropathic mice also exhibit hypersensitivity to cold stimuli (Balayssac *et al.*, 2014). Using the operant measure of cold place preference, neuropathic mice from both groups spent less time at 16ºC compared to baseline. This cold zone avoidance was completely lost post IVM in αβ but not β-only expressing mice, suggesting a recovery from cold hypersensitivity (Fig. 6C). There was a discrepancy that the mechanical hypersensitivity was partially recovered and the cold hypersensitivity full recovered following silencing. It was reasoned that perhaps mechanical sensitivity requires a larger population of cells to be silenced and therefore requires higher GluCl transduction. To address this, αβ tissue was analysed *post-hoc* and GluCl expression plotted against the percentage rescue (Fig. 6D). Indeed, there was a strong correlation between the percentage of neurons expressing GluCl and the degree of rescue (Fig. 6D).

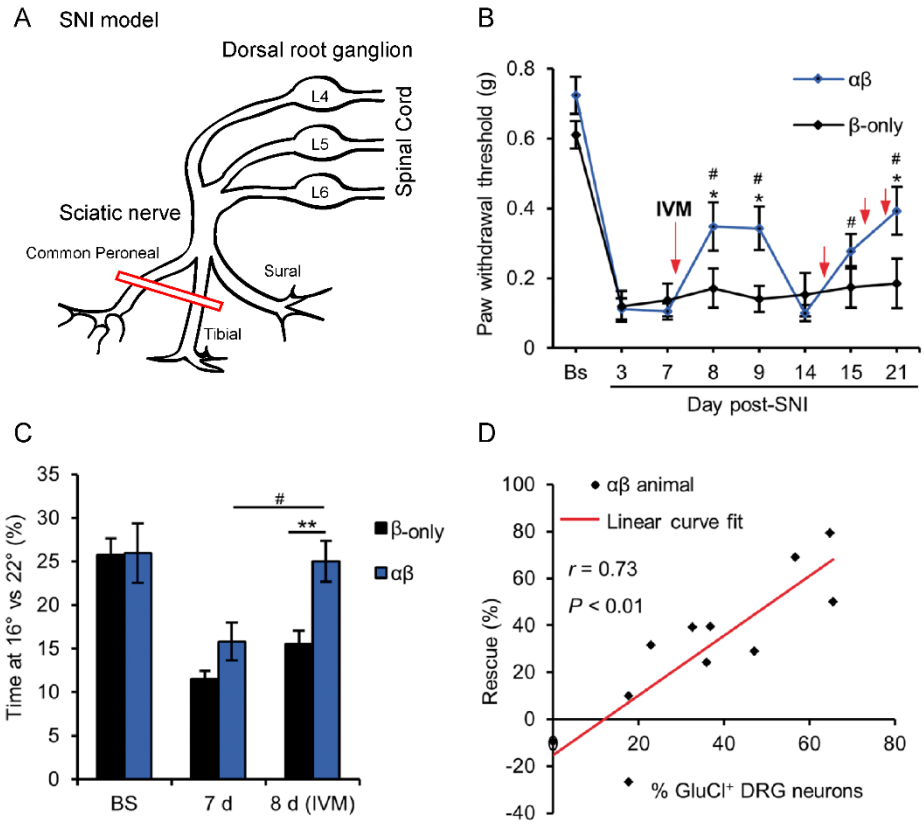

Figure 6: GluCl mediated silencing elevates neuropathic pain-related hypersensitivity.

A) The spared nerve injury (SNI) model of neuropathic pain. Red bar illustrates nerve transection. **B)** The mechanical hypersensitivity tracked post-SNI in both GluClβ and GluClαβ expressing mice. Red arrow indicates the time of IVM (5 mg/kg) administration (n = β-only 11 mice, αβ = 11 mice, RM two-way ANOVA with *post hoc* Bonferroni test, β-only vs αβ, d8: $t = 3.144$, $df = 160$, $P = 0.015$, *, d9: $t = 2.845$, $df = 160$, $P = 0.0395$, *, d21: $t = 3.148$, $df = 160$, $P = 0.0156$, *. *Post hoc* Bonferroni test, αβ post-SNI time points compared to day 7, d8: $t = 4.288$, $df = 140$, $P = 0.0002$, # , d9: $t = 4.192$, $df = 140$, $P = 0.0003$, #, d15: $t = 3.093$, $df = 140$, $P = 0.016$, #, d21: $t = 5.051$, $df = 140$, $P < 0.0001$, #). **C)** Cold hypersensitivity assayed for using cold place preference at day 7 and 8 post-SNI. A single dose of IVM recovered the cold hypersensitivity in the GluClαβ expressing cohort (n = β-only 11 mice, αβ = 11 mice, RM two-way ANOVA with *post hoc* Bonferroni test, β-only vs αβ, d8: $t = 3.065$, $df = 60$, $P = 0.0098$, **. Post hoc Bonferroni test, d7 vs d8, αβ: $t = 3.452$, $df = 40$, $P = 0.0027$, #). **D)** The observed correlation between L4 DRG neurons expressing GluCl and the rescue of mechanical hypersensitivity following IVM in GluClαβ expressing mice (n = 11 mice, Pearson's correlation co-efficient, $r = 0.73$, $P = 0.0057$). All data is mean ± S.E.M.

Primary afferent driven ectopic activity is thought to underly the spontaneous non-evoked component of neuropathic pain (Haroutounian *et al.*, 2014). Assessing spontaneous pain in rodents is challenging, however groups have successfully shown that using a CPP assay on rodents experiencing neuropathic pain exhibit a preference for environments where a non-addictive analgesic is given (King *et al.*, 2009). We argue that primary afferent chemogenetic silencing could cease on-going primary afferent activity and spontaneous pain. To address this, a pilot experiment was designed whereby the CPP paradigm was conducted while DRGs were silenced, the expected outcome being a loss of analgesic preference. The pilot experiment timeline and CPP paradigm used are illustrated in Fig. 7A-B. Neuropathic β-only control mice exhibited a preference for the clonidine paired chamber and αβ mice did not show a clear preference for the clonidine paired chamber. Significance was not reached because of the small group size, however this pilot experiment indicates that chemogenetic silencing of primary afferents may abolish an analgesic CPP as αβ expressing mice are not experiencing on-going tonic pain.

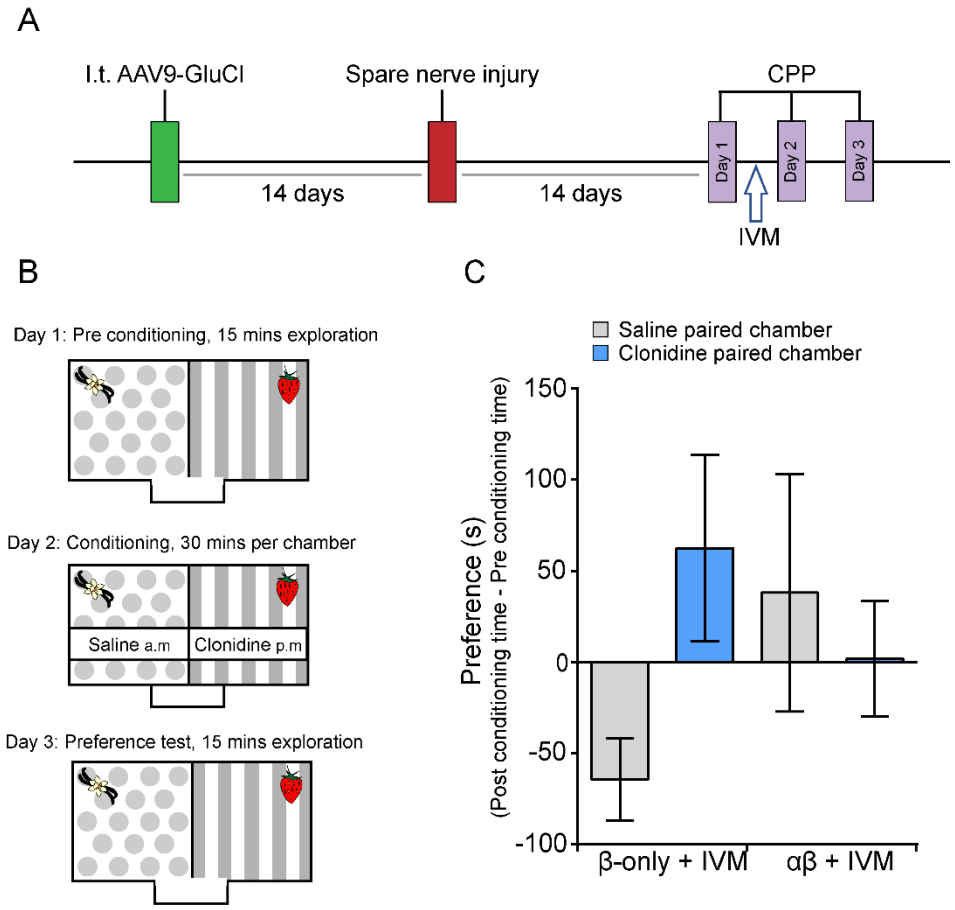

Figure 7: GluCl activation can alleviate the non-evoked spontaneous component of neuropathic pain.

A) The timeline of the experiment. **B)** The conditioned place preference paradigm used to assess tonic on-going pain. **C)** The preference for the saline-paired chamber (grey) and clonidine paired chamber (blue). There is a trend for preference for the clonidine-paired chamber in the control group and no clear preference in the experimental group. (n = 4 mice per group, two-way ANONA *post hoc* Bonferroni, clonidine chamber β vs αβ, $t = 0.939$, $df = 12$, $P = 0.732$). Using this preliminary data and G*Power 3.1.9.2. the sample size required to see a significant difference in preference for the clonidine paired chamber between the two groups, when $\alpha = 0.05$, power = 80%, n = 19 mice per group.

4. Discussion

The optimised GluClv2.0 was employed *in vivo* to target and silence peripheral sensory neurons. AAV9 successfully targeted DRG neurons following a single intrathecal injection without off target expression in other regions. Upon administration of low doses of IVM, multimodal sensory hyposensitivity was observed, without motor deficits. Additionally, the chemogenetic silencing of primary afferents lead to the recovery of neuropathic pain.

The intention to use GluClv2.0 *in vivo* required the generation and delivery of AAVs containing optimised GluClα and β subunits. Many AAV serotypes have been trialled for the targeting of rodent DRG neurons, but AAV9 was considered superior (Mason *et al.*, 2010; Schuster *et al.*, 2014). AAV9 has been praised for its ability to cross the blood-brain barrier allowing the targeting of CNS tissues (Foust *et al.*, 2009; Gray *et al.*, 2011). One study carried out a detailed analysis of AAV9 introduced intravenously or intrathecally in mice (Schuster *et al.*, 2014). Intravenous AAV9.GFP showed modest efficiency at transducing DRG neurons, while lumbar puncture style intrathecal AAV9-GFP was extremely effective (Schuster *et al.*, 2014). However, Schuster *et al*. (2014), noted that their intrathecal injections of AAV9 led to transgene expression in CNS regions. This was likely due to viral particles having entered the subarachnoid space. This is common for lumbar puncture style intrathecal injections due to limited control over injections and their delivery to subdural/subarachnoid spaces. To retain DRG specificity, we employed a system for intrathecal injections, where mice received an intrathecal slow viral infusion (via a canula) into the subdural space in a controlled surgical setting (Chisholm *et al.*, 2018). We confirmed that using this cannula style intrathecal approach, a single i.t. injection of AAV9.GFP lead to robust and high GFP expression in DRG sensory neurons. Our collaborators informed us this method prevents CNS expression, something investigated later in this chapter. This work

suggests our injection method was efficient and that AAV9 was a suitable serotype for further work.

AAV9.GluClα and AAV9.GluClβ were generated and intrathecally injected into C57BL/6 mice. Four weeks post a single injection of both GluCl subunits transduction efficiency averaged at 66.02 ± 0.16% and was non-preferential and equally distributed between DRG subpopulations. Transduced DRG neurons also showed expression in cutaneous primary afferent terminals and in central projections into the dorsal horn of the spinal cord. Importantly, there was no GluCl expression in dorsal horn or ventral horn neurons themselves. Silencing any of these two cell types would have been a major confound to this work. To confirm DRG specificity of our system, GluCl expression was assessed in other sensory and sympathetic ganglia as well as the brain. All structures, other than DRG neurons, were absent for GluCl expression, suggesting intrathecal delivery of our GluCl viruses was a suitable method to specifically target DRG neurons. This was encouraging as future interpretations of using GluCl chemogenetic silencing will not be confounded by the silencing of undesired regions.

Not only was it possible to specifically target DRG neurons with GluCl, but long term expression did not caused any obvious cellular injury or peripheral neuropathy. However, we did observe a lower percentage of transduction at 7 months compared to 4 weeks post injection. This could have been a surgical batch effect or perhaps there is a small degree of transgene down regulation over time. IVM use is FDA approved and routinely used in humans and small animals. Collectively, the GluCl silencing system can be considered safe and non-toxic.

There is some evidence that chemogenetic silencing of primary afferent results in acute pain inhibition (Iyer *et al.*, 2016; Saloman *et al.*, 2016). However, these studies used the inhibitory hM4Di DREADD and as discussed in Chapter 2, DREADDs may not be suitable for use in sensory neurons. Therefore, a major aim was to use GluCl silencing in primary afferents and interrogate the efficacy of our system *in vivo*. As a proof of

principle, GluCl was expressed in a broad and non-selective population of DRG neurons *in vivo.* Following IVM administration both mechanical and thermal pain thresholds were elevated. It is known that IVM has other binding partners including P2X4 and $GABA_A$ receptors (Asatryan *et al.*, 2010; Franklin *et al.*, 2014; Estrada-Mondragon and Lynch, 2015). However, due to GluCl's enhanced IVM sensitivity and no requirement for IVM to cross the blood brain barrier, we were able to use IVM at doses low enough to not activate other receptors. In addition, we saw no sensory changes in control mice treated with our IVM dose. Interestingly, these *in vivo* experiments did not alter proprioceptive function despite the presence of GluCl in parvalbumin (PV) positive proprioceptive neurons. This was an unexpected advantage and perhaps suggests redundancy in the proprioceptive system that we do not yet fully understand. In addition, there is evidence that there is strong interplay between vision and proprioception (Sarlegna and Sainburg, 2009; Malik, Cote and Lam, 2017). Therefore, future assays could asses proprioception in darkness to remove the potential compensation from the visual system. Additionally, one major advantage of GluCl is the long lasting silencing following a single dose of IVM. It is possible this is due to slow IVM clearance and IVM being sequestered in the cell membrane and readily available for re-binding. Although, it is also possible that IVM sensitivity is so enhanced that it binds permanently and it is not until GluCl receptor turn over that we observe silencing recovery. These factors could also speak to the slow onset and off set of GluCl response. The IVM binding site is located in the membrane region of GluCl, therefore membrane IVM accumulation and clearance likely contribute to these onset and off set kinetics (Atif *et al.*, 2019). Further experiments are required to fully determine this mechanism of action of GluClv2.0, and it would be greatly aided by the generation of a tagged IVM molecule (Atif *et al.*, 2019). While, the IVM induced silencing was long lasting it was also slow in its onset. Therefore, experiments which require fast temporal resolution might not benefit from using the GluCl/IVM system. The ability to silencing sensory neurons for days was ideally suited to the study of chronic conditions such as neuropathic pain. The GluClv2.0 system was used in a mouse model

of neuropathic pain following a traumatic nerve injury (SNI). Following IVM administration the pain related mechanical hypersensitivity was alleviated, in a repeatable manner. The degree of recovery was strongly correlated to the percentage of DRG neurons expressing GluCl, a key point to consider if this was to ever to be translated therapeutically. GluCl mediated primary afferent silencing also fully reversed the cold hypersensitivity associated with the SNI model of neuropathic pain. This is the first demonstration of using a chemogenetic silencing system in a model of neuropathic pain. Since this work, a report has shown that the chemogenetic (DREADD) inhibition of nociceptors resulted in the prevention of high fat diet induced diabetic small fibre neuropathy in mice (Jayaraj *et al.*, 2018). In particular, the prevention of neuropathic pain related mechanical hypersensitivity. A second study developed a novel optogenetic silencer, termed BLINK2. This tool was employed and alleviated chemotherapy induced neuropathic hypersensitivity in rats (Alberio *et al.*, 2018). Together with our findings, this further supports that suppression of DRG neuron excitability can ameliorate neuropathic pain at its source.

However, Jayaraj *et al* (2018) and Alberio *et al* (2018), as well as many other studies in the neuropathic pain field, failed to interrogate the spontaneous non-evoked component of neuropathic pain, which is often the largest clinical complaint in patients with neuropathic pain (Colloca *et al.*, 2017). The pain field has trialled various new approaches to accurately assess spontaneous pain in rodent models. These include facial grimace scores and spontaneous nocifensive behaviours such as paw lifting or vocalisation. These methods are often very subjective and likely represent extreme pain. In addition, a hurdle using these methods is that rodents, as a pray species, often hide their pain for survival. However, one method to interrogate on-going spontaneous pain in rodents is an operant condition place preference assay, where neuropathic rodents form a preference for a non-addictive analgesic paired chamber (King *et al.*, 2009; Navratilova and Porreca, 2014). This assay is much less subjective and does not rely on

‘visualising’ pain in rodents. A pilot study was carried out to understand if the chemogenetic silencing of primary afferents was sufficient to cease tonic on-going pain following peripheral nerve injury. Indeed, the preliminary data looked encouraging and the chemogenetic silencing of DRG neurons may reduce the analgesic preference in neuropathic mice. One interpretation of this is that GluCl/IVM silenced the aberrant DRG activity and spontaneous tonic pain in neuropathic mice, which resulted in these mice not seeking the conditioning analgesic. This data is in its infancy but warrants replication alongside vigorous controls to ensure no other factors altered chamber preference.

To summarise, GluClv2.0 was selectively expressed in peripheral sensory neurons *in vivo.* This works provides proof of principle that GluCl chemogenetic silencing is an efficient and effective technology in the somatosensory system, *in vivo.* AAV9.GluClv2.0 can be used to silence a broad population of DRG sensory neurons, to elevate acute pain thresholds and treat neuropathic pain at its source. This work also shows that there is a necessity for primary afferent activity in neuropathic pain, in agreement with the early literature showing the efficacy of local anaesthetic block in the treatment of neuropathic pain. These data lay the foundations for the potential use of GluCl as a gene therapy, and as a powerful tool to silence distinct primary afferent populations to understand their circuitry and function in sensory biology.

5. Acknowledgements

All rodent surgeries and behaviour in this chapter were performed together and/or equally split between Dr Weir and myself. I produced the data presented in this chapter, which has been published in a peer reviewed journal. I have permission from the senior author to include my published work in this thesis.

6. References

Agbandje-McKenna, M. and Kleinschmidt, J. (2011) 'AAV capsid structure and cell interactions', *Methods in Molecular Biology*, pp. 47–92. doi: 10.1007/978-1-61779-370-7_3.

Alberio, L. *et al.* (2018) 'A light-gated potassium channel for sustained neuronal inhibition', *Nature Methods*. Nature Publishing Group, 15(11), pp. 969–976. doi: 10.1038/s41592-018-0186-9.

Arcourt, A. *et al.* (2016) 'Touch Receptor-Derived Sensory Information Alleviates Acute Pain Signaling and Fine-Tunes Nociceptive Reflex Coordination', *Neuron*. Elsevier Inc., 93(1), pp. 179–193. doi: 10.1016/j.neuron.2016.11.027.

Asatryan, L. *et al.* (2010) 'Ivermectin antagonizes ethanol inhibition in purinergic P2X4 receptors', *Journal of Pharmacology and Experimental Therapeutics*. American Society for Pharmacology and Experimental Therapy, 334(3), pp. 720–728. doi: 10.1124/jpet.110.167908.

Atchison, R. W., Casto, B. C. and Hammon, W. M. (1965) 'Adenovirus-Associated Defective Virus Particles', *Science*. American Association for the Advancement of Science (AAAS), 149(3685), pp. 754–755. doi: 10.1126/science.149.3685.754.

Atif, M. *et al.* (2019) 'GluClR-mediated inhibitory postsynaptic currents reveal targets for ivermectin and potential mechanisms of ivermectin resistance', *PLOS Pathogens*. Edited by A. J. Wolstenholme. Public Library of Science, 15(1), p. e1007570. doi: 10.1371/journal.ppat.1007570.

Balayssac, D. *et al.* (2014) 'Assessment of thermal sensitivity in rats using the thermal place preference test: Description and application in the study of oxaliplatin-induced acute thermal hypersensitivity and inflammatory pain models', *Behavioural Pharmacology*. Lippincott Williams and Wilkins, 25(2), pp. 99–111. doi:

10.1097/FBP.0000000000000026.

Bello, A. *et al.* (2009) ‘Isolation and evaluation of novel adeno-associated virus sequences from porcine tissues’, *Gene Therapy*, 16(11), pp. 1320–1328. doi: 10.1038/gt.2009.82.

Borgeat, A. and Aguirre, J. (2010) ‘Update on local anesthetics’, *Current Opinion in Anaesthesiology*. Lippincott Williams and Wilkins, pp. 466–471. doi: 10.1097/ACO.0b013e328339eef2.

Boucher, T. J. *et al.* (2000) ‘Potent analgesic effects of GDNF in neuropathic pain states’, *Science*, 290(5489), pp. 124–127. doi: 10.1126/science.290.5489.124.

Boutin, S. *et al.* (2010) ‘Prevalence of serum IgG and neutralizing factors against adeno-associated virus (AAV) types 1, 2, 5, 6, 8, and 9 in the healthy population: Implications for gene therapy using AAV vectors’, *Human Gene Therapy*, 21(6), pp. 704–712. doi: 10.1089/hum.2009.182.

Calcedo, R. *et al.* (2009) ‘Worldwide Epidemiology of Neutralizing Antibodies to Adeno-Associated Viruses’, *The Journal of Infectious Diseases*. Oxford University Press (OUP), 199(3), pp. 381–390. doi: 10.1086/595830.

Carter, R. J., Morton, J. and Dunnett, S. B. (2001) ‘Motor Coordination and Balance in Rodents’, *Current Protocols in Neuroscience*, 15(1), pp. 8.12.1-8.12.14. doi: 10.1002/0471142301.ns0812s15.

Chabal, C., Russell, L. C. and Burchiel, K. J. (1989) ‘The effect of intravenous lidocaine, tocainide, and mexiletine on spontaneously active fibers originating in rat sciatic neuromas’, *Pain*, 38(3), pp. 333–338. doi: 10.1016/0304-3959(89)90220-0.

Chan, K. Y. *et al.* (2017) ‘Engineered AAVs for efficient noninvasive gene delivery to the central and peripheral nervous systems’, *Nature Neuroscience*. Nature Publishing Group, 20(8), pp. 1172–1179. doi: 10.1038/nn.4593.

Chisholm, K. I. *et al.* (2018) ‘Large scale in vivo recording of sensory neuron activity with GCaMP6’, *eNeuro*. Society for Neuroscience, 5(1). doi: 10.1523/ENEURO.0417-17.2018.

Colloca, L. *et al.* (2017) ‘Neuropathic pain’, *Nature Reviews Disease Primers*. Macmillan Publishers Limited, 3, pp. 1–20. doi: 10.1038/nrdp.2017.2.

Dawes, J. M. *et al.* (2018) ‘Immune or Genetic-Mediated Disruption of CASPR2 Causes Pain Hypersensitivity Due to Enhanced Primary Afferent Excitability’, *Neuron*, 97(4), pp. 806-822.e10. doi: 10.1016/j.neuron.2018.01.033.

Deer, T. R. *et al.* (2017) ‘Dorsal root ganglion stimulation yielded higher treatment success rate for complex regional pain syndrome and causalgia at 3 and 12 months: A randomized comparative trial’, *Pain*. Lippincott Williams and Wilkins, 158(4), pp. 669–681. doi: 10.1097/j.pain.0000000000000814.

Deverman, B. E. *et al.* (2016) ‘Cre-dependent selection yields AAV variants for widespread gene transfer to the adult brain’, *Nature Biotechnology*. Nature Publishing Group, 34(2), pp. 204–209. doi: 10.1038/nbt.3440.

Devor, M., Wall, P. D. and Catalan, N. (1992) ‘Systemic lidocaine silences ectopic neuroma and DRG discharge without blocking nerve conduction.’, *Pain*, 48(2), pp. 261–8. doi: 10.1016/0304-3959(92)90067-l.

Dixon, W. J. (1980) ‘Efficient Analysis of Experimental Observations’, *Annual Review of Pharmacology and Toxicology*, 20(1), pp. 441–462. doi: 10.1146/annurev.pa.20.040180.002301.

Dong, J. Y., Fan, P. D. and Frizzell, R. A. (1996) ‘Quantitative analysis of the packaging capacity of recombinant adeno-associated virus’, *Human Gene Therapy*. Mary Ann Liebert Inc., 7(17), pp. 2101–2112. doi: 10.1089/hum.1996.7.17-2101.

Dudek, A. M. *et al.* (2018) ‘An Alternate Route for Adeno-associated Virus (AAV) Entry

Independent of AAV Receptor.', *Journal of virology*, 92(7). doi: 10.1128/JVI.02213-17.

Esposito, M. F. *et al.* (2019) 'Unique Characteristics of the Dorsal Root Ganglion as a Target for Neuromodulation', *Pain Medicine*, 20(Supplement_1), pp. S23–S30. doi: 10.1093/pm/pnz012.

Estrada-Mondragon, A. and Lynch, J. W. (2015) 'Functional characterization of ivermectin binding sites in α1β2γ2L gaba(A) receptors', *Frontiers in Molecular Neuroscience*. Frontiers Research Foundation, 8(September). doi: 10.3389/fnmol.2015.00055.

Ferrari, F. K. *et al.* (1996) 'Second-strand synthesis is a rate-limiting step for efficient transduction by recombinant adeno-associated virus vectors.', *Journal of virology*, 70(5), pp. 3227–34. Available at: http://www.ncbi.nlm.nih.gov/pubmed/8627803 (Accessed: 8 December 2019).

Fisher, K. J. *et al.* (1996) 'Transduction with recombinant adeno-associated virus for gene therapy is limited by leading-strand synthesis.', *Journal of virology*, 70(1), pp. 520–32. Available at: http://www.ncbi.nlm.nih.gov/pubmed/8523565 (Accessed: 8 December 2019).

Foust, K. D. *et al.* (2009) 'Intravascular AAV9 preferentially targets neonatal neurons and adult astrocytes', *Nature Biotechnology*, 27(1), pp. 59–65. doi: 10.1038/nbt.1515.

Franklin, K. M. *et al.* (2014) 'P2X4 receptors (P2X4Rs) represent a novel target for the development of drugs to prevent and/or treat alcohol use disorders', *Frontiers in Neuroscience*. Frontiers Research Foundation. doi: 10.3389/fnins.2014.00176.

Gao, G. P. *et al.* (2002) 'Novel adeno-associated viruses from rhesus monkeys as vectors for human gene therapy', *Proceedings of the National Academy of Sciences of the United States of America*, 99(18), pp. 11854–11859. doi: 10.1073/pnas.182412299.

Gemes, G. *et al.* (2013) ‘Failure of action potential propagation in sensory neurons: Mechanisms and loss of afferent filtering in C-type units after painful nerve injury’, *Journal of Physiology*, 591(4), pp. 1111–1131. doi: 10.1113/jphysiol.2012.242750.

Glatzel, M. *et al.* (2000) ‘Adenoviral and adeno-associated viral transfer of genes to the peripheral nervous system’, *Proceedings of the National Academy of Sciences of the United States of America*, 97(1), pp. 442–447. doi: 10.1073/pnas.97.1.442.

Glorioso, J. C. and Fink, D. J. (2009) ‘Herpes vector-mediated gene transfer in the treatment of chronic pain’, *Molecular Therapy*, pp. 13–18. doi: 10.1038/mt.2008.213.

Gray, S. J. *et al.* (2011) ‘Preclinical differences of intravascular aav9 delivery to neurons and glia: A comparative study of adult mice and nonhuman primates’, *Molecular Therapy*. Nature Publishing Group, 19(6), pp. 1058–1069. doi: 10.1038/mt.2011.72.

Haroutounian, S. *et al.* (2014) ‘Primary afferent input critical for maintaining spontaneous pain in peripheral neuropathy’, *Pain*. Elsevier B.V., 155(7), pp. 1272–1279. doi: 10.1016/j.pain.2014.03.022.

He, Y. *et al.* (2012) ‘Negative reinforcement reveals non-evoked ongoing pain in mice with tissue or nerve injury’, *Journal of Pain*, 13(6), pp. 598–607. doi: 10.1016/j.jpain.2012.03.011.

Iyer, S. M. *et al.* (2016) ‘Optogenetic and chemogenetic strategies for sustained inhibition of pain’, *Scientific Reports*. Nature Publishing Group, 6. doi: 10.1038/srep30570.

Jacques, S. J. *et al.* (2012) ‘AAV8 gfp preferentially targets large diameter dorsal root ganglion neurones after both intra-dorsal root ganglion and intrathecal injection’, *Molecular and Cellular Neuroscience*, 49(4), pp. 464–474. doi: 10.1016/j.mcn.2012.03.002.

Jayaraj, N. D. *et al.* (2018) ‘Reducing CXCR4-mediated nociceptor hyperexcitability reverses painful diabetic neuropathy’, *Journal of Clinical Investigation*. American Society for Clinical Investigation, 128(6), pp. 2205–2225. doi: 10.1172/JCI92117.

Kajander, K. C. and Bennett, G. J. (1992) ‘Onset of a painful peripheral neuropathy in rat: A partial and differential deafferentation and spontaneous discharge in Aβ and Aδ primary afferent neurons’, *Journal of Neurophysiology*, 68(3), pp. 734–744. doi: 10.1152/jn.1992.68.3.734.

Kent, A. R. *et al.* (2018) ‘Mechanisms of Dorsal Root Ganglion Stimulation in Pain Suppression: A Computational Modeling Analysis’, *Neuromodulation*. Blackwell Publishing Inc., pp. 234–246. doi: 10.1111/ner.12754.

Kilkenny, C. *et al.* (2010) ‘Improving Bioscience Research Reporting: The ARRIVE Guidelines for Reporting Animal Research’, *PLoS Biology*. Public Library of Science, 8(6), p. e1000412. doi: 10.1371/journal.pbio.1000412.

King, T. *et al.* (2009) ‘Unmasking the tonic-aversive state in neuropathic pain’, *Nature Neuroscience*, 12(11), pp. 1364–1366. doi: 10.1038/nn.2407.

Malik, R. N., Cote, R. and Lam, T. (2017) ‘Sensorimotor integration of vision and proprioception for obstacle crossing in ambulatory individuals with spinal cord injury’, *Journal of Neurophysiology*. American Physiological Society, 117(1), pp. 36–46. doi: 10.1152/jn.00169.2016.

Mason, M. R. J. *et al.* (2010) ‘Comparison of AAV serotypes for gene delivery to dorsal root ganglion neurons’, *Molecular Therapy*, 18(4), pp. 715–724. doi: 10.1038/mt.2010.19.

Navratilova, E. and Porreca, F. (2014) ‘Reward and motivation in pain and pain relief’, *Nature Neuroscience*. Nature Publishing Group, pp. 1304–1312. doi: 10.1038/nn.3811.

Nicolson, S. C. and Samulski, R. J. (2014) ‘Recombinant adeno-associated virus

utilizes host cell nuclear import machinery to enter the nucleus.', *Journal of virology*, 88(8), pp. 4132–44. doi: 10.1128/JVI.02660-13.

Nonnenmacher, M. and Weber, T. (2011) 'Adeno-associated virus 2 infection requires endocytosis through the CLIC/GEEC pathway', *Cell Host and Microbe*, 10(6), pp. 563–576. doi: 10.1016/j.chom.2011.10.014.

Nonnenmacher, M. and Weber, T. (2012) 'Intracellular transport of recombinant adeno-associated virus vectors', *Gene Therapy*, pp. 649–658. doi: 10.1038/gt.2012.6.

Pan, B. *et al.* (2018) 'Dorsal Root Ganglion Field Stimulation Prevents Inflammation and Joint Damage in a Rat Model of Rheumatoid Arthritis', *Neuromodulation: Technology at the Neural Interface*, 21(3), pp. 247–253. doi: 10.1111/ner.12648.

Philpott, N. J. *et al.* (2002) 'A p5 integration efficiency element mediates Rep-dependent integration into AAVS1 at chromosome 19', *Proceedings of the National Academy of Sciences of the United States of America*, 99(19), pp. 12381–12385. doi: 10.1073/pnas.182430299.

Pillay, S. *et al.* (2016) 'An essential receptor for adeno-associated virus infection', *Nature*. Nature Publishing Group, 530(7588), pp. 108–112. doi: 10.1038/nature16465.

Pillay, S. and Carette, J. E. (2017) 'Host determinants of adeno-associated viral vector entry', *Current Opinion in Virology*. Elsevier B.V., pp. 124–131. doi: 10.1016/j.coviro.2017.06.003.

Saloman, J. L. *et al.* (2016) 'Gi-DREADD Expression in Peripheral Nerves Produces Ligand-Dependent Analgesia, as well as Ligand-Independent Functional Changes in Sensory Neurons', *Journal of Neuroscience*, 36(42), pp. 10769–10781. doi: 10.1523/JNEUROSCI.3480-15.2016.

Samulski, R. J. *et al.* (1991) 'Targeted integration of adeno-associated virus (AAV) into human chromosome 19.', *The EMBO Journal*. Wiley, 10(12), pp. 3941–3950. doi:

10.1002/j.1460-2075.1991.tb04964.x.

Sarlegna, F. R. and Sainburg, R. L. (2009) ‘The roles of vision and proprioception in the planning of reaching movements’, *Advances in Experimental Medicine and Biology*. NIH Public Access, 629, pp. 317–335. doi: 10.1007/978-0-387-77064-2_16.

Schuster, D. J. *et al.* (2014) ‘Biodistribution of adeno-associated virus serotype 9 (AAV9) vector after intrathecal and intravenous delivery in mouse’, *Frontiers in Neuroanatomy*, 8. doi: 10.3389/fnana.2014.00042.

Shim, B. *et al.* (2005) ‘Mechanical and heat sensitization of cutaneous nociceptors in rats with experimental peripheral neuropathy’, *Neuroscience*. Elsevier Ltd, 132(1), pp. 193–201. doi: 10.1016/j.neuroscience.2004.12.036.

Smith, A. K., O’Hara, C. L. and Stucky, C. L. (2013) ‘Mechanical Sensitization of Cutaneous Sensory Fibers in the Spared Nerve Injury Mouse Model’, *Molecular Pain*, 9, pp. 1744-8069-9–61. doi: 10.1186/1744-8069-9-61.

Sonntag, F., Schmidt, K. and Kleinschmidt, J. A. (2010) ‘A viral assembly factor promotes AAV2 capsid formation in the nucleolus’, *Proceedings of the National Academy of Sciences of the United States of America*, 107(22), pp. 10220–10225. doi: 10.1073/pnas.1001673107.

Srivastava, A., Lusby, E. W. and Berns, K. I. (1983) ‘Nucleotide sequence and organization of the adeno-associated virus 2 genome.’, *Journal of virology*, 45(2), pp. 555–64. Available at: http://www.ncbi.nlm.nih.gov/pubmed/6300419 (Accessed: 8 December 2019).

Summerford, C. and Samulski, R. J. (2016) ‘AAVR: A multi-serotype receptor for AAV’, *Molecular Therapy*. Nature Publishing Group, pp. 663–666. doi: 10.1038/mt.2016.49.

Tanguy, Y. *et al.* (2015) ‘Systemic AAVrh10 provides higher transgene expression than AAV9 in the brain and the spinal cord of neonatal mice’, *Frontiers in Molecular*

Neuroscience, 8. doi: 10.3389/fnmol.2015.00036.

Towne, C. *et al.* (2009) 'Recombinant adeno-associated virus serotype 6 (rAAV2/6)-mediated gene transfer to nociceptive neurons through different routes of delivery', *Molecular Pain*, 5. doi: 10.1186/1744-8069-5-52.

Tsujino, H. *et al.* (2000) 'Activating transcription factor 3 (ATF3) induction by axotomy in sensory and motoneurons: A novel neuronal marker of nerve injury', *Molecular and Cellular Neurosciences*. Academic Press Inc., 15(2), pp. 170–182. doi: 10.1006/mcne.1999.0814.

Vaso, A. *et al.* (2014) 'Peripheral nervous system origin of phantom limb pain', *Pain*. Elsevier B.V., 155(7), pp. 1384–1391. doi: 10.1016/j.pain.2014.04.018.

Vulchanova, L. *et al.* (2010) 'Differential adeno-associated virus mediated gene transfer to sensory neurons following intrathecal delivery by direct lumbar puncture', *Molecular Pain*, 6. doi: 10.1186/1744-8069-6-31.

Wall, P. D. and Devor, M. (1983) 'Sensory afferent impulses originate from dorsal root ganglia as well as from the periphery in normal and nerve injured rats', *Pain*, 17(4), pp. 321–339. doi: 10.1016/0304-3959(83)90164-1.

Wall, P. D. and Gutnick, M. (1974) 'Properties of afferent nerve impulses originating from a neuroma', *Nature*, 248(5451), pp. 740–743. doi: 10.1038/248740a0.

Wang, D., Tai, P. W. L. and Gao, G. (2019) 'Adeno-associated virus vector as a platform for gene therapy delivery', *Nature Reviews Drug Discovery*. Nature Publishing Group, pp. 358–378. doi: 10.1038/s41573-019-0012-9.

Wu, G. *et al.* (2001) 'Early onset of spontaneous activity in uninjured C-fiber nociceptors after injury to neighboring nerve fibers.', *The Journal of neuroscience : the official journal of the Society for Neuroscience*, 21(8). doi: 10.1523/jneurosci.21-08-j0002.2001.

Xiao, P.-J. and Samulski, R. J. (2012) ‘Cytoplasmic trafficking, endosomal escape, and perinuclear accumulation of adeno-associated virus type 2 particles are facilitated by microtubule network.’, *Journal of virology*, 86(19), pp. 10462–73. doi: 10.1128/JVI.00935-12.

Yu, H. *et al.* (2011) ‘Lentiviral gene transfer into the dorsal root ganglion of adult rats’, *Molecular Pain*, 7. doi: 10.1186/1744-8069-7-63.

Yu, H., Fischer, G. and Hogan, Q. H. (2016) ‘AAV-mediated gene transfer to dorsal root ganglion’, in *Methods in Molecular Biology*. Humana Press Inc., pp. 251–261. doi: 10.1007/978-1-4939-3271-9_18.

Chapter 4: Using GluCl.Cre^{ON} to silence DRG subpopulations

1. Introduction

Neurons of the dorsal root ganglia are highly heterogenous, which is becoming increasingly apparent due to single cell sequencing studies (Usoskin *et al.*, 2015; Zeisel *et al.*, 2018). There is a need to investigate the contributions of primary afferent populations to the different components of pain related behaviour. Not only will this elucidate valuable information about each sensory neuron population but also it will inform future studies the therapeutic targeting of specific sensory neuron populations. The rationale of this chapter is to validate and use the GluCl.Cre^{ON} silencing system *in vivo* to target Cre recombinase expressing populations. The selective refinement of GluCl expression within the DRG will facilitate investigations into DRG heterogeneity, allowing us to ascribe function to different and novel populations.

1.1. Previous modulation of DRG subpopulations

This is not the first time groups have aimed to understand the heterogeneity of DRG primary afferent populations. There is a wealth of literature investigating the function of particular genes that show selectivity of expression for particular sensory neuron subpopulations, using genetic knockout or over-expression models. Consequently, these studies have provided valuable information about sensory neuron populations and their function. However, genetic manipulation of genes might not elucidate their full role. What is required is the systematic inactivation or activation of defined populations, while the consequence to somatosensory processing is assessed.

1.1.1. Ligand mediated ablation/inactivation

Indeed, early studies ablated populations of sensory neurons using high doses of agonists and toxins. For example capsaicin (Yaksh *et al.*, 1979; Fitzgerald and Woolf, 1982; Cavanaugh *et al.*, 2009; Wang *et al.*, 2017) and

resiniferatoxin (RTX) (Neubert *et al.*, 2003; Karai *et al.*, 2004; Tender, Li and Cui, 2008; Mishra and Hoon, 2010) which strongly activate TRPV1 leading to Ca^{2+} mediated excitotoxicity in order to ascribe function to the TRPV1+ population (primarily peptidergic nociceptors). It was found that high doses of capsaicin or RTX largely resulted in heat hyposensitivity in naïve and inflammatory states (Yaksh *et al.*, 1979; Fitzgerald and Woolf, 1982; Neubert *et al.*, 2003; Karai *et al.*, 2004; Cavanaugh *et al.*, 2009; Mishra and Hoon, 2010). There is some evidence that RTX reversed neuropathic mechanical hypersensitivities (Tender, Li and Cui, 2008) (Table 1). Others have tried to investigate non-peptidergic nociceptors through administration of Saporin conjugated IB4, which leads to hyposensitivity to mechanical and thermal stimuli in the naive state and recovery from neuropathic injury induced mechanical hypersensitivity (Vulchanova *et al.*, 2001; Tarpley, Kohler and Martin, 2004; Joseph and Levine, 2010; Pinto *et al.*, 2019) (Table 1). Other studies developed means to inactivate populations via the soluble lidocaine derivative QX-314, in combination with non-selective ion channel agonists such as capsaicin, WS-12 and flagellin to inactivate defined populations (Binshtok, Bean and Woolf, 2007; Xu *et al.*, 2015; Ongun, Sarkisian and McKemy, 2018) (Table 1). Most recently, a more advanced approach was designed and used of the photosensitizer IR700 fused to NGF^{SNAP} (and painless $NGF^{R121W\text{-}SNAP}$) and $BDNF^{SNAP}$, to target different sensory afferent terminals (Dhandapani *et al.*, 2018; Nocchi *et al.*, 2019). Indeed, photoablation of TrkA positive afferents (largely peptidergic nociceptors) resulted in hyposensitivity to punctate, noxious mechanical and heat stimuli. Photoablation of TrkA+ terminals resulted in the reversal of von Frey but not dynamic brush hypersensitivity following neuropathic injury (Nocchi *et al.*, 2019) (Table 1). Photoablation of TrkB positive afferents (Aδ-LTMRs and Aβ RA-LTMRs) resulted in hyposensitivity to dynamic stimuli pre-injury and punctate and dynamic stimuli post injury (Dhandapani *et al.*, 2018) (Table 1). However, the availability of Cre driver lines

has enabled groups to use mouse genetics to selectively overexpress effector molecules in order to ablate, silence or activate defined sensory neuron populations.

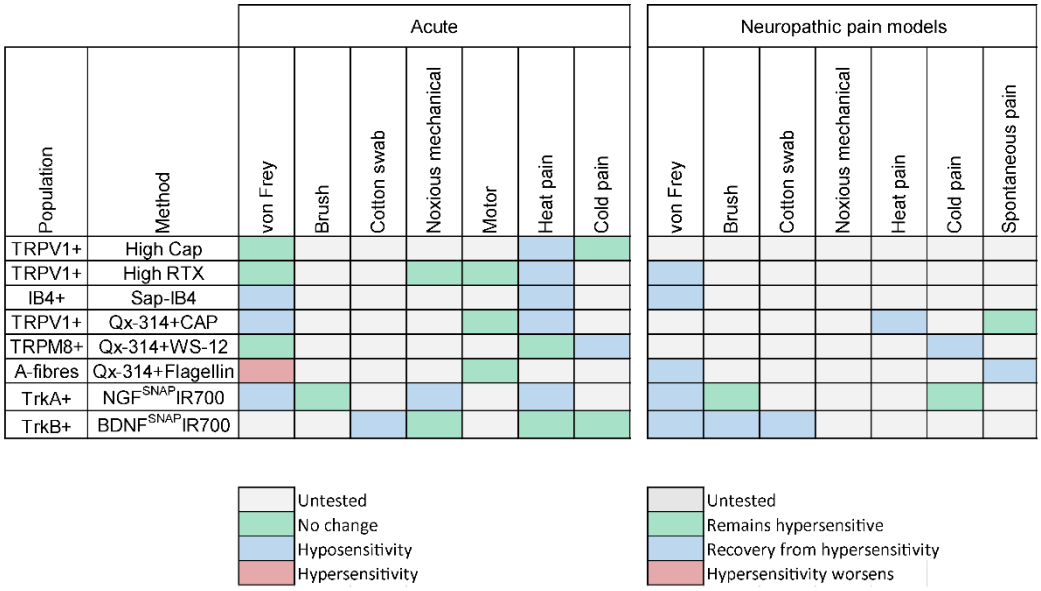

Table 1: Summarising studies that used ligand mediated ablation or inactivation to investigate sensory neuron populations. The results summarised in this table focus on acute sensory behaviours in naïve rodents and rodent neuropathic pain models, which include, traumatic nerve injury, chronic constriction injury, diabetic neuropathy, chemotherapy-induced neuropathy. (Yaksh *et al.*, 1979; Fitzgerald and Woolf, 1982; Vulchanova *et al.*, 2001; Neubert *et al.*, 2003; Karai *et al.*, 2004; Tarpley, Kohler and Martin, 2004; Binshtok, Bean and Woolf, 2007; Tender, Li and Cui, 2008; Cavanaugh *et al.*, 2009; Joseph and Levine, 2010; Mishra and Hoon, 2010; Xu *et al.*, 2015; Wang *et al.*, 2017; Dhandapani *et al.*, 2018; Ongun, Sarkisian and McKemy, 2018; Nocchi *et al.*, 2019; Pinto *et al.*, 2019)

1.1.2. Diphtheria toxin mediated ablation

A more selective method of inducing sensory neuron dysfunction to interrogate heterogeneity is using mouse genetics to overexpress the Diphtheria toxin receptor (DTR) in defined populations using Cre recombinase. Following administration of diphtheria toxin (DTX), cells expressing the receptor undergo cell death and are irreversibly ablated (detailed description see Chapter 1).

The first study to ablate a population of sensory neurons was Abrahamsen *et al* (2008) who used the DTR/DTX system to ablate Nav1.8 positive sensory neurons. The study identified Nav1.8 as a nociceptive specific marker and therefore intended to investigate nociceptive contribution to acute, inflammatory and neuropathic pain (Abrahamsen *et al.*, 2008). DTX ablation of Nav1.8+ sensory neurons resulted in the almost complete resistance to cold behaviours and hyposensitivity to mechanical pain but no motor, light touch or heat deficits (Abrahamsen *et al.*, 2008). In the context of injury, the ablation of Nav1.8+ afferents inhibited inflammatory pain but did not alter neuropathic pain (Abrahamsen *et al.*, 2008) (Table 2).

A later study used an alternative Cre line to interrogate nociceptor function. Mishra *et al* (2011), used DTR/DTX to ablate TRPV1-lineage neurons which encompass both peptidergic and non-peptidergic nociceptors through the large expression profile of TRPV1 during development (Hjerling-Leffler *et al.*, 2007; Mishra *et al.*, 2011). Mishra *et al.* (2011) demonstrated that TRPV1-lineage neuronal ablation resulted in hyposensitivity to cold and heat stimuli, deficits in thermal regulation and hyposensitivity to pruritogens. The study concluded that the TRPV1-lineage population is required for inflammatory but not neuropathic pain hypersensitivities (Mishra *et al.*, 2011) (Table 2).

While both Cre driver lines used above are thought to encompass most nociceptors, others have tried to pass out the roles and contribution of nociceptor subpopulations. For instance, Cavanaugh *et al.* (2009) used DTX to selectively ablate MRGPRD positive non-peptidergic nociceptors and observed that ablation of this subpopulation resulted in mechanical detection deficits and the absence of CFA-induced inflammatory mechanical hypersensitivity (Cavanaugh *et al.*, 2009). Following MRGPRD ablation, mice retained thermal sensitivity (Cavanaugh *et al.*, 2009) (Table 2). To investigate in detail the contribution of

peptidergic primary afferents, McCoy *et al* (2013) later used the targeted DTR/DTX system to selectively ablate peptidergic sensory neurons using a $CGRP\alpha^{Cre}$ line (McCoy *et al.*, 2013). This study found that CGRPα positive neurons are required to detect noxious heat, capsaicin, histamine and chloroquine (McCoy *et al.*, 2013). It was shown that loss of CGRPα neurons resulted in increased sensitivity to cold stimuli (likely due to a loss of spinal inhibition on cold circuits, that is usually driven by CGRPα afferents), impaired thermoregulation, and that this population is required for heat hypersensitivity post inflammatory pain and neuropathic pain (McCoy *et al.*, 2013) (Table 2). CGRPα is also expressed in a subpopulation of Aδ-nociceptors. The marker Npy2r was found to be expressed in this population and DTR was expressed in $Npy2r^{Cre}$ mice and DTX given to ablate the population. Ablating this population saw a deficit in the latency of mice to respond to pin prick stimuli (Arcourt *et al.*, 2016)(Table 2).

A population of sensory neurons that express GINIP co-express markers of non-peptidergic nociceptors and C-LTMRs (Urien *et al.*, 2017). The DTR/DTX ablation of this population of sensory neurons results in fewer attempts to remove sticky tape and almost a total loss of all formalin induced nocifensive behaviour (Urien *et al.*, 2017).

The DTR/DTX ablation system has also been used in non-nociceptive sensory neuron populations. A small population of somatostatin (SST) positive sensory neurons were DTX ablated using a SST^{Cre} driver line and an Advillin-LSL-DTR effector line (Stantcheva *et al.*, 2016). This revealed that this population was involved in itch and represented a novel population of pruritoceptors. Additionally, Aδ-LTMRs and Aβ-RA-LTMRs were targeted through the generation of a $TrkB^{CreERT2}$ driver line (Dhandapani *et al.*, 2018). The sensory neuron specific ablation of TrkB positive afferents revealed that they are critical

for dynamic light touch pre-injury (Table 2). It was shown that the ablation of TrkB positive sensory neurons prevented tactile hypersensitivity to punctate and dynamic stimuli in multiple models of neuropathic injury (Dhandapani *et al.*, 2018) (Table 2).

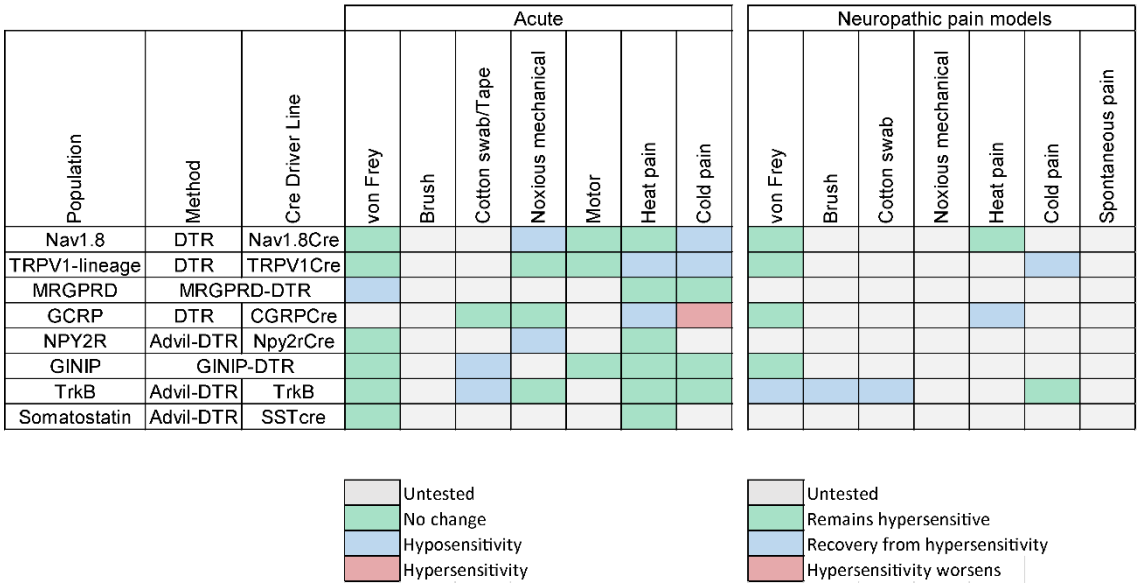

Table 2: Summarising studies that used DTR/DTX mediated ablation to investigate sensory neuron populations. The results summarised in this table focus on acute sensory behaviours in naïve rodents and rodent neuropathic pain models, which include, traumatic nerve injury, diabetic neuropathy, chemotherapy-induced neuropathy. (Abrahamsen *et al.*, 2008; Cavanaugh *et al.*, 2009; Mishra *et al.*, 2011; McCoy *et al.*, 2013; Arcourt *et al.*, 2016; Stantcheva *et al.*, 2016; Urien *et al.*, 2017; Dhandapani *et al.*, 2018).

1.1.3. Optogenetic and chemogenetic inactivation of DRG populations

1.1.3.1. Population specific optogenetic silencing

To address some of the concerns surrounding the chemical or genetic ablation of different populations, groups have adopted optogenetic techniques to inhibit sensory neuron function in a reversible and repeatable manner. In addition, optogenetics offers fast spatiotemporal resolution allowing time locked stimulus response experimental designs.

Daou *et al* (2016) used the inhibitory optogenetic tool Archaerhodopsin which in the presence of yellow light pumps protons into the extracellular space. The extrusion of protons results in membrane hyperpolarisation and subsequent silencing of neuronal activity. In this study, Arch was selectively expressed in Nav1.8 positive sensory neurons. In naïve conditions, optogenetic silencing did not change mechanical sensitivity (Daou *et al.*, 2016). However, following a 1hr transdermal illumination (under anaesthesia) session, neuropathic and inflammatory mice were less hypersensitive to mechanical or thermal stimuli (Daou *et al.*, 2016)(Table 3), implicating Nav1.8+ afferents in inflammatory and neuropathic pain. Arch mediated silencing of Nav1.8 positive afferents was also used to silence bladder nociceptive afferents and reduced evoked and non-evoked bladder pain (Samineni *et al.*, 2017).

Cowie *et al* (2018) employed the same tool to investigate the role of the CGRPα positive peptidergic population through the inducible expression of Arch in $CGRP^{CreERT2}$ mice. They showed that in the uninjured state inhibiting CGRP positive afferents results in hypersensitivity to cold stimuli and hyposensitivity to hot stimuli, with no effect on mechanical detection

thresholds (Cowie *et al.*, 2018)(Table 3). Inhibiting CGRP afferents post-SNI resulted in cold hyposensitivity and a reversal of nerve-injury induced mechanical and thermal hypersensitivity (Cowie *et al.*, 2018)(Table 3). Unlike the majority of preclinical studies, the authors did not overlook tonic ongoing pain and developed a real-time optogenetic place-preference assay to interrogate the contribution of CGRP afferents to spontaneous non-evoked pain. Neuropathic mice expressing Arch in CGRP afferents demonstrated a preference for the chamber illuminated with yellow light, which suggested that silencing of CGRP afferents could alleviate spontaneous ongoing pain (Cowie *et al.*, 2018)(Table 3). In contrast, CGRP afferent inhibition had no effect on incisional pain hypersensitivities (Cowie *et al.*, 2018).

1.1.3.2. Population specific chemogenetic silencing.

While optogenetics offers fast spatiotemporal resolution, chemogenetics offers the ability to silence sensory neurons over longer durations. Chronic silencing can elucidate the role of sensory neuron populations over time and is ideally suited for the study of chronic conditions such as neuropathic pain.

The first group to use transgenics to express inhibitory DREADDs in sensory neurons used the TRPV1-linage Cre driver line. Expression of Gi-DREADD (hM4Di) in TRPV1-lineage neurons and administration of CNO resulted in hyposensitivity to noxious thermal stimuli but not mechanical stimuli (Saloman *et al.*, 2016)(Table 3). This study also highlighted major concerns with using DREADDs in peripheral sensory neurons (see Chapter 2). Despite concerns over using inhibitory DREADDs, subsequent studies have expressed them in Nav1.8 positive sensory neurons to investigate their role in osteoarthritis and diabetic neuropathy (Miller *et al.*, 2017; Jayaraj *et al.*, 2018). DREADD inhibition of Nav1.8 positive neurons reduces knee

hyperalgesia and mechanical hypersensitivity during the early stages of osteoarthritis (Miller *et al.*, 2017). Equally, chemogenetic inhibition of Nav1.8 neurons in a model of high fat diet induced diabetic neuropathy, prevented small fibre degeneration and the associated mechanical hypersensitivity (Jayaraj *et al.*, 2018)(Table 3).

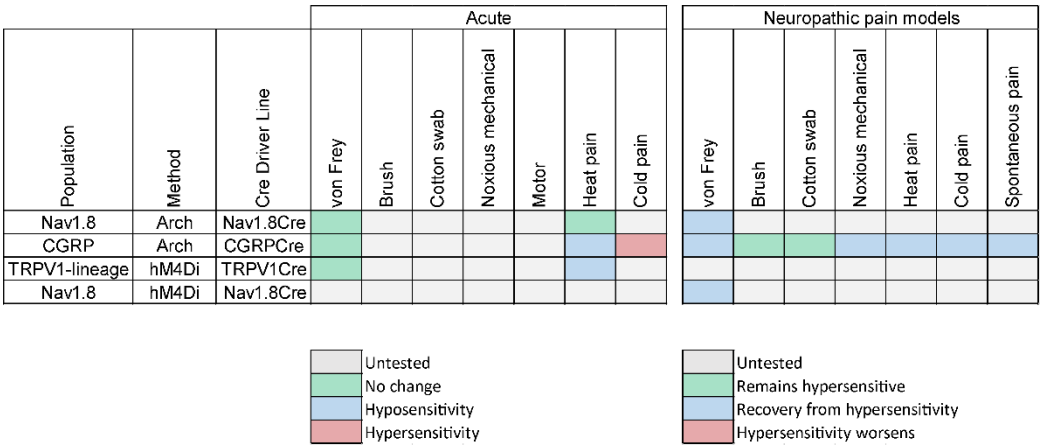

Table 3: Summarising studies that used optogenetic or chemogenetic mediated inactivation of sensory neuron populations. The results summarised in this table focus on acute sensory behaviours in naïve rodents and rodent neuropathic pain models, which include, traumatic nerve injury, diabetic neuropathy and chemotherapy-induced neuropathy. (Daou *et al.*, 2016; Saloman *et al.*, 2016; Miller *et al.*, 2017; Samineni *et al.*, 2017; Cowie et al., 2018; Jayaraj *et al.*, 2018).

1.2. Targeting Nav1.8 positive and TH positive afferents.

What is lacking and subsequently required is the ability to study both the classic and novel populations of DRG neurons using a systematic and precise approach which allows reversible silencing or activation of specific cells while performing a plethora of standard and complex pain related behavioural assays. We therefore aim to use the viral GluCl.Cre^{ON} system to target all Nav1.8 expressing sensory neurons, (which are largely nociceptors) as a proof of principle that our system works.

It is clear from the reviewed literature above that there is contrasting data when investigating the roles of the Nav1.8, CGRP or IB4 positive populations and it is possible that previous methods used may be contributing to phenotypes, beyond simply inactivating a population. Therefore, this provided the opportunity to use our method to bridge some of the discrepancies in the literature surrounding the role of the Nav1.8 population. The Nav1.8 population of sensory neurons express the VGSC Nav1.8, which is thought to be a marker of nociceptive afferents and as a population has been discussed in detail above.

The second aim is to use the GluCl.Cre^{ON} system to interrogate the role of a subpopulation of C-fibres termed C-low threshold mechanoreceptors (C-LTMRs) using the TH^{CreERT2} driver line. Both human and rodent C-LTMRs will be discussed in detail in the next chapter. However, briefly, C-LTMRs are low threshold mechanoreceptors, which respond to punctate mechanical and brush stimuli in humans (Vallbo, Olausson and Wessberg, 1999; Löken *et al.*, 2009). The C-LTMR population is a non-nociceptive population and is believed by many to encode pleasant touch in humans (Löken *et al.*, 2009; Morrison *et al.*, 2011). The likely species equivalent is the rodent tyrosine hydroxylase (TH) positive population, which have low mechanical thresholds, C-fibre range conduction velocities and innervate hairy skin (Li *et al.*, 2011). Previous studies have attempted to understand rodent C-

LTMRs through genetic KO studies, and the role of rodent C-LTMRs in the naïve and neuropathic setting is debated (Seal *et al.*, 2009; Delfini *et al.*, 2013; François *et al.*, 2015; Peirs *et al.*, 2015; Urien *et al.*, 2017). No study has selectively inactivated or ablated the population and therefore using our newly developed tool, we aim to interrogate C-LTMR function in rodents, particularly in the context of neuropathic pain.

2. Methods

2.1. Animals

All mice were group-housed in individually ventilated cages with free access to food and water, in humidity and temperature controlled rooms with a 12 hr light-dark cycle, in a pathogen free facility. All animal procedures adhered to the UK Home Office (Scientific Procedures) Act (1986) and were performed under a UK Home Office Project Licence. All animal experiments were carried out in accordance with University of Oxford Policy on the Use of Animals in Scientific Research. The work within this study also conforms to the ARRIVE guidelines (Kilkenny *et al.*, 2010). All experiments were carried out on adult male and female mice.

The Nav1.8^{Cre} line was a gift from John Wood (UCL) and was previous generated by Nassar *et al* (2004). Briefly, the Cre recombinase gene with the 3'UTR of the Nav1.8 gene was knocked into the translation start site of Nav1.8 gene. This resulted in Nav1.8 being substituted for the Cre gene. The targeting vector contained an frt flanked neomycin cassette which was used for positive selection of embryonic stem cells that successfully underwent homologous recombination. This was later removed using a FLPe deleter mouse (Nassar *et al.*, 2004). For histological studies Nav1.8^{Cre} mice were bred with Cre dependent report lines Ai14 (tdTomato; JAX) or Ai32 (ChR2-YFP; JAX).

The TH^{CreERT2} mouse line was obtained from Jackson labs and was previously generated by Abraira *et al* (2017). Briefly, the TH^{CreERT2} line was generated using a two-step protocol of the highly efficient recombineering-based method for generating knockout or knockin mutations (Liu, Jenkins and Copeland, 2003). The sequence for exon 13 of the tyrosine hydroxylase gene was obtained and a 9.1kb region was subcloned into a new plasmid. This region included the sequence prior to the 3'UTR, the 3'UTR itself and a region after the 3'UTR. The Cre recombinase estrogen receptor T2 (CreERT2) sequence was cloned after a T2A cleavage peptide. The

T2A-CreERT2 sequence was introduced into the 9.1kb TH region immediately before the start of the 3'UTR. An frt site flanked neomycin cassette was introduced after the 3'UTR to aid successful clone selection and later removed (Abraira *et al.*, 2017).

2.2. Tamoxifen dosing

$TH^{CreERT2}$:Ai14 mice were given tamoxifen dissolved in corn oil (1x 50 mg/kg I.P) at 8-10 weeks of age and tissue was taken for histology at least 2 weeks later. $TH^{CreERT2}$ mice that received AAV intrathecal injections were tamoxifen dosed 1 week post-surgery to allow GluCl.Cre^{ON} expression.

2.3. Surgery

2.3.1. Intrathecal injection

$Nav1.8^{Cre}$ or $TH^{CreERT2}$ mice, 6-8 weeks old and of mixed sex, were used for intrathecal (i.t.) injection surgery. Each animal was anaesthetised using 2% isoflurane and prepared for surgery by shaving a region over the thoracic vertebrae. Following incision site sterilisation (Iodine, alcohol wipe) a 1-2 cm incision was made to the back (rostral to caudal) above the spine. T-10 and T-11 vertebrae were located, soft tissue was carefully and sparingly removed lateral to the midline to expose the dura and spinal cord. A drop of lidocaine was applied to the dura for approximately 1-2 mins then removed. Using a 30 gauge needle the dura was carefully punctured (CSF leak at this point suggested a successful puncture). An "in house" developed cannula system was designed by connecting tubing of decreasing size until the final cannula tip measured 0.008 in (O.D) x 0.004 in (I.D). The end of the cannula was inserted approximately 1 cm caudal into the subdural space. Using a syringe pump driver, 8 µl of AAV (AAV9-GluCl.Cre^{ON}α and/or AAV9-GluCl.Cre^{ON}β) was injected into the subdural space at a rate of 1 µl/min. Following injection, the cannula was allowed to rest in

position for 2 min to avoid back flow and then slowly removed. The dura was coated with a single drop of dura gel (Cambridge NeuroCare) to seal the dura and prevent further CSF leak. Finally, the incision site was sutured closed and appropriate post-operative care and analgesics given (local 2 mg/kg Marcain, AstraZeneca and systemic 5 mg/kg Rimadyl, Pfizer). Animals were used for behaviour or histology at least 3 weeks post-surgery.

2.3.2. Spared nerve injury (SNI)

Mice were anesthetised using 2% isoflurane and prepared for surgery by shaving and sterilising the leg. A small incision was made to the thigh skin parallel to the thigh bone. The sciatic nerve was identified through separation of muscle and connective tissue. The sciatic nerve branches into three nerves, the common peroneal, tibial and sural. The branching points were identified and a non-absorbable suture was used to tie the common perineal and tibial nerves prior to nerve transection. The sural nerve was untouched and left intact. The site was closed and appropriate post-operative care given (local 2 mg/kg Marcain, AstraZeneca and systemic 5 mg/kg Rimadyl, Pfizer).

2.4. Immunohistochemistry (IHC)

Animals were deeply anesthetised with pentobarbital, and the blood cleared from all tissues by perfusing saline through the vascular system. Mice were then perfuse-fixed using 4% paraformaldehyde (PFA). Tissues were then collected and post-fixed in 4% PFA accordingly (DRG: 1-2 hrs, Spinal Cord: 24 hrs, Skin: 1-2 hrs). All tissues were cryoprotected in 30% Sucrose for a minimum of 48 hrs followed by embedding the tissue and sectioning on a cryostat. (DRG 12 µm, Spinal cord 20 µm, Skin 30 µm). Cultured cells were fixed with 4% PFA for 10 mins and treated similarly to other tissues. Briefly, samples were washed in PBS and blocked in a blocking solution (5% normal donkey serum, 0.3% TritonX-100, PBS) for 1 hr at room temperature (RT). Primary antibodies (appendix table 1) were diluted in blocking

solution and applied to tissue or cells overnight at RT. The next day samples were washed in a wash solution (0.3% TritonX-100, PBS) followed by a 2 hr incubation with secondary antibodies (appendix table 1) diluted in wash solution at RT. Samples were mounted using Vectorshield and imaged on a confocal microscope (Zeiss LSM-710). Images were analysed using Fuji/ImageJ (NIH). For quantification at least three sections per animal were used, with at least 3 animals per group.

2.5. *In situ* hybridisation (ISH)

ISH was performed by following the user instructions for the RNAScope2.5 RED Chromogenic assay kit (Advanced Cell Diagnostics). Briefly, tissue was pre-treated using hydrogen peroxide and a protease treatment. Tissue was next incubated for 2 hrs at 40^{o}C with a TRPV1 mRNA specific probe (Cat no. 313331). Next, a series of 6 probe amplification steps were carried out followed by a fast red detection step.

2.6. Whole cell patch-clamp recordings

Voltage-clamp recordings using an Axopatch 200B amplifier and Digidata 1550 acquisition system (Molecular Devices) were performed at room temperature (21°C - the standard for the field when not assessing temperature sensitivity). Data were sampled at 20 kHz and low-pass filtered at 5 kHz. Series resistance was compensated 60%–80% to reduce voltage errors. All data were analysed by Clampfit 10 software (Molecular Devices). GFP/XFP+ DRG neurons were detected with an Olympus microscope with an inbuilt GFP filter set (470/40x excitation filter, dichroic LP 495 mirror and 525/50 emission filter). Filamental borosilicate glass capillaries (1.5 mm OD, 0.84 mm ID; World Precision Instruments) were pulled to form patch pipettes of 2–4 MΩ tip resistance and filled with an internal solution containing (mM): 100 K-gluconate, 28 KCl, 1 $MgCl_2$, 5 MgATP, 10 HEPES, and 0.5 EGTA; pH was adjusted to 7.3 with KOH and osmolarity set at 305 mOsm (by adding glucose). Cells

were maintained in a chamber constantly perfused with a physiological extracellular buffer containing (mM): 140 NaCl, 4.7 KCl, 2.5 $CaCl_2$, 1.2 $MgCl_2$, 10 HEPES and 10 glucose; pH was adjusted to 7.4 with NaOH and osmolarity set at 315 mOsm (by adding glucose). Membrane conductance was measured in voltage clamp with a 100 ms voltage ramp from -90 mV to +40 mV every 10 s. The resultant linear current gradient was used to calculate membrane conductance. Resting membrane potential was calculated in bridge mode. In current clamp mode DRGs were held at -60 mV. Input resistance was derived by measuring the membrane deflection caused by a 20 pA current step. Rheobase was determined by applying 50 ms depolarising currents of increasing steps of 25 pA until action potential (AP) generation.

2.7. Mechanical Sensory testing

Both male and female mice were used in this study and mice were tested at a consistent time of day, in the same environment. Mice were habituated to their testing environment and equipment prior to behavioural test days. The experimenter was blind to animal genotype prior to testing and until after behavioural analysis was complete.

Mice were randomly assigned a test box (5 x 5 x 10 cm) which was elevated on a wire mesh base and were acclimatised to the equipment for 30-60 mins. All tests were conducted to achieve a baseline then repeated once 24 hrs post IVM administration, unless other wise stated.

2.7.1. von Frey testing*:* Mice were then tested on their plantar hind paws (between their running pads pre injury, sural territory post injury) using calibrated von Frey hairs (Linton Instrumentation) using the ‘up-down’ method (Dixon, 1980) to evaluate their 50% paw withdrawal thresholds. Mice were tested on 3 different days to obtain an average baseline value.

Post SNI: von Frey stimuli were applied to the ipsilateral paw to obtain the 50% paw withdrawal threshold post injury.

2.7.2. Brush/cotton swab*:* The plantar hind paws of mice were brushed (1 cm/s) with a fine artists paint brush or a cotton swab that had been puffed out to 3 times its original size. Each mouse received 5 successive stimuli on alternate hind paws (10 s apart), twice. The number of responses were recorded. A response included, lifting, flicking or moving the hind paw or walking away from the stimulus. Mice were tested on 3 different days to obtain an average baseline value. Post SNI: Brush stimuli were applied to the ipsilateral hind paw post injury and responses scored (1-3) to assess the dynamic score/allodynic response as previously described (Cheng *et al.*, 2017).

2.7.3. Pinprick: Mice were randomly assigned a test box (5 x 5 x 10 cm) which was elevated on a wire mesh base and were acclimatised to the equipment for 30-60 mins. Mice were then tested on their plantar hind paws using a pin attached to a 1 g calibrated von Frey filament (Arcourt *et al.*, 2016). Mice were video recorded using a Sony Xperia phone at 120 fps (8.33 ms per frame) and the latency to withdraw from the pinprick analysed, three times per paw, on three different days.

2.7.4. Tape test: A small 1 cm by 1 cm piece of tape was places onto the hindlimb of mice and the time taken from mice to detect the tape was measured (sense time), on three different days to obtain a baseline

2.8. Thermal Sensory testing

The experimenter was blind to animal genotype prior to testing and until after behavioural analysis was complete. All tests were conducted to achieve a baseline then repeated once 24 hrs post IVM administration, unless other wise stated. All Mice

were randomly selected from their home cages in order to randomise the order of thermal sensory assessment.

2.8.1. ***53ºC Hotplate****:* Mice were placed onto a Perspex enclosed Hotplate (UgoBasile) and were observed until mice displayed pain behaviours on their hind paws i.e. lifting, flicking, licking of the hind paw (cut off 30 s to prevent tissue damage). The latency to respond was recorded and mice were tested on 3 different days to obtain average baseline value.

2.8.2. Cold place preference: Mice were briefly acclimatised to the cold place preference apparatus (temperature not set, equipment at RT). Mice were placed in a two chamber paradigm consisting of two chambers, divided by a small corridor, where one base was set to room temperature 22^{o}C and the other set to 16^{o}C. To avoid learning, chamber temperature was randomised. Mice were allowed to freely explore over a 10 min period and time in each chamber live scored. Mice were assayed on two different days to achieve a pre injury baseline value, and on day 7 for a post injury baseline value and on day 8 (24 hrs post IVM).

2.9. Other behaviour tests

2.9.1. Rotarod: Mice were briefly acclimatised to the rotarod apparatus (Ugo Basile, 47600). Mice were placed onto the rotarod equipment while the central rod rotated at a speed of 32 rpm. The latency to fall was recorded on two different days to achieve a baseline.

2.9.2. Nesting: The ability of mice to nest was carried out as previously described (Deacon, 2006). Briefly, mice were individually housed overnight in a fresh cage with all enrichment removed except exactly 3 g of nestlet (pressed cotton square). The next morning nests were assed and scored 1-

5 according to Deacon (2006). All nesting behaviour was assayed 24 hrs post IVM.

2.10. Formalin assay

A hind paw of each mouse was injected subcutaneously with 4% formalin and the nocifensive behaviours of the injected hind paw (lifting, licking, flinching, shaking) immediately recorded (live timed) every 5 mins for 60 mins. The formalin assay was also analysed in 2 phases; 1st phase 0-15 mins 2nd phase 15-60 mins. All formalin behaviour was assayed 24 hrs post IVM.

2.11. Statistical analysis

All data was tested for normality using the D'Agostino-Pearson normality test and the appropriate parametric or non-parametric statistical tests used accordingly. All statistical tests used were two-tailed. Statistical comparisons were made using a Student's t-test or Mann Whitney U-test. In experimental groups in which multiple comparisons and repeated measures were made two-way analysis of variance (ANOVA) tests with appropriate *post-hoc* tests were performed. All ANOVA results, details, and tables can be found in the appendix. All data is represented as mean ± the standard error of the mean (S.E.M.) unless otherwise stated. Statistical significance is indicated as follows * $P < 0.05$, ** $P < 0.01$, *** $P < 0.001$, **** $P < 0.0001$. The statistical test used is reported in the appropriate figure legend. Graph Pad prism 6 was used to perform statistical tests and graph data. Adobe illustrator CS5 was used to create schematics and medical graphics were obtained from Smart servier free medical art (smart.servier.com).

3. Results

3.1. Characterisation of Nav1.8 positive sensory neurons.

The aim was to use chemogenetics to silence Nav1.8 primary afferents and interrogate their role in acute and neuropathic pain states. Prior to this investigation, studies have suggested that Nav1.8 is a selective marker for nociceptors (Abrahamsen *et al.*, 2008), while others suggest that Nav1.8 is present in non-nociceptive populations (Shields *et al.*, 2012). Therefore, it was important to characterise the Nav1.8^{Cre} line in our hands.

In order to characterise the Nav1.8^{Cre} line, it was crossed with a Cre dependent reporter line. The reporter line chosen was the Ai32 strain which encoded ChR2 fused to YFP. In this instance, the YFP was used to report the Nav1.8^{Cre} population. Using histology, the proportion of Nav1.8 positive neurons within the DRG was determined and found to be 68.7 ± 3.79% (Fig. 1A+G). Unfortunately, there is no good Nav1.8 antibody available to assess specificity. Instead, further characterisation was carried out to determine the frequency of other population markers within the Nav1.8 positive population (Fig. 1 B-F+H). There was high frequency of the nociceptive population markers TRPV1, CGRP and IB4 overlapping with the Nav1.8 population (Fig. 1H). There was a 13.6 ± 0.21% overlap of S100β (myelinated marker) and Nav1.8 (Fig. 1H). This 13.6% of the Nav1.8 population made up 22.7 ± 3.74% of the S100β population. There was a low, but still detectable 2.77% ±0.21 frequency of calbindin (RA-LTMR marker) and Nav1.8 co-expressing neurons (Fig. 1H). However, this 2.77% of the Nav1.8 population made up 17.89 ± 3.58% of the calbindin population. The Nav1.8 positive sensory neuron terminals which enter the dorsal horn of the spinal cord were also visualised (Fig. 1I-L). There was co-localisation laminae I (above IB4+ terminations), with Laminae II^{o} (IB4+) and laminae II^{i} (Below IB4+ terminations). The Nav1.8+ laminae II^{i} terminations are C-LTMRs (also shown at the DRG level later in this chapter). There were also some

projections which terminated in deeper laminae (white boxes), which includes the LTMR zone. Taken together, Nav1.8^{Cre} mice target 68.7% of DRG neurons and is a population largely comprised of nociceptors, but is also co-expressed by 22.7% of all myelinated afferents, C-LTMRs and 17.89% of all calbindin positive RA-LTMRs.

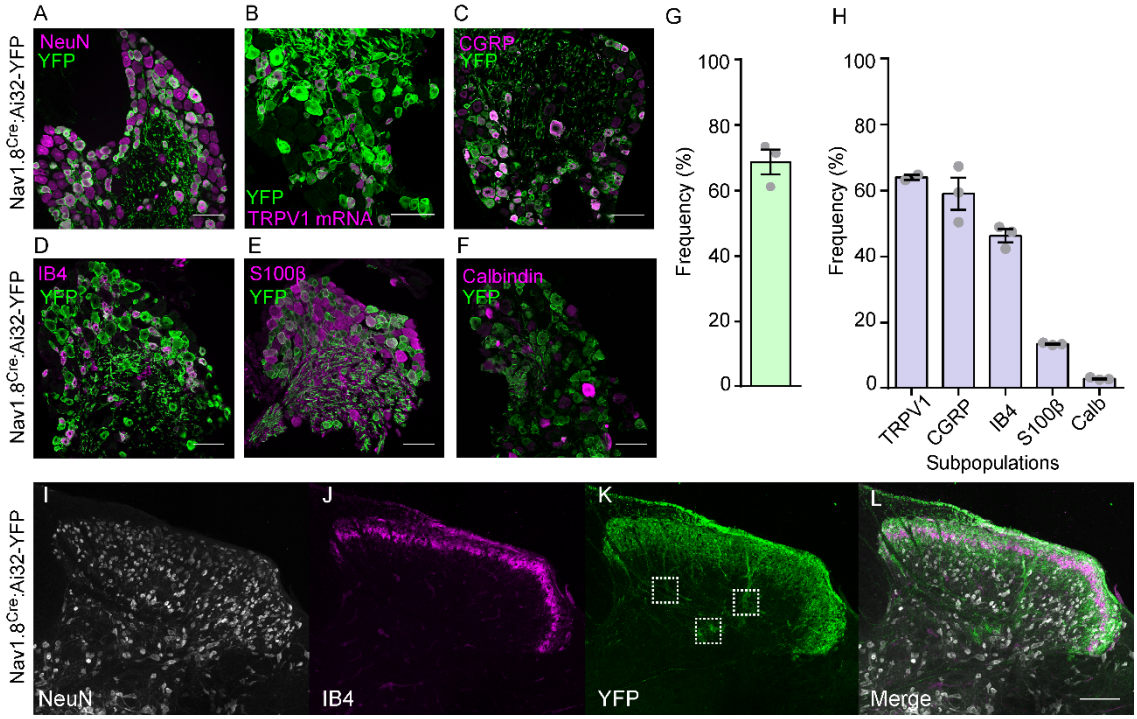

Figure 1: Histological characterisation of Nav1.8 positive sensory neurons

DRG sections from Nav1.8^{Cre}:Ai32-YFP mice co-stained for **A)** NeuN **B)** TRPV1 mRNA **C)** CGRP **D)** IB4 **E)** S100β **F)** Calbindin, scale bar = 100 μm **G)** Quantification of Nav1.8 positive neuron frequency in lumbar DRG. (n = 3 mice, total of 4466 Nav1.8 positive cells from a total of 6754 counted cells). **H)** The frequency of other sensory neurons markers in the Nav1.8 positive population (n= 3 mice per group, overlap averaged from 3 sections per mouse, TRPV1 (n = 2) = 243/382 cells, CGRP = 424/792 cells, IB4 = 513/1105 cells, S100β = 102/832 cells, Calbindin = 29/892 cells). **I-J)** Immunostaining of Nav1.8 positive terminals entering lumbar dorsal horn of the spinal cord, co-stained with IB4 and NeuN. White boxes indicate deep laminae termination of Nav1.8 sensory afferents. Scale bar = 100 μm. All data mean ± S.E.M.

3.2. Using GluCl.Cre^{ON} to chemogenetically silence Nav1.8 positive afferents.

It was important to validate that *in vivo* delivery of GluCl.Cre^{ON} combined with *in vivo* IVM dosing, could successfully silence Nav1.8 neuron activity. To achieve this GluCl.Cre^{ON} constructs were commercially packaged into AAV9 viruses. AAV9.GluCl.Cre^{ON}αβ or β-only was i.t. injected into Nav1.8^{Cre} mice (Fig. 2A) and three weeks later injected *in vivo* with 5 mg/kg IVM. DRG neurons were cultured 24 hrs later from these mice and patch-clamp recordings carried out within 48hrs (Fig. 2A). Patch-clamp analysis was used to record fluorescent β-only or αβ expressing neurons. The capacitance and the resting membrane potential of the recorded cells were comparable between groups (Fig. 2B-C). However, in voltage-clamp mode the recorded conductance of αβ expressing Nav1.8 neurons was significantly higher than β-only expressing neurons after *in vivo* IVM dosing (Fig. 2D). In current-clamp mode, the input resistance was significantly reduced in the αβ expressing group compared the β-only control neurons (Fig 2E). Finally, it was important to assess excitability after *in vivo* IVM dosing and αβ expressing neurons were significantly hypo-excitable compared to β-only control neurons. Thus, we can conclude that GluCl.Cre^{ON} is effective at silencing Nav1.8^{Cre} positive neurons when delivered and activated *in vivo*.

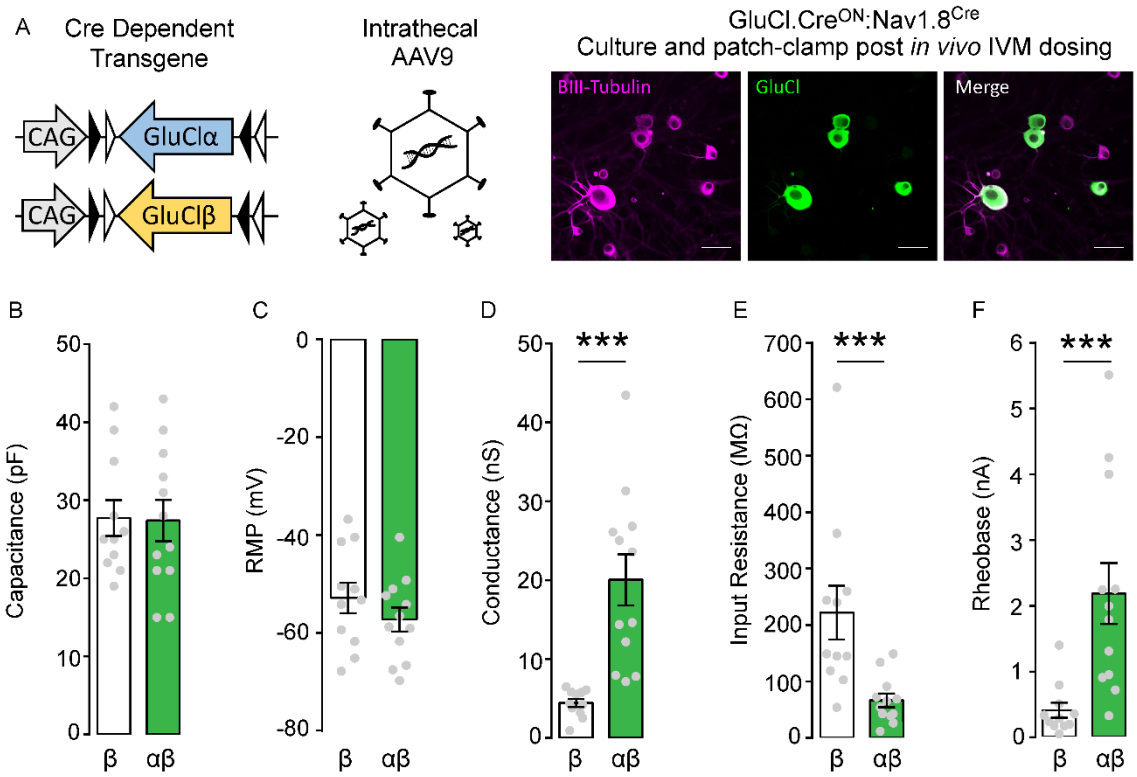

Figure 2: Validation of *in vivo* silencing of Nav1.8 positive nociceptors.

A) AAV9-GluCl.Cre^{ON} subunits were generated and intrathecally injected into Nav1.8^{Cre} mice. Three weeks after AAV injection mice were dosed *in vivo* with 5 mg/kg IVM. DRG neurons were cultured 24 hrs later and patch-clamp carried out within 36 hrs. Example image of GluCl+ cultured DRG neurons. Scale bar 25µm. **B)** The recorded capacitance of either Nav1.8^{Cre}GluCl.βonly (White) or Nav1.8^{Cre}GluClαβ (Green) neurons. The cell capacitance was on average the same for each group (two-tailed, unpaired t-test, n = β 11 cells, αβ 12 cells, t = 0.088 df = 21, P = 0.930). **C)** The resting membrane potential was not significantly different between Nav1.8^{Cre}GluCl.βonly or Nav1.8^{Cre}GluClαβ neurons (two-tailed, unpaired t-test, n = β 11 cells, αβ 12 cells, t = 1.125, df = 21, P = 0.272). **D)** Membrane conductance was measured in voltage clamp mode with a 100ms voltage ramp from -90mV to +40mV. Nav1.8^{Cre}GluClαβ neurons had a significantly higher conductance than β-only expressing neurons following *in vivo* IVM dosing (two-tailed, unpaired t-test, n = β 11 cells, αβ 12 cells, t = 4.562, df = 21, P = 0.0002, ***). **E)** The input resistance of Nav1.8^{Cre}GluClαβ expressing neurons was significantly lower than β-only expressing neurons after IVM dosing *in vivo* (two-tailed, Mann Whitney U test, n = β 11 cells, αβ 12 cells, U = 13, P = 0.0005, ***). **F)** Following IVM dosing *in vivo*, the rheobase (minimum current required to elicit an AP) of Nav1.8^{Cre}GluClαβ expressing neurons was significantly higher than β-only expressing neurons (two-tailed, Mann Whitney U test, n = β 11 cells, αβ 12 cells, U = 10, P = 0.0002, ***). All data mean ± S.E.M.

Next, it was key to address how the selective silencing of Nav1.8 positive neurons might alter acute and neuropathic pain sensitivities. Nav1.8^{Cre} mice were i.t. injected with AAV9.GluCl.Cre^{ON} (Fig 3A) which successfully transduced small/medium but not large DRG neurons (Fig 3B). These mice entered a behavioural paradigm where their sensory processing was tested pre and post IVM treatment (Fig. 3C). The cohort then received a spared nerve injury. The neuropathic cohort was tracked for 3 weeks with weekly IVM dosing and testing (Fig 3C).

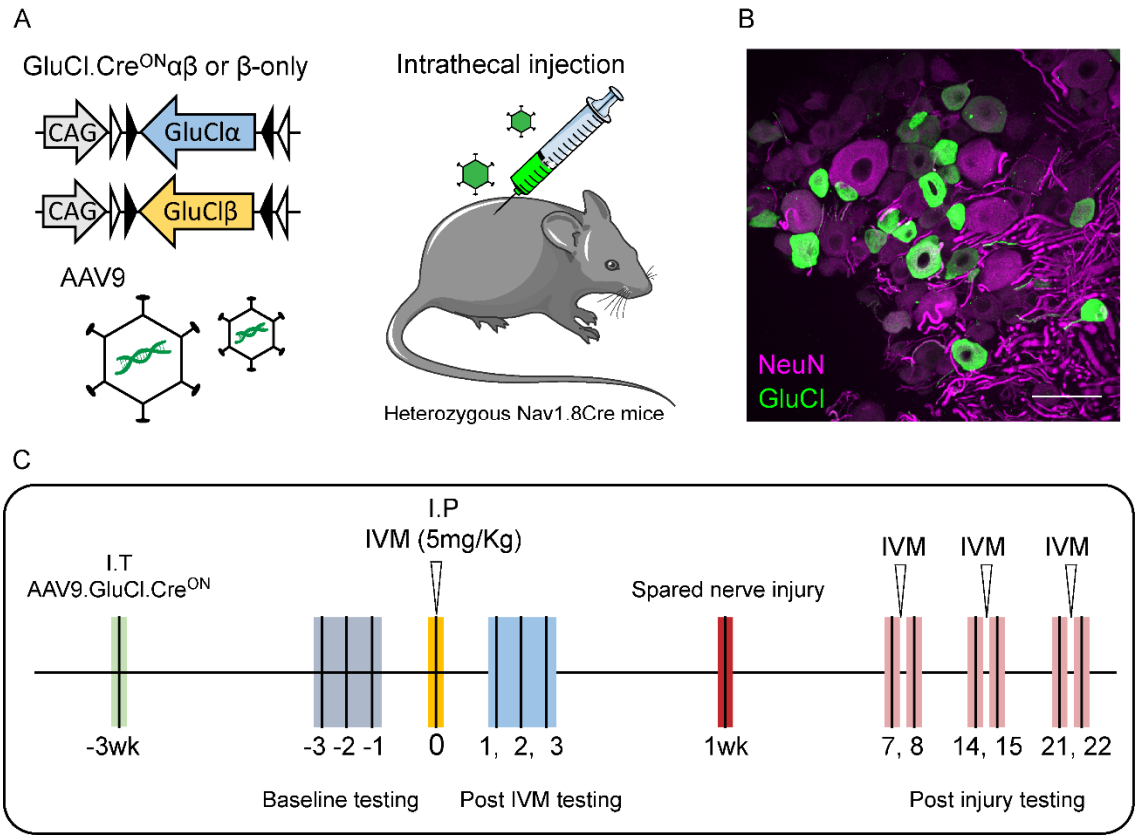

Figure 3: The timeline of the experimental setup of silencing Nav1.8 positive sensory neurons. A) Schematic illustrating the intrathecal injection of AAV9.GluCl.Cre^{ON} into heterozygous Nav1.8^{Cre} mice. **B)** Example of GluCl.Cre^{ON} expression in Nav1.8^{Cre} injected mice. Scale bar 50 µm. **C)** Timeline of events following intrathecal injection of GluCl.Cre^{ON}. Baseline testing, IVM dosing, post IVM testing, SNI, post SNI mechanical sensitivity testing over 3 weeks.

Mechanical detection of punctate stimuli (Fig 4A), light touch cotton swab (Fig 4B) and brush stimuli (Fig 4C), were unchanged when silencing Nav1.8 positive sensory afferents. However, silencing the Nav1.8 positive population resulted in

significant hyposensitivity to the noxious 53^{o}C hotplate assay, while no change was seen in β-only expressing control mice (Fig 4D). The silencing of Nav1.8 positive neurons did not result in significant changes in the latency to withdraw from a noxious pinprick. However, there is a strong trend towards hyposensitivity in the αβ-expressing group (Fig. 4E). Silencing Nav1.8 positive neurons did not alter motor function (Fig 4F). The silencing of Nav1.8 sensory neurons alters the response to noxious stimuli and provides good proof of principle that selective GluCl expression can alter population specific modalities.

In the context of neuropathic pain there is a large debate as to the contribution of the Nav1.8 positive population (Abrahamsen *et al.*, 2008; Daou *et al.*, 2016). To address this, Nav1.8^{Cre}:GluClαβ and β-only mice received a spared nerve injury and were behaviourally tracked for three weeks (Fig 5A). Both groups of mice became behaviourally hypersensitive to punctate von Frey stimuli following SNI, however no recovery of hypersensitivity was observed following IVM silencing (Fig 5B). Neuropathic mice also developed mechanical hypersensitivity to dynamic brush stimuli as seen by an increase in the dynamic score (Fig 5C). When compared to baseline (αβ vs β-only comparison was not made due to small sample size), all dynamic scores in both groups were significantly higher post SNI, except αβ day 8 post IVM. This time point was not significantly different from baseline suggestive of a partial recovery of dynamic hypersensitivity. There was a trend for a reduction in the dynamic hypersensitivity at day 15 (a post IVM day). Neuropathic mice were also assayed for the recovery of cold hypersensitivity, both groups developed cold hypersensitivity one week post SNI as measured by the ColdPP assay. However, recovery following IVM administration was unclear due to data variability in both groups. These data suggest a limited role for NaV1.8+ neurons post-nerve injury, but are hampered by low group numbers and will have to be replicated.

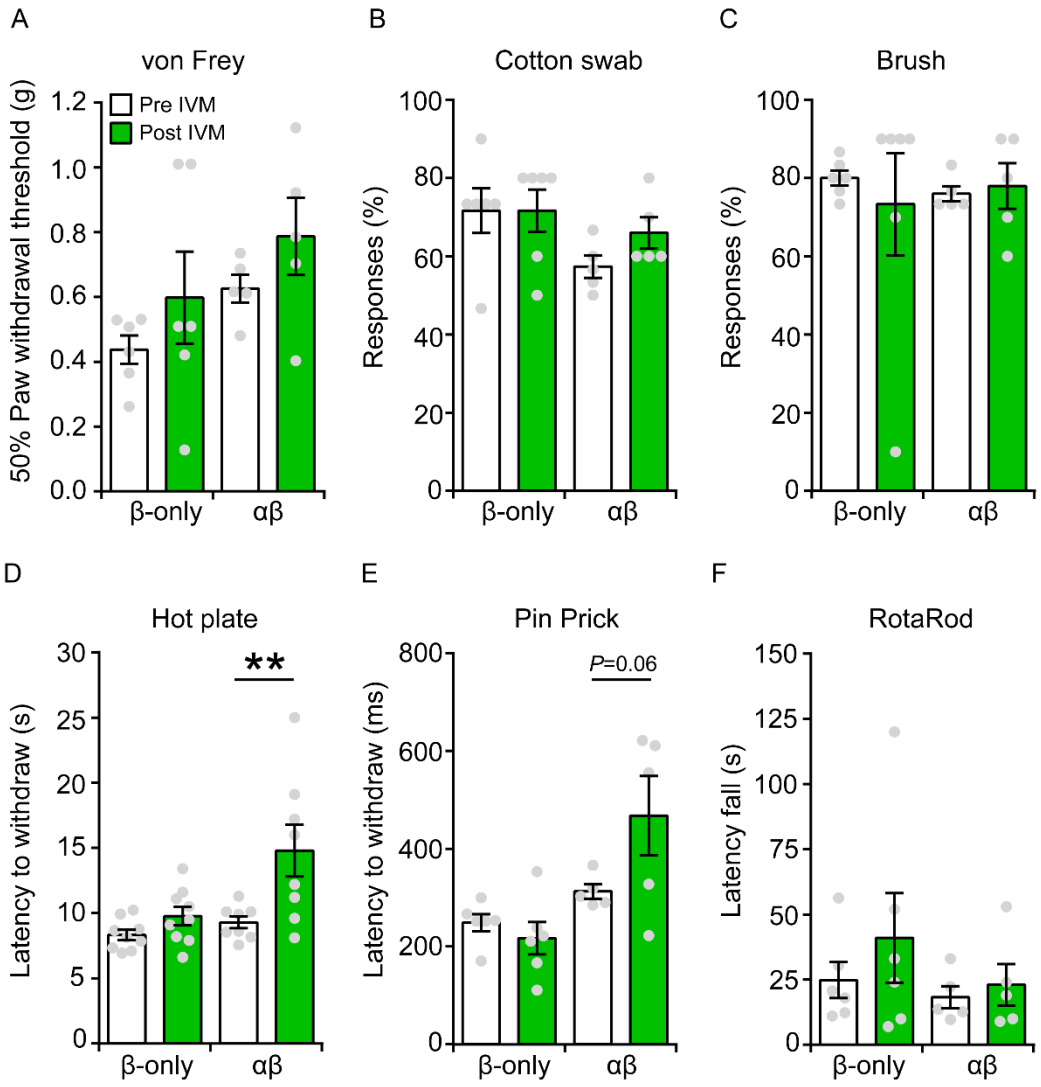

Figure 4: Naïve sensory testing following Nav1.8 specific silencing using AAV9.GluCl.Cre^{ON}

A) There were no significant changes in the mechanical detection of punctate von Frey in either Nav1.8^{Cre}GluClβonly control mice or Nav1.8^{Cre}GluClαβ expressing mice following IVM (RM two-way ANOVA, with Bonferroni *post hoc* test pre vs post IVM, β-only; n = 6 mice, t = 1.09, df = 9, P = 0.66, αβ; n = 5 mice, t = 0.93, df = 9, P = 0.74). **B)** There were no significant changes in the mechanical detection of light touch (cotton swab) in either Nav1.8^{Cre}GluClβonly or Nav1.8^{Cre}GluClαβ expressing mice following IVM (RM two-way ANOVA, with Bonferroni *post hoc* test pre vs post IVM, β-only; n = 6 mice, t = 0.00, df = 9, P >0.99, αβ; n = 5 mice, t = 1.96, df = 9, P = 0.163). **C)** There were no significant changes in the mechanical detection of light touch (brush) in either Nav1.8^{Cre}GluClβonly or Nav1.8^{Cre}GluClαβ expressing mice following IVM (RM two-way ANOVA, with Bonferroni *post hoc* test pre vs post IVM, β-only; n = 6 mice, t = 0.59, df = 9, P > 0.99, αβ; n = 5 mice, t = 0.163, df = 9, P > 0.99). **D)** Nav1.8^{Cre}GluClαβ mice exhibited significant hyposensitivity to a noxious 53^{o}C hot plate. (RM two-way ANOVA, with Bonferroni *post*

hoc test pre vs post IVM, β-only; n = 9 mice, $t = 1.15$, $df = 15$, $P = 0.536$, αβ; n = 8 mice, $t = 4.151$, $df = 15$, $P = 0.0017$,**). **E)** Nav1.8^{Cre} Mice expressing GluClαβ, and not β-only show a trend towards significant hyposensitivity in the noxious pin prick assay following IVM (RM two-way ANOVA, with Bonferroni *post hoc* test pre vs post IVM, β-only; n = 6 mice, $t = 0.569$, $df = 9$, $P > 0.99$, αβ; n = 5 mice, $t = 2.532$, $df = 9$, $P = 0.0642$). **F)** Silencing Nav1.8 positive primary afferents does not affect motor function (RM two-way ANOVA, with Bonferroni *post hoc* test pre vs post IVM, β-only; n = 6 mice, $t = 1.924$, $df = 9$, $P = 0.173$, αβ; n = 5 mice, $t = 0.512$, $df = 9$, $P > 0.99$). All data mean ± S.E.M.

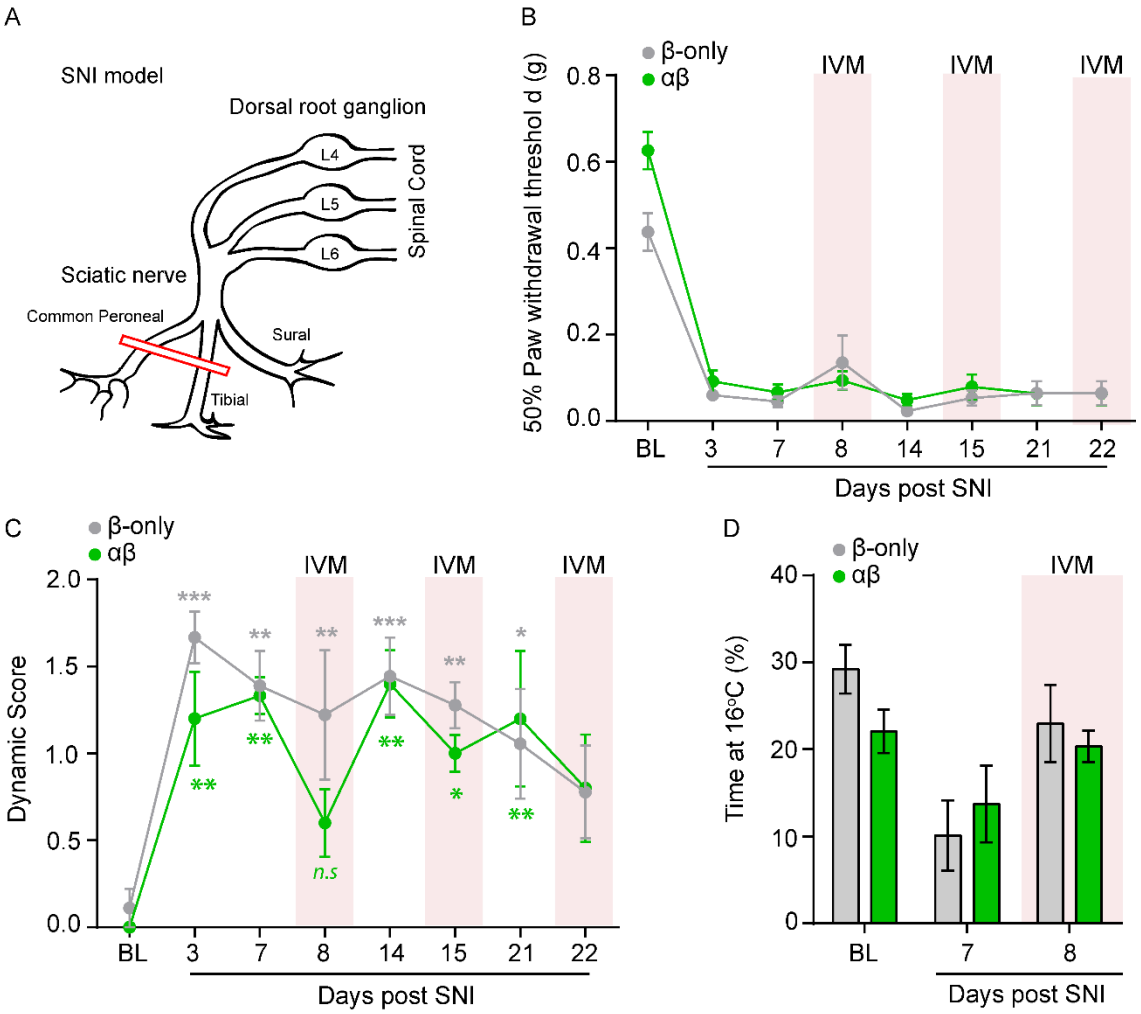

Figure 5: Early dynamic mechanical hypersensitivity, but not punctate mechanical or cold hypersensitivity, is alleviated after silencing Nav1.8 positive neurons.

A) Schematic of the SNI model of neuropathic pain used. **B)** Tracking of the punctate (v Frey) mechanical hypersensitivity following SNI in Nav1.8^{Cre}GluClαβ and GluClβ-only expressing mice. There were no changes in the punctate mechanical hypersensitivity following IVM in either αβ or β-only expressing Nav1.8 neurons (RM two-way ANOVA, with Bonferroni *post hoc* test β-only vs αβ, β-only; n = 6 mice, αβ; n = 5 mice, $t < 0.97$, $df = 72$, $P > 0.99$). **C)** Tracking of dynamic (Brush) mechanical hypersensitivity following SNI in mice expressing GluClαβ or β-only in the Nav1.8 population. Nav1.8^{Cre}GluClαβ mice remained significantly hypersensitive compared to BL, except day 8, IVM treatment day (RM two-way ANOVA, with Bonferroni *post hoc* test αβ BL vs αβ d8, n = 5 mice, $t < 1.705$, $df = 63$, $P = 0.65$). **D)** Cold hypersensitivity in αβ and β-only expressing Nav1.8^{Cre} mice following SNI. Following IVM, there were no significant changes in cold hypersensitivity in αβ or β-only controls (RM two-way ANOVA, with Bonferroni *post hoc* test, d8 β-only vs d8 αβ, β-only; n = 6 mice, αβ; n = 5 mice, $t = 0.523$, $df = 27$, $P > 0.99$). All data mean ± S.E.M.

3.3. The $TH^{CreERT2}$ transgenic mouse efficiently targets C-LTMRs

We characterised the $TH^{CreERT2}$ line generated by Abraira *et al.* (2017) as a means to target the C-LTMR population. This line was previously used to demonstrate C-LTMR central projections terminating in lamina II^{i} of the DH (Abraira *et al.*, 2017). We bred the $TH^{CreERT2}$ line with a Cre dependent tdTomato reporter line and induced tdTomato expression in adulthood in order to characterise the C-LTMR population at the level of the DRG, spinal cord and skin. We show that the labelled C-LTMR population makes up 4.7 ± 0.5% of lumbar and 9.8 ± 1.9% of thoracic DRG neurons (Fig. 6A-B), similar to previous studies (Li *et al.*, 2011). We confirmed that these neurons are indeed small neurons with an average neuronal area of 238.6 ± 8.3 μm^2 (an area below 490 μm^2 denotes a small DRG neuron with a diameter of 25μm). We have shown consistent and expected lamina II^{i} tdTomato C-LTMR terminations in the DH of the spinal cord (Fig. 6C) as reported previously (Abraira *et al.*, 2017). We assessed labelled sensory ending structures in the skin and identified longitudinal lanceolate endings associated with hair follicles on hind paw hairy skin (Fig. 6D). It has been recently reported that some species of rodent (including C57BL/6 strains) have hair follicles located between the running pads of their paws, which have been evolutionary conserved (Walcher *et al.*, 2018). Interestingly, we found that C-LTMR sensory endings are also present on the plantar surface of rodent glabrous skin and indeed innervate hairs located between rodent running pads (Fig. 6E). Finally, we did not see any labelled epidermal small fibres (nociceptors) (Fig. 6F). We have also shown that the $TH^{CreERT2}$ line is 87.41 ± 4.48% efficient at targeting the population when tamoxifen is given in adulthood (Fig. 6G+M). Genetically labelled TH positive C-LTMRs form a distinct non-overlapping population that do not express/bind, Parvalbumin (PV), IB4, CGRP, or S100β and 94.23% ±2.17 of C-LTMRs express the VGSC Nav1.8 (Fig. 6H-M).

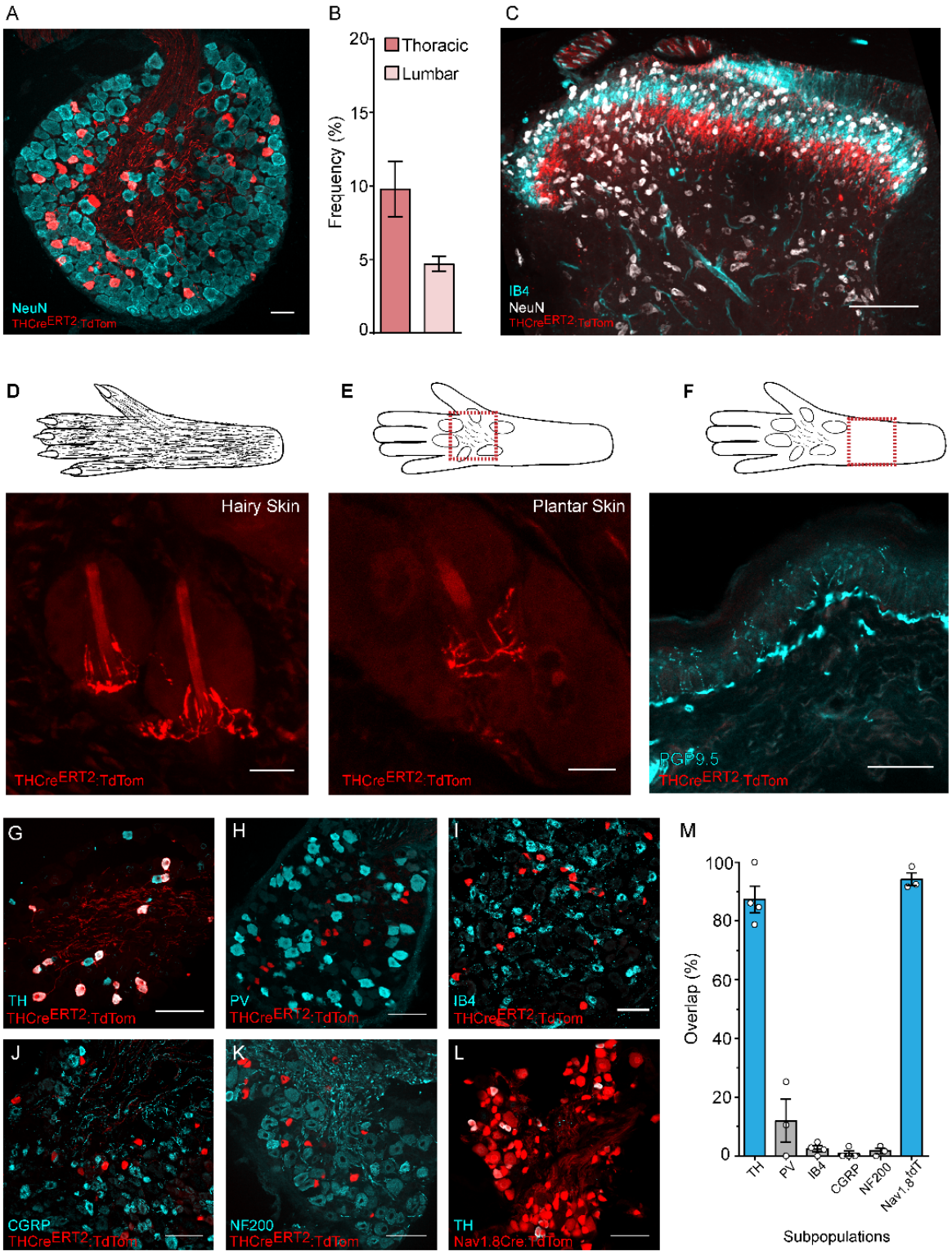

Figure 6: Characterisation of TH^{CreERT2} mouse line.

A) Example of genetically labelled C-LTMRs using the TH^{CreERT2} mouse line crossed with the Cre dependent reporter (tdTomato), scale bar 50 µm. **B)** Quantification of TH positive neuron frequency in thoracic and lumbar DRG. **C)** Dorsal horn of the spinal Cord showing C-LTMR termination in Lamina II^{i} below IB4 positive afferents which terminate in Lamina II^{o}. Scale bar 100

μm. **D)** tdTomato labelled C-LTMRs forming longitudinal lanceolate endings around hair follicles in hind-paw hairy skin. Scale bar 25μm. **E)** tdTomato positive C-LTMR innervating the hair follicles found on the plantar surface (located between the running pads) of mice. Scale bar 25μm. **F)** TH positive C-LTMRs do not terminate in the skin as PGP9.5+ epidermal free nerve endings. Scale bar 50 μm. **G)** Co-localisation of genetically labelled C-LTMRs and TH antibody labelled C-LTMR cell bodies in the DRG. $TH^{CreERT2}$ positive C-LTMRs are a largely non-overlapping population and minimal co-localisation was seen between Parvalbumin (PV) **(H)**, IB4 **(I)**, CGRP **(J)**, NF200 **(K)**. **L)** Almost all TH positive C-LTMRs co-express Nav1.8 as seen by co-localisation of genetically labelled Nav1.8 afferents ($Nav1.8^{Cre}$TdTom) and the TH antibody. G-L, scale bar 100 μm. **M)** Quantification of the $TH^{CreERT2}$tdTom co-localisation with other sensory neuron markers. (n = 3 or 4 mice, overlap averaged from 3 sections per mouse). All data represented as mean ± S.E.M.

3.4. Using AAV9.GluCl.Cre^{ON} to chemogenetically silence C-LTMRs

As C-LTMRs are a subpopulation of the Nav1.8 positive population, we wanted to interrogate their contribution to touch and pain sensation. To address this, cohorts of mice were generated, $TH^{CreERT2}$ mice were i.t. injected with AAV9.GluCl.Cre^{ON} (Fig 7A) and tamoxifen given 1 week later, which successfully transduced small TH+ DRG neurons (Fig 7B). These cohorts were behavioural characterised pre and post IVM treatment (Fig. 7C). The cohorts then received a spared nerve injury to investigate C-LTMR contribution to neuropathic pain. The neuropathic cohorts were tracked for 3 weeks with weekly IVM dosing and testing (Fig 7C).

Initially, we performed mechanical sensory testing on our cohorts. GluCl.Cre^{ON}αβ expressed in C-LTMRs resulted in hyposensitivity to punctate mechanical stimuli applied to the plantar surface of the paw post IVM (Fig. 8A). There were no significant changes in the detection of sticky tape placed onto the hind limb of mice, or the ability of mice to detect a light touch cotton swab when silencing C-LTMRs (Fig. 8B-C). When silencing C-LTMRs there was also no change in the latency to withdraw from a noxious hotplate (Fig. 8D). Mice were allowed to explore

the cold place preference apparatus and freely explored a 22°C zone and a 16°C zone. When silencing C-LMTRs mice spent longer at 22°C vs 16°C compared to β-only controls. There is still a lack of assays available to interrogate pleasure in rodents, we therefore hypothesised that perhaps mice find nesting pleasurable and lack of C-LTMR function might alter nesting ability. However, using a small cohort of mice, those that expressed αβ in C-LTMRs performed normally compared to control mice post IVM.

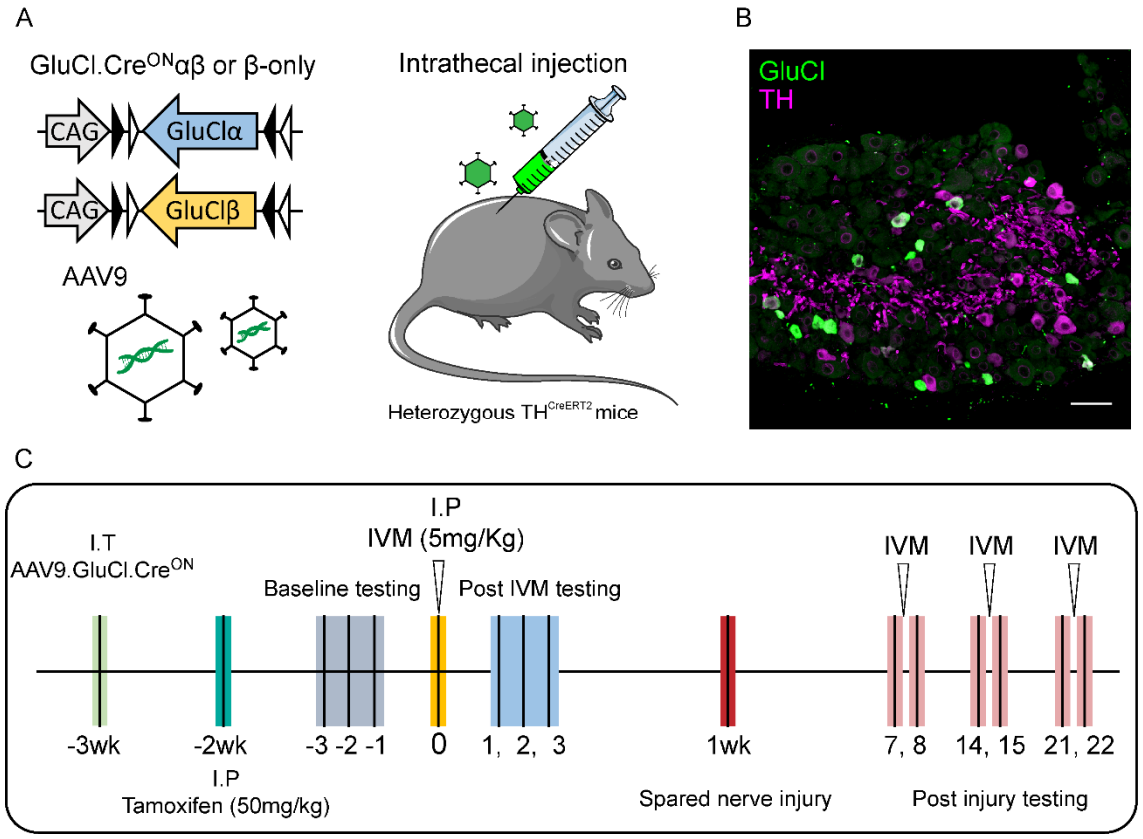

Figure 7: The timeline of the experimental setup of silencing TH positive C-LTMRs.

A) Schematic illustrating the intrathecal injection of AAV9.GluCl.Cre^{ON} into heterozygous TH^{CreERT2} mice. **B)** Example of GluCl.Cre^{ON} expression in TH^{CreERT2} injected mice, co-stained with TH antibody. Scale bar 50 µm. **C)** Timeline of events following intrathecal injection of GluCl.Cre^{ON}. Tamoxifen dosing, baseline testing, IVM dosing, post IVM testing, SNI, post SNI mechanical sensitivity testing over 3 weeks.

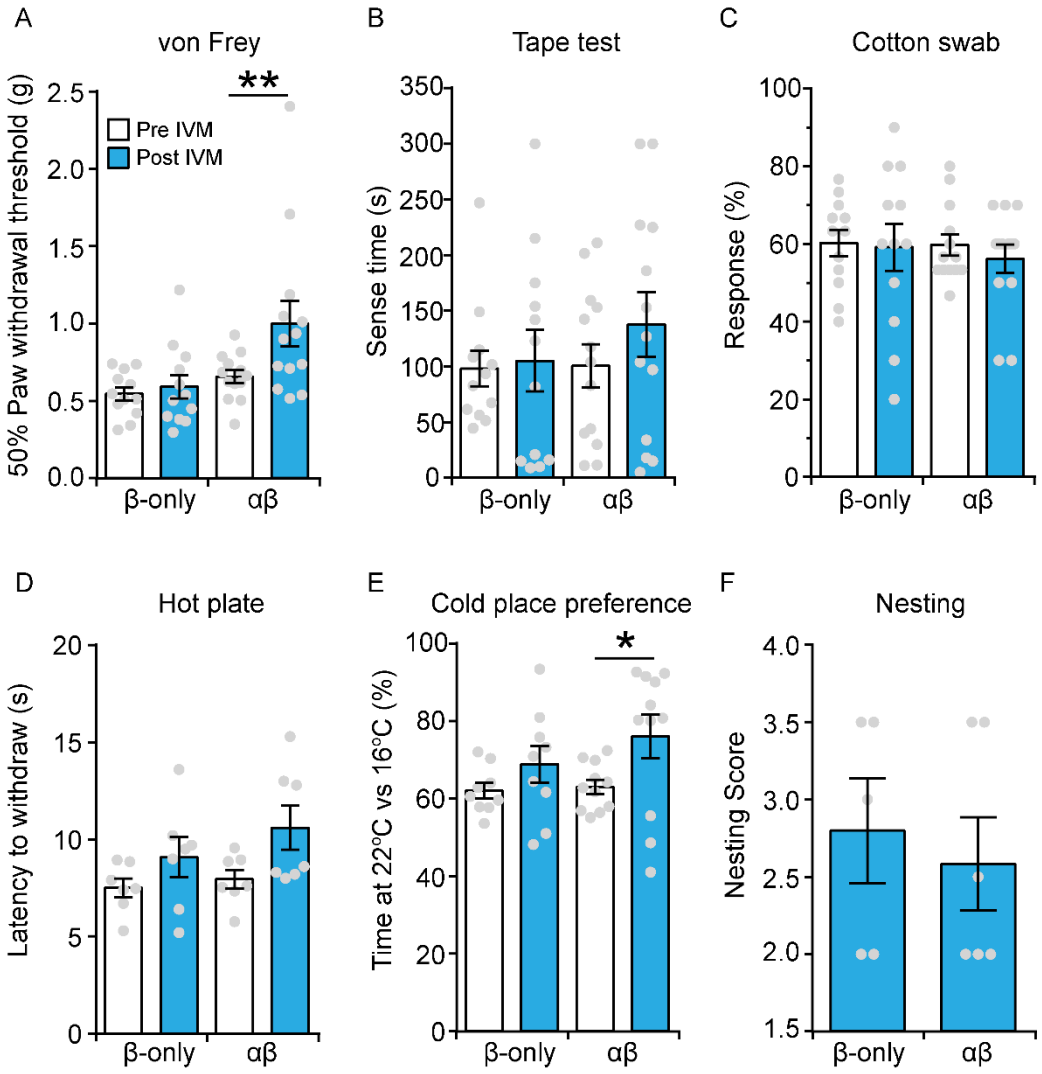

Figure 8: Acute sensory phenotyping after silencing TH^{CreERT2} positive C-LTMRs

A) Following IVM TH^{CreERT2} mice expressing αβ but not β-only become hyposensitive to punctate von Frey mechanical stimuli. (RM two-way ANOVA, with Bonferroni *post hoc* test, pre vs post IVM; β-only; n = 12 mice, t = 0.4269, df = 23, P > 0.99, αβ; n = 13 mice, t = 3.334, df = 23, P = 0.0058, **). **B)** Silencing C-LTMRs does not affect sense time during the tape test (RM two-way ANOVA, with Bonferroni *post hoc* test, pre vs post IVM; β-only; n = 12 mice, t = 0.213, df = 23, P > 0.99, αβ; n = 13 mice, t = 1.186, df = 23, P = 0.495). **C)** Silencing C-LTMRs does not affect the detection of a cotton swab (RM two-way ANOVA, with Bonferroni *post hoc* test, pre vs post IVM; β-only; n = 12 mice, t = 0.233, df = 23, P > 0.99, αβ; n = 13 mice, t = 0.784, df = 23, P = 0.881). **D)** Silencing C-LTMRs does not alter the response to a noxious 53°C hotplate (RM two-way ANOVA, with Bonferroni *post hoc* test, pre vs post IVM; β-only; n = 7 mice, t = 1.380, df = 12, P = 0.385, αβ; n = 7 mice, t = 2.321, df = 12, P = 0.077). **E)** TH^{CreERT2}GluClαβ expressing mice spend longer in 22°C vs 16°C compared to β-only expressing mice (RM two-way ANOVA, with Bonferroni *post hoc* test, pre vs post IVM; β-only; n = 9 mice, t = 1.162, df = 18, P = 0.520, αβ; n

= 11 mice, t = 2.476, df = 18, P = 0.0469, *). **F)** Silencing C-LTMRs does not alter the nesting ability of a small cohort of mice post IVM (two-tailed unpaired t-test, β-only; n = 5 mice, vs αβ; n = 6 mice, t = 0.479, df = 9, P = 0.642). All data represented as mean ± S.E.M.

To try to address the contribution of C-LTMRs to neuropathic pain like hypersensitivities, $TH^{CreERT2}$ mice expressing αβ and β-only received the spared nerve injury and were behaviourally assessed for the subsequent three weeks (Fig 9A). Both groups of mice became behaviourally hypersensitive to punctate von Frey and dynamic brush stimuli following SNI, however there was no recovery to either following IVM silencing (Fig 9B-C). Neuropathic mice were also assayed for the recovery of cold hypersensitivity. Cold hypersensitivity was maintained in both groups on day 8 when IVM was given and C-LTMRs silenced. Taken together C-LTMRs may not have a role in SNI induced neuropathic pain.

A previous study ablated GINIP+ sensory neurons which encompass C-LMTRs and non-peptidergic nociceptors. The study suggested that C-LTMRs are uniquely responsible for the inflammatory pain behaviour that presents following an injection of formalin (Urien *et al.*, 2017). Formalin injections induce nocifensive behaviour that occurs in two phases over 60 minutes (Fig 10A-B). Formalin was given to mice that expressed GluCl.Cre^{ON}αβ and β-only specifically in C-LTMRs. Contrary to the literature, silencing of C-LTMRs did not alter formalin-evoked pain in either the first or second phase (Fig. 10C).

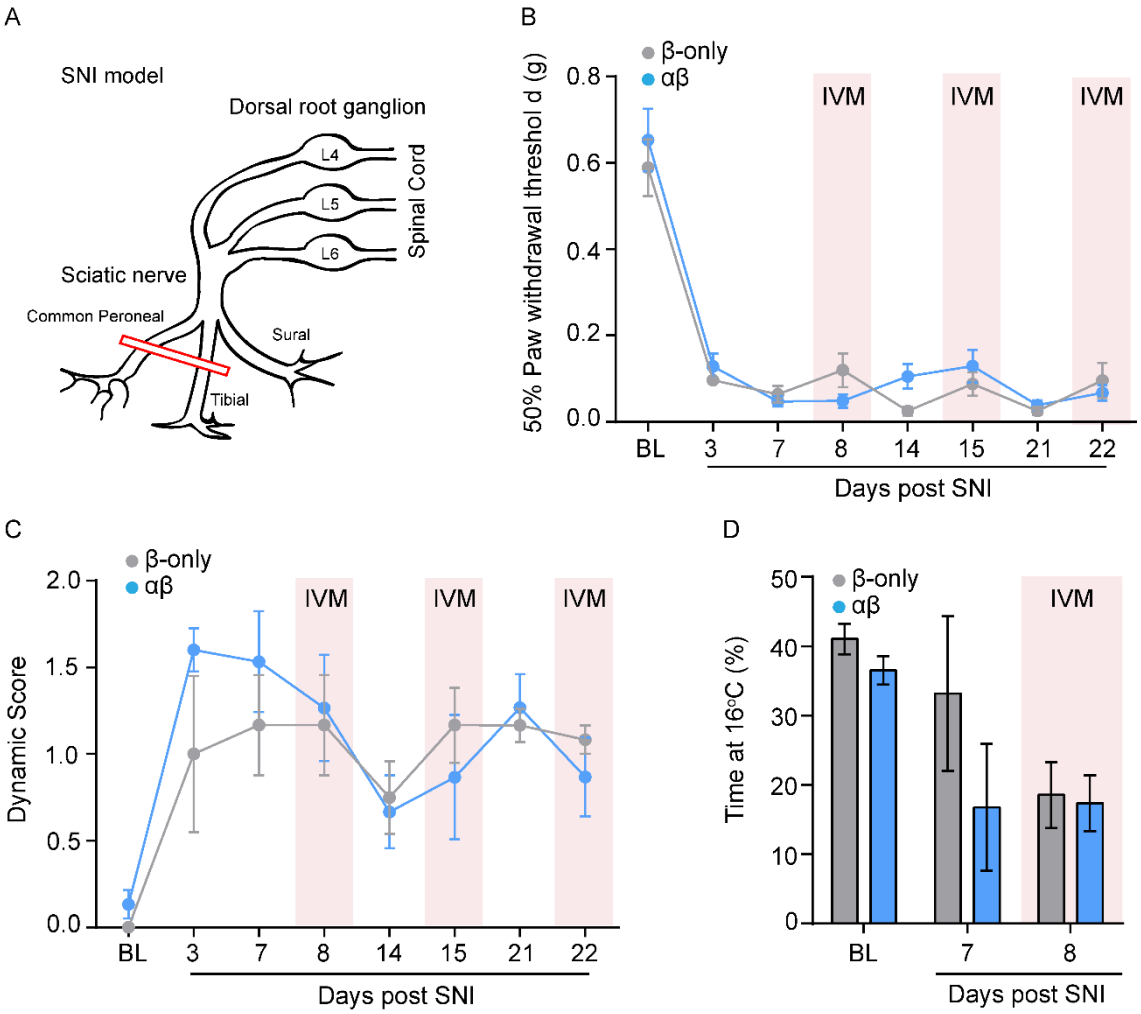

Figure 9: Neuropathic pain-related mechanical and cold hypersensitivities are unchanged after silencing TH+ positive neurons

A) Schematic of the SNI model of neuropathic pain used. **B)** Tracking of the punctate (von Frey) mechanical hypersensitivity following SNI in TH^{CreERT2}GluClαβ and GluClβ-only expressing mice. There were no changes in the punctate mechanical hypersensitivity following IVM in either group (RM two-way ANOVA, with Bonferroni *post hoc* test β-only vs αβ, β-only; n = 10 mice, αβ; n = 11 mice, $t < 2.158$, $df = 158$, $P > 0.99$). **C)** Tracking of dynamic (Brush) mechanical hypersensitivity following SNI in TH^{CreERT2}GluClαβ and GluClβ-only expressing mice. Following IVM mice from both groups remained significantly hypersensitive compared to BL, except d14 but this was not a treatment day. (RM two-way ANOVA, with Bonferroni *post hoc* test BL vs all other time points (except d14). β-only; n = 4 mice, αβ; n = 5 mice, $t > 3.29$, $df = 49$, P<0.05). **D)** The cold hypersensitivity in TH^{CreERT2}GluClαβ and β-only expressing mice following SNI. Following IVM there were no significant difference in day 8 cold hypersensitivity between the two groups. (RM two-way ANOVA, with Bonferroni *post hoc* test d8 β-only vs d8 αβ, β-only; n = 4 mice, αβ; n = 5 mice, $t = 0.127$, $df = 21$, $P > 0.99$). All data represented as mean ± S.E.M.

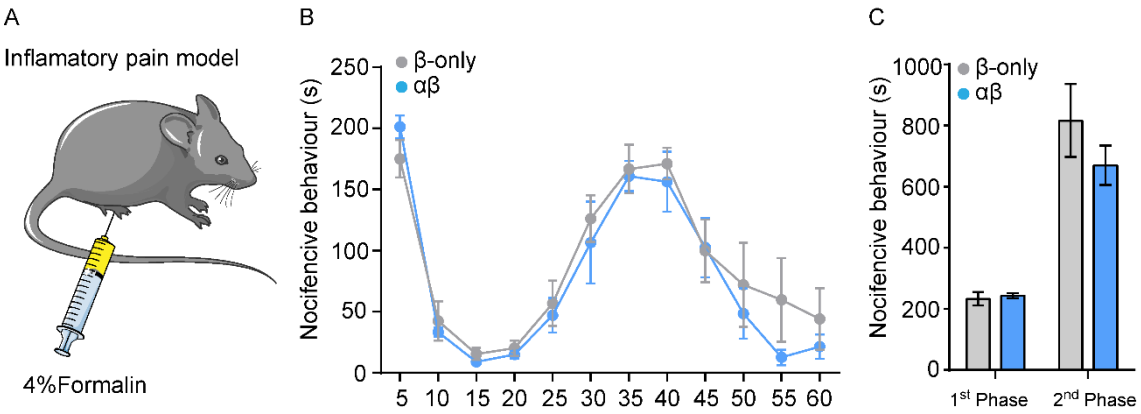

Figure 10. Formalin evoked inflammatory pain does not require C-LTMRs.

A) An illustration of the model used. 4% formalin injected subcutaneously into the hind paw. **B)** Nocifensive behaviour was live scored for 1 hr post formalin injection which was given 24 hrs post IVM administration. There were no differences in nocifensive behaviour between $TH^{CreERT2}$GluClαβ and GluClβ-only expressing mice. (RM two-way ANOVA, with Bonferroni *post hoc* test β-only vs αβ, β-only; n = 5 mice, αβ; n = 6 mice, $t < 1.76$, $df = 108$, $P > 0.99$). **C)** Nocifensive behaviours categorised into the 1st and 2nd phase of the model also did not differ between groups (RM two-way ANOVA, with Bonferroni *post hoc* test β-only vs αβ, β-only; n = 5 mice, αβ; n = 6 mice, 1st phase; $t = 0.011$, $df = 18$, $P > 0.99$, 2nd phase; $t = 1.57$, $df = 18$, $P = 0.265$). All data mean ± S.E.M.

4. Discussion

The Cre dependent GluCl.Cre^{ON} system was employed in two sensory neuron populations using the transgenic Nav1.8^{Cre} and inducible TH^{CreERT2} driver mouse lines. Selective silencing of Nav1.8 positive neurons resulted in hyposensitivity to noxious thermal stimuli and early hyposensitivity to dynamic brush stimuli following traumatic nerve injury. The selective silencing of C-LTMRs resulted in hyposensitivity to punctate mechanical stimuli but no major changes in evoked neuropathic pain related sensitivities. These findings provide evidence that our approach can be used to selectively modulate different populations of sensory neurons, giving rise to population specific changes in sensory modalities.

The Nav1.8^{Cre} line used herein, has been well characterised. However, some studies question the specificity of the Nav1.8^{Cre} to purely nociceptive populations. Shields *et al*. (2012) used the Nav1.8^{Cre} line crossed with a Cre-dependent reporter to show that the Nav1.8^{Cre} line largely labels nociceptors. However, they also reported that some cutaneous Meissner corpuscles and C-LTMRs, which are associated with mechanosensation, were genetically labelled (Shields *et al.*, 2012). It was therefore important to analyse the Nav1.8^{Cre} population in our hands. In line with the wealth of previous literature, the labelled Nav1.8^{Cre} neurons show strong overlap with nociceptive markers such as TRPV1, CGRP and IB4 (Novakovic *et al.*, 1998; Amaya *et al.*, 2000; Abrahamsen *et al.*, 2008). Some Nav1.8+ neurons express the marker of myelinated afferents S100β. The Nav1.8+ S100β+ population likely include myelinated Aδ and Aβ nociceptors, but may also include some Aβ-LTMRs (Shields *et al.*, 2012). Therefore we looked at the co-expression of Calbindin a marker of RA-LTMRs that are thought to form Meissner corpuscles and hair follicle endings. 2.77 ± 0.21% of Nav1.8 positive neurons were Calbindin positive. However, as the calbindin population is a small population (~10% of total DRG neurons) this 2.77% of the Nav1.8 population corresponds to 17.89 ± 3.58% of the Calbindin population. Suggesting, 17.89% of RA-LTMRs are Nav1.8

positive. In addition nearly all TH positive C-LTMRs express Nav1.8, consistent with Shields *et al.* (2012) who observed Nav1.8 and VGLUT3 co-expression. The dorsal horn of the spinal cord was investigated and there were laminae II^{i} terminations consistent with C-LTMRs, and interestingly deep terminal projections which are within the LTMR zone (Abraira *et al.*, 2017). These could relate to Nav1.8 positive LTMRs or some CGRP positive afferents which are also known to terminate (McCoy *et al.*, 2013). Taken together, Nav1.8 is not restricted to nociceptors, and interpretation of previous studies and the data herein need to be considered in this light.

Regardless of the nociceptor specificity issue of the $Nav1.8^{Cre}$ line, we wanted to use it to validate our system and there is a wealth of previous studies to which we can compare our findings. We showed that $GluCl.Cre^{ON}$ was functional when virally expressed in Nav1.8 positive neurons and IVM given *in vivo*. Neurons were subsequently cultured and assessed using patch-clamp. While silencing does not alter RMP, αβ expressing neurons exhibited a large chloride conductance, low input resistance and increased rheobase. On average the rheobase was 5.4x larger compared to β-only control expressing neurons. While this increase was large, it was not as large as the excitability changes seen previously (>10x rheobase, Chapter 2). This could be due to differences in IVM given *in vitro* vs *in vivo*. Perhaps the dose we prescribe does not fully sequester DRG neurons (like *in vitro*) due to IVM clearance, or perhaps the level of GluCl expression is lower, as there is a requirement for multiple processes to occur. Unlike GluClv2.0, $GluCl.Cre^{ON}$ requires successful viral transduction and Cre-mediated recombination of each subunit, potentially reducing transcription efficiency. $GluCl.Cre^{ON}$ was also designed using a shorter CAG promoter which could account for the variation between GluClv2.0 and $GluCl.Cre^{ON}$. Regardless, the 5.4x increase in rheobase can be interpreted as physiologically relevant and certainly in excess of that demonstrated for both DREADD and optogenetic silencing of sensory neurons (Saloman *et al.*, 2016; Samineni *et al.*, 2017). We assessed acute behavioural responses pre and post Nav1.8+

population silencing. We confirmed that our observed silencing was enough to produce hyposensitivity to noxious heat stimuli and a trend for hyposensitivity to noxious pin prick, but not light touch sensibility or motor function. Unfortunately, the sample size was small (except for hot plate) so these experiments warrant replication. We were powered enough to see a functional change in thermal nociception, which is not in accordance with previous studies which ablated the Nav1.8 population (Abrahamsen *et al.*, 2008). Abrahamsen *et al.* (2008) saw a near absence of cold pain detection when ablating Nav1.8 nociceptors, which was not investigated here. Future work should look at the cold response of GluCl.Cre^{ON} silenced Nav1.8+ neurons. Our work is also contrary to the optogenetic silencing of the Nav1.8 population which did not observe changes in heat pain in naïve mice (Daou *et al.*, 2016)). It is not logical that these two studies did not see changes in heat nociception when we show that 64.02 ± 0.81% of the Nav1.8 population express the heat activated ion channel TRPV1. Indeed ablation or inactivation of the TRPV1-lineage or CGRPα populations (which are both Nav1.8 positive) resulted in heat hyposensitivity (Mishra *et al.*, 2011; Cowie *et al.*, 2018). Perhaps this highlights the issue with using ablation and proton pumps to investigate the function of sensory neuron populations. Ablation studies have provided valuable insight into sensory neuron heterogeneity and population function both pre and post neuropathic injury. However, caution needs to be taken when interpreting these data for the following reasons. Ablation using the diphtheria toxin system is irreversible and in itself could be considered an injury. It is also unclear how the anatomical loss of a population might after the function of other populations and their networks within the CNS (Foster *et al.*, 2015). In particular, ablation could lead to synaptic plasticity in the spinal cord dorsal horn and/or an immune response related to the cell death. This is particularly important as there is strong interplay between the immune system and pathological pain (Calvo, Dawes and Bennett, 2012). Equally, the optogenetic silencing of Nav1.8 neurons used a tool which extruded protons for 1 hr. Increasing the extracellular proton concentration for 1 hr would likely have other consequences, and may activate acid-sensing ion channels (ASICs)

and other pH sensitive proteins. Indeed, heterologously expressed ASICs were activated by yellow light/Arch mediated proton efflux (Zeng *et al.*, 2015). Furthermore, computational models predicted the peak proton concentration at the extracellular membrane, as a result of Arch activation would reach pH 6.7, enough to activate ASICs *in vivo* (Zeng *et al.*, 2015). This is particularly pertinent as ASICs are known to modulate mechanosensory function (Omerbašić *et al.*, 2015).

Due to GluCl.Cre^{ON} working *in vivo* we wanted to selectively target the Nav1.8 population after neuropathic injury as there is debate in the literature over their contribution (Nassar *et al.*, 2005; Joshi *et al.*, 2006; Abrahamsen *et al.*, 2008; Daou *et al.*, 2016). We tracked neuropathic mice over three weeks and did not see changes in punctate mechanical or cold hypersensitivity post silencing. However, 8 day post injury, during a Nav1.8 silencing period dynamic brush hypersensitivity was not significantly different from baseline, suggesting a reduction in dynamic hypersensitivity. The only other studies which assessed dynamic hypersensitivity post nociceptor ablation/inactivation following SNI were Nocchi *et al* (2019) and Cowie *et al* (2018). They used NGF targeted photoablation to ablate TrkA+ sensory terminals and the optogenetic silencing of GCRPα positive afferents, respectively. Both of these studies did not see changes in injury induced dynamic sensitivity (Cowie *et al.*, 2018; Nocchi *et al.*, 2019). Our findings suggest, this may represent sensitization of Nav1.8+ population or related spinal circuits following SNI, which relay dynamic hypersensitivity. However, this observation may relate to non-nociceptor specific expression of Nav1.8 in 17.89% of the Calbindin+ RA-LMTR population. Calbindin positive neurons likely co-express low levels of TrkB (Aδ-LTMR and RA-LTMR marker) and previous work has implicated the TrkB+ population of sensory neurons as key contributors to post SNI punctate and dynamic mechanical hypersensitivity (Dhandapani *et al.*, 2018). Parsing out which portion of the Nav1.8 population is responsible for this partial recovery will be difficult, but investigating smaller subpopulations of afferents using GluCl will facilitate this. This observation also

warrants further investigation to see if this is a replicable finding and future work will aim to look at the contribution of Nav1.8 afferents to tonic ongoing pain following SNI, using the conditioned place preference paradigm. There is literature outlining that post-injury spontaneous activity occurs initially in A-fibres (Wall and Gutnick, 1974; Boucher *et al.*, 2000; Liu *et al.*, 2000; Wu *et al.*, 2001) and is followed by C-fibres (Wu *et al.*, 2001, 2002). Assaying for the contribution of Nav1.8 afferents at different time points would provide valuable insight to tonic pain mechanisms.

Next, we wanted to use GluCl.Cre^{ON} to target a sparse population of sensory neurons termed the C-low threshold mechanoreceptors. Until recently this population has been difficult to target and modulate due to the lack of efficient Cre driver lines (Badea *et al.*, 2009). The TH positive population have C-fibre range conduction velocities and detect low threshold mechanical stimuli (Li *et al.*, 2011). The population is also specifically marked by VGlut3, Tafa4 and Cav3.3 (Seal *et al.*, 2009; Delfini *et al.*, 2013; Reynders *et al.*, 2015). The initially generated TH^{CreER} line only sparsely marked the population (Badea *et al.*, 2009). A new TH^{CreERT2} line was generated and we carried out a thorough population characterisation and identified that this Cre driver line efficiently targets the TH positive population, and is a good model to interrogate C-LTMR function. We provide evidence that TH positive sensory neurons innervate the small hairs that are found on the glabrous surface of hindpaws, which were previously thought to only be innervated by Aδ LTMRs (Dawes *et al.*, 2018; Walcher *et al.*, 2018). Importantly, this region (between the running pads) is where we test our mice for mechanical sensitivity. To confirm further that these TH positive cutaneous afferents are C-LTMRs, future work using primary afferent recordings could be conducted on TH^{CreERT2} mice that have been crossed with a Cre dependent channelrhodopsin 2 effector line. This would allow skin-nerve characterisation of optically activated TH positive afferents.

However, after confirming that the TH^{CreERT2} driver line was a good model to investigate C-LTMR function we wanted to use GluCl.Cre^{ON} to target and silence the

population. Interestingly, we found that when silencing this population mice were hyposensitive to punctate mechanical stimuli. This is in line with a previous study that investigated C-LTMR function through gene KO strategies (François *et al.*, 2015). One discrepancy in this chapter of work is that C-LTMRs which express Nav1.8 appear to modulate punctate mechanical detection, but silencing the Nav1.8 population has little effect on punctate von Frey thresholds. It is important to note that the Nav1.8 silencing study is underpowered and has resulted in large data variability particularly apparent in the von Frey results. Looking at the data there is a trend for hyposensitivity in the experimental group in this assay and future replication studies will parse out if this is a significant effect. Alternatively, it is possible that at the level of the spinal cord, TH positive neurons are part of a circuit that modulates other Nav1.8 subpopulations and loss of this modulation results in punctate hyposensitivity, only when silencing TH+ neurons and not all Nav1.8 neurons.

Some C-LMTRs are thought to respond to cooling stimuli (Li *et al.*, 2011; François *et al.*, 2015), therefore we aimed to investigate cool sensibility while silencing the population. Using the cold place preference assay, there is a slight preference for the 22^{o}C vs 16^{o}C. This could suggest that C-LTMRs are responsible for cool sensibility and detection. However, the interpretation of the cold place preference assay is difficult in non-injured states; are we observing a reduced preference for 16^{o}C or a gained preference for 22^{o}C? Equally, the two temperatures alone might not be ideally suited to address the question and a more sensitive assay should be used in the future to look in detail at the consequences of silencing TH positive neurons on thermal sensibility. For instance, using the thermal gradient apparatus. In addition, silencing TH positive afferents did not alter the detection of cotton swab, tape or rodents motivation to nest. These findings are in accordance to those results presented in the next chapter where Nav1.7 is selectively ablated in C-LTMRs.

There is debate over the role of C-LTMRs in neuropathic and painful conditions (Seal *et al.*, 2009; Delfini *et al.*, 2013; François *et al.*, 2015; Peirs *et al.*, 2015; Kambrun *et al.*, 2018). However, silencing C-LTMRs did not alter evoked hypersensitivities following SNI. Due to low sample sizes these experiments require repeating. The involvement of C-LTMRs in tonic ongoing pain has never been investigated and is something that will be followed up in future cohorts. A previous study used DTR/DTX ablation to ablate a population of sensory neurons which express GINIP. GINIP is expressed by C-LMTRs and IB4+ neurons. The authors concluded that ablating GINIP+ sensory neurons resulted in the absence of formalin evoked pain, a model of inflammatory pain (Urien *et al.*, 2017). We therefore wanted to ask if silencing C-LTMRs specifically altered formalin pain behaviours. Contrary to Urien *et al*. (2017), we did not observe any changes to the formalin evoked behaviour when silencing C-LMTRs. Suggesting that this population may not have a role in formalin evoked inflammatory pain. Alternatively, formalin pain may require the interplay of two populations, IB4+ and C-LTMRs, however at present, this mechanism is unclear.

An important point to note is that there were difficulties in detecting GluCl.Cre^{ON} expression when analysing sectioned tissue when targeting both the Nav1.8 and Th positive populations. However, when neurons were cultured expression was easier to detect. This could be due to the large area GluCl needs to cover *in vivo*, where as cultured neuron neurites are stunted which could allow GluCl to accumulate. This could also indicate our Cre^{ON} expressing constructs are lowly expressed, limiting the ability to fully silence a population, which could lead to behavioural false negative phenotypes. However, despite this technical issue we saw effective GluCl.Cre^{ON} silencing both *in vivo* and *in vitro.* Future work, will investigate how to increase this Cre-dependent expression of GluCl.Cre^{ON}.

To summarise, I have employed the newly developed AAV9.GluCl.Cre^{ON} tool and employed it to investigate two sensory neuron populations. The selective silencing of

Nav1.8 nociceptors resulted in robust hyposensitivity to heat stimuli without affecting light mechanosensation. The selective silencing of TH+ C-LTMRs resulted in large hyposensitivity to punctate mechanical stimuli. These data suggest that the C-LTMR population, which has been largely understudied may play a large role in mechanosensation and we show that C-LTMR afferents are present on the plantar surface of rodents. At present, silencing the Nav1.8 positive population mildly attenuates dynamic hypersensitivity following SNI. This work is still in its infancy and requires replication and investigation into non-evoked ongoing pain. This work has validated our novel GluCl.Cre^{ON} tool which can now be applied to defined sensory neuron populations to investigate their role in sensory biology.

5. Acknowledgements:

All rodent surgeries and behaviour in this chapter were performed together and/or equally split between Dr Weir and myself.

6. References

Abrahamsen, B. *et al.* (2008) 'The cell and molecular basis of mechanical, cold, and inflammatory pain', *Science*, 321(5889), pp. 702–705. doi: 10.1126/science.1156916.

Abraira, V. E. *et al.* (2017) 'The Cellular and Synaptic Architecture of the Mechanosensory Dorsal Horn', *Cell*. Cell Press, 168(1–2), pp. 295-310.e19. doi: 10.1016/J.CELL.2016.12.010.

Amaya, F. *et al.* (2000) 'Diversity of expression of the sensory neuron-specific TTX-resistant voltage-gated sodium ion channels SNS and SNS2', *Molecular and Cellular Neurosciences*. Academic Press Inc., 15(4), pp. 331–342. doi: 10.1006/mcne.1999.0828.

Arcourt, A. *et al.* (2016) 'Touch Receptor-Derived Sensory Information Alleviates Acute Pain Signaling and Fine-Tunes Nociceptive Reflex Coordination', *Neuron*. Elsevier Inc., 93(1), pp. 179–193. doi: 10.1016/j.neuron.2016.11.027.

Badea, T. C. *et al.* (2009) 'New Mouse Lines for the Analysis of Neuronal Morphology Using CreER(T)/loxP-Directed Sparse Labeling', *PLoS ONE*. Edited by T. Ikezu, 4(11), p. e7859. doi: 10.1371/journal.pone.0007859.

Binshtok, A. M., Bean, B. P. and Woolf, C. J. (2007) 'Inhibition of nociceptors by TRPV1-mediated entry of impermeant sodium channel blockers', *Nature*. Nature Publishing Group, 449(7162), pp. 607–610. doi: 10.1038/nature06191.

Boucher, T. J. *et al.* (2000) 'Potent analgesic effects of GDNF in neuropathic pain states', *Science*, 290(5489), pp. 124–127. doi: 10.1126/science.290.5489.124.

Calvo, M., Dawes, J. M. and Bennett, D. L. H. (2012) 'The role of the immune system in the generation of neuropathic pain', *The Lancet Neurology*, pp. 629–642. doi: 10.1016/S1474-4422(12)70134-5.

Cavanaugh, D. J. *et al.* (2009) 'Distinct subsets of unmyelinated primary sensory fibers

mediate behavioral responses to noxious thermal and mechanical stimuli', *Proceedings of the National Academy of Sciences of the United States of America*. National Academy of Sciences, 106(22), pp. 9075–9080. doi: 10.1073/pnas.0901507106.

Cheng, L. *et al.* (2017) 'Identification of spinal circuits involved in touch-evoked dynamic mechanical pain', *Nature Neuroscience*. Nature Publishing Group, 20(6), pp. 804–814. doi: 10.1038/nn.4549.

Cowie, A. *et al.* (2018) 'Optogenetic Inhibition of CGRP␣ Sensory Neurons Reveals Their Distinct Roles in Neuropathic and Incisional Pain', 38(25), pp. 5807–5825. doi: 10.1523/JNEUROSCI.3565-17.2018.

Daou, I. *et al.* (2016) 'Optogenetic silencing of Nav1.8-positive afferents alleviates inflammatory and neuropathic pain', *eNeuro*. Society for Neuroscience, 3(1), pp. 702–705. doi: 10.1523/ENEURO.0140-15.2016.

Dawes, J. M. *et al.* (2018) 'Immune or Genetic-Mediated Disruption of CASPR2 Causes Pain Hypersensitivity Due to Enhanced Primary Afferent Excitability', *Neuron*, 97(4), pp. 806-822.e10. doi: 10.1016/j.neuron.2018.01.033.

Deacon, R. M. J. (2006) 'Assessing nest building in mice', *Nature Protocols*, 1(3), pp. 1117–1119. doi: 10.1038/nprot.2006.170.

Delfini, M.-C. *et al.* (2013) 'TAFA4, a Chemokine-like Protein, Modulates Injury-Induced Mechanical and Chemical Pain Hypersensitivity in Mice', *Cell Reports*. Cell Press, 5(2), pp. 378–388. doi: 10.1016/J.CELREP.2013.09.013.

Dhandapani, R. *et al.* (2018) 'Control of mechanical pain hypersensitivity in mice through ligand-targeted photoablation of TrkB-positive sensory neurons', *Nature Communications*. Nature Publishing Group, 9(1), p. 1640. doi: 10.1038/s41467-018-04049-3.

Dixon, W. J. (1980) 'Efficient Analysis of Experimental Observations', *Annual Review*

of Pharmacology and Toxicology, 20(1), pp. 441–462. doi: 10.1146/annurev.pa.20.040180.002301.

Fitzgerald, M. and Woolf, C. J. (1982) 'The time course and specificity of the changes in the behavioural and dorsal horn cell responses to noxious stimuli following peripheral nerve capsaicin treatment in the rat', *Neuroscience*, 7(9), pp. 2051–2056. doi: 10.1016/0306-4522(82)90119-1.

Foster, E. *et al.* (2015) 'Targeted ablation, silencing, and activation establish glycinergic dorsal horn neurons as key components of a spinal gate for pain and itch', *Neuron*. Cell Press, 85(6), pp. 1289–1304. doi: 10.1016/j.neuron.2015.02.028.

François, A. *et al.* (2015) 'The Low-Threshold Calcium Channel Cav3.2 Determines Low-Threshold Mechanoreceptor Function', *Cell Reports*. Cell Press, 10(3), pp. 370–382. doi: 10.1016/J.CELREP.2014.12.042.

Hjerling-Leffler, J. *et al.* (2007) 'Emergence of functional sensory subtypes as defined by transient receptor potential channel expression', *Journal of Neuroscience*, 27(10), pp. 2435–2443. doi: 10.1523/JNEUROSCI.5614-06.2007.

Jayaraj, N. D. *et al.* (2018) 'Reducing CXCR4-mediated nociceptor hyperexcitability reverses painful diabetic neuropathy', *Journal of Clinical Investigation*. American Society for Clinical Investigation, 128(6), pp. 2205–2225. doi: 10.1172/JCI92117.

Joseph, E. K. and Levine, J. D. (2010) 'Hyperalgesic priming is restricted to isolectin B4-positive nociceptors', *Neuroscience*, 169(1), pp. 431–435. doi: 10.1016/j.neuroscience.2010.04.082.

Joshi, S. K. *et al.* (2006) 'Involvement of the TTX-resistant sodium channel Nav 1.8 in inflammatory and neuropathic, but not post-operative, pain states', *Pain*, 123(1–2), pp. 75–82. doi: 10.1016/j.pain.2006.02.011.

Kambrun, C. *et al.* (2018) 'TAFA4 Reverses Mechanical Allodynia through Activation of

GABAergic Transmission and Microglial Process Retraction', *Cell Reports*. Cell Press, 22(11), pp. 2886–2897. doi: 10.1016/J.CELREP.2018.02.068.

Karai, L. *et al.* (2004) 'Deletion of vanilloid receptor 1-expressing primary afferent neurons for pain control', *Journal of Clinical Investigation*. The American Society for Clinical Investigation, 113(9), pp. 1344–1352. doi: 10.1172/JCI20449.

Kilkenny, C. *et al.* (2010) 'Improving Bioscience Research Reporting: The ARRIVE Guidelines for Reporting Animal Research', *PLoS Biology*. Public Library of Science, 8(6), p. e1000412. doi: 10.1371/journal.pbio.1000412.

Li, L. *et al.* (2011) 'The Functional Organization of Cutaneous Low-Threshold Mechanosensory Neurons', *Cell*. Cell Press, 147(7), pp. 1615–1627. doi: 10.1016/J.CELL.2011.11.027.

Liu, C. N. *et al.* (2000) 'Tactile allodynia in the absence of C-fiber activation: Altered firing properties of DRG neurons following spinal nerve injury', *Pain*. Elsevier, 85(3), pp. 503–521. doi: 10.1016/S0304-3959(00)00251-7.

Liu, P., Jenkins, N. A. and Copeland, N. G. (2003) 'A highly efficient recombineering-based method for generating conditional knockout mutations', *Genome Research*, 13(3), pp. 476–484. doi: 10.1101/gr.749203.

Löken, L. S. *et al.* (2009) 'Coding of pleasant touch by unmyelinated afferents in humans', *Nature Neuroscience*. Nature Publishing Group, 12(5), pp. 547–548. doi: 10.1038/nn.2312.

McCoy, Eric S. *et al.* (2013) 'Peptidergic CGRPα Primary Sensory Neurons Encode Heat and Itch and Tonically Suppress Sensitivity to Cold', *Neuron*, 78(1), pp. 138–151. doi: 10.1016/j.neuron.2013.01.030.

McCoy, Eric S. *et al.* (2013) 'Peptidergic CGRPα Primary Sensory Neurons Encode Heat and Itch and Tonically Suppress Sensitivity to Cold', *Neuron*. Cell Press, 78(1),

pp. 138–151. doi: 10.1016/j.neuron.2013.01.030.

Miller, R. E. *et al.* (2017) ‘Chemogenetic Inhibition of Pain Neurons in a Mouse Model of Osteoarthritis’, *Arthritis & Rheumatology*, 69(7), pp. 1429–1439. doi: 10.1002/art.40118.

Mishra, S. K. *et al.* (2011) ‘TRPV1-lineage neurons are required for thermal sensation’, *EMBO Journal*, 30(3), pp. 582–593. doi: 10.1038/emboj.2010.325.

Mishra, S. K. and Hoon, M. A. (2010) ‘Ablation of TrpV1 neurons reveals their selective role in thermal pain sensation’, *Molecular and Cellular Neuroscience*, 43(1), pp. 157–163. doi: 10.1016/j.mcn.2009.10.006.

Morrison, I. *et al.* (2011) ‘Reduced C-afferent fibre density affects perceived pleasantness and empathy for touch’, *Brain*. Narnia, 134(4), pp. 1116–1126. doi: 10.1093/brain/awr011.

Nassar, M. A. *et al.* (2004) ‘Nociceptor-specific gene deletion reveals a major role for Nav1.7 (PN1) in acute and inflammatory pain’, *Proceedings of the National Academy of Sciences*, 101(34), pp. 12706–12711. doi: 10.1073/pnas.0404915101.

Nassar, M. A. *et al.* (2005) ‘Neuropathic pain develops normally in mice lacking both Na(v)1.7 and Na(v)1.8.’, *Molecular pain*, 1, p. 24. doi: 10.1186/1744-8069-1-24.

Neubert, J. K. *et al.* (2003) ‘Peripherally induced resiniferatoxin analgesia’, *Pain*. Elsevier, 104(1–2), pp. 219–228. doi: 10.1016/S0304-3959(03)00009-5.

Nocchi, L. *et al.* (2019) ‘Nerve growth factor-mediated photoablation of nociceptors reduces pain behavior in mice’, *Pain*. NLM (Medline), 160(10), pp. 2305–2315. doi: 10.1097/j.pain.0000000000001620.

Novakovic, S. D. *et al.* (1998) ‘Distribution of the tetrodotoxin-resistant sodium channel PN3 in rat sensory neurons in normal and neuropathic conditions.’, *The Journal of neuroscience : the official journal of the Society for Neuroscience*, 18(6), pp. 2174–87.

Available at: http://www.ncbi.nlm.nih.gov/pubmed/9482802 (Accessed: 31 December 2019).

Omerbašić, D. *et al.* (2015) 'ASICs and mammalian mechanoreceptor function', *Neuropharmacology*. Pergamon, pp. 80–86. doi: 10.1016/j.neuropharm.2014.12.007.

Ongun, S., Sarkisian, A. and McKemy, D. D. (2018) 'Selective cold pain inhibition by targeted block of TRPM8-expressing neurons with quaternary lidocaine derivative QX-314', *Communications Biology*. Nature Research, 1(1). doi: 10.1038/s42003-018-0062-2.

Peirs, C. *et al.* (2015) 'Dorsal Horn Circuits for Persistent Mechanical Pain', *Neuron*. Cell Press, 87(4), pp. 797–812. doi: 10.1016/J.NEURON.2015.07.029.

Pinto, L. G. *et al.* (2019) 'Non-Peptidergic Nociceptive Neurons Are Essential for Mechanical Inflammatory Hypersensitivity in Mice', *Molecular Neurobiology*. Humana Press Inc., 56(8), pp. 5715–5728. doi: 10.1007/s12035-019-1494-5.

Reynders, A. *et al.* (2015) 'Transcriptional Profiling of Cutaneous MRGPRD Free Nerve Endings and C-LTMRs', *Cell Reports*. Cell Press, 10(6), pp. 1007–1019. doi: 10.1016/J.CELREP.2015.01.022.

Saloman, J. L. *et al.* (2016) 'Gi-DREADD expression in peripheral nerves produces ligand-dependent analgesia, as well as ligand-independent functional changes in sensory neurons', *Journal of Neuroscience*. Society for Neuroscience, 36(42), pp. 10769–10781. doi: 10.1523/JNEUROSCI.3480-15.2016.

Samineni, V. K. *et al.* (2017) 'Optogenetic silencing of nociceptive primary afferents reduces evoked and ongoing bladder pain', *Scientific Reports*. Nature Publishing Group, 7(1). doi: 10.1038/s41598-017-16129-3.

Seal, R. P. *et al.* (2009) 'Injury-induced mechanical hypersensitivity requires C-low threshold mechanoreceptors', *Nature*. Nature Publishing Group, 462(7273), pp. 651–

655. doi: 10.1038/nature08505.

Shields, S. D. *et al.* (2012) 'Nav1.8 expression is not restricted to nociceptors in mouse peripheral nervous system.', *Pain*, 153(10), pp. 2017–30. doi: 10.1016/j.pain.2012.04.022.

Stantcheva, K. K. *et al.* (2016) 'A subpopulation of itch-sensing neurons marked by Ret and somatostatin expression', *EMBO reports*. EMBO, 17(4), pp. 585–600. doi: 10.15252/embr.201540983.

Tarpley, J. W., Kohler, M. G. and Martin, W. J. (2004) 'The behavioral and neuroanatomical effects of IB 4-saporin treatment in rat models of nociceptive and neuropathic pain', *Brain Research*, 1029(1), pp. 65–76. doi: 10.1016/j.brainres.2004.09.027.

Tender, G. C., Li, Y. Y. and Cui, J. G. (2008) 'Vanilloid receptor 1-positive neurons mediate thermal hyperalgesia and tactile allodynia', *Spine Journal*, 8(2), pp. 351–358. doi: 10.1016/j.spinee.2007.08.005.

Urien, L. *et al.* (2017) 'Genetic ablation of GINIP-expressing primary sensory neurons strongly impairs Formalinevoked pain', *Scientific Reports*. Nature Publishing Group, 7. doi: 10.1038/srep43493.

Usoskin, D. *et al.* (2015) 'Unbiased classification of sensory neuron types by large-scale single-cell RNA sequencing', *Nature Neuroscience*. Nature Publishing Group, 18(1), pp. 145–153. doi: 10.1038/nn.3881.

Vallbo, Å. B., Olausson, H. and Wessberg, J. (1999) 'Unmyelinated Afferents Constitute a Second System Coding Tactile Stimuli of the Human Hairy Skin', *Journal of Neurophysiology*. American Physiological SocietyBethesda, MD , 81(6), pp. 2753–2763. doi: 10.1152/jn.1999.81.6.2753.

Vulchanova, L. *et al.* (2001) 'Cytotoxic targeting of isolectin IB4-binding sensory

neurons.', *Neuroscience*, 108(1), pp. 143–55. doi: 10.1016/s0306-4522(01)00377-3.

Walcher, J. *et al.* (2018) 'Specialized mechanoreceptor systems in rodent glabrous skin', *The Journal of Physiology*. John Wiley & Sons, Ltd (10.1111), 596(20), pp. 4995–5016. doi: 10.1113/JP276608.

Wall, P. D. and Gutnick, M. (1974) 'Properties of afferent nerve impulses originating from a neuroma', *Nature*, 248(5451), pp. 740–743. doi: 10.1038/248740a0.

Wang, Sheng *et al.* (2017) 'Ca2+ and calpain mediate capsaicin-induced ablation of axonal terminals expressing transient receptor potential vanilloid 1', *Journal of Biological Chemistry*. American Society for Biochemistry and Molecular Biology Inc., 292(20), pp. 8291–8303. doi: 10.1074/jbc.M117.778290.

Wu, G. *et al.* (2001) 'Early onset of spontaneous activity in uninjured C-fiber nociceptors after injury to neighboring nerve fibers.', *The Journal of neuroscience : the official journal of the Society for Neuroscience*, 21(8). doi: 10.1523/jneurosci.21-08-j0002.2001.

Wu, G. *et al.* (2002) 'Degeneration of myelinated efferent fibers induces spontaneous activity in uninjured C-fiber afferents', *Journal of Neuroscience*, 22(17), pp. 7746–7753. doi: 10.1523/jneurosci.22-17-07746.2002.

Xu, Z. Z. *et al.* (2015) 'Inhibition of mechanical allodynia in neuropathic pain by TLR5-mediated A-fiber blockade', *Nature Medicine*. Nature Publishing Group, 21(11), pp. 1326–1331. doi: 10.1038/nm.3978.

Yaksh, T. L. *et al.* (1979) 'Intrathecal capsaicin depletes substance P in the rat spinal cord and produces prolonged thermal analgesia', *Science*, 206(4417), pp. 481–483. doi: 10.1126/science.228392.

Zeisel, A. *et al.* (2018) 'Molecular Architecture of the Mouse Nervous System', *Cell*. Cell Press, 174(4), pp. 999-1014.e22. doi: 10.1016/J.CELL.2018.06.021.

Zeng, W. Z. *et al.* (2015) ‘Activation of acid-sensing ion channels by localized proton transient reveals their role in proton signaling’, *Scientific Reports*. Nature Publishing Group, 5. doi: 10.1038/srep14125.

Chapter 5: Nav1.7 is required for normal C-Low threshold mechanoreceptor function in humans and mice

1. Introduction

Touch sensation is a critical component of the sensory system giving us the ability to detect, discriminate and explore our environment and also provides a substrate for social interaction. Low threshold mechanoreceptors (LTMRs) are a heterogenous group of sensory neurons which encode mechanical stimuli and can be classified according to their conduction velocity, stimulus-response function and the end-organs which they innervate. Although the majority of C-fibre sensory afferents are nociceptors and thermoceptors, an unmyelinated C-fibre population, termed C-low threshold mechanoreceptors (C-LTMRs, often termed CT- afferents in humans) exist. Following on from the chemogenetic silencing of C-LTMRs in Chapter 4, the rationale for this chapter was to investigate C-LTMR function when loss of function might occur as a result of altered human and mouse genetics or pharmacological intervention. In this case, we investigated the role Nav1.7 and C-LTMR function.

1.1. C-Low threshold mechanoreceptors

C-LTMRs were first discovered 80 years ago in the cat (Zotterman, 1939) and much later in humans (Nordin, 1990; Vallbo, Olausson and Wessberg, 1999). In humans, C-LTMRs respond to low threshold punctate indentations and have conduction velocities in the C-fibre range (Vallbo, Olausson and Wessberg, 1999). Human C-LTMRs also underpin pleasant touch, a category of tactile perception which until recently has been largely understudied. Yet evidence now suggests they are highly important for social contact, communication, relationships, pain relief, and empathy for touch observed in others (Olausson *et al.*, 2010; Morrison, Björnsdotter and Olausson, 2011; Liljencrantz and Olausson, 2014). These afferents respond to brushing stimuli between 1-10 cm/s and show an inverted U-shape relationship, with

peak firing rates and peak perceived pleasantness seen at 3 cm/s (Löken *et al.*, 2009).

C-LTMRs have been identified in other mammals, including rodents (Lynn and Carpenter, 1982; Leem, Willis and Chung, 1993). Several studies have identified molecular markers of rodent C-LTMRs (vGLUT3 (Seal *et al.*, 2009), Tafa4 (Delfini *et al.*, 2013) and IB4-GINIP+ (Urien *et al.*, 2017)), one of which being Tyrosine hydroxylase (TH), a marker of all C-LTMRs (Li *et al.*, 2011). In addition, recent single-cell RNA sequencing studies have provided further evidence confirming that C-LTMRs have a very distinct transcriptional profile compared to other sensory neuron populations (Usoskin *et al.*, 2015; Zeisel *et al.*, 2018). The TH positive population makes up ~10% of all dorsal root ganglion (DRG) neurons and sparse genetic labelling of TH positive C-LTMRs revealed sensory endings innervating mouse hairy skin as longitudinal lanceolate endings surrounding hair follicles (Li *et al.*, 2011). C-LTMR sensory neurons also project centrally to the spinal cord and terminate in lamina II^{i} of the dorsal horn (DH) where they synapse with distinct inhibitory (parvalbumin) and excitatory (PKCγ) interneuron populations (Li *et al.*, 2011; Larsson and Broman, 2019). Li *et al.* (2011) also confirmed that TH positive DRG neurons function like human C-LTMRs and have low mechanical thresholds, C-fibre range conduction velocities, and respond to cooling stimuli.

1.2. The voltage-gated sodium channel, Nav1.7

The voltage-gated sodium channel (VGSC) Nav1.7, is a predominant VGSC in the peripheral nervous system (Toledo-Aral *et al.*, 1997). Nav1.7 is a tetrodotoxin sensitive sodium channel which contributes to the rising phase of the nociceptor action potential, amplifies subthreshold stimuli, has a low activation threshold and fast channel kinetics (Bennett *et al.*, 2019). Because molecular identifiers of C-LTMRs have emerged relatively recently, there has been a dearth of studies into the role of sodium channel genes and their mutations in C-LTMRs, in either humans or

rodents. This is particularly relevant as VGSCs have emerged as important analgesic drug targets. Two recent studies suggest that C-LTMRs show significant expression of *SCN9A* (Zeisel *et al.*, 2018; Zheng *et al.*, 2019), the gene encoding the VGSC Nav1.7 which human genetics has strongly linked to nociception and pain (Bennett *et al.*, 2019). Gain of function (GOF) mutations in Nav1.7 can result in painful conditions such as erythromelalgia, paroxysmal extreme pain disorder (PEPD), small fibre neuropathy and painful diabetic neuropathy (Yang, 2004; Dib-Hajj *et al.*, 2005; Fertleman *et al.*, 2006; Faber *et al.*, 2012; Blesneac *et al.*, 2018). Whilst bi-allelic loss of function (LOF) mutations lead to congenital insensitivity to pain (CIP) in which patients do not perceive pain in response to noxious mechanical, thermal or chemical stimuli (Cox *et al.*, 2006; Goldberg *et al.*, 2007; McDermott *et al.*, 2019). These striking psychophysical features are accompanied by a loss of functional C-nociceptors (assessed using microneurography) highlighting Nav1.7 as an important modulator of the nociceptive system. This sensory loss has been thought to be relatively selective with an absence of pain perception, chemogenic itch and smell; touch and proprioceptive function were reportedly normal (Cox *et al.*, 2006; Goldberg *et al.*, 2007; Weiss *et al.*, 2011; McDermott *et al.*, 2019). This human genetic data, the relatively selective expression of Nav1.7 in the peripheral versus central nervous system and preclinical studies have made Nav1.7 an attractive druggable target to treat painful conditions (Minett *et al.*, 2015; Cao *et al.*, 2016; Shields *et al.*, 2018; Meents *et al.*, 2019; Mis *et al.*, 2019). A number of small molecule blockers targeting Nav1.7 are currently in clinical development.

Whilst understandably there has been a focus linking Nav1.7 to human nociception, C-LTMR function has never been specifically interrogated. We have used a multi-disciplinary approach to answer this question by studying humans with LOF mutations in Nav1.7 alongside mice in which Nav1.7 has been ablated in C-LTMRs. We find that Nav1.7 LOF in the human not only leads to CIP, but also an

impairment in affective touch and that the stimulus-response function of C-LTMRs is critically dependent on functional Nav1.7. Finally, we challenge the current dogma that therapeutics targeting Nav1.7 will act only on the nociceptive system and provide evidence that treatments may have undesired impacts on affective touch sensation.

2. Methods

2.1. Participants.

Six participants with bi-allelic loss of function mutations in *SCN9A* and congenital insensitivity to pain (CIP, 2 males and 4 females, mean age = 35, SD = 11.02, (Appendix Table 2) participated in the study and were compared to a large normative sample of healthy subjects (Morrison, Björnsdotter and Olausson, 2011; Perini, Morrison and Olausson, 2015; Sehlstedt *et al.*, 2016), which included age and gender matched controls (N = 86, 42 females, age range = 16 - 60, mean age = 36, SD = 12.2). All of the participants exhibited the typical features of congenital insensitivity to pain with a history of never having experienced pain and multiple painless injuries such as burns and fractures. Psychophysical correlates to affective touch were collected in one participant in Gainesville, Florida, USA (participant 1), three participants at the John Radcliffe Hospital, Oxford, United Kingdom (participants 2-4) and two participants at Addenbrook's Hospital, Cambridge, United Kingdom (participants 5 and 6). CIP participants and healthy control participants were examined following the same paradigm. All centres had been trained in carrying out the brush paradigm in exactly the same manner. Facial electromyography was collected in two participants (participants 2, and 3) and 8 age matched controls in Linköping, Sweden. Ethical approval was obtained by the ethics board of Linköping University and the National Research Ethics of the United Kingdom (Painful Channelopathies Study, NRES-UK reference: 12/LO/0017). Participants gave informed consent in accordance with the Declaration of Helsinki.

2.2. Affective touch testing: psychophysics.

Single brush strokes were manually delivered to the 9 cm of the forearm of the participants (N = 6 CIP participants and N = 86 healthy controls) using a soft 7 cm-wide goat hair artist's brush. Brush strokes were delivered in a distal to proximal direction at 5 different velocities: 0.3 cm/s, 1 cm/s, 3 cm/s, 10 cm/s, and 30 cm/s.

The experimenter was guided regarding brushing velocity by a visual meter on a monitor, not visible to the subject. Six repetitions of each velocity were presented in pseudo-randomized order. The participants performed ratings of unpleasantness or pleasantness using visual-analogue scale (VAS) with the anchor points 'unpleasant' (-10) and 'pleasant' (+10). In each trial instructions appeared above the visual-analogue scale to "rate how pleasant the touch feels to you" followed by a 4–6 s response interval.

To ensure that their arm and the experimenter were out of view, participants positioned the stimulated arm behind a curtain or wore goggles flanked by occluders. For each participant the average of the visual-analogue scale scores for each velocity was calculated. To determine the effect of the mutation on affective touch evaluation we compared pleasantness rating patterns across groups. Average scores per velocity per participant were entered in a 2x5 factorial analysis of variance (ANOVA) with dependent variables, the five velocities and the two groups as between subject variable. Greenhouse-Geisser correction was performed when assumption of sphericity was not met. Additional *post-hoc* Mann-Whitney analysis was performed to compare ratings at each velocity between groups when assumption of normality was not met. All data was analysed using the Statistical Package for the Social Sciences (SPSS Inc., Chicago, IL, USA).

2.3. Affective touch testing: facial electromyography (facial EMG) session.

Participants (participants 2 and 3, N = 8 age and gender matched healthy controls) were fitted with surface electrodes placed above the eyebrow, to measure corrugator supercilii ("corrugator") muscle region activity, and over the cheek, measuring zygomaticus major ("zygomatic") muscle region reactivity according to Fridlund and Cacioppo *et al.* (1986). EMG was measured using 4 mm Ag/AgCl

electrodes and an 8 mm gel-filled Ag/AgCl ground sensor on the forehead. Sites were cleaned with alcohol and lightly abraded until impedance was below 20 kΩ (measured with a Model 1089 MK III Checktrode; UFI, Morro Bay, CA, USA). EMG signals were amplified 5000x, 10–500 Hz band pass filtered, and digitized at 1000 Hz using EMG100C amplifiers and MP150 Data Acquisition System from Biopac Systems (Goleta, CA, USA). Acknowledge software (Biopac Systems) was used to apply a comb band stop filter and signals were then rectified and integrated over 20 ms. Tasks were presented using Presentation Software (Neurobehavioral Systems, Berkley, CA, USA). Affective responses were assessed by measuring corrugator and zygomatic reactivity in response to each stimulus, quantified as mean EMG activation during the 6 s stimulus presentation minus the mean EMG activation during the 1 s before the stimulus was presented. Trained raters, blinded for experimental conditions, identified and excluded trials with excessive baseline activity or artefactual activations (Fridlund and Cacioppo, 1986).

Touch was administered using a soft 5 cm-wide goat hair artist's brush applied to a 9 cm section of the forearm, as detailed previously (Mayo *et al.*, 2018; Ree, Morrison, *et al.*, 2019). Participants were on one side of a curtain with the left arm extending to the other side of the curtain, where the experimenter administered the brushing. Participants were instructed to look straight ahead at a fixation cross that was presented on a computer screen throughout the brushing trials. Using the same settings as for affective touch testing, participants were precluded from receiving any visual cues regarding touch administration. The task consisted of four blocks; each block consisted of 8 trials, four at each velocity, 3 cm/s (slow) and 30 cm/s (fast), with velocity order within each block pseudorandomized but not repeated more than 3 times. In total, each participant completed 32 trials; 16 at each velocity. Participant 3 completed two extra blocks of trials but only self-report ratings were collected during these final blocks due to inadvertent sensor removal. During the

inter-trial intervals, participants gave self-report ratings using a visual analog scale (VAS) presented on the computer screen as described. Participants were asked “How PLEASANT was the touch?” or “How INTENSE was the touch?” and could choose from -10 (extremely unpleasant) to +10 (extremely pleasant) or -10 (not at all intense) to +10 (extremely intense), respectively, using the mouse to move the VAS slider. Self-report ratings (pleasantness, intensity) alternated so that 50% of the trials at each velocity were followed by pleasantness ratings, and 50% were followed by intensity ratings. Ratings were pseudorandomised so that no velocity x question combination repeated more than two times. Ratings were followed by a 7- 9 s variable interval before the next trial began.

2.4. Animals

All mice were group-housed in individually ventilated cages with free access to food and water, in humidity and temperature controlled rooms with a 12 hr light-dark cycle, in a pathogen free facility. All animal procedures adhered to the UK Home Office (Scientific Procedures) Act (1986) and performed under a UK Home Office Project Licence. All animal experiments were carried out in accordance with University of Oxford Policy on the Use of Animals in Scientific Research. The work within this study also conforms to the ARRIVE guidelines (Kilkenny *et al.*, 2010).

The $TH^{CreERT2}$ mice were purchased from Jackson Labs (Bar harbour, Maine, USA) and have been previously described (Abraira *et al.*, 2017). The floxed Nav1.7 (Nav1.7flox/flox) and $Nav1.8^{Cre}$ mice were a kind gift from John Wood (UCL, UK) and have been previously described (Nassar *et al.*, 2004). The following lines were used as Cre dependent reporter lines, R26-Flox-Stop-TdTomato reporter mice (Ai14) and RCL-ChR2(H134R)/EYFP (Ai32), and were purchased from Jackson labs. C57BL/6 mice were purchased form the Oxford University Breeding Unit.

All experiments were carried out on adult male and female mice. C57BL/6 mice were used for skin-nerve pharmacology and *In situ* hybridisation experiments. $TH^{CreERT2+/-}Ai14^{+/-}$ mice and $Nav1.8^{Cre+/-}Ai14^{+/-}$ mice were used for histological experiments. $TH^{CreERT2+/-}Ai32^{+/-}$ mice were used for patch-clamp pharmacology experiments. Intrathecal injections and patch-clamp electrophysiology were conducted on $TH^{CreERT2+/-}$ and $TH^{CreERT2+/-}Nav1.7^{flox/flox}$ ($TH^{CreERT2}$:Nav1.7-KO) mice. All behaviour and skin-nerve electrophysiology was carried out on $TH^{CreERT2-/-}Nav1.7^{flox/flox}$ (Nav1.7-WT) and $TH^{CreERT2+/-}Nav1.7^{flox/flox}$ ($TH^{CreERT2}$:Nav1.7-KO) littermate mice.

2.5. Tamoxifen dosing

Nav1.7-WT and $TH^{CreERT2}$:Nav1.7-KO mice were given tamoxifen dissolved in corn oil (1x 50 mg/kg I.P) at 8-10 wks of age and behaviour and electrophysiology carried out 4-6 weeks later. This time point was chosen as Shields *et al.* (2018) have previously shown that when using $Nav1.7^{flox/flox}$ mice, the Nav1.7 protein can still be detected prior to 3 weeks (but not at 4 weeks) post tamoxifen. $TH^{CreERT2}$:Ai14 and $TH^{CreERT2}$:Ai32 and mice were given tamoxifen at 8-10 weeks of age and tissue was taken for histology or electrophysiology at least 2 weeks later. Animals that received intrathecal injections were tamoxifen dosed 1 week post-surgery to allow simultaneous Nav1.7 KO and eGFP expression.

2.6. Immunohistochemistry (IHC)

Animals were deeply anaesthetised with pentobarbital, and the blood cleared from all tissues by perfusing saline through the vascular system. Mice were then perfuse-fixed using 4% paraformaldehyde (PFA). Tissues were then collected and post-fixed in 4% PFA accordingly (DRG: 1-2 hrs, spinal cord: 24 hrs, skin: 1-2 hrs).

All tissues were cryoprotected in 30% sucrose for a minimum of 48 hrs followed by embedding the tissue and sectioning on a cryostat. (DRG 12 µm, spinal cord 20 µm, skin 30 µm). Cultured cells were fixed with 4% PFA for 10 mins and treated similarly to other tissues. Briefly, samples were washed in PBS and blocked in a blocking solution (5% normal donkey serum, 0.3% TritonX-100, PBS) for 1 hr at room temperature (RT). Primary antibodies (Appendix Table 1) were diluted in blocking solution and applied to tissue or cells overnight at RT. The next day samples were washed in a wash solution (0.3% TritonX-100, PBS) followed by a 2 hr incubation with secondary antibodies (Appendix Table 1) diluted in wash solution at RT. Samples were mounted using Vectorshield and imaged on a confocal microscope (Zeiss LSM-710). Images were analysed using Fuji/ImageJ (NIH). For quantification at least three sections per animal were used, with at least 3 animals per group.

2.7. *In situ* hybridisation (ISH)

ISH was performed using two methods; the first method (Fig. 3 c-d) was performed by following the user instructions for the RNAScope2.5 RED Chromogenic assay kit (Advanced Cell Diagnostics). Briefly, tissue was pre-treated using hydrogen peroxide and a protease treatment. Tissue was next incubated for 2 hrs at 40^{o}C with a Nav1.7mRNA specific probe (Cat no. 457641). Next, a series of 6 probe amplification steps were carried out followed by a fast red detection step. The second method of ISH (Fig. 3b) was performed using digoxigenin labelled probes. Probes were hybridized overnight at 55°C, and the slides incubated with the horseradish peroxidase anti-digoxigenin antibody (Roche). Final detection was achieved using cy3 TSA plus kit (Perkin Elmer). RNA probes were synthesized using gene-specific PCR primers and cDNA templates from adult mouse DRG. The following oligonucleotides were used for *SCN9A* PCR probe synthesis snc9a-F : 5′-GAAGGTGACTCACTCGTG-3′ and snc9a-R : 5′-CATGTGCGCCTGAATTTC-3′

(Ahmad *et al.*, 2007). Samples were also co-stained using IHC using a standard IHC protocol. ISH tissue was imaged on a confocal microscope and analysis was carried out on Fuji/imageJ. TH+ cells were selected using Fuji/imageJ and the Nav1.7mRNA fluorescence intensity was measured. Three random regions of the imaged section not containing cells was selected and intensity measured to determine signal background. An intensity cut off (3x average background intensity) was applied to distinguish Nav1.7mRNA positive and negative cells.

2.8. Animal Behaviour

Both male and female mice were used in this study and mice were tested at a consistent time of day, in the same environment by the same experimenter. Mice were habituated to their testing environment and equipment prior to behavioural test days. The experimenter was blind to animal genotype prior to testing and until after behavioural analysis was complete.

2.8.1. Mechanical Sensory testing

Mice were randomly assigned a test box (5 x 5 x 10 cm) which was elevated on a wire mesh base and were acclimatised to the equipment for 30-60 mins.

2.8.1.1. von Frey testing: Mice were then tested on their plantar hind paws (between the running pads) using calibrated von Frey hairs (Linton Instrumentation) using the ‘up-down’ method (Dixson 1980) to evaluate their 50% paw withdrawal thresholds. Mice were tested on 3 different days to obtain an average baseline value.

2.8.1.2. Brush/cotton swab*:* The plantar hind paws of mice were brushed (1 cm/s) with a fine artists paint brush or a cotton swab that had been puffed out to 3 times its original size. Each mouse received 5

successive stimuli on alternate hind paws (10 s apart), twice. The number of responses were recorded. A response included, lifting, flicking or moving the hind paw or walking away from the stimulus. Mice were tested on 3 different days to obtain an average baseline value.

2.8.2. Thermal Sensory testing

Mice were randomly selected from their home cages in order to randomise the order of thermal sensory assessment

2.8.2.1. 53ºC Hotplate*:* Mice were placed onto a Perspex enclosed Hotplate (UgoBasile) and were observed until mice displayed pain behaviours on their hind paws i.e. lifting, flicking, licking of the hind paw (cut off 30 s to prevent tissue damage). The latency to respond was recorded and mice were tested on 3 different days to obtain average baseline value.

2.8.2.2. Thermal Gradient*:* Mice were able to freely explore a thermal gradient apparatus (UgoBasile) where a metal platform was heated in a gradient from 54ºC to 6ºC. Mice were allowed to freely explore the thermal gradient for 30 mins and their activity was monitored and tracked using a HD webcam and ANYMaze software.

2.9. Intrathecal injections

Adult $TH^{CreERT2}$ and $TH^{CreERT2}$:Nav1.7-KO mice received an intrathecal injection (i.t) as previously described. Briefly, mice were anaesthetised using 2% isoflurane, a rostral to caudal incision (1-2 cm) was made, and the T10-11 vertebra were exposed. Lateral to the midline the dura was identified and carefully punctured with a 30 gauge needle. A polyethelene cannula (designed of connecting tubing of decreasing size until the final cannula tip measured 0.008 in (O.D) x 0.004 in (I.D)), was prefilled with virus and inserted 1 cm caudal into the subdural space. Using a

pump system 5 µl of AAV9.Flex.eGFP at $1x10^{13}$ vg/ml (VVF, Zurich, Switzerland) was injected at a rate of 1 µl/min. The cannula was maintained for 2 min after the viral bolus was delivered to prevent viral backflow. The cannula was removed and the dura sealed using DuraGel (Cambridge, NeuroCare). Finally, the incision site was sutured closed and appropriate post-operative care and analgesics given (local 2 mg/kg Marcain, AstraZeneca and systemic 5 mg/kg Rimadyl, Pfizer).

2.10. Dorsal root ganglion (DRG) culture

DRG neuron cultures were prepared as detailed previously (Weir *et al.*, 2017). DRG were harvested and enzymatically digested at 37°C for 90 min in HBSS without Ca^{2+} and Mg^{2+} (ThermoFisher Scientific) with dispase type II (4.7 mg/ml) and collagenase type II (4 mg/ml) (Worthington Biochemical). Neurons were mechanically dissociated into a single-cell suspension with fire polished glass capillaries and plated in complete Neurobasal® medium (Neurobasal® media supplemented with 2% (v/v) B27 and 1% (v/v) penicillin streptomycin (ThermoFisher Scientific)) onto laminin/poly-D-lysine (BD Biosciences) treated coverslips. Murine growth factors (50 ng/ml; mouse nerve growth factor, PeproTech and 10 ng/ml; glial-derived neurotrophic factor; Peprotech) were added to the media and cultures used for experiments 24–48 hrs later.

2.11. Single cell 'picking', RT-PCR, and qPCR

All solutions were made in an RNAse-free environment and with 1% DEPC-treated water. Patch pipettes of 2-3 MΩ were pulled from borosilicate glass capillaries (WPI) and filled with ~ 2 µl of a standard internal solution: (mM) 100 K-gluconate, 28 KCl, 1 $MgCl_2$, 5 MgATP, 10 HEPES, and 0.5 EGTA. Solution was pH adjusted to 7.3 with KOH and osmolarity adjusted to 305 with glucose. eGFP+ DRG neurons (from at least 3 mice per group) were detected with an Olympus microscope

with an inbuilt GFP filter set (470/40x excitation filter, dichroic LP 495 mirror and 525/50 emission filter) and 'picked' individually using patch pipettes and negative pressure. Samples were transferred into Eppendorfs containing 2 µl resuspension buffer and lysis enhancer (CellDirect One-Step qRT-PCR Kit, ThermoFisher) supplemented with 1 U/µl Ribonuclease Inhibitor (Takara). Negative 'no cell' controls - where cell collection was mimicked but only solution was aspirated - were taken throughout sample collection to ensure solutions were not contaminated. Samples were snap-frozen immediately prior to downstream processing. After DNAse treatment using manufacturer's protocol (CellDirect), cDNA was synthesized with SuperScript III First Strand SuperMix (ThermoFisher). Each cell lysate was treated as a double reaction and the manufacturer's protocol using random hexamers was followed, allowing for multiple PCR reactions from a single cell. cDNA was stored at -20°C until further use.

Prior to Nav1.7 quantification, RT-PCR for βIII tubulin (F primer: GGCCTCCTCTCACAAGTATGT, R primer: CAGGGAATCGAAGGGAGGTG) was performed to confirm each single cell sample was successfully collected. RT-PCRs used a gene-specific preamplification with Platinum Taq DNA Polymerase (ThermoFisher) followed by RedTaq ReadyMix (Sigma). βIII tubulin positive samples and no-cell controls were then used for Nav1.7 qPCR reaction, performed in triplicate (SYBR Green LightCycler 480, Roche). Nav1.7 primers used were those previously published by Shield *et al.* 2018, and concentrations were calculated as 2^{-Cp}. Reference genes are not typically used for single cell normalisation (due to temporal fluctuations in RNA synthesis), thus Nav1.7 mRNA data were normalised to the mean WT expression for presentation. To verify Nav1.7 specificity, RT-PCRs were subsequently performed to verify band size, and bands were gel extracted for sequencing (QiaQuick Gel Extraction Kit, Qiagen).

2.12. Whole-cell patch clamp recordings

Voltage-clamp recordings using an Axopatch 200B amplifier and Digidata 1550 acquisition system (Molecular Devices) were performed at room temperature (21^{o}C - the standard for the field when investigating sodium currents). Data were sampled at 20 kHz and low-pass filtered at 5 kHz. Series resistance was compensated 80%–90% to reduce voltage errors. All data were analysed by Clampfit 10 software (Molecular Devices). GFP/eYFP+ DRG neurons were detected with an Olympus microscope with an inbuilt GFP filter set (470/40x excitation filter, dichroic LP 495 mirror and 525/50 emission filter).

Filamental borosilicate glass capillaries (1.5 mm OD, 0.84 mm ID; World Precision Instruments) were pulled to form patch pipettes of 2–4 MΩ tip resistance and filled with an internal solution containing (mM): 140 CsF, 10 NaCl, 1 EGTA and 10 HEPES; pH was adjusted to 7.3 with CsOH and osmolarity set to 300 mOsm with glucose. The extracellular solution contained (mM): 70 NaCl, 50 N-methyl-d-glucamine, 20 Tetraethylammonium chloride, 1 $CaCl_2$, 3 KCl, 1 $MgCl_2$, 10 HEPES, 10 Glucose and 0.1 $CdCl_2$; pH was adjusted to 7.3 with NaOH and osmolarity set to 310 mOsm with glucose.

The protocol used to assess peak voltage-gated Na^+ currents consisted of a 20ms test pulse to 0 mV, from a holding potential of -120 mV. The protocol used to assess the effect of PF-05089771 on Na^+ currents consisted of a step from -120 mV to -75 mV for 8 s to inactivate a proportion of NaV1.7 channels, followed by a recovery step to -120 mV for 2 ms and a test pulse to 0 mV for 20 ms. This inactivation step was necessary as PF-05089771 blocks Nav1.7 by binding in the inactivated state. We were guided by previous literature that -77 mV is the half inactivation of hNav1.7 (Alexandrou *et al.*, 2016). In both instances, three sweeps were taken, with an intersweep interval of 10s and the peak inward current during the test pulse was measured for each recording. I/V curves were generated from a

series of incremental (Δ+5 mV) 300 ms voltage steps from -80 to +35 mV, evoked every 10 s from a holding potential of -120 mV. Recordings were discarded if series resistance > 15 MΩ or deviated by > 20% during the recording. Linear leak subtraction was performed using P/4 leak subtraction.

2.13. Ex vivo skin-nerve preparation

The hind paw hairy skin and saphenous nerve was dissected and maintained in the inside-out orientation (hypodermis face up) in a recording chamber constantly perfused with synthetic interstitial fluid (SIF: 2.0 mM $CaCl_2$, 5.5 mM Glucose, 10 mM HEPES, 3.5 mM KCl, 0.7 mM $MgSO_4$, 123 mM NaCl, 1.5 mM NaH_2PO_4, 9.5 mM Na-gluconate, 7.5 mM Sucrose, 1M NaOH; dH_20) at 32°C (Important to maintain skin temperature of 32^{o}C when assessing excitability of temperature sensitive afferents). The saphenous nerve was isolated using mineral oil (Sigma) in an adjacent chamber. Here the nerve was, by hand, de-sheathed and nerve fibres teased apart and placed onto a silver recording electrode. Single fibre receptive fields were located using a blunt probe, and conduction velocity measured using pulsed supra-threshold electrical currents. C-LTMRs were identified on the basis of two main factors; conduction velocities below 1.2 m/s and von Frey mechanical thresholds below 5.8 mN. C-LTMR receptive fields were stimulated using a piezoelectric stimulator (Physik Instrument) in conjunction with a force transducer (Kleindiek). To measure stimulus response functions, the receptive fields were stimulated using an increasing stimulus force protocol and/or an increasing stimulus velocity protocol. All stimuli evoked action potentials were visualized using an oscilloscope and recorded using a Powerlab 4.0 system in conjunction with LabChart v7.3 software (ADInstruments). Nav1.7-WT and $TH^{CreERT2}$:Nav1.7-KO mice were used to characterise the inducible genetic loss of Nav1.7 in C-LTMRs, the experimenter was blind to animal genotype prior to the experiment until post analysis. Once C-LTMRs were identified in C57BL/6 mice, receptive fields were isolated using a metal ring and the skin was stimulated

pre and 10 mins post application of 10 nM of the selective Nav1.7 channel blocker PF-05089771 or vehicle. The experimenter was blind to the treatment group until post-analysis. On average, only 1-2 C-LTMRs were found per preparation and each preparation lasted up to 8hrs.

2.14. Computational modelling of C-LTMRs

The C-LTMR computational model used was previously described in detail by Zheng *et al.* (2019) and was accessed from ModelDB (https://senselab.med.yale.edu/modeldb/, accession No. 256632) (Zheng *et al.*, 2019). Briefly, the C-LTMR model was executed using the NEURON simulation environment. The model was constructed as such the membrane capacitance (Cm) was 12 pF and contained the voltage-gated ion channels; Nav1.7, Nav1.8, Kv1, Kv2, Kv3, Kv4 and a leak channel. The voltage dependence and current kinetics of each ion channel in the model was described by Zheng *et al* (2019). The maximal conductance ($\bar{g}$) for each ion channel is as follows: Nav1.7 (30 mS/cm^2), Nav1.8 (40 mS/cm^2), Kv1 (0.06 mS/cm^2), Kv2 (2 mS/cm^2), Kv3 (0.05 mS/cm^2) and Kv4 (11 mS/cm^2). The model also included a non-voltage dependent leak conductance (0.02 mS/cm^2) with a reversal potential of -80 mV. CIP participant mutations from participant 2, 3 and 4 were previously characterised by McDermott *et al.* (2019) in a heterologous expression system. The fold change decrease in the mutant Nav1.7 conductance, compared to wild type conductance was calculated. In the C-LTMR model, the maximal Nav1.7 conductance was altered according to the conductance fold change due to each mutation (Table 1) to create a new model for each mutation. The model was run in the naïve setting to model healthy controls without Nav1.7 mutations. The models applied successive current injections in increments of 1 pA in order to assess threshold excitability and 25 pA to assess suprathreshold excitability.

2.15. Statistical analysis

All data was tested for normality using the D'Agostino-Pearson normality test and the appropriate parametric or non-parametric statistical tests were used accordingly. All statistical tests used were two-tailed. Statistical comparisons were made using a Student's t-test or Mann Whitney U-test. In experimental groups in which multiple comparisons were made one way or two-way analysis of variance (ANOVA) tests with appropriate *post-hoc* tests were performed. All ANOVA results, details and tables can be found in the appendix. The non-linear regression Gaussian fitted curves were used to analyse thermal gradient experiments. All data is represented as mean ± the standard error of the mean (S.E.M.) unless otherwise stated. Statistical significance is indicated as follows * $P < 0.05$, ** $P < 0.01$, *** $P < 0.001$, **** $P < 0.0001$). The statistical test used is reported in the appropriate figure legend. Graph Pad prism 6 was used to perform statistical tests and graph data. Adobe Illustrator CS5 was used to create schematics and medical graphics were obtained from Smart servier free medical art (smart.servier.com).

3. Results

3.1. CIP participants have an altered affective touch experience

We investigated affective touch in 6 participants with LOF mutations in *SCN9A* which principally results in CIP. Details about the participants who were recruited for this study are outlined in the appendix Table 2. We presented healthy control participants and CIP participants with an affective touch paradigm (Fig. 1a) in which pleasantness was rated in response to brushing the forearm at different velocities. The self-reported scores from a large sample of healthy participants were consistent with previous literature demonstrating an inverted U-shaped VAS pleasantness pattern with stimulus speed and the optimal brushing speed being 3 cm s^{-1} (Fig. 1b) (Löken et al., 2009; Morrison, Björnsdotter and Olausson, 2011; Triscoli et al., 2013; Perini, Morrison and Olausson, 2015; Sehlstedt et al., 2016). However, the CIP participant group reported significantly lower pleasantness ratings for slow brushing touch and they do not show the classical U-shaped VAS score response (Fig. 1b). The change in self-reported pleasantness in the CIP participant group is specific to slow brushing speeds and no difference was observed for faster speeds (10 cm/s and 30 cm/s) (Fig. 1b). This suggests mutations in Nav1.7 have an impact on the affective perception of gentle touch.

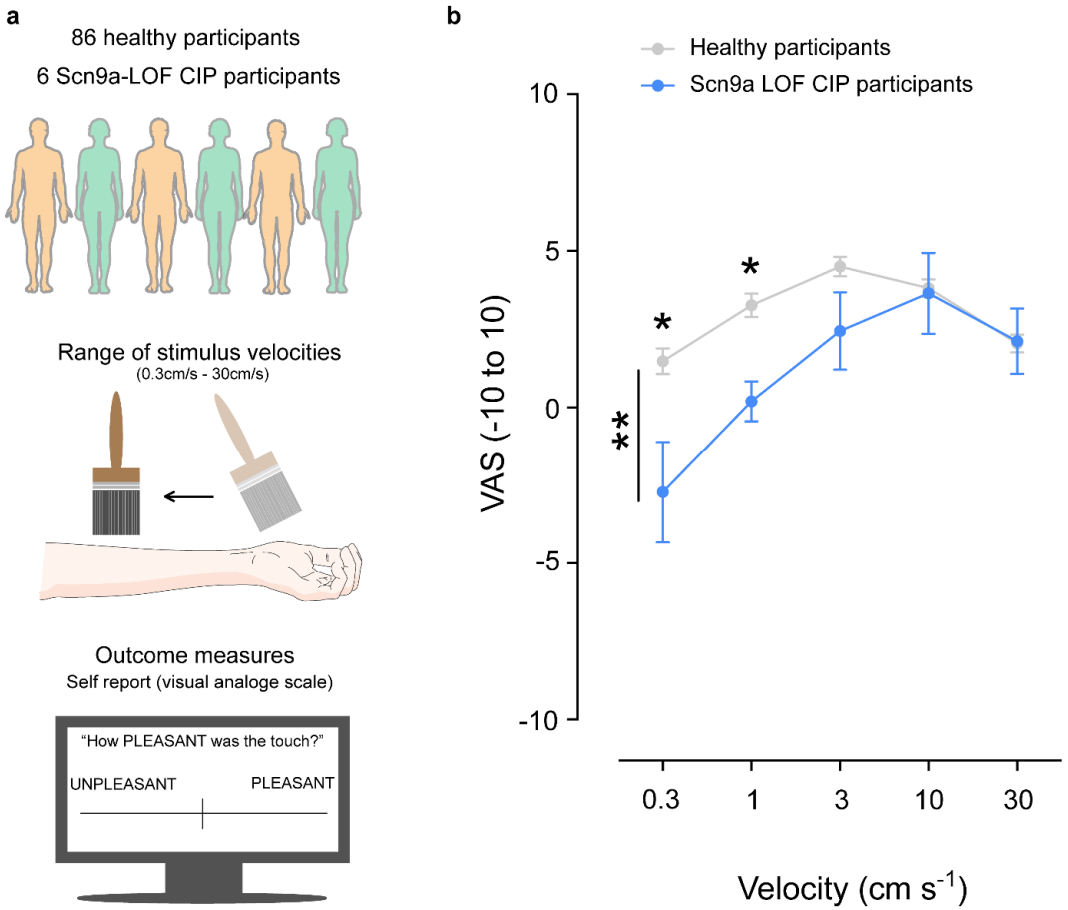

Figure 1: Humans with CIP perceive affective brush stimuli as less pleasant.

a) A schematic outlining the two cohorts of participants that were recruited, the affective touch paradigm used and the self-report visual analogue scale (VAS) outcome measure. **b)** Average affective touch ratings across five stroking velocities in CIP participants with *SCN9A* mutations and healthy control participants. CIP participants find affective brush stimuli significantly less pleasant compared to healthy controls. A 2x5 repeated measures ANOVA revealed a significant main effect of speed (F = 13.55, P < 0.001, n^2p = 0.13) and a significant speed*group interaction (black line) (F = 3.80, P = 0.01, n^2p = 0.04, **). *Post-hoc* Mann-Whitney revealed a significant difference for 0.3 cm/s (U = 117, P = 0.03, *), 1 cm/s (U = 95, P = 0.01, *) and a trend for 3 cm/s (U = 149, P = 0.08). For 10 cm/s and 30 cm/s P > 0.8. Data are mean ± S.E.M..

An extended examination, that included facial electromyography (EMG) as an indicator of emotional responses, was conducted on two of the CIP participants (participant no. 2 and 3) and in eight control participants (Fig 2a). Again, consistent with Fig. 1 and previous studies Löken et al., 2009; Morrison, Björnsdotter and Olausson, 2011; Triscoli et al., 2013; Perini, Morrison and Olausson, 2015; Sehlstedt et al., 2016), control participants rated slow stroking touch as significantly more pleasant and less intense than fast stroking touch (Fig 2b). Facial EMG in healthy control participants revealed that the pleasant slow stroking was associated with a relaxation of the corrugator (frowning) facial muscle, whereas the less pleasant fast stroking was associated with a contraction of the corrugator muscle (Mayo *et al.*, 2018; Ree, Mayo, *et al.*, 2019; Ree, Morrison, *et al.*, 2019) (Fig. 2b). In contrast, the CIP participants showed no consistent corrugator activity to slow or fast brushing (Fig. 2c-d). Despite not rating either stimulus as more or less pleasant, the CIP participants were able to discriminate stimulus intensity (Fig. 2c-d). Thus, the *SCN9A* mutations influenced not only the perception of affective touch but also the emotional reactions to touch, as measured using facial EMG.

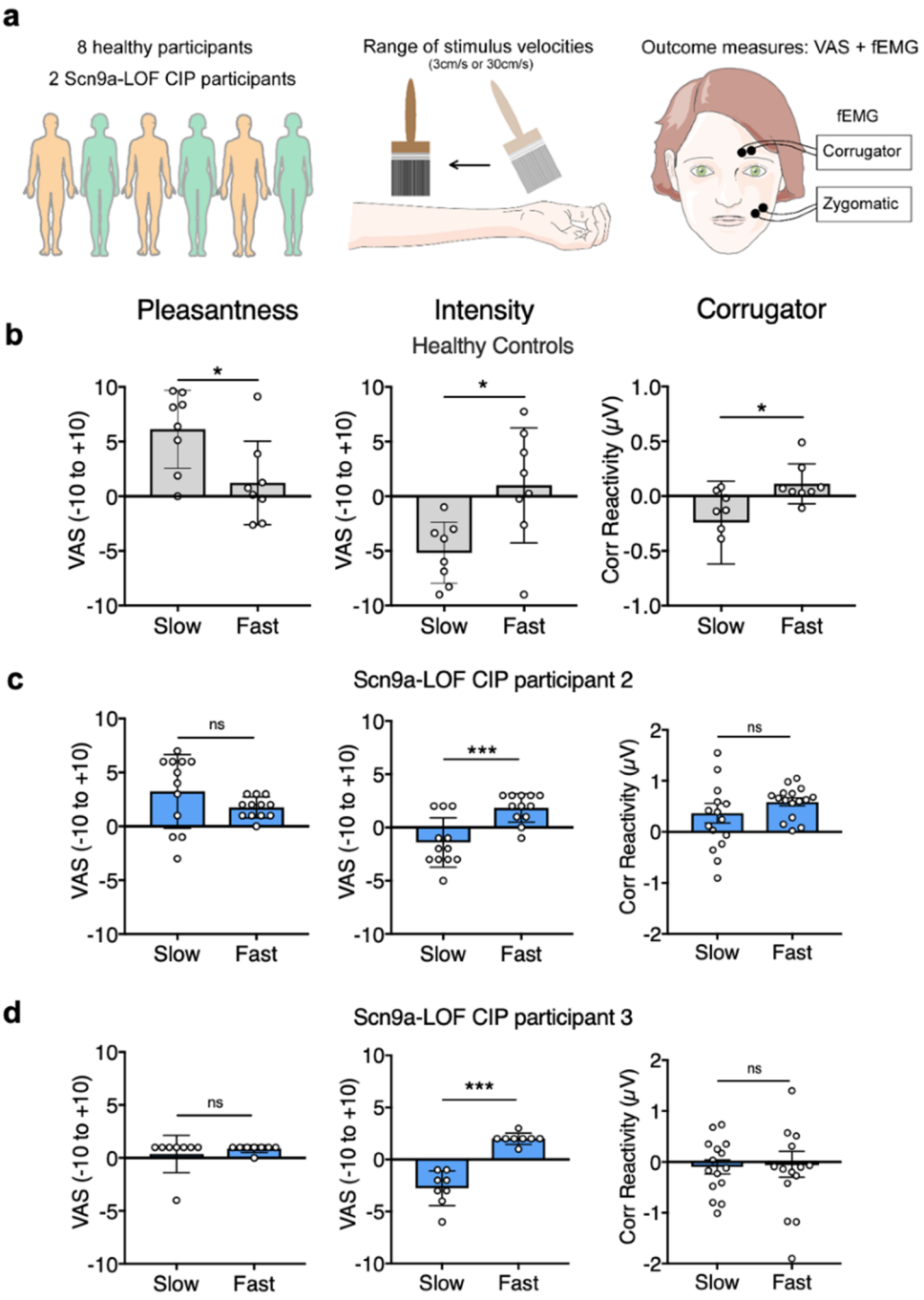

Figure 2: SCN9A LOF participants do not show the classical fEMG response to affective touch stimuli.

a) A diagram illustrating that participants were recruited, stimuli applied and the outcome measures (VAS ratings and facial electromyography, facial EMG) **b)** Average and individual ratings of pleasantness, intensity, and average facial EMG (corrugator) respectively, in response to slow (3 cm/s) or fast (30 cm/s) brush stroking on the forearm of healthy participants. Healthy participants rate slow brushing as significantly more pleasant and less intense compared to fast brushing stimuli (ratings of touch

pleasantness [*F(1,7)* 23.8, *P* = 0.002] and intensity [*F(1,7)* = 9.21; *P* = 0.019]). In addition, there was significantly greater corrugator activity elicited from fast brush stimuli and a reduction in activity elicited by slow brush stimuli (corrugator activity [*F(1,7)* = 8.56; *P* = 0.022]). There was no significant effect of velocity on zygomatic activity (not illustrated [*F(1,7)* = 3.71; *P* = 0.095]). **c-d)** Average and trial-by-trial affective touch ratings and facial EMG responses for two *SCN9A* mutation participants. Data from individual trials. Participant 2 reported no difference in pleasantness between brushing velocities [paired t-test; *t(14)* = 0.78; *P* = 0.45] but rated fast touch as more intense than slow touch [paired t-test; *t(14)* = 7.67; *P* < 0.001]. There was no velocity-based difference in corrugator [paired t-test; *t(28)* = 0.19; *P* = 0.85] or zygomatic activity (not illustrated) [paired t-test; *t(27)* = 0.76, *P* = 0.45]. Participant 3 also reported no difference in ratings of pleasantness for slow and fast touch [paired t-test; *t(22)* = 1.46; *P* = 0.16] but rated fast touch as more intense than slow touch [paired t-test; *t(22)* = 4.21; *P* = 0.004]. Corrugator [paired t-test; *t(30)* = 1.06; *P* = 0.30] and zygomatic (not illustrated) [paired t-test; *t(27)* = 0.35, *P* = 0.73] response to fast and slow touch were not significantly different.

3.2. C-LTMRs express Nav1.7

Nav1.7 is highly expressed in the peripheral nervous system with restricted expression within the CNS in sub-cortical structures, including the thalamus, medial amygdala, hypothalamus, and the axons of the olfactory epithelium projecting to the olfactory bulb (Branco *et al.*, 2016; Kanellopoulos *et al.*, 2018). Nav1.7 is highly expressed in C-nociceptors (Black *et al.*, 2012). It has been shown through mRNA sequencing of the C-LTMR population that they also express Nav1.7 (Reynders *et al.*, 2015). Using the data set provided by Reynders *et al.* (2015) we identified *SCN9A* expression in three sensory neuron populations: C-LTMRs (GINIP+/IB4-), non-peptidergic nociceptors (GINIP+/IB4+) and all other DRG neurons (IB4-/GINIP-), with the highest reads per kilobase of transcript per million mapped reads (RPKM) seen in C-LTMRs (Fig. 3a). To validate these sequencing results, we carried out *in situ* hybridisation (ISH) combined with immunohistochemistry (IHC) and Nav1.7mRNA was indeed present in the C-LTMR population (GINIP+/IB4-) (Fig. 3b).

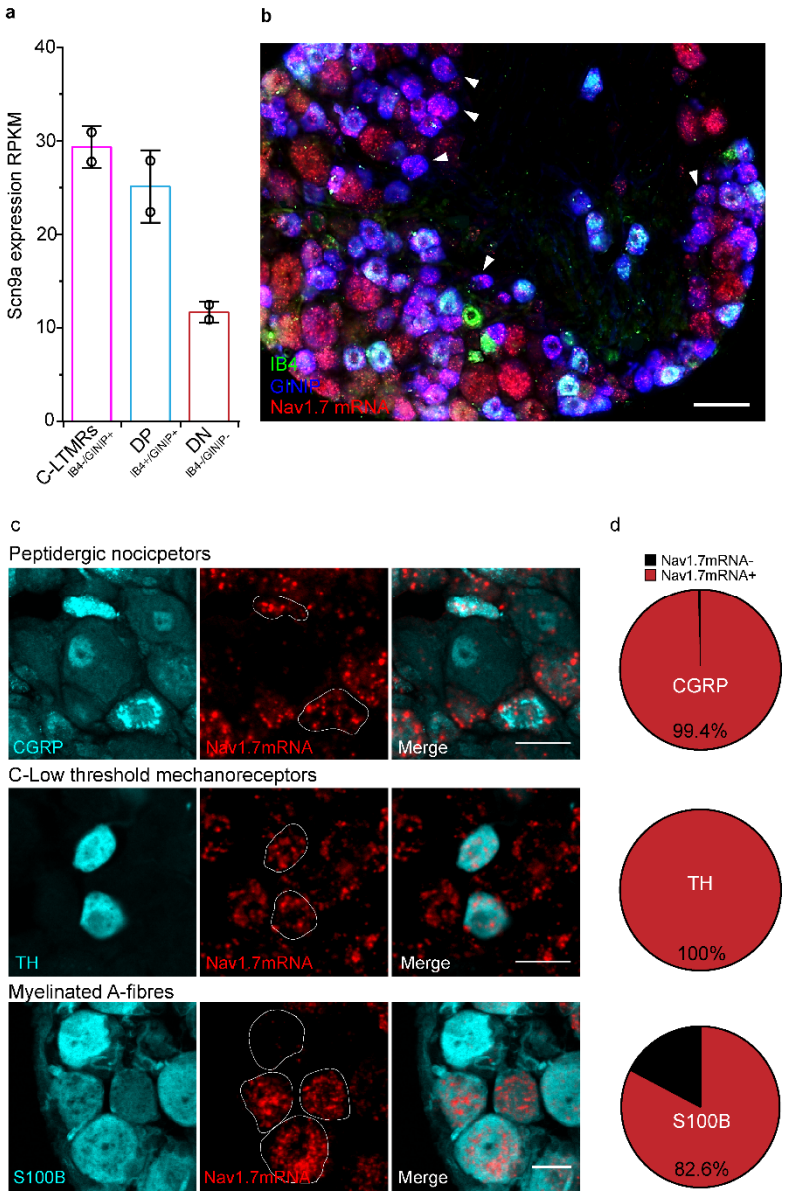

Figure 3: *SCN9A* mRNA expression in C-LTMRs and other sensory neuron populations. a) Relative gene expression for SCN9A was quantified by the normalised reads per kilobase per million mapped reads (RPKM) using the mean and the standard deviation across three distinct neuronal populations, C-LTMRs, double positive non-peptidergic nociceptors (IB4+GINIP+) and double negative all other neurons (IB4-GINIP-). RPKM data were downloaded from GSE64091. Data was originally presented in Reynders *et al.* (2015). N = 3 per respective neuronal subpopulation. **b)** Validation of the sequencing data shown by ISH of Nav1.7mRNA and IHC co-localisation of IB4 and GINIP in wild type DRG sections. Example C-LTMRs shown with arrows. Scale bar 50 µm. **c-d)** ISH of DRG sections showing the percentage co-localisation of CGRP positive (peptidergic) nociceptors, TH+ C-LTMRs, S100β positive (myelinated) afferents and Nav1.7mRNA. Scale bars 25µm.

We also found that 99.4% of peptidergic nociceptors and 82.6% of myelinated fibres express Nav1.7 mRNA (Fig. 3c-d). More recently, Zheng *et al.* (2019) carried out deep sequencing of seven transgenically labelled sensory neurons populations, including C-LTMRs (Zheng *et al.*, 2019). This work demonstrated that C-LTMRs identified by expression of TH, express Nav1.7 mRNA and surprisingly this expression is highest in C-LTMRs as compared to seven other sensory neuron populations, including nociceptors (Zheng *et al.*, 2019). To validate these sequencing results from Zheng *et al* (2019) and ask what proportion of C-LTMRs express Nav1.7, we carried out ISH and IHC and found that 100% of TH positive C-LTMRs express Nav1.7 mRNA (Fig. 3c-d).

Taken together with the characterisation of the $TH^{CreERT2}$ line (Chapter 4), all C-LTMRs express Nav1.7 mRNA and the $TH^{CreERT2}$ line first published by Abraira *et al* (2017) is a good model to study C-LTMR function.

3.3. Genetic loss of Nav1.7 in rodent C-LTMRs results in mechanical and cooling deficits

To understand the role of Nav1.7 in mouse C-LTMRs we generated a conditional C-LTMR specific Nav1.7 knock-out (KO) mouse, using the previously discussed $TH^{CreERT2}$ model crossed with a floxed Nav1.7 mouse line. Following administration of tamoxifen and the conditional KO of Nav1.7 we conducted an array of behaviour assays in order to profile sensory function. We found that mice lacking Nav1.7 in C-LTMRs exhibit a small but significant hyposensitivity to punctate mechanical stimuli (Fig. 4a). There was no difference in the number of responses to light brush stimuli as measured by a cotton swab or brush (Fig. 4b-c). As expected, the loss of Nav1.7 in C-LTMRs did not affect the latency to withdraw from a nociceptive hotplate (Fig. 4d). Since C-LTMRs are known to respond to cooling

stimuli, we therefore sought to assess the loss of Nav1.7 in cold stimuli coding. We allowed mice to freely explore a temperature gradient apparatus which ranged from 6-54^{o}C for 30 minutes. Nav1.7-WT mice had the expected bell shaped response to the thermal gradient apparatus while TH^{CreERT2}:Nav1.7-KO mice spend more time in cooler zones as seen by a significant leftward shift in the non-linearly regressed Gaussian curve (Fig. 4e), suggestive of a deficit in cold detection. Additionally, there is a ~4^{o}C reduction in the average preferred temperature (the temperature at which mice spent most of their time) in TH^{CreERT2}:Nav1.7-KO mice compared to wild type mice (Fig. 4f). These data showing that the genetic loss of Nav1.7 in rodent C-LTMRs results in mechanical and cold sensory deficits, illustrate that Nav1.7 is necessary for normal C-LTMR function.

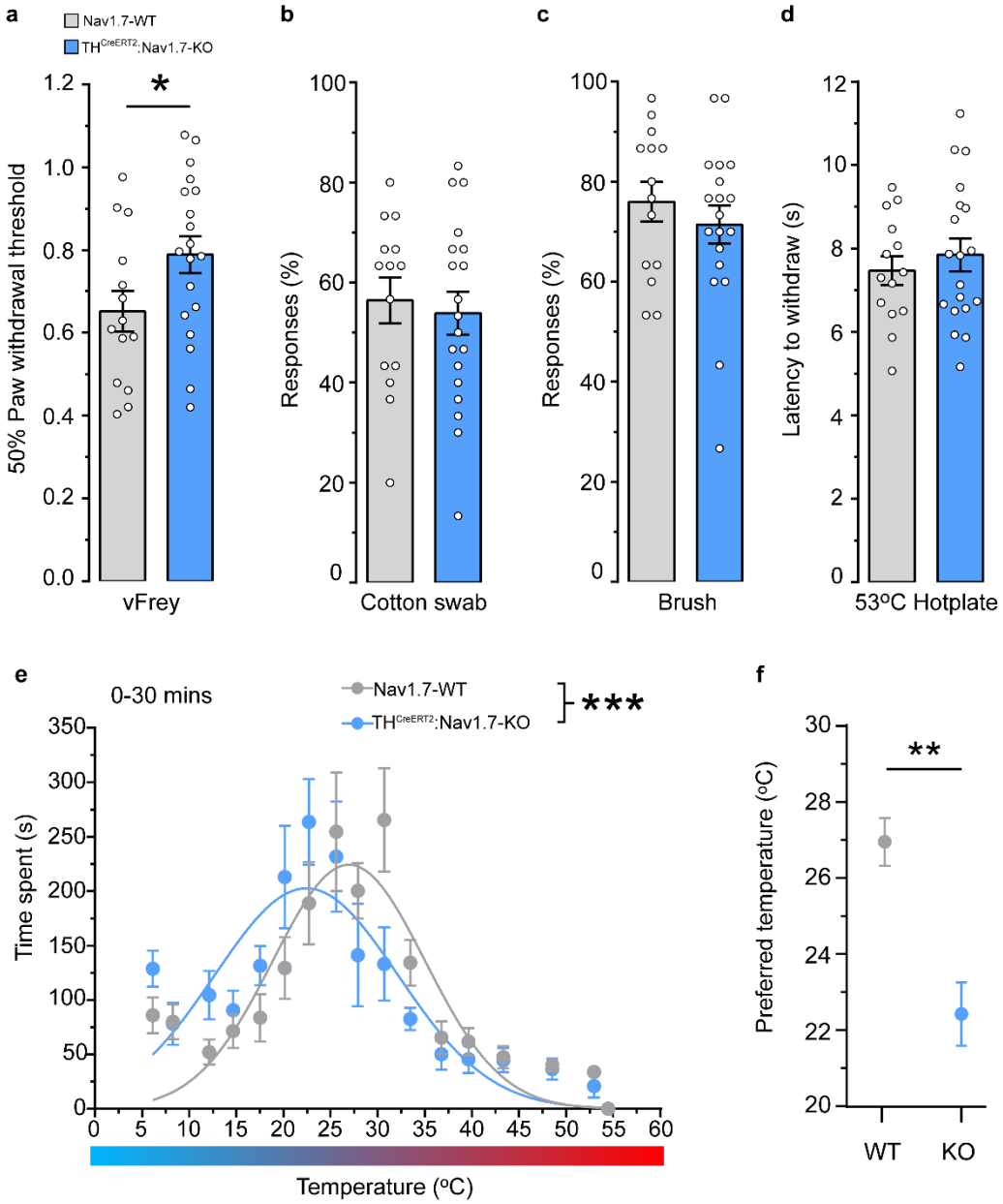

Figure. 4: The genetic loss of Nav1.7 in rodent C-LTMRs results in mechanical hyposensitivity and abnormalities in cooling detection.

Acute sensory testing of mice lacking Nav1.7 in the TH positive C-LTMR population (Blue – TH^{CreERT2}:Nav1.7-KO) compared to controls (Grey – Nav1.7-WT). **a)** C-LTMR specific deletion of Nav1.7 results in significant hyposensitivity to punctate mechanical von Frey stimuli (WT n = 14 mice, KO n = 19 mice, two-tailed Student's unpaired t-Test, t = 2.054, df = 31, P = 0.048, *). **b)** The number of responses to a cotton swab or **c)** to a brush are not affected by the loss of Nav1.7 in rodent C-LTMRs (WT n = 14 mice, KO n = 19 mice, two-tailed Student's unpaired t-Test, t = 0.402, df = 31, P = 0.69 and t = 0.809, df = 31, P = 0.42, respectively, n.s). **d)** Mice specifically lacking Nav1.7 in C-LTMRs show no changes in their latency to withdraw from a noxious 53ºC hotplate. (WT n = 14 mice, KO n = 19 mice, two-tailed Student's unpaired t-Test, t = 0.703, df = 31, P > 0.48, n.s). **e)** Mice lacking Nav1.7 in C-LTMRs spend more time in colder zones during

0-30 minutes of the thermal gradient test. The non-linear regression Gaussian fitted curves are significantly different between WT and KO mice, with KO mice showing a leftward shift toward colder temperatures (WT n = 7 mice, KO n=5 mice, non-linear fit F-Test, *F (dfn, dfd)* = 5.753 (1, 198), *P* = 0.0009, ***). **f)** The preferred temperature (the average temperature at which most time was spent) is significantly lower in KO mice compared to WT mice during 0-30 minutes of a thermal gradient test (WT n = 7 mice, KO n = 5 mice, two-tailed Student's unpaired t-Test, *t* = 4.422, *df* = 10, *P* = 0.0013, **). All data represented as mean ± S.E.M..

3.4. C-LTMRs lacking Nav1.7 are hypo-excitable

Given the changes in sensory behaviour in the $TH^{CreERT2}$:Nav1.7-KO mice we wanted to confirm our C-LTMR Nav1.7 KO and interrogate the contribution of Nav1.7 to the total sodium currents in this population. We labelled the C-LTMR population using the Cre dependent virus, AAV9.Flex.eGFP, giving us the ability to study the C-LTMRs *in vitro*. We performed intrathecal (i.t) injections of the reporter virus into $TH^{CreERT2}$ and $TH^{CreERT2}$:$Nav1.7^{flox/flox}$ mice and administered tamoxifen one week later to initiate simultaneous eGFP expression and Nav1.7 ablation (Fig. 5a). Four weeks following tamoxifen dosing we cultured lumbar DRG neurons from injected animals and performed voltage clamp analysis and single cell qPCR on eGFP positive cells (Fig. 5b). Using single cell qPCR, we confirm that the Nav1.7 mRNA transcript level is significantly reduced in $TH^{CreERT2}$:Nav1.7-KO C-LTMRs (Nav1.7-WT, n=7 cells, relative Nav1.7 mRNA expression 1.0 ± 0.3 and $TH^{CreERT2}$:Nav1.7-KO, n= 7 cells, relative Nav1.7 mRNA expression 0.3 ± 0.1. Mann Whitney *U* = 7, *P* = 0.0256). Patch clamp recordings showed a reduced peak inward current upon membrane depolarisation to 0mV (Fig. 5c-d) and lower current densities across a range of voltages at which voltage-gated sodium channels are known to activate (Fig. 5e-f), in C-LTMRs that lack Nav1.7 compared to wild type neurons.

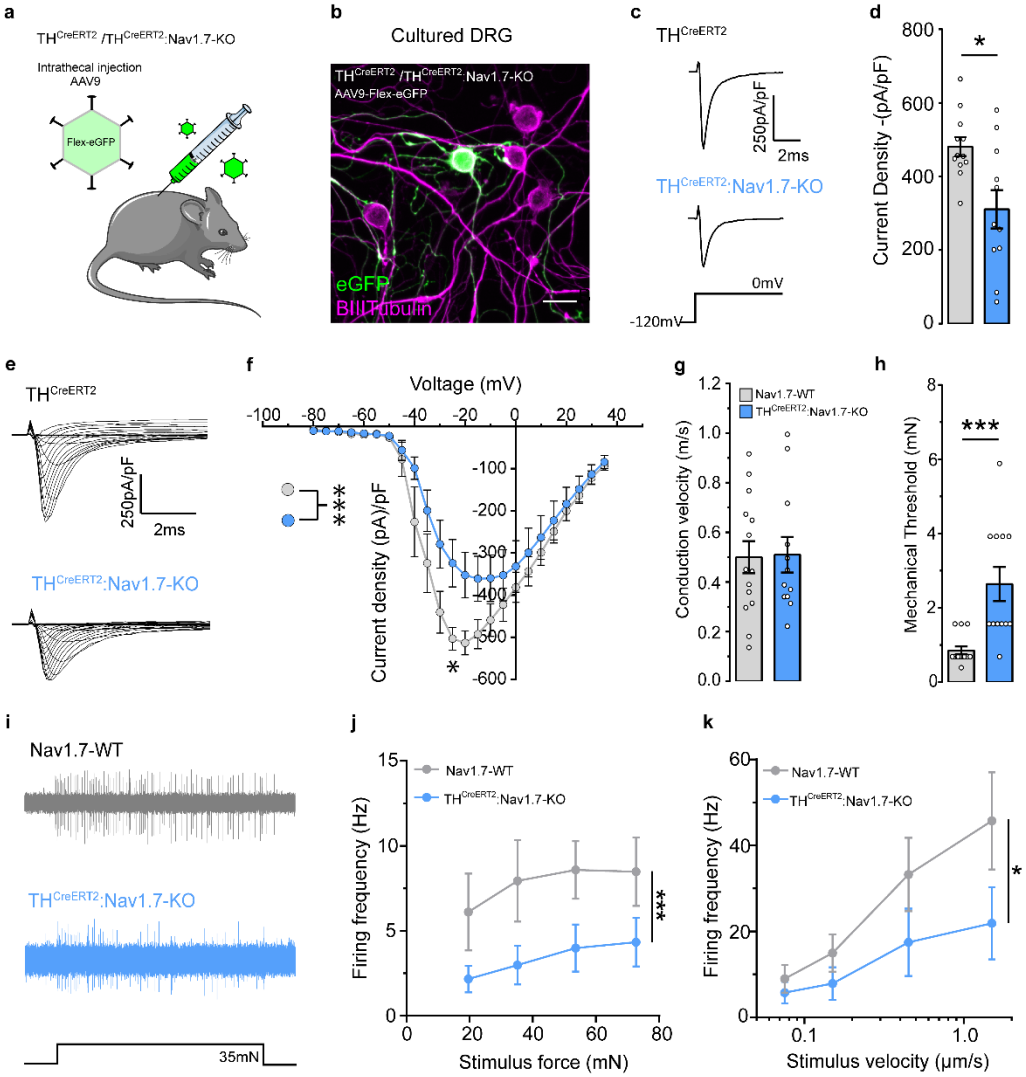

Figure. 5: Rodent C-LTMRs that lack Nav1.7 show smaller sodium currents and hypo-excitability.

a) $TH^{CreERT2}$ (control) or $TH^{CreERT2}Nav1.7^{flox/flox}$ ($TH^{CreERT2}$Nav1.7-KO) mice received and intrathecal injection of AAV.Flex.eGFP to target C-LTMRs prior to tamoxifen administration. Subsequent tamoxifen injection initiated simultaneous eGFP and Nav1.7 ablation. **b)** Virally targeted C-LTMRs were cultured, eGFP expression used to identify the population and voltage-clamp used to analyse sodium currents in both control and $TH^{CreERT2}$Nav1.7-KO mice. **c)** Example traces of recorded total sodium currents in eGFP positive C-LTMRs from $TH^{CreERT2}$ and $TH^{CreERT2}$Nav1.7-KO mice. **d)** C-LTMRs lacking Nav1.7 have a significantly reduced sodium current density compared to control C-LTMRs ($TH^{CreERT2}$ n = 12 cells, $TH^{CreERT2}$Nav1.7-KO n = 11 cells. Mann Whitney U test, $U = 28$, $P < 0.018$, *). **e)** Example sodium current traces from $TH^{CreERT2}$ and $TH^{CreERT2}$Nav1.7-KO C-LTMRs, in order to determine the sodium current-voltage (I/V) relationship. **f)** Quantification of the I/V relationship displayed as I/V curves. C-LTMRs from $TH^{CreERT2}$Nav1.7-KO mice show a significantly smaller I/V curve compared to C-LTMRs from $TH^{CreERT2}$ mice ($TH^{CreERT2}$ n = 12 cells, $TH^{CreERT2}$Nav1.7-KO n = 11 cells. Two-way ANOVA, *F (dfn,*

dfd) = 24.05 (1, 432), *P* < 0.0001, ***, with Sidak-Holm *post-hoc* test, -25pA, *t* = 3.342, *df* = 432, *P* = 0.021, *). **g)** Single fibre recordings from the mouse skin-nerve (saphenous) preparation comparing recordings from Nav1.7-WT (Grey) and $TH^{CreERT2}$:Nav1.7-KO (Blue) mice. C-LTMR conduction velocities are normal and comparable between both WT and C-LTMRs lacking Nav1.7. (WT n = 14 units, KO n = 12 units, two-tailed Student's unpaired t-Test, *t* = 0.103, *df* = 24, *P* > 0.91, n.s.) **h)** The mechanical thresholds of $TH^{CreERT2}$:Nav1.7-KO C-LTMRs are significantly higher than Nav1.7-WT control C-LTMRs (WT n = 14 units, KO n = 12 units, two-tailed Student's unpaired t-Test, *t* = 4.070, *df* = 24, *P* = 0.0004,***) **i)** Example trace of evoked action potentials in response to a supra-threshold mechanical stimulus applied to a single Nav1.7-WT and $TH^{CreERT2}$:Nav1.7-KO C-LTMR receptive field. **j)** The increasing force stimulus-response function showing that C-LTMRs lacking Nav1.7 are significantly hypo-excitable to supra-threshold stimuli compared to control C-LTMRs (WT n = 14 units, KO n = 12 units, two-way ANOVA, *F (dfn, dfd)* = 11.87 (1, 95), *P* = 0.0008, ***). **k)** The increasing velocity stimulus-response function of Nav1.7-WT and $TH^{CreERT2}$:Nav1.7-KO C-LTMRs. C-LTMRs lacking Nav1.7 are hypo-excitable with a significantly reduced firing frequency to dynamic stimuli (WT n = 14 units, KO n = 12 units, two-way ANOVA, *F (dfn, dfd)* = 6.212 (1, 96), *P* = 0.014, *). All data represented as mean ± S.E.M..

Due to Nav1.7's large contribution to sodium currents in C-LTMRs, we next examined whether Nav1.7 directly regulated C-LTMR excitability. We performed single-fibre primary afferent characterisation of C-LMTRs in hind paw hairy skin from Nav1.7-WT and $TH^{CreERT2}$:Nav1.7-KO mice. The conduction velocity of recorded C-LTMRs were within the mouse C-fibre range (<1.2m/s) and comparable between both WT and KO mice (Fig. 5g). However, there was a significant increase in the mechanical thresholds of $TH^{CreERT2}$:Nav1.7-KO C-LTMRs compared to those recorded from Nav1.7-WT mice (Fig. 5h). We next analysed the stimulus response functions of C-LTMRs to suprathreshold mechanical stimuli and saw that C-LTMRs lacking Nav1.7 fire less and display significant hypo-excitability (Fig. 5I-J). We also investigated the stimulus response functions in response to repeated punctate mechanical stimuli, where each downward skin indentation increases its velocity. Rodent C-LTMRs from $TH^{CreERT2}$:Nav1.7-KO mice exhibited a reduced firing frequency and are hypo-excitable to moving punctate stimuli compared to Nav1.7-WT mice (Fig. 5k). Collectively, we demonstrate that Nav1.7 is a key regulator of C-LTMR excitability.

3.5. Small molecule blockade of Nav1.7 reduces C-LTMR excitability

The small molecule inhibitor PF-05089771 shows selectivity for Nav1.7 (Alexandrou *et al.*, 2016) and has been in clinical development; it has shown potential in the treatment of patients with inherited erythromelalgia (Cao *et al.*, 2016). We performed voltage clamp recordings of labelled C-LTMRs (Fig. 6a) to investigate the effects of PF-05089771 (10 nM) on sodium current densities. Small molecule blockade of Nav1.7 significantly reduced the total sodium current density in C-LTMRs (Fig. 6b-c). We next performed primary afferent recordings using the *ex vivo* skin-nerve preparation from wild type mice in the presence or absence of PF-05089771, to determine whether this selective small molecule blocker could impact on rodent C-LTMR function. We identified and isolated C-LTMR receptive fields in rodent hairy skin and applied either vehicle or PF-05089771 and assessed excitability (Fig. 6d). We compared the mechanical thresholds of the isolated C-LTMR receptive fields before and after treatment and discovered that, compared to vehicle, there is a significant increase in mechanical threshold fold when PF-05089771 was applied (Fig. 6e). In addition, when we assessed the stimulus response function using suprathreshold mechanical stimuli we observed a significant reduction in C-LTMR activity in the presence of PF-05089771 compared to vehicle (Fig. 6f). To summarise, selective small molecule blockade of Nav1.7 reduced total sodium currents and altered C-LTMR function, resulting in hypo-excitability.

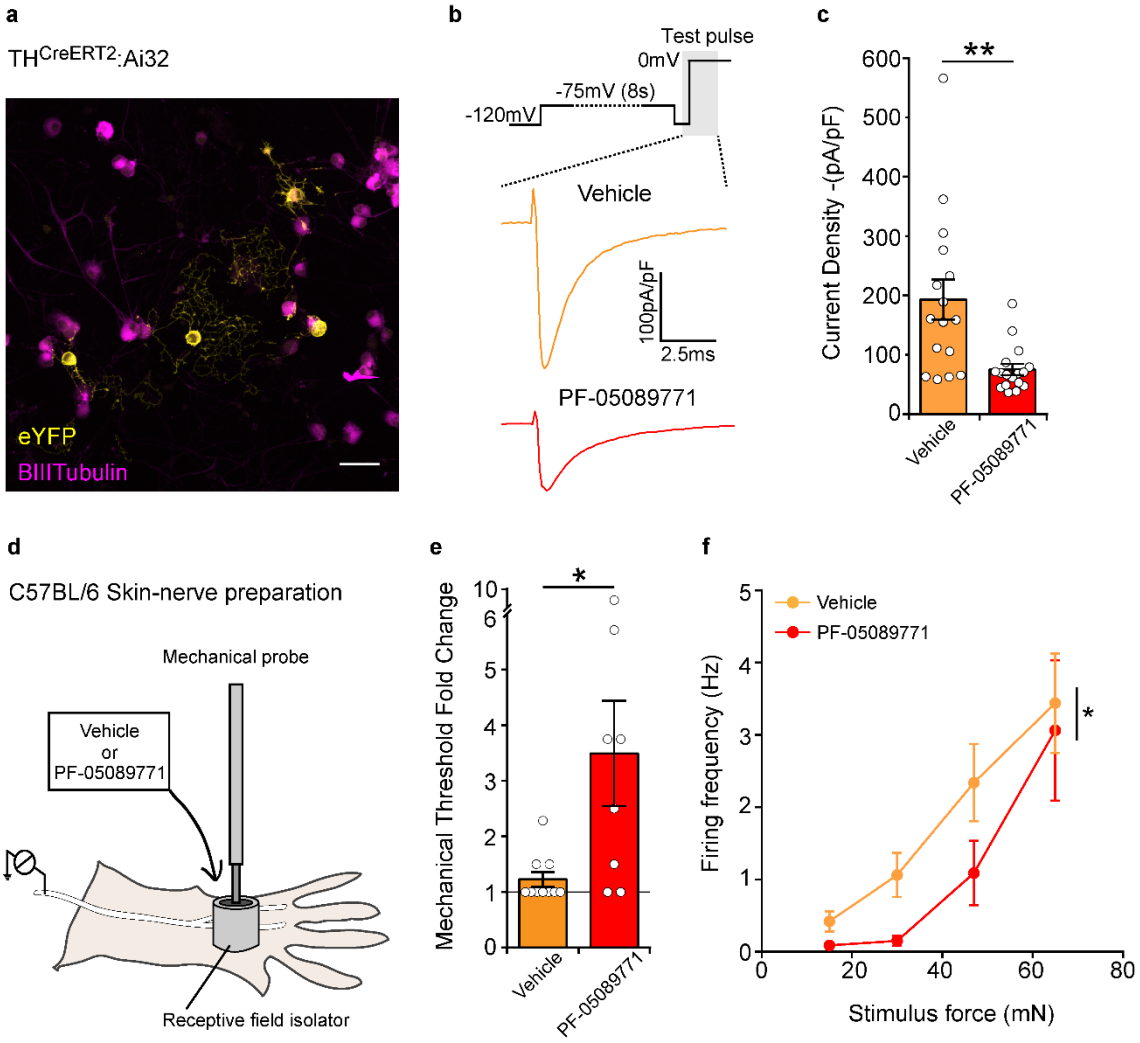

Figure 6: Selective small molecule inhibition of Nav1.7 currents results in hypo-excitable C-LTMR sensory endings.

a) DRG neuronal cultures were made from genetically labelled C-LTMRs ($TH^{CreERT2}$Ai32/eYFP) and used for subsequent voltage clamp analysis. **b)** *Top*, During the voltage-clamp protocol, neurons were depolarised to -75mV from a holding potential of -120mV for 8s (to inactivate a proportion of $Na_V1.7$ channels), followed by a 2ms recovery step to -120mV and a test pulse to 0 mV. *Bottom*, example traces of total sodium currents induced during the test pulse (shaded region of protocol schematic) in the presence of vehicle or PF-05089771 (10 nM). **c)** Quantification of the sodium current densities in wild type C-LTMRs in the presence of vehicle or PF-05089771. Blockage of Nav1.7 using PF-05089771 in C-LTMRs results in a significant reduction in the sodium current density compared to vehicle treated C-LTMRs (Vehicle n=16 cells, PF-05089771 n=17 cells, Mann Whitney U test, $U = 49$, $P = 0.0012$, **) **d)** Example illustration of single fibre C-LTMR recordings from wild type mice. C-LTMRs were identified and subsequently recorded following a 10 minute incubation of vehicle or PF-05089771 (10 nM) applied directly to the isolated receptive field. **e)** The fold change (1 = no change) of C-LTMR mechanical thresholds following vehicle or PF-05089771. Small molecule inhibition of Nav1.7 in C-LTMR sensory endings results

in a significant fold change increase in the mechanical threshold compared to vehicle. (Vehicle n=10 units, PF-05089771 n=8 units, Mann Whitney U test, $U = 15$, $P = 0.015$, *). **f)** The increasing force stimulus-response function showing that PF-05089771 treated C-LTMRs are significantly hypo-excitable to supra-threshold stimuli compared to vehicle treated C-LTMRs (Vehicle n=10 units, PF-05089771 n=8 units, two-way ANOVA, $F\ (dfn, dfd) = 4.101\ (1, 64)$, $P = 0.047$, *). All data represented as mean ± S.E.M..

3.6. Computational modelling of human *SCN9A* mutations in C-LTMRs

Given the clinical data that CIP participants experience an altered affective touch perception and that genetic ablation or pharmacological blockade of Nav1.7 in rodents reduced C-LTMR excitability, we investigated the impact of the CIP participant mutations on C-LTMR excitability and function. To address this question we took advantage of the recent Nav1.7 mutation characterisation from three CIP participants in our cohort (McDermott *et al.*, 2019). From the data available in McDermott *et al.* (2019) we were able to calculate the fold decrease in Nav1.7 conductance as a consequence of each *SCN9A* mutation (Table 1). We used a publicly available computational model of C-LTMR sensory neurons (Zheng *et al.*, 2019) to model C-LTMR excitability while altering the Nav1.7 conductance (Nav1.7 g-CLTMR, mS/cm^2) in accordance with the conductance decrease observed in each CIP participant mutation (Table 1). We ran the model in the naïve setting, without changing the Nav1.7 conductance, in order to resemble healthy control participant excitability measures (Fig. 7a). Next, we ran the model for four mutations, from three CIP participants using the new Nav1.7 conductance values calculated (Fig. 7b-e). C-LTMR excitability is strikingly impaired when modelling CIP participant mutations in C-LTMRs (Fig. 7b-e). The minimum current required to elicit an action potential in healthy control models is 40 pA; however, in CIP mutation models this ranges from 550pA-767 pA, depending on the mutation (Fig. 7a-e). We also used these computational models to look at suprathreshold excitability. We modelled C-LTMRs receiving incremental current injections (Δ25 pA) and there is clear hypo-excitability

observed in all CIP mutation models compared to the healthy control model (Fig. 7f-k). This is the first example of using a C-LTMR specific model to investigate Nav1.7 function in this popualtion. This is particularly important as C-LTMRs are electrophysiologically and transcriptionally distinct from C-fibre nociceptors (Campero *et al*., 2011; Roger Watkins *et al*., 2017; Zeisel *et al.,* 2018; Zheng *et al.,* 2019.)

Participant identifier	***SCN9A* mutation**	**Fold Decrease in Conductance**	**gNav1.7-C-LTMR (mS/cm^2)**
Healthy control	-	-	30.00
CIP participant 4	R839X	7.62	3.99
CIP participant 2	G1725R	30.20	1.01
CIP participant 3	R896W	62.39	0.49
CIP participant 4	FS1773	169.36	0.18

Table 1. CIP participants, their mutations and subsequent changes in Nav1.7 conductance applied to the C-LTMR computational model. Calculated from mutation characterisation in McDermott *et al* (2019).

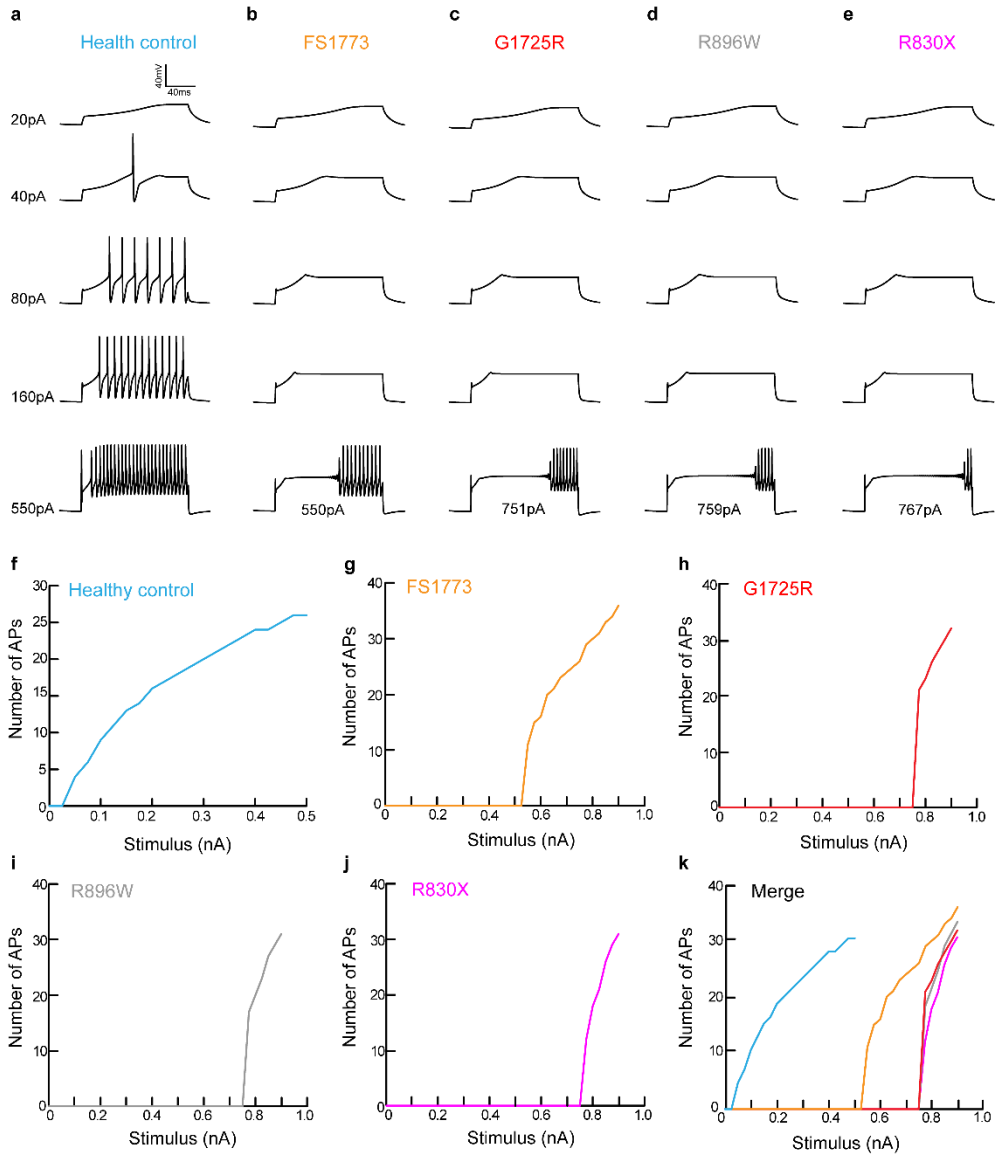

Figure 7: Modelling of human SCN9A mutations in a C-LTMR computational model shows multimodal hypo-excitability.

a) Computational modelling of healthy control participant C-LTMRs with no mutations in Nav1.7. Example traces of C-LTMR excitability and firing patterns assessed by increasing the current injected into the model. Examples of C-LTMR excitability and firing patterns when the model was adapted to take into account the changes in Nav1.7 conductance due to the following SCN9A mutations; **b)** FS1773, **c)** G1725R, **d)** R896W, **e)** R830X. The overlaid current value denotes the threshold of each model. All SCN9A mutations have increased thresholds to current injections. **f)** The healthy control model was subsequently ran to increase the current injection successively by 25pA in order to assess suprathreshold excitability. The model was adapted (change in Nav1.7 conductance) to take into account each SCN9A mutation **g)** FS1773, **h)** G1725R, **i)** R896W, **j)** R830X and executed to assess suprathreshold excitability. **k)** The merge of all models clearly illustrates that all SCN9A mutation models are hypo-excitable and require much larger current injections in order to repetitively fire to the same frequency as the healthy control C-LTMR model.

4. Discussion

We have found that not only do humans with *SCN9A*-LOF mutations have CIP but also an altered experience and perception of affective touch sensation. We demonstrate that rodent C-LTMRs express high levels of Nav1.7. We used selective genetic strategies in order to attribute this LOF phenotype to hypo-excitable C-LTMR primary afferents. We also challenged the current concept that pharmacological blockade of Nav1.7 is selective to the nociceptive system and show the affective touch system also requires functional Nav1.7.

The CIP participants in this study were all bi-allelic compound heterozygotes and all of their mutations have been previously characterised and shown to abolish almost all Nav1.7 driven sodium currents. The CIP participants have also been extensively studied in the context of nociception (Cox *et al.,* 2006; Bennett *et al.,* 2019). These participants have never experienced pain and as a result have had multiple injuries throughout their lives due to a loss of functional C-nociceptors, a lack of epidermal small fibres (McDermott *et al.*, 2019) and up-regulation of endogenous opioids (Minett *et al.*, 2015). These patients also lack itch perception in response to pruritogens, such as histamine, and exhibit mild hyposensitivity to warm and cool stimuli. Vibration and mechanical detection thresholds have not been found to differ from control whilst the affective touch system has never previously been investigated.

The identification of human mutations affecting C-LTMRs and affective touch is scarce. Patients with hereditary sensory and autonomic neuropathy type-V (HSAN-V) due to a mutation in the nerve growth factor beta (*NGFβ*) gene and who also have congenital insensitivity to pain have a reduced affective touch percept (Morrison *et al.*, 2011). NGF mediates its effects by binding to the NTRK1 receptor; the $NTRK1^{+}$ lineage of small diameter, unmyelinated neurons derive from the *Neurog1* wave of neurogenesis and these mutations likely impede the initial development of C-LTMRs (Marmigère and Ernfors, 2007). We have now shown that LOF mutations in the voltage-gated ion channel

Nav1.7, have negative impacts on affective touch. Our cohort of CIP participants exhibit altered self-reported pleasantness for gentle brush stimulation and do not show the classical inverted U-shaped response pattern. Compared to a less pleasant fast touch stimulus, affective touch reliably attenuates activity of the corrugator muscle in an unbiased facial EMG measure of affective touch, suggestive of a reduction in negative affect (Mayo *et al.*, 2018; Ree, Mayo, *et al.*, 2019). Here, 3 cm/s stroking stimulation failed to influence corrugator activity in CIP participants, suggesting that touch which normally elicits human C-LTMR activation does not attenuate negative affect in these individuals. This was selective for the affective aspect of the stimulus, since all CIP participants were able to rate the stimulus intensity similarly to healthy control participants. This confirms previous literature suggesting that in cases of CIP the large myelinated touch fibres are not compromised (McDermott *et al.*, 2019). Collectively, these findings demonstrate that human *SCN9A*-LOF mutations can alter the affective component of pleasant touch sensation.

To interrogate further the expression and role of Nav1.7 in C-LTMR function we took advantage of rodent models. Nav1.7 is known to be expressed in nociceptors (Black *et al.*, 2012; Rostock *et al.*, 2018). Using ISH and analysis of previously published data sets (Reynders *et al.*, 2015) we show that *SCN9A* is expressed in all C-LTMRs and to a high level. This data adds to the recent sequencing data showing that *SCN9A* is most highly expressed in the rodent C-LTMR population (Zheng *et al.*, 2019). Interestingly many A-LTMRs also show some expression of Nav1.7 however there is no evidence of impairments either in large fibre mediated touch modalities or the electrophysiological properties of these afferents in *SCN9A*-LOF CIP patients (Cox *et al.*, 2006; Goldberg *et al.*, 2007; McDermott *et al.*, 2019). This is likely due to functional redundancy and the co-expression (unlike in C-LTMRs (Zheng *et al.*, 2019)) of other TTX-S VGSCs such as Nav 1.1 and 1.6 in these neurons which can compensate for the loss of Nav1.7 (Bennett *et al.*, 2019).

A number of genetic knock-out strategies have previously been used to investigate the role of C-LTMRs in rodents. A global vGLUT3 KO, initially thought to be C-LTMR specific, resulted in altered noxious mechanical thresholds (Seal *et al.*, 2009), a phenotype which was later shown to be driven by loss of spinal vGLUT3 (Peirs *et al.*, 2015). Other studies suggest deficits in acute light touch, cold detection and chemical pain responses when Nav1.8 positive sensory neurons (which include C-LTMRs) lack Cav3.2 a voltage-gated calcium channel enriched in C-LTMRs (François *et al.*, 2015). In contrast, the global KO of the chemokine-like protein Tafa4, which is thought to only be expressed and released by C-LTMRs, resulted in a pro-nociceptive phenotype (Delfini *et al.*, 2013). This phenotype was recovered by administration of exogenous Tafa4 a mechanism which involves GABAergic transmission and spinal microglia (Delfini *et al.*, 2013; Kambrun *et al.*, 2018). Vrontou *et al.* (2013) identified a population of sensory neurons that expressed the G-protein coupled receptor MrgprB4. There is some evidence that this population is involved in massage-like stroking of hairy skin (Vrontou *et al.*, 2013). Unfortunately, Vrontou *et al.* (2013) were not able to identify this population as a low-threshold mechanoreceptive population and could only infer that they are C-fibres due to small cell body size and IB4 expression (Liu *et al.*, 2007; Vrontou *et al.*, 2013) . In addition, there has been no physiological evidence of C-fibre range conduction velocities of MrgprB4+ afferents. There is closer alliance and more physiological evidence that the TH/vGLUT3/Tafa4 population is the likely species equivalent of human C-LTMRs (Seal *et al.*, 2009; Li *et al.*, 2011; Delfini *et al.*, 2013). However, we cannot exclude the possibility that both populations co-exist and that perhaps relate to modality specific pleasure perception.

Hitherto, there has been a lack of transgenic tools available to selectively target the C-LTMR population; the discovery that TH is a marker of C-LTMRs and development of the $TH^{CreERT2}$ line has helped delineate the physiology and connectivity of these neurons in the rodent (Li *et al.*, 2011; Abraira *et al.*, 2017). In validating the $TH^{CreERT2}$

mouse (and confirming that it is a good model system to target C-LTMRs (Abraira *et al.*, 2017)) we have found that C-LTMRs innervate not only hairy skin on the dorsum of the paw but also the hind paw plantar surface of mice, as longitudinal lanceolate endings (as shown in chapter 4). These hair follicles located between hind-paw running pads were thought to exclusively be innervated by the Aδ-LTMR population known as D-hairs (Dawes *et al.*, 2018; Walcher *et al.*, 2018). This is an important finding, as studies often overlook these particular hair follicles and the dogma currently suggests that C-LTMRs do not innervate rodent plantar skin. We provide evidence that this population does innervate the running pad region, which is commonly tested in rodent sensory biology.

We saw that when we ablated Nav1.7 in rodent C-LTMRs, the response to noxious heat remained intact but mice became hyposensitive to punctate mechanical stimuli. This finding is consistent with previous rodent studies which also show that C-LTMRs have a modest contribution to punctate mechanical stimuli (François *et al.*, 2015). There is debate in the literature over the perceptual correlate of a withdrawal to a von Frey hair in rodents. It is likely that von Frey withdrawal relates to stimulus detection rather than a painful aversion. The genetic ablation of all TRPV1-lineage neurons (all nociceptors) or the optogenetic silencing of CGRP+ peptidergic neurons did not alter von Frey thresholds in the naïve, uninjured state (Mishra *et al.*, 2011; Cowie *et al.*, 2018). In addition, the early human data which first characterised C-LTMRs, clearly demonstrated that C-LTMRs do respond to both punctate and brush stimuli (Vallbo, Olausson and Wessberg, 1999), and patients lacking A-fibre function are still able to detect low-force punctate monofilaments, but only in hairy skin (Cole *et al.*, 2006). Together this highlights that C-LTMRs play a role in punctate mechanical detection in rodents and humans.

Interestingly, using our mouse KO model we did not see any changes in the number of responses to dynamic light touch stimuli. However, one must consider that these assays interrogate stimulus detection, not the affective component of the stimulus.

It has been recently demonstrated in rodents that the TrkB+ population (Aδ LTMRs and Aβ RA-LTMRs) are responsible for the detection of dynamic brush and cotton swab (Dhandapani *et al.*, 2018). TrkB is not present in TH+ C-LTMRs (Dhandapani et al. 2018). We would therefore have expected the dynamic response to brush and cotton wool to be unaltered as a consequence of impaired C-LTMR function. We have shown with our EMG cohort that CIP participants can still detect the brushing stimulus intensity (as distinct to affective response) and this therefore is consistent with our mouse findings. The sensory biology field is currently challenged in not having a reliable read-out for affective pleasure sensation in rodents, an obstacle that as a community we need to overcome.

The loss of C-LTMR Nav1.7 resulted in deficits in cool coding, suggesting without Nav1.7 in the C-LTMR population mice are unable to properly code the cooling stimuli and, as a consequence spend a longer amount of time in colder regions. This could speak to the possibility that wild type C-LTMRs signal aversive stimuli promoting avoidance, which is lacking in our C-LTMR Nav1.7 KO. However, this loss of avoidance is not in noxious temperature range and likely relates to cool sensibility. It is also important to note that these behavioural changes can also be interpreted as C-LTMR Nav1.7 KO mice losing their preference for the temperature that is usually most pleasant. Furthermore, in a previous study, quantitative sensory testing (QST) was used to sensory profile CIP participants (3 which were recruited as part of this study) and it was found that they were hypo-sensitive to cooling stimuli (McDermott *et al.*, 2019). This highlights further similarities between the rodent and human phenotypes and future work should interrogate the thermo-response of C-LTMRs at a single fibre level in C-LTMRs lacking Nav1.7.

There are few other regions of the nervous system that also co-express TH and Nav1.7 where ablation would also occur in our model. Sympathetic neurons express both (Zeisel *et al.*, 2018) however they unlikely require Nav1.7 as CIP participants do

not present with sympathetic deficits. Equally, dopaminergic neurons in the periaqueductal grey and ventral midbrain express TH but show very low levels of *SCN9A* expression (Zeisel *et al.*, 2018). Given our expression data and that the observed phenotypes represent very selective deficits in sensory processing, it is highly likely that the locus of action is in primary afferents.

Given the high expression of Nav1.7 in C-LTMRs and the important role of Nav1.7 as a threshold channel within sensory neurons, we investigated whether the observed behavioural changes were due to alterations in the excitability of C-LTMRs. Using voltage-clamp recordings *in vitro,* we saw a reduction of the sodium current density in C-LTMRs which lack Nav1.7 and found that there is a large contribution of Nav1.7 to the total sodium currents in this population. A previous study used the skin-nerve preparation to interrogate Nav1.7 contribution to peripheral nerve excitability, using a sensory neuron specific Nav1.7 KO mouse (Hoffmann *et al.*, 2018). However, Hoffmann *et al.* (2018), did not characterise in detail the loss of Nav1.7 in C-LTMRs and were underpowered to perform such analysis. Therefore, we assessed C-LTMR primary afferent terminal excitability using the skin-nerve preparation. Here, we found that loss of Nav1.7 results in hypo-excitability and, in particular, alters C-LTMR stimulus response functions to mechanical stimuli. From this, we propose a mechanism whereby Nav1.7, which has a large contribution to C-LTMR sodium currents, is important in regulating C-LTMR excitability and function. We propose that loss of functional Nav1.7 in our CIP participants likely results in hypo-excitable C-LTMRs which can no longer effectively drive the affective component of pleasant brush stimuli.

Targeting Nav1.7 to therapeutically treat painful conditions may therefore have unintended consequences on the affective touch system. We indeed saw a reduction in both C-LTMR sodium currents and terminal excitability when using a Nav1.7 selective small molecule blocker. These data suggest that current and future strategies, which target Nav1.7 to treat pain, need to consider the consequences of reducing the

excitability, of this non-nociceptive population and how this might, alter pleasant touch, social contact, communication, relationships and empathy for touch observed in others. One clinical example might be the prescription of Nav1.7 blockers in early life where social contact, communication, relationships and empathy are still developing. A second example is that blocking C-LTMR function in adulthood when pleasant touch, social contact, communication, relationships and empathy are already established may also negatively affect the patient, despite any pain relief. In addition, there may be novel roles of C-LTMRs that are not yet identified. For instance there is a growing literature illustrating that autism candidate genes also regulate LTMR function (Orefice et al. 2016; Dawes et al. 2018; Orefice et al. 2019). This is yet to include C-LTMRs but this is a field in its infancy.

We know from previous studies that human *SCN9A*-LOF mutations can reduce neuronal excitability (McDermott *et al.*, 2019). As such, we sought to investigate the effects of human *SCN9A*-LOF mutations in the context of C-LTMRs, using a recently developed C-LTMR computational model (Zheng *et al.*, 2019). While models of C-nociceptors exist there is strong evidence that this would not generalise to C-LTMRs (Tigerholm *et al.*, 2014). For instance, C-LTMR activity dependent slowing is very different compared to C-nociceptors (Campero *et al.*, 2011; Roger Watkins *et al.*, 2017). Therefore, using a C-LTMR specific computational model, we recapitulated mutations from a subset of our CIP participant cohort and consistent with our empirical findings these led to hypo-excitability in C-LTMRs. The CIP-participants have compound heterozygote mutations so the outcome *in vivo* is the combinatorial effect of two mutations.

To summarise, we have used a multidisciplinary approach to investigate the role of Nav1.7 in C-LTMR function in humans and mice. Psychophysical testing showed CIP participants have an altered perception of affective touch sensation. We used a mouse model to selectively ablate Nav1.7 in C-LTMRs in order to determine this mechanism.

We found that loss of Nav1.7 in C-LTMRs results in mechanical and cold hyposensitivity, a reduction in sodium currents and hypo-excitability to threshold and suprathreshold mechanical stimuli. Pharmacological blockade of Nav1.7 also led to hypo-excitable C-LTMRs. The impact of loss of function in one VGSC alpha subunit within different sensory neuron subpopulations is dependent on co-expression with other VGSCs, which vary between fibre types, and the non-redundant role of Nav1.7 in C-LTMRs which we observed, is supported by a recent computational model of C-LTMRs. The phenotype of bi-allelic LOF gene mutations in *SCN9A* has therefore been widened to not only include pain perception but also impaired affective touch and furthermore targeting Nav1.7 to therapeutically treat painful conditions may have implications on the affective touch system.

5. Acknowledgements

Dr Andreas Themistocleous from the University of Oxford, UK and Dr Irene Perini from Linkoping University, Sweden (together with their collaborators), collected all of the human data in Figures 1 and 2 of this chapter. The ISH in Figure 3b was carried out by Dr Manon Bohic from Rutgers, USA. The voltage-clamp recordings in Figure 5c-f and Figure 6b-c, was carried out by Dr Greg Weir. Single cell qPCR was carried out by Allison Barry, University of Oxford. All other data in this chapter was carried out by myself.

6. References

Abraira, V. E. *et al.* (2017) 'The Cellular and Synaptic Architecture of the Mechanosensory Dorsal Horn', *Cell*. Cell Press, 168(1–2), pp. 295-310.e19. doi: 10.1016/J.CELL.2016.12.010.

Ahmad, S. *et al.* (2007) 'A stop codon mutation in SCN9A causes lack of pain sensation', *Human Molecular Genetics*. Narnia, 16(17), pp. 2114–2121. doi: 10.1093/hmg/ddm160.

Alexandrou, A. J. *et al.* (2016) 'Subtype-Selective Small Molecule Inhibitors Reveal a Fundamental Role for Nav1.7 in Nociceptor Electrogenesis, Axonal Conduction and Presynaptic Release', *PLOS ONE*. Edited by T. J. Price. Public Library of Science, 11(4), p. e0152405. doi: 10.1371/journal.pone.0152405.

Bennett, D. L. *et al.* (2019) 'The Role of Voltage-Gated Sodium Channels in Pain Signaling', *Physiological Reviews*. American Physiological Society Bethesda, MD , 99(2), pp. 1079–1151. doi: 10.1152/physrev.00052.2017.

Black, J. A. *et al.* (2012) 'Expression of Nav1.7 in DRG neurons extends from peripheral terminals in the skin to central preterminal branches and terminals in the dorsal horn.', *Molecular pain*. SAGE Publications, 8, p. 82. doi: 10.1186/1744-8069-8-82.

Blesneac, I. *et al.* (2018) 'Rare NaV1.7 variants associated with painful diabetic peripheral neuropathy', *Pain*. Wolters Kluwer Health, 159(3), p. 469. doi: 10.1097/J.PAIN.0000000000001116.

Branco, T. *et al.* (2016) 'Near-Perfect Synaptic Integration by Nav1.7 in Hypothalamic Neurons Regulates Body Weight.', *Cell*. Elsevier, 165(7), pp. 1749–1761. doi: 10.1016/j.cell.2016.05.019.

Campero, M. *et al.* (2011) 'Activity-dependent slowing properties of an unmyelinated

low threshold mechanoreceptor in human hairy skin', *Neuroscience Letters*, 493(3), pp. 92–96. doi: 10.1016/j.neulet.2011.02.012.

Cao, L. *et al.* (2016) 'Pharmacological reversal of a pain phenotype in iPSC-derived sensory neurons and patients with inherited erythromelalgia.', *Science translational medicine*. American Association for the Advancement of Science, 8(335), p. 335ra56. doi: 10.1126/scitranslmed.aad7653.

Cole, J. *et al.* (2006) 'Unmyelinated tactile afferents underpin detection of low-force monofilaments', *Muscle & Nerve*. John Wiley & Sons, Ltd, 34(1), pp. 105–107. doi: 10.1002/mus.20534.

Cowie, A. M. *et al.* (2018) 'Optogenetic Inhibition of CGRPα Sensory Neurons Reveals Their Distinct Roles in Neuropathic and Incisional Pain.', *The Journal of neuroscience*. Society for Neuroscience, 38(25), pp. 5807–5825. doi: 10.1523/JNEUROSCI.3565-17.2018.

Cox, J. J. *et al.* (2006) 'An SCN9A channelopathy causes congenital inability to experience pain', *Nature*. Nature Publishing Group, 444(7121), pp. 894–898. doi: 10.1038/nature05413.

Dawes, J. M. *et al.* (2018) 'Immune or Genetic-Mediated Disruption of CASPR2 Causes Pain Hypersensitivity Due to Enhanced Primary Afferent Excitability', *Neuron*, 97(4), pp. 806-822.e10. doi: 10.1016/j.neuron.2018.01.033.

Delfini, M.-C. *et al.* (2013) 'TAFA4, a Chemokine-like Protein, Modulates Injury-Induced Mechanical and Chemical Pain Hypersensitivity in Mice', *Cell Reports*. Cell Press, 5(2), pp. 378–388. doi: 10.1016/J.CELREP.2013.09.013.

Dhandapani, R. *et al.* (2018) 'Control of mechanical pain hypersensitivity in mice through ligand-targeted photoablation of TrkB-positive sensory neurons', *Nature Communications*. Nature Publishing Group, 9(1), p. 1640. doi: 10.1038/s41467-018-

04049-3.

Dib-Hajj, S. D. *et al.* (2005) ‘Gain-of-function mutation in Nav1.7 in familial erythromelalgia induces bursting of sensory neurons’, *Brain*. Narnia, 128(8), pp. 1847–1854. doi: 10.1093/brain/awh514.

Faber, C. G. *et al.* (2012) ‘Gain of function NaV1.7 mutations in idiopathic small fiber neuropathy’, *Annals of Neurology*, 71(1), pp. 26–39. doi: 10.1002/ana.22485.

Fertleman, C. R. *et al.* (2006) ‘SCN9A Mutations in Paroxysmal Extreme Pain Disorder: Allelic Variants Underlie Distinct Channel Defects and Phenotypes’, *Neuron*. Elsevier, 52(5), pp. 767–774. doi: 10.1016/J.NEURON.2006.10.006.

François, A. *et al.* (2015) ‘The Low-Threshold Calcium Channel Cav3.2 Determines Low-Threshold Mechanoreceptor Function’, *Cell Reports*. Cell Press, 10(3), pp. 370–382. doi: 10.1016/J.CELREP.2014.12.042.

Fridlund, A. J. and Cacioppo, J. T. (1986) ‘Guidelines for Human Electromyographic Research’, *Psychophysiology*. John Wiley & Sons, Ltd (10.1111), 23(5), pp. 567–589. doi: 10.1111/j.1469-8986.1986.tb00676.x.

Goldberg, Y. *et al.* (2007) ‘Loss-of-function mutations in the Nav1.7 gene underlie congenital indifference to pain in multiple human populations’, *Clinical Genetics*. John Wiley & Sons, Ltd (10.1111), 71(4), pp. 311–319. doi: 10.1111/j.1399-0004.2007.00790.x.

Hoffmann, T. *et al.* (2018) ‘NaV1.7 and pain: contribution of peripheral nerves’, *Pain*. NLM (Medline), 159(3), pp. 496–506. doi: 10.1097/j.pain.0000000000001119.

Kambrun, C. *et al.* (2018) ‘TAFA4 Reverses Mechanical Allodynia through Activation of GABAergic Transmission and Microglial Process Retraction’, *Cell Reports*. Cell Press, 22(11), pp. 2886–2897. doi: 10.1016/J.CELREP.2018.02.068.

Kanellopoulos, A. H. *et al.* (2018) ‘Mapping protein interactions of sodium channel Na $_{V}$

1.7 using epitope-tagged gene-targeted mice', *The EMBO Journal*. John Wiley & Sons, Ltd, 37(3), pp. 427–445. doi: 10.15252/embj.201796692.

Kilkenny, C. *et al.* (2010) 'Improving Bioscience Research Reporting: The ARRIVE Guidelines for Reporting Animal Research', *PLoS Biology*. Public Library of Science, 8(6), p. e1000412. doi: 10.1371/journal.pbio.1000412.

Larsson, M. and Broman, J. (2019) 'Synaptic Organization of VGLUT3 Expressing Low-Threshold Mechanosensitive C Fiber Terminals in the Rodent Spinal Cord', *eNeuro*. Society for Neuroscience, 6(1), p. ENEURO.0007-19.2019. doi: 10.1523/ENEURO.0007-19.2019.

Leem, J. W., Willis, W. D. and Chung, J. M. (1993) 'Cutaneous sensory receptors in the rat foot', *https://doi.org/10.1152/jn.1993.69.5.1684*. American Physiological Society Bethesda, MD . doi: 10.1152/JN.1993.69.5.1684.

Li, L. *et al.* (2011) 'The Functional Organization of Cutaneous Low-Threshold Mechanosensory Neurons', *Cell*. Cell Press, 147(7), pp. 1615–1627. doi: 10.1016/J.CELL.2011.11.027.

Liljencrantz, J. and Olausson, H. (2014) 'Tactile C fibers and their contributions to pleasant sensations and to tactile allodynia', *Frontiers in Behavioral Neuroscience*. Frontiers, 8, p. 37. doi: 10.3389/fnbeh.2014.00037.

Liu, Q. *et al.* (2007) 'Molecular genetic visualization of a rare subset of unmyelinated sensory neurons that may detect gentle touch', *Nature Neuroscience*, 10(8), pp. 946–948. doi: 10.1038/nn1937.

Löken, L. S. *et al.* (2009) 'Coding of pleasant touch by unmyelinated afferents in humans', *Nature Neuroscience*. Nature Publishing Group, 12(5), pp. 547–548. doi: 10.1038/nn.2312.

Lynn, B. and Carpenter, S. E. (1982) 'Primary afferent units from the hairy skin of the

rat hind limb', *Brain Research*. Elsevier, 238(1), pp. 29–43. doi: 10.1016/0006-8993(82)90768-5.

Marmigère, F. and Ernfors, P. (2007) 'Specification and connectivity of neuronal subtypes in the sensory lineage', *Nature Reviews Neuroscience*. Nature Publishing Group, 8(2), pp. 114–127. doi: 10.1038/nrn2057.

Mayo, L. M. *et al.* (2018) 'Putting a good face on touch: Facial expression reflects the affective valence of caress-like touch across modalities', *Biological Psychology*. Elsevier, 137, pp. 83–90. doi: 10.1016/J.BIOPSYCHO.2018.07.001.

McDermott, L. A. *et al.* (2019) 'Defining the Functional Role of NaV1.7 in Human Nociception', *Neuron*. Elsevier, 101(5), pp. 905-919.e8. doi: 10.1016/J.NEURON.2019.01.047.

Meents, J. E. *et al.* (2019) 'The role of Nav1.7 in human nociceptors: insights from human induced pluripotent stem cell-derived sensory neurons of erythromelalgia patients.', *Pain*, 160(6), pp. 1327–1341. doi: 10.1097/j.pain.0000000000001511.

Minett, M. S. *et al.* (2015) 'Endogenous opioids contribute to insensitivity to pain in humans and mice lacking sodium channel Nav1.7', *Nature Communications*. Nature Publishing Group, 6(1), p. 8967. doi: 10.1038/ncomms9967.

Mis, M. A. *et al.* (2019) 'Resilience to Pain: A Peripheral Component Identified Using Induced Pluripotent Stem Cells and Dynamic Clamp.', *The Journal of neuroscience : the official journal of the Society for Neuroscience*. Society for Neuroscience, 39(3), pp. 382–392. doi: 10.1523/JNEUROSCI.2433-18.2018.

Mishra, S. K. *et al.* (2011) 'TRPV1-lineage neurons are required for thermal sensation', *EMBO Journal*, 30(3), pp. 582–593. doi: 10.1038/emboj.2010.325.

Morrison, I. *et al.* (2011) 'Reduced C-afferent fibre density affects perceived pleasantness and empathy for touch', *Brain*. Narnia, 134(4), pp. 1116–1126. doi:

10.1093/brain/awr011.

Morrison, I., Björnsdotter, M. and Olausson, H. (2011) ‘Vicarious responses to social touch in posterior insular cortex are tuned to pleasant caressing speeds.’, *The Journal of neuroscience : the official journal of the Society for Neuroscience*. Society for Neuroscience, 31(26), pp. 9554–62. doi: 10.1523/JNEUROSCI.0397-11.2011.

Nassar, M. A. *et al.* (2004) ‘Nociceptor-specific gene deletion reveals a major role for Nav1.7 (PN1) in acute and inflammatory pain’, *Proceedings of the National Academy of Sciences*, 101(34), pp. 12706–12711. doi: 10.1073/pnas.0404915101.

Nordin, M. (1990) ‘Low-threshold mechanoreceptive and nociceptive units with unmyelinated (C) fibres in the human supraorbital nerve.’, *The Journal of physiology*. Wiley-Blackwell, 426, pp. 229–40. doi: 10.1113/jphysiol.1990.sp018135.

Olausson, H. *et al.* (2010) ‘The neurophysiology of unmyelinated tactile afferents’, *Neuroscience & Biobehavioral Reviews*. Pergamon, 34(2), pp. 185–191. doi: 10.1016/J.NEUBIOREV.2008.09.011.

Orefice, L. L. *et al.* (2019) ‘Targeting Peripheral Somatosensory Neurons to Improve Tactile-Related Phenotypes in ASD Models’, *Cell*. Cell Press, 178(4), pp. 867-886.e24. doi: 10.1016/j.cell.2019.07.024.

Orefice, L. L. L. *et al.* (2016) ‘Peripheral Mechanosensory Neuron Dysfunction Underlies Tactile and Behavioral Deficits in Mouse Models of ASDs’, *Cell*. Cell Press, 166(2), pp. 299–313. doi: 10.1016/j.cell.2016.05.033.

Peirs, C. *et al.* (2015) ‘Dorsal Horn Circuits for Persistent Mechanical Pain’, *Neuron*. Cell Press, 87(4), pp. 797–812. doi: 10.1016/J.NEURON.2015.07.029.

Perini, I., Morrison, I. and Olausson, H. (2015) ‘Seeking pleasant touch: neural correlates of behavioral preferences for skin stroking’, *Frontiers in Behavioral Neuroscience*. Frontiers, 9, p. 8. doi: 10.3389/fnbeh.2015.00008.

Ree, A., Mayo, L. M., *et al.* (2019) ‘Touch targeting C-tactile afferent fibers has a unique physiological pattern: A combined electrodermal and facial electromyography study’, *Biological Psychology*. Elsevier, 140, pp. 55–63. doi: 10.1016/J.BIOPSYCHO.2018.11.006.

Ree, A., Morrison, I., *et al.* (2019) ‘Using Facial Electromyography to Assess Facial Muscle Reactions to Experienced and Observed Affective Touch in Humans’, *Journal of Visualized Experiments*, (145), p. e59228. doi: 10.3791/59228.

Reynders, A. *et al.* (2015) ‘Transcriptional Profiling of Cutaneous MRGPRD Free Nerve Endings and C-LTMRs’, *Cell Reports*. Cell Press, 10(6), pp. 1007–1019. doi: 10.1016/J.CELREP.2015.01.022.

Roger Watkins, X. H. *et al.* (2017) ‘RAPID REPORT Sensory Processing Optimal delineation of single C-tactile and C-nociceptive afferents in humans by latency slowing Optimal delineation of single C-tactile and C-nociceptive afferents in humans by latency slowing’, *J Neuro-physiol*, 117, pp. 1608–1614. doi: 10.1152/jn.00939.2016.-C-mechanoreceptors.

Rostock, C. *et al.* (2018) ‘Human vs. Mouse Nociceptors – Similarities and Differences’, *Neuroscience*, 387, pp. 13–27. doi: 10.1016/j.neuroscience.2017.11.047.

Seal, R. P. *et al.* (2009) ‘Injury-induced mechanical hypersensitivity requires C-low threshold mechanoreceptors’, *Nature*. Nature Publishing Group, 462(7273), pp. 651–655. doi: 10.1038/nature08505.

Sehlstedt, I. *et al.* (2016) ‘Gentle touch perception across the lifespan.’, *Psychology and Aging*, 31(2), pp. 176–184. doi: 10.1037/pag0000074.

Shields, S. D. *et al.* (2018) ‘Insensitivity to Pain upon Adult-Onset Deletion of Nav1.7 or Its Blockade with Selective Inhibitors’, *Journal of Neuroscience*. Society for Neuroscience, 38(47), pp. 10180–10201. doi: 10.1523/JNEUROSCI.1049-18.2018.

Tigerholm, J. *et al.* (2014) 'Modeling activity-dependent changes of axonal spike conduction in primary afferent C-nociceptors', *Journal of Neurophysiology*. American Physiological Society, 111(9), pp. 1721–1735. doi: 10.1152/jn.00777.2012.

Toledo-Aral, J. J. *et al.* (1997) 'Identification of PN1, a predominant voltage-dependent sodium channel expressed principally in peripheral neurons', *Proceedings of the National Academy of Sciences of the United States of America*, 94(4), pp. 1527–1532. doi: 10.1073/pnas.94.4.1527.

Triscoli, C. *et al.* (2013) 'CT-optimized skin stroking delivered by hand or robot is comparable.', *Frontiers in behavioral neuroscience*. Frontiers Media SA, 7, p. 208. doi: 10.3389/fnbeh.2013.00208.

Urien, L. *et al.* (2017) 'Genetic ablation of GINIP-expressing primary sensory neurons strongly impairs Formalin-evoked pain', *Scientific Reports*. Nature Publishing Group, 7(1), p. 43493. doi: 10.1038/srep43493.

Usoskin, D. *et al.* (2015) 'Unbiased classification of sensory neuron types by large-scale single-cell RNA sequencing', *Nature Neuroscience*. Nature Publishing Group, 18(1), pp. 145–153. doi: 10.1038/nn.3881.

Vallbo, Å. B., Olausson, H. and Wessberg, J. (1999) 'Unmyelinated Afferents Constitute a Second System Coding Tactile Stimuli of the Human Hairy Skin', *Journal of Neurophysiology*. American Physiological SocietyBethesda, MD , 81(6), pp. 2753–2763. doi: 10.1152/jn.1999.81.6.2753.

Vrontou, S. *et al.* (2013) 'Genetic identification of C fibres that detect massage-like stroking of hairy skin in vivo', *Nature*. NIH Public Access, 493(7434), pp. 669–673. doi: 10.1038/nature11810.

Walcher, J. *et al.* (2018) 'Specialized mechanoreceptor systems in rodent glabrous skin', *The Journal of Physiology*. John Wiley & Sons, Ltd (10.1111), 596(20), pp. 4995–

5016. doi: 10.1113/JP276608.

Weir, G. A. *et al.* (2017) ‘Using an engineered glutamate-gated chloride channel to silence sensory neurons and treat neuropathic pain at the source’, *Brain*, 140(10), pp. 2570–2585. doi: 10.1093/brain/awx201.

Weiss, J. *et al.* (2011) ‘Loss-of-function mutations in sodium channel Nav1.7 cause anosmia’, *Nature*. Nature Publishing Group, 472(7342), pp. 186–190. doi: 10.1038/nature09975.

Yang, Y. (2004) ‘Mutations in SCN9A, encoding a sodium channel alpha subunit, in patients with primary erythermalgia’, *Journal of Medical Genetics*, 41(3), pp. 171–174. doi: 10.1136/jmg.2003.012153.

Zeisel, A. *et al.* (2018) ‘Molecular Architecture of the Mouse Nervous System’, *Cell*. Cell Press, 174(4), pp. 999-1014.e22. doi: 10.1016/J.CELL.2018.06.021.

Zheng, Y. *et al.* (2019) ‘Deep Sequencing of Somatosensory Neurons Reveals Molecular Determinants of Intrinsic Physiological Properties’, *Neuron*. Cell Press. doi: 10.1016/J.NEURON.2019.05.039.

Zotterman, Y. (1939) ‘Touch, pain and tickling: an electro-physiological investigation on cutaneous sensory nerves’, *The Journal of Physiology*, 95(1), pp. 1–28. doi: 10.1113/jphysiol.1939.sp003707.

Chapter 6: General discussion

1. The next generation of GluCl chemogenetic tools

This body of work has led to the production of multiple chemogenetic tools which allow the precise and targeted expression of neural modulators that can inhibit sensory neuron activity in a reversible and repeatable manner. These tools were designed to turn on or turn off GluCl expression in defined populations of sensory neurons. The use of GluCl.Cre^{ON} was the major focus of this thesis. However, GluCl.Cre^{OFF} was also developed, but has not yet been employed *in vivo*. This tool offers opportunity to silence all sensory neurons that do not express Cre recombinase, offering an alternative approach to investigate sensory neuron heterogeneity.

However, these tools could be developed further to build the next generation of GluCl modulators. Further, cloning strategies could be employed to alter the reporters so that they are instead red florescent proteins or small epitopes such as HA, c-Myc or His. This might be advantageous in studies which hope to combine the use of GluCl chemogenetic silencing and calcium imaging using genetically encoded calcium indicators such as GCaMP6 (Chen *et al.*, 2013). GCaMP6 is a modified version of GFP and therefore the YFP reporter currently present on the GluClβ subunit will prevent the accurate recording of calcium transients in GluClβ expressing cells.

In addition, while using Cre driver lines can aid the investigation into DRG heterogeneity, it is clear that these definitions may be too simplistic (Usoskin *et al.*, 2015; Zeisel *et al.*, 2018) and that subpopulations may exist that cannot be defined on the basis of a singular molecular marker. Future studies may opt to use intersectional viral strategies to express GluCl in a Cre and Flp recombinase dependent manner, using transgenic mice expressing Cre and Flp . This would facilitate GluCl expression in neurons expressing the combination of two molecular markers and would give finer control over population targeting. To achieve this, variants of the GluCl subunits could

be generated flanked with FRT sites (Flp recombinase but not Cre recombinase sensitive). Alternatively, a recombinase dependent effector line could be generated containing the Rosa26 harboured CAG promoted conditional GluCl KI (GluClα and GluClβ preceded with a lox site flanked stop codon and a frt flanked stop codon). This GluCl$^{Cre:Flp}$ line would allow the transgenic overexpression of GluCl using Cre and Flp driver lines in a non-viral manner. However, to fully utilise this approach more Flp recombinase expressing lines need to be generated within the neuroscience community. These efforts are underway and will likely be accelerated given the appreciation that singular molecular markers cannot be used to target all populations of interest. Nevertheless, my work provides proof of principle that these applications should be achievable with the GluCl system.

2. Primary afferent activity driving neuropathic pain

This thesis has generated and used novel chemogenetic tools to interrogate sensory neuron function in naïve mice and in the context of neuropathic pain. The work using optimised GluClv2.0 to broadly silence DRG neurons not only provided a proof of principle that the developed tool is efficacious, but that primary afferent drive is necessary for the maintenance of neuropathic pain. This supports the literature where local DRG anaesthetic block (ultrasound guided administration of lidocaine) provided neuropathic pain relief in humans (Haroutounian *et al.*, 2014). Our work in silencing primary afferents studied animals in which neuropathic pain behaviour was established and IVM was always applied within 4 weeks of nerve injury. It did not look at the role of the initial afferent barrage known to occur acutely following injury, this barrage may be important for the processes of plasticity and sensitization that initially establish neuropathic pain. We chose these timepoints to give more clinical relevance than silencing at the acute time of injury. Future work could build on this hypothesis by silencing primary afferents for an extended period of time, i.e. at the time of nerve injury onwards. Previous studies hypothesise that it is the ongoing aberrant activity of primary

afferents which initiates and drives neuropathic pain. It would be interesting to confirm this using the GluCl silencing system to prevent on-going activity from ever initiating and assessing the behavioural consequence in mice. In addition, is primary afferent silencing effective at alleviating neuropathic pain at more chronic time points? Human data from Haroutounian *et al.* (2014) would suggest yes, however this needs to be confirmed in rodent models. This would be something that we should be able to test as we have shown that our AAV-GluCl expression lasts for 7 months. These experiments may give insights into a 'critical treatment period' for neuropathic pain.

In this thesis, two populations of sensory neurons were silenced and their roles investigated pre and post nerve injury induced neuropathic pain. The silencing of these two populations revealed subtle or little involvement in the maintenance of evoked hypersensitivity using the SNI model of neuropathic pain (albeit replication is required). It is not clear that all models of neuropathic pain share a single mechanism leading to pain pathophysiology. In addition, due to the increased use of chemotherapeutic agents for the treatment of cancers, and the increased prevalence of diabetes, the incidence of neuropathic pain is predicted to rise (Van Hecke *et al.*, 2014). Therefore, due to its clinical importance, the study of systemic neuropathies has increased. Using the GluCl tool box, future work could identify the Nav1.8+ or the TH+ population as being critical in driving and maintaining chemotherapy or diabetes induced neuropathic pain.

A large part of this thesis focused on using evoked measures of neuropathic pain. The preliminary data using GluClv2.0 to eliminate an analgesic preference in neuropathic mice suggested primary afferent activity also maintains the non-evoked spontaneous component of neuropathic pain. Previous work has suggested that the TRPV1+ fibres are involved in spontaneous pain in the SNL model of neuropathic pain (King *et al.*, 2011). However, it is important to further refine exactly which population(s) underlie spontaneous pain, in multiple models. CPP will be used to further explore on-going spontaneous pain and will be employed when silencing distinct sensory neuron

populations in order to identify which population maintains this component, as it is most clinically relevant.

3. The translational potential of this work

This work hopes to offer a contribution to the understanding and mechanisms behind the maintenance of neuropathic pain and has begun to interrogate the role of Nav1.8+ and TH+ sensory neurons in nerve injury induced neuropathic pain and will facilitate the investigation of other sensory neuron populations in the future. Once a key population(s) is identified (in either evoked and/or non-evoked pain) future work could look in detail at transcription changes pre- and post-injury within a genetically labelled population, using FACS sorting and deep RNA sequencing. Similar work has achieved this (pre-injury) and identified key ion channels that regulate population specific electrophysiological characteristics (Zheng *et al.*, 2019). This will elude to peripheral mechanisms of neuropathic pain and will hopefully identify novel and population specific targets which are either druggable using existing or novel compounds.

Due to the clear evidence for both peripheral and central components of neuropathic pain, the identification of key sensory neuron populations that maintain neuropathic pain will enable studies to investigate peripheral population contribution to the central pathophysiological changes seen such as synaptic plasticity, immune responses, intrinsic dorsal horn hyperexcitability and circuit disinhibition (Woolf, 2011).

4. Could AAV-GluCl be utilised as gene therapy for human neuropathic pain disorders?

Gene therapies involve the introduction of new genetic information into targeted cells to treat disease. Gene therapies are classically split into two categories; *ex vivo* gene therapy and *in vivo* gene therapy. The former being the introduction of genetic material into cells *ex vivo*, that are later transferred into the patient, and the latter being

the introduction of viral vectors containing transgenes directly into patients (Anguela and High, 2019). There are a large number of pre-clinical studies which have developed gene therapy strategies for the treatment of many neurological disorders. However, at present, gene therapies are not regularly used in humans. Since the first clinical trials using gene therapies there has been progress but also challenges and setbacks which have slowed progress (Anguela and High, 2019). However, there are now eight gene therapies that have been approved for clinical use for patients with the following conditions; familial lipoprotein lipase deficiency, unresectable melanoma, adenosine deaminase deficiency resulting in severe combined immunodeficiency, non-Hodgkin lymphoma, acute lymphoblastic leukaemia and RPE65 mutation associated retinal dystrophy (Anguela and High, 2019). Other therapies which have demonstrated success include the gene replacement therapy used to treat spinal motor atrophy 1 (SMA1) (Mendell *et al.*, 2017), and the RNA interference therapy used to treat familial amyloid neuropathy (Adams *et al.*, 2019). Indeed, both of these therapies have been approved and are used clinically.

A major challenge with gene therapies is the reliance on effective viral delivery. Recent efforts suggest that AAVs are well tolerated in humans, they successfully transduce human neurons, and they are being using in clinical trials (Hadaczek *et al.*, 2010; Kotterman and Schaffer, 2014; Mendell *et al.*, 2017). The pre-clinical work within this thesis suggests that AAVs can be used to express GluCl in DRG neurons. This supports the idea that AAV-GluCl could be used to transfect human DRG neurons and supress on-going excitability that is maintaining neuropathic pain states. An added benefit of this system is that the GluCl agonist IVM is an approved drug and is currently prescribed to humans. This is advantageous over DREADD agonists such as CNO, that requires back conversion to clozapine (Gomez *et al.*, 2017). As clozapine is an antipsychotic it would be difficult to prescribe CNO clinically. The longevity of GluCl silencing after one dose of IVM could also be considered a translational benefit. In patients, IVM could be administered daily or every few days, rather than hourly. The

GluCl silencing system is also reversible which would be beneficial if patients were to ever experience negative side effects. Taken together, it is possible that in the future the AAV-GluCl/IVM system could be employed in humans to treat neuropathic pain and even extended to other disorders of hyperexcitability, such as epilepsy (Lieb *et al.*, 2018).

However, it is important to consider that GluCl is a protein that is originally derived from nematode *C.elegans*. Careful consideration would need to ensure expression of a non-human protein does not cause an immune-mediated response. This is particularly important as primary afferents are not protected by the blood brain barrier like CNS regions. In addition, while GluCl having two subunits could be considered an advantage in pre-clinical studies, this is less advantageous in a clinical setting, as two viruses would need to be co-administered. For these reasons, other chemogenetic tools might be best suited for human gene therapies to silence aberrant neuronal activity. For instance, the recently developed PSAM^4-GlyR is an engineered human channel, requires a single viral construct, has a clinically approved agonist (varenicline) and has shown efficacy in silencing neurons in non-human primates (Magnus *et al.*, 2019). This construct has never been employed in the sensory system; I have begun work to validate its use in rodent sensory neurons and human induced pluripotent stem cell derived nociceptors. PSAM^4-GlyR, acts in a very similar way to GluCl, in that activation mediates a chloride conductance that reduces membrane input resistance. Therefore it would be expected that PSAM^4-GlyR would be just as efficacious as GluCl.

Considering AAV-GluCl as potential gene therapy would also require targeting the construct to sensory neurons and ideally the appropriate sensory neuron population. As recombinase based genetics in not possible in humans, once a preclinical population is identified efforts should focus on identification of population specific viral tropism or the design of short synthetic population specific promoters.

5. The importance of targeting sensory neuron populations

The work in this thesis has provided argument for the development of therapeutics that target appropriate sensory neuron populations. The data in this thesis exemplify the importance of targeting the correct sub-population of sensory neurons. We provide evidence using human genetics and preclinical techniques that Nav1.7 is required for human and rodent C-LTMR function. The current dogma is that therapeutics targeting Nav1.7 are specific to the nociceptive system. As such many pharmaceutical companies have programs dedicated to the development of Nav1.7 specific blockers. The data in this thesis exemplifies that the pharmacological blockade of Nav1.7 significantly reduces sodium currents and the excitability of C-LTMRs (a non-nociceptive population). This has major implications for the use of Nav1.7 blockers to treating pain, in large due to their inability to offer true specificity for nociceptors. Careful consideration needs to be taken going forward as reducing the excitability of C-LTMRs could lead to undesired side effects, particularly with pro-longed treatment and treatment early in life.

6. General conclusions

To conclude, a novel selection of chemogenetic tools have been generated and validated in the peripheral sensory nervous system. These tools allow the expression of an engineered GluCl ion channel that in the presence of low doses of its agonist IVM, results in robust and reversible neuronal silencing. *In vivo* neuronal silencing was used to alleviate neuropathic pain in the rodent SNI model. GluCl.Cre^{ON} and GluCl.Cre^{OFF} tools were also generated and in particular GluCl.Cre^{ON} was used to target and silence two different populations, Nav1.8 positive neurons and TH+ C-LTMRs. Silencing Nav1.8+ neurons resulted in heat hyposensitivity and subtle dynamic sensitivity changes post SNI. Silencing C-LTMRs led to hyposensitivity to punctate von Frey stimuli and but no changes in post-SNI evoked mechanical sensitivity. This suggested that C-LTMRs may play a major role in punctate mechanical detection thresholds pre injury. This lead to the investigation into the role of the VGSC Nav1.7 and C-LTMR function in both

humans and mice. Humans who have bi-allelic LOF mutations in Nav1.7, have an altered perception of pleasant touch stimuli. Mouse genetics were used to demonstrate behaviour hyposensitivity to punctate mechanical stimuli and cool stimuli. Primary afferent recordings were used to characterise the ablation of Nav1.7 in C-LTMRs, and terminal hypo-excitability was observed. This finding was supported by the computational modelling of C-LMTRs, with altered Nav1.7 conductance's informed by each patient mutation. Finally, Nav1.7 selective blockers were applied to C-LMTRs and resulted in C-LTMR hypo-excitability.

Collectively, this body of work investigates the role of different sensory neurons populations and DRG heterogeneity. It highlights that there is still much more to understand in terms of sensory neuron populations and their contributions to somatosensation and pathological pain. It also highlights why this is an important issue and why future therapeutics need to be developed in order to target the appropriate sensory neuron population.

7. References

Adams, D. *et al.* (2019) ‘Hereditary transthyretin amyloidosis: a model of medical progress for a fatal disease’, *Nature Reviews Neurology*. Nature Publishing Group, pp. 387–404. doi: 10.1038/s41582-019-0210-4.

Anguela, X. M. and High, K. A. (2019) ‘Entering the Modern Era of Gene Therapy’, *Annual Review of Medicine*. Annual Reviews, 70(1), pp. 273–288. doi: 10.1146/annurev-med-012017-043332.

Chen, T. W. *et al.* (2013) ‘Ultrasensitive fluorescent proteins for imaging neuronal activity’, *Nature*, 499(7458), pp. 295–300. doi: 10.1038/nature12354.

Gomez, J. L. *et al.* (2017) ‘Chemogenetics revealed: DREADD occupancy and activation via converted clozapine’, *Science*. American Association for the Advancement of Science, 357(6350), pp. 503–507. doi: 10.1126/science.aan2475.

Hadaczek, P. *et al.* (2010) ‘Eight years of clinical improvement in MPTP-lesioned primates after gene therapy with AAV2-hAADC’, *Molecular Therapy*. Nature Publishing Group, 18(8), pp. 1458–1461. doi: 10.1038/mt.2010.106.

Haroutounian, S. *et al.* (2014) ‘Primary afferent input critical for maintaining spontaneous pain in peripheral neuropathy’, *Pain*. Elsevier B.V., 155(7), pp. 1272–1279. doi: 10.1016/j.pain.2014.03.022.

Van Hecke, O. *et al.* (2014) ‘Neuropathic pain in the general population: A systematic review of epidemiological studies’, *Pain*. Elsevier B.V., pp. 654–662. doi: 10.1016/j.pain.2013.11.013.

King, T. *et al.* (2011) ‘Contribution of afferent pathways to nerve injury-induced spontaneous pain and evoked hypersensitivity’, *Pain*, 152(9), pp. 1997–2005. doi: 10.1016/j.pain.2011.04.020.

Kotterman, M. A. and Schaffer, D. V. (2014) ‘Engineering adeno-associated viruses for

clinical gene therapy', *Nature Reviews Genetics*. Nature Publishing Group, 15(7), pp. 445–451. doi: 10.1038/nrg3742.

Lieb, A. *et al.* (2018) 'Biochemical autoregulatory gene therapy for focal epilepsy', *Nature Medicine*. Nature Publishing Group, pp. 1324–1329. doi: 10.1038/s41591-018-0103-x.

Magnus, C. J. *et al.* (2019) 'Ultrapotent chemogenetics for research and potential clinical applications', *Science*. American Association for the Advancement of Science, 364(6436). doi: 10.1126/science.aav5282.

Mendell, J. R. *et al.* (2017) 'Single-Dose Gene-Replacement Therapy for Spinal Muscular Atrophy', *New England Journal of Medicine*, 377(18), pp. 1713–1722. doi: 10.1056/NEJMoa1706198.

Usoskin, D. *et al.* (2015) 'Unbiased classification of sensory neuron types by large-scale single-cell RNA sequencing', *Nature Neuroscience*. Nature Publishing Group, 18(1), pp. 145–153. doi: 10.1038/nn.3881.

Woolf, C. J. (2011) 'Central sensitization: Implications for the diagnosis and treatment of pain', *Pain*. doi: 10.1016/j.pain.2010.09.030.

Zeisel, A. *et al.* (2018) 'Molecular Architecture of the Mouse Nervous System Resource Molecular Architecture of the Mouse Nervous System', *Cell*, 174, pp. 999-1014.e22. doi: 10.1016/j.cell.2018.06.021.

Zheng, Y. *et al.* (2019) 'Deep Sequencing of Somatosensory Neurons Reveals Molecular Determinants of Intrinsic Physiological Properties', *Neuron*. Cell Press, 103(4), pp. 598-616.e7. doi: 10.1016/J.NEURON.2019.05.039.

Appendix

Primary Antibodies	Source	Identifier
NeuN (1:500, Rabbit)	Abcam	Ab177487
NeuN (1:500, Chicken)	Merck Millipore	Abn91
dsRed (1:1000, Rabbit)	Clone tech	632392
Tyrosine Hydroxylase (1:250, Sheep)	Merck Millipore	Ab1542
βIII-Tubulin (1:500, Mouse)	R&D	Mab1195
IB4 (1:50, Streptavidin conjugated)	Sigma-Aldrich	L2140
IB4-Alexa Fluor 488 dye (1:200)	Invitrogen	I21411
GFP (1:500, Chicken)	Abcam	Ab13970
GFP (1:500, Rabbit)	Invitrogen	A6455
PGP9.5 (1:200, Rabbit)	Zytomed	516-3344
CGRP (1:250, Sheep)	Enzo	Ca1137
Parvalbumin (1:200, Guinea pig)	Frontier Insitute	Af1000
GINIP (1:1000, Rat)	(Gaillard *et al* 2014)	(Gaillard *et al* 2014)
NF200 (1,1000 Rabbit)	Merck Millipore	ABN76
S100β (1:500, Rabbit)	Abcam	Ab41548
ATF3 (1:500, Rabbit)	Santa Cruz	c-19, sc-188
Calbindin (1:200, Rabbit)	Swant	CB38
Secondary Antibodies	**Source**	**Identifier**
Alexa Fluor 488 (1:500)	Thermo Fischer Scientific	Alexa Fluor
Alexa Fluor 546 (1:500)	Thermo Fischer Scientific	Alexa Fluor
Alexa Fluor 647 (1:500)	Invitrogen	Alexa Fluor
Pacific Blue (1:100)	Thermo Fischer Scientific	Alexa Fluor
Cy3 (1:500)	Jackson	713-166-147

Appendix Table 1: List of primary and secondary antibodies

Participant's identifier	Age	Sex	Mutation	Reference
CIP Participant 1	16	F	Compound heterozygous mutations: c.5155 T>C; C1719R – in exon 26 causing an amino acid substitution of arginine for cysteine (c.5155 T>C; C1719R) c.3467+3 delA, or IVS17+3delA – in intron 17. This deletion alters the splice donor consensus sequence, which causes exon 17 to be skipped at the mRNA level.	(Staud *et al*., 2011)[1]
CIP Participant 2	44/47*	F	Compound heterozygous mutations: c.2691G>A (Y897X) – premature stop codon c.5173G>C (G1725R) – in exon 27, affects a highly conserved region of the protein and is predicted to cause major alteration in the sixth transmembrane region of the protein	(Bogdanova-Mihaylova *et al*., 2015)[2] (McDermott *et al.,* 2019)[3]
CIP Participant 3	34/36*	M	Compound heterozygous mutations: c.377+5C>T – intronic variant c.2686C>T (R896W) – in exon 16, affects a highly conserved region of the protein, and is predicted to cause an alteration in the ion transport region of the protein	(McDermott *et al*., 2019)[3]
CIP Participant 4	31	M	Compound heterozygous mutations: c.2488C>T (R830X) - premature stop codon in coding exon 15 c.5318delA (FS1773) - in exon 26,1 bp deletion that induces a frameshift at position 1773 in the C terminal domain of the channel.	(Ramirez *et al*., 2014)[4] (McDermott *et al*., 2019)[3] (Weiss *et al*., 2011)[5]
CIP Participant 5	42	F	Compound heterozygous mutations: Exon 22: c.3699_3709delATGGATAGCAT p.Ile1235LeufsX and in exon 29: c.4975A>T p.Lys1659X. As both of these exons are not last or penultimate, nonsense mediated decay would be predicted for both mutations. *Patient 5 and 6 are siblings	(Weiss *et al*., 2011)[5]
CIP Participant 6	45	F	Compound heterozygous mutations: Exon 22: c.3699_3709delATGGATAGCAT p.Ile1235LeufsX and in exon 29: c.4975A>T p.Lys1659X. As both of these exons are not last or penultimate, nonsense mediated decay would be predicted for both mutations. *Patient 5 and 6 are siblings	(Weiss *et al*., 2011)[5]

Appendix Table 2. Demographics and the relevant Scn9a-LOF mutations of the recruited CIP cohort. *Age during facial EMG testing.

Appendix ANOVA results and tables

Chapter 2 ANOVA results

Cp2 - Figure 2E

Two-way RM ANOVA	Matching: Across row				
Alpha	0.05				
Source of Variation	% of total variation	P value	P value summary	Significant?	
Interaction	12.58	0.0222	*	Yes	
subunit	2.984	0.3151	ns	No	
IVM	4.325	0.1571	ns	No	
Subjects (matching)	44.38	0.2484	ns	No	
ANOVA table	SS	DF	MS	F (DFn, DFd)	P value
Interaction	141607	1	141607	F (1, 16) = 6.409	P = 0.0222
subunit	33594	1	33594	F (1, 16) = 1.076	P = 0.3151
IVM	48689	1	48689	F (1, 16) = 2.204	P = 0.1571
Subjects (matching)	499647	16	31228	F (16, 16) = 1.413	P = 0.2484
Residual	353494	16	22093		
Number of missing values	0				

Cp2- Figure 6A

Two-way RM ANOVA	Matching: Across row				
Alpha	0.05				
Source of Variation	% of total variation	P value	P value summary	Significant?	
Interaction	0.1888	0.9141	ns	No	
Cell type	1.541	0.5715	ns	No	
Pre/Post	62.70	< 0.0001	****	Yes	
Subjects (matching)	19.90	0.3250	ns	No	
ANOVA table	SS	DF	MS	F (DFn, DFd)	P value
Interaction	23.77	2	11.89	F (2, 15) = 0.09036	P = 0.9141
Cell type	194.0	2	97.01	F (2, 15) = 0.5809	P = 0.5715
Pre/Post	7894	1	7894	F (1, 15) = 60.01	P < 0.0001
Subjects (matching)	2505	15	167.0	F (15, 15) = 1.269	P = 0.3250
Residual	1973	15	131.6		
Number of missing values	0				

Cp2 - Figure 6B

Two-way RM ANOVA	Matching: Across row				
Alpha	0.05				
Source of Variation	% of total variation	P value	P value summary	Significant?	
Interaction	0.1936	0.7618	ns	No	
Pre/Post	0.3419	0.7281	ns	No	
Cell type	52.76	0.0004	***	Yes	
Subjects (matching)	26.75	0.3258	ns	No	
ANOVA table	SS	DF	MS	F (DFn, DFd)	P value
Interaction	346.9	1	346.9	F (1, 10) = 0.09707	P = 0.7618
Pre/Post	612.6	1	612.6	F (1, 10) = 0.1278	P = 0.7281
Cell type	94533	1	94533	F (1, 10) = 26.45	P = 0.0004
Subjects (matching)	47924	10	4792	F (10, 10) = 1.341	P = 0.3258
Residual	35743	10	3574		
Number of missing values	0				

Cp 2 - Figure 8D

Two-way RM ANOVA	Matching: Across row				
Alpha	0.05				
Source of Variation	% of total variation	P value	P value summary	Significant?	
Interaction	31.23	0.0001	***	Yes	
Time	32.48	< 0.0001	****	Yes	
Pre/Post	35.56	< 0.0001	****	Yes	
Subjects (matching)	0.1744	0.8535	ns	No	
ANOVA table	SS	DF	MS	F (DFn, DFd)	P value
Interaction	1505	1	1505	F (1, 4) = 227.8	P = 0.0001
Time	1565	1	1565	F (1, 4) = 745.2	P < 0.0001
Pre/Post	1713	1	1713	F (1, 4) = 259.4	P < 0.0001
Subjects (matching)	8.399	4	2.100	F (4, 4) = 0.3179	P = 0.8535
Residual	26.42	4	6.605		
Number of missing values	0				

Chapter 3 ANOVA results

Cp3 – Figure 4B

One-way ANOVA summary	
F	37.74
P value	< 0.0001
P value summary	****
Are differences among means statistically significant? (P < 0.05)	Yes
R square	0.9188

ANOVA table	SS	DF	MS	F (DFn, DFd)	P value
Treatment (between columns)	6012	3	2004	F (3, 10) = 37.74	P < 0.0001
Residual (within columns)	531.0	10	53.10		
Total	6543	13			

Cp3 – Figure 4C

One-way ANOVA summary	
F	2.269
P value	0.1251
P value summary	ns
Are differences among means statistically significant? (P < 0.05)	No
R square	0.1590

ANOVA table	SS	DF	MS	F (DFn, DFd)	P value
Treatment (between columns)	255.3	2	127.6	F (2, 24) = 2.269	P = 0.1251
Residual (within columns)	1350	24	56.24		
Total	1605	26			

Cp3 – Figure 5A

Two-way RM ANOVA	Matching: Across row				
Alpha	0.05				
Source of Variation	% of total variation	P value	P value summary	Significant?	
Interaction	5.309	0.0774	ns	No	
GluCl subunit	5.458	0.0775	ns	No	
Pre/Post	10.39	0.0163	*	Yes	
Subjects (matching)	40.26	0.4714	ns	No	
ANOVA table	SS	DF	MS	F (DFn, DFd)	P value
Interaction	0.3756	1	0.3756	F (1, 25) = 3.393	P = 0.0774
GluCl subunit	0.3861	1	0.3861	F (1, 25) = 3.389	P = 0.0775
Pre/Post	0.7347	1	0.7347	F (1, 25) = 6.638	P = 0.0163
Subjects (matching)	2.849	25	0.1139	F (25, 25) = 1.029	P = 0.4714
Residual	2.767	25	0.1107		
Number of missing values	0				

Cp3 – Figure 5B

Two-way RM ANOVA	Matching: Across row				
Alpha	0.05				
Source of Variation	% of total variation	P value	P value summary	Significant?	
Interaction	18.19	0.0006	***	Yes	
GluCl subunit	9.696	0.0194	*	Yes	
Pre/Post	3.935	0.0820	ns	No	
Subjects (matching)	38.81	0.2614	ns	No	
ANOVA table	SS	DF	MS	F (DFn, DFd)	P value
Interaction	129.3	1	129.3	F (1, 25) = 15.18	P = 0.0006
GluCl subunit	68.92	1	68.92	F (1, 25) = 6.246	P = 0.0194
Pre/Post	27.97	1	27.97	F (1, 25) = 3.283	P = 0.0820
Subjects (matching)	275.8	25	11.03	F (25, 25) = 1.295	P = 0.2614
Residual	213.0	25	8.520		
Number of missing values	0				

Cp3 – Figure 5C

Two-way RM ANOVA	Matching: Across row				
Alpha	0.05				
Source of Variation	% of total variation	P value	P value summary	Significant?	
Interaction	4.108	0.1601	ns	No	
GluCl subunit	0.3393	0.7043	ns	No	
Pre/Post	16.36	0.0088	**	Yes	
Subjects (matching)	43.42	0.3548	ns	No	
ANOVA table	SS	DF	MS	F (DFn, DFd)	P value
Interaction	16894	1	16894	F (1, 19) = 2.138	P = 0.1601
GluCl subunit	1395	1	1395	F (1, 19) = 0.1485	P = 0.7043
Pre/Post	67267	1	67267	F (1, 19) = 8.512	P = 0.0088
Subjects (matching)	178561	19	9398	F (19, 19) = 1.189	P = 0.3548
Residual	150151	19	7903		
Number of missing values	0				

Cp3 – Figure 5D

Two-way RM ANOVA	Matching: Across row				
Alpha	0.05				
Source of Variation	% of total variation	P value	P value summary	Significant?	
Interaction	0.1978	0.7164	ns	No	
GluCl subunit	1.269	0.4716	ns	No	
Pre/Post	2.543	0.1997	ns	No	
Subjects (matching)	59.39	0.1171	ns	No	
ANOVA table	SS	DF	MS	F (DFn, DFd)	P value
Interaction	16.88	1	16.88	F (1, 25) = 0.1350	P = 0.7164
GluCl subunit	108.3	1	108.3	F (1, 25) = 0.5343	P = 0.4716
Pre/Post	217.0	1	217.0	F (1, 25) = 1.735	P = 0.1997
Subjects (matching)	5068	25	202.7	F (25, 25) = 1.621	P = 0.1171
Residual	3127	25	125.1		
Number of missing values	0				

Cp3 – Figure 5E

Two-way RM ANOVA	Matching: Across row				
Alpha	0.05				
Source of Variation	% of total variation	P value	P value summary	Significant?	
Interaction	3.003	0.3054	ns	No	
GluCl subunit	0.4716	0.7254	ns	No	
Pre/Post	1.523	0.4616	ns	No	
Subjects (matching)	55.24	0.2698	ns	No	
ANOVA table	SS	DF	MS	F (DFn, DFd)	P value
Interaction	21.49	1	21.49	F (1, 15) = 1.126	P = 0.3054
GluCl subunit	3.374	1	3.374	F (1, 15) = 0.1281	P = 0.7254
Pre/Post	10.90	1	10.90	F (1, 15) = 0.5710	P = 0.4616
Subjects (matching)	395.2	15	26.35	F (15, 15) = 1.381	P = 0.2698
Residual	286.2	15	19.08		
Number of missing values	0				

Cp3 – Figure 5F

Two-way RM ANOVA	Matching: Stacked				
Alpha	0.05				
Source of Variation	% of total variation	P value	P value summary	Significant?	
Interaction	9.265	0.0061	**	Yes	
Time	7.744	0.0172	*	Yes	
GluCl subunit	3.902	0.0509	ns	No	
Subjects (matching)	20.12	0.0377	*	Yes	
ANOVA table	SS	DF	MS	F (DFn, DFd)	P value
Interaction	218.6	5	43.71	F (5, 110) = 3.457	P = 0.0061
Time	182.7	5	36.54	F (5, 110) = 2.889	P = 0.0172
GluCl subunit	92.04	1	92.04	F (1, 22) = 4.266	P = 0.0509
Subjects (matching)	474.6	22	21.57	F (22, 110) = 1.706	P = 0.0377
Residual	1391	110	12.65		
Number of missing values	0				

Cp3 – Figure 5G

Two-way RM ANOVA	Matching: Across row				
Alpha	0.05				
Source of Variation	% of total variation	P value	P value summary	Significant?	
Interaction	0.0001680	0.9935	ns	No	
GluCl subunit	3.022	0.2570	ns	No	
Pre/Post	51.93	0.0009	***	Yes	
Subjects (matching)	20.91	0.5875	ns	No	
ANOVA table	SS	DF	MS	F (DFn, DFd)	P value
Interaction	0.001052	1	0.001052	F (1, 10) = 6.959e-005	P = 0.9935
GluCl subunit	18.92	1	18.92	F (1, 10) = 1.445	P = 0.2570
Pre/Post	325.2	1	325.2	F (1, 10) = 21.52	P = 0.0009
Subjects (matching)	130.9	10	13.09	F (10, 10) = 0.8663	P = 0.5875
Residual	151.1	10	15.11		
Number of missing values	0				

Cp3 – Figure 6B

Two-way RM ANOVA	Matching: Stacked				
Alpha	0.05				
Source of Variation	% of total variation	P value	P value summary	Significant?	
Interaction	5.128	0.0006	***	Yes	
Time	48.13	< 0.0001	****	Yes	
GluCl subunit	3.841	0.0460	*	Yes	
Subjects (matching)	16.97	< 0.0001	****	Yes	
ANOVA table	SS	DF	MS	F (DFn, DFd)	P value
Interaction	0.5315	7	0.07594	F (7, 140) = 3.955	P = 0.0006
Time	4.989	7	0.7127	F (7, 140) = 37.12	P < 0.0001
GluCl subunit	0.3981	1	0.3981	F (1, 20) = 4.527	P = 0.0460
Subjects (matching)	1.759	20	0.08794	F (20, 140) = 4.580	P < 0.0001
Residual	2.688	140	0.01920		
Number of missing values	0				

Cp3 – Figure 6C

Two-way RM ANOVA	Matching: Stacked				
Alpha	0.05				
Source of Variation	% of total variation	P value	P value summary	Significant?	
Interaction	4.411	0.0580	ns	No	
Time	30.13	< 0.0001	****	Yes	
GluCl Subunit	6.690	0.0473	*	Yes	
Subjects (matching)	29.94	0.0243	*	Yes	
ANOVA table	SS	DF	MS	F (DFn, DFd)	P value
Interaction	238.8	2	119.4	F (2, 40) = 3.061	P = 0.0580
Time	1631	2	815.5	F (2, 40) = 20.91	P < 0.0001
GluCl Subunit	362.1	1	362.1	F (1, 20) = 4.469	P = 0.0473
Subjects (matching)	1621	20	81.03	F (20, 40) = 2.077	P = 0.0243
Residual	1560	40	39.01		
Number of missing values	0				

Cp3 – Figure 7C

Two-way ANOVA	Ordinary				
Alpha	0.05				
Source of Variation	% of total variation	P value	P value summary	Significant?	
Interaction	19.45	0.0996	ns	No	
GluCl subunit	1.271	0.6564	ns	No	
Drug/Vehicle	5.988	0.3416	ns	No	
ANOVA table	SS	DF	MS	F (DFn, DFd)	P value
Interaction	26708	1	26708	F (1, 12) = 3.185	P = 0.0996
GluCl subunit	1745	1	1745	F (1, 12) = 0.2081	P = 0.6564
Drug/Vehicle	8222	1	8222	F (1, 12) = 0.9805	P = 0.3416
Residual	100626	12	8386		
Number of missing values	0				

Chapter 4 ANOVA results

Cp4 – Figure 4A

Two-way RM ANOVA	Matching: Across row				
Alpha	0.05				
Source of Variation	% of total variation	P value	P value summary	Significant?	
Interaction	7.303e-005	0.9972	ns	No	
GluCl subunit	14.68	0.0437	*	Yes	
Pre/Post	10.65	0.2017	ns	No	
Subjects (matching)	24.04	0.8582	ns	No	
ANOVA table	SS	DF	MS	F (DFn, DFd)	P value
Interaction	9.677e-007	1	9.677e-007	F (1, 9) = 1.300e-005	P = 0.9972
GluCl subunit	0.1945	1	0.1945	F (1, 9) = 5.494	P = 0.0437
Pre/Post	0.1412	1	0.1412	F (1, 9) = 1.897	P = 0.2017
Subjects (matching)	0.3186	9	0.03540	F (9, 9) = 0.4757	P = 0.8582
Residual	0.6697	9	0.07441		
Number of missing values	0				

Cp4 – Figure 4B

Two-way RM ANOVA	Matching: Across row				
Alpha	0.05				
Source of Variation	% of total variation	P value	P value summary	Significant?	
Interaction	3.333	0.1817	ns	No	
GluCl subunit	17.75	0.1424	ns	No	
Pre/Post	3.333	0.1817	ns	No	
Subjects (matching)	61.82	0.0201	*	Yes	
ANOVA table	SS	DF	MS	F (DFn, DFd)	P value
Interaction	102.4	1	102.4	F (1, 9) = 2.095	P = 0.1817
GluCl subunit	545.5	1	545.5	F (1, 9) = 2.584	P = 0.1424
Pre/Post	102.4	1	102.4	F (1, 9) = 2.095	P = 0.1817
Subjects (matching)	1900	9	211.1	F (9, 9) = 4.318	P = 0.0201
Residual	440.0	9	48.89		
Number of missing values	0				

Cp4 – Figure 4C

Two-way RM ANOVA	Matching: Across row				
Alpha	0.05				
Source of Variation	% of total variation	P value	P value summary	Significant?	
Interaction	1.667	0.6138	ns	No	
GluCl subunit	0.009865	0.9646	ns	No	
Pre/Post	0.4834	0.7847	ns	No	
Subjects (matching)	42.75	0.6423	ns	No	
ANOVA table	SS	DF	MS	F (DFn, DFd)	P value
Interaction	102.4	1	102.4	F (1, 9) = 0.2733	P = 0.6138
GluCl subunit	0.6061	1	0.6061	F (1, 9) = 0.002077	P = 0.9646
Pre/Post	29.70	1	29.70	F (1, 9) = 0.07923	P = 0.7847
Subjects (matching)	2627	9	291.9	F (9, 9) = 0.7787	P = 0.6423
Residual	3373	9	374.8		
Number of missing values	0				

Cp4 – Figure 4D

Two-way RM ANOVA	Matching: Across row				
Alpha	0.05				
Source of Variation	% of total variation	P value	P value summary	Significant?	
Interaction	7.238	0.0413	*	Yes	
GluCl subunit	15.64	0.0215	*	Yes	
Pre/Post	21.09	0.0017	**	Yes	
Subjects (matching)	35.60	0.1763	ns	No	
ANOVA table	SS	DF	MS	F (DFn, DFd)	P value
Interaction	35.18	1	35.18	F (1, 15) = 4.981	P = 0.0413
GluCl subunit	76.00	1	76.00	F (1, 15) = 6.588	P = 0.0215
Pre/Post	102.5	1	102.5	F (1, 15) = 14.51	P = 0.0017
Subjects (matching)	173.0	15	11.54	F (15, 15) = 1.633	P = 0.1763
Residual	106.0	15	7.064		
Number of missing values	0				

Cp4 – Figure 4E

Two-way RM ANOVA	Matching: Across row				
Alpha	0.05				
Source of Variation	% of total variation	P value	P value summary	Significant?	
Interaction	12.67	0.0507	ns	No	
GluCl subunit	35.82	0.0058	**	Yes	
Pre/Post	5.505	0.1714	ns	No	
Subjects (matching)	24.95	0.4383	ns	No	
ANOVA table	SS	DF	MS	F (DFn, DFd)	P value
Interaction	47562	1	47562	F (1, 9) = 5.081	P = 0.0507
GluCl subunit	134504	1	134504	F (1, 9) = 12.92	P = 0.0058
Pre/Post	20671	1	20671	F (1, 9) = 2.208	P = 0.1714
Subjects (matching)	93697	9	10411	F (9, 9) = 1.112	P = 0.4383
Residual	84240	9	9360		
Number of missing values	0				

Cp4 – Figure 4F

Two-way RM ANOVA	Matching: Across row				
Alpha	0.05				
Source of Variation	% of total variation	P value	P value summary	Significant?	
Interaction	1.326	0.3822	ns	No	
GluCl subunit	6.036	0.4125	ns	No	
Pre/Post	4.412	0.1281	ns	No	
Subjects (matching)	73.59	0.0110	*	Yes	
ANOVA table	SS	DF	MS	F (DFn, DFd)	P value
Interaction	180.0	1	180.0	F (1, 9) = 0.8440	P = 0.3822
GluCl subunit	819.3	1	819.3	F (1, 9) = 0.7382	P = 0.4125
Pre/Post	598.8	1	598.8	F (1, 9) = 2.808	P = 0.1281
Subjects (matching)	9989	9	1110	F (9, 9) = 5.204	P = 0.0110
Residual	1919	9	213.3		
Number of missing values	0				

Cp4 – Figure 5B

Two-way RM ANOVA	Matching: Stacked				
Alpha	0.05				
Source of Variation	% of total variation	P value	P value summary	Significant?	
Interaction	3.504	0.0096	**	Yes	
Time	83.56	< 0.0001	****	Yes	
GluCl subunit	0.8574	0.1707	ns	No	
Subjects (matching)	3.482	0.0274	*	Yes	
ANOVA table	SS	DF	MS	F (DFn, DFd)	P value
Interaction	0.08777	7	0.01254	F (7, 63) = 2.957	P = 0.0096
Time	2.093	7	0.2990	F (7, 63) = 70.52	P < 0.0001
GluCl subunit	0.02147	1	0.02147	F (1, 9) = 2.216	P = 0.1707
Subjects (matching)	0.08720	9	0.009689	F (9, 63) = 2.285	P = 0.0274
Residual	0.2671	63	0.004240		
Number of missing values	0				

Cp4 – Figure 5C

Two-way RM ANOVA	Matching: Stacked				
Alpha	0.05				
Source of Variation	% of total variation	P value	P value summary	Significant?	
Interaction	3.210	0.7584	ns	No	
Time	39.98	< 0.0001	****	Yes	
GluCl subunit	1.693	0.1443	ns	No	
Subjects (matching)	5.959	0.5671	ns	No	
ANOVA table	SS	DF	MS	F (DFn, DFd)	P value
Interaction	1.287	7	0.1839	F (7, 63) = 0.5940	P = 0.7584
Time	16.03	7	2.290	F (7, 63) = 7.397	P < 0.0001
GluCl subunit	0.6788	1	0.6788	F (1, 9) = 2.557	P = 0.1443
Subjects (matching)	2.389	9	0.2655	F (9, 63) = 0.8576	P = 0.5671
Residual	19.50	63	0.3096		
Number of missing values	0				

Cp4 – Figure 5D

Two-way RM ANOVA	Matching: Stacked				
Alpha	0.05				
Source of Variation	% of total variation	P value	P value summary	Significant?	
Interaction	4.897	0.3846	ns	No	
Time	33.33	0.0061	**	Yes	
GluCl subunit	1.064	0.4351	ns	No	
Subjects (matching)	14.36	0.7360	ns	No	
ANOVA table	SS	DF	MS	F (DFn, DFd)	P value
Interaction	160.2	2	80.08	F (2, 18) = 1.008	P = 0.3846
Time	1090	2	545.0	F (2, 18) = 6.862	P = 0.0061
GluCl subunit	34.80	1	34.80	F (1, 9) = 0.6672	P = 0.4351
Subjects (matching)	469.5	9	52.17	F (9, 18) = 0.6568	P = 0.7360
Residual	1430	18	79.42		
Number of missing values	0				

Cp4 – Figure 8A

Two-way RM ANOVA	Matching: Across row				
Alpha	0.05				
Source of Variation	% of total variation	P value	P value summary	Significant?	
Interaction	4.415	0.0572	ns	No	
GluCl subunit	13.37	0.0196	*	Yes	
Pre/Post	7.549	0.0154	*	Yes	
Subjects (matching)	48.84	0.0614	ns	No	
ANOVA table	SS	DF	MS	F (DFn, DFd)	P value
Interaction	0.2762	1	0.2762	F (1, 23) = 4.007	P = 0.0572
GluCl subunit	0.8365	1	0.8365	F (1, 23) = 6.296	P = 0.0196
Pre/Post	0.4722	1	0.4722	F (1, 23) = 6.851	P = 0.0154
Subjects (matching)	3.055	23	0.1328	F (23, 23) = 1.927	P = 0.0614
Residual	1.585	23	0.06892		
Number of missing values	0				

Cp4 – Figure 8B

Two-way RM ANOVA	Matching: Across row				
Alpha	0.05				
Source of Variation	% of total variation	P value	P value summary	Significant?	
Interaction	0.8367	0.5111	ns	No	
GluCl subunit	1.132	0.4902	ns	No	
Pre/Post	1.788	0.3394	ns	No	
Subjects (matching)	52.94	0.3149	ns	No	
ANOVA table	SS	DF	MS	F (DFn, DFd)	P value
Interaction	2835	1	2835	F (1, 23) = 0.4455	P = 0.5111
GluCl subunit	3835	1	3835	F (1, 23) = 0.4918	P = 0.4902
Pre/Post	6057	1	6057	F (1, 23) = 0.9518	P = 0.3394
Subjects (matching)	179378	23	7799	F (23, 23) = 1.226	P = 0.3149
Residual	146369	23	6364		
Number of missing values	0				

Cp4 – Figure 8C

Two-way RM ANOVA	Matching: Across row				
Alpha	0.05				
Source of Variation	% of total variation	P value	P value summary	Significant?	
Interaction	0.1948	0.7109	ns	No	
GluCl subunit	0.3990	0.7144	ns	No	
Pre/Post	0.7007	0.4838	ns	No	
Subjects (matching)	66.85	0.0408	*	Yes	
ANOVA table	SS	DF	MS	F (DFn, DFd)	P value
Interaction	19.17	1	19.17	F (1, 23) = 0.1408	P = 0.7109
GluCl subunit	39.25	1	39.25	F (1, 23) = 0.1373	P = 0.7144
Pre/Post	68.95	1	68.95	F (1, 23) = 0.5065	P = 0.4838
Subjects (matching)	6578	23	286.0	F (23, 23) = 2.101	P = 0.0408
Residual	3131	23	136.1		
Number of missing values	0				

Cp4 – Figure 8D

Two-way RM ANOVA	Matching: Across row				
Alpha	0.05				
Source of Variation	% of total variation	P value	P value summary	Significant?	
Interaction	1.279	0.5185	ns	No	
GluCl subunit	4.209	0.2833	ns	No	
Pre/Post	19.79	0.0225	*	Yes	
Subjects (matching)	40.03	0.4040	ns	No	
ANOVA table	SS	DF	MS	F (DFn, DFd)	P value
Interaction	2.027	1	2.027	F (1, 12) = 0.4425	P = 0.5185
GluCl subunit	6.671	1	6.671	F (1, 12) = 1.262	P = 0.2833
Pre/Post	31.36	1	31.36	F (1, 12) = 6.846	P = 0.0225
Subjects (matching)	63.44	12	5.287	F (12, 12) = 1.154	P = 0.4040
Residual	54.97	12	4.581		
Number of missing values	0				

Cp4 – Figure 8E

Two-way RM ANOVA	Matching: Across row				
Alpha	0.05				
Source of Variation	% of total variation	P value	P value summary	Significant?	
Interaction	1.374	0.4346	ns	No	
GluCl subunit	2.348	0.3337	ns	No	
Pre/Post	13.69	0.0213	*	Yes	
Subjects (matching)	42.82	0.4168	ns	No	
ANOVA table	SS	DF	MS	F (DFn, DFd)	P value
Interaction	97.60	1	97.60	F (1, 18) = 0.6387	P = 0.4346
GluCl subunit	166.7	1	166.7	F (1, 18) = 0.9868	P = 0.3337
Pre/Post	972.4	1	972.4	F (1, 18) = 6.364	P = 0.0213
Subjects (matching)	3041	18	168.9	F (18, 18) = 1.106	P = 0.4168
Residual	2750	18	152.8		
Number of missing values	0				

Cp4 – Figure 9B

Two-way RM ANOVA	Matching: Stacked				
Alpha	0.05				
Source of Variation	% of total variation	P value	P value summary	Significant?	
Interaction	1.256	0.1213	ns	No	
Time	81.41	< 0.0001	****	Yes	
GluCl subunit	0.07855	0.4516	ns	No	
Subjects (matching)	2.527	0.2368	ns	No	
ANOVA table	SS	DF	MS	F (DFn, DFd)	P value
Interaction	0.08416	7	0.01202	F (7, 133) = 1.671	P = 0.1213
Time	5.453	7	0.7790	F (7, 133) = 108.3	P < 0.0001
GluCl subunit	0.005262	1	0.005262	F (1, 19) = 0.5907	P = 0.4516
Subjects (matching)	0.1692	19	0.008908	F (19, 133) = 1.238	P = 0.2368
Residual	0.9568	133	0.007194		
Number of missing values	0				

Cp4 – Figure 9C

Two-way RM ANOVA	Matching: Stacked				
Alpha	0.05				
Source of Variation	% of total variation	P value	P value summary	Significant?	
Interaction	4.852	0.5140	ns	No	
Time	39.88	< 0.0001	****	Yes	
GluCl subunit	0.4874	0.6537	ns	No	
Subjects (matching)	15.55	0.0132	*	Yes	
ANOVA table	SS	DF	MS	F (DFn, DFd)	P value
Interaction	1.363	7	0.1948	F (7, 49) = 0.9001	P = 0.5140
Time	11.21	7	1.601	F (7, 49) = 7.398	P < 0.0001
GluCl subunit	0.1370	1	0.1370	F (1, 7) = 0.2195	P = 0.6537
Subjects (matching)	4.368	7	0.6241	F (7, 49) = 2.884	P = 0.0132
Residual	10.60	49	0.2164		
Number of missing values	0				

Cp4 – Figure 9D

Two-way RM ANOVA	Matching: Stacked				
Alpha	0.05				
Source of Variation	% of total variation	P value	P value summary	Significant?	
Interaction	4.341	0.4849	ns	No	
Time	30.40	0.0189	*	Yes	
GluCl subunit	5.497	0.2034	ns	No	
Subjects (matching)	19.55	0.4818	ns	No	
ANOVA table	SS	DF	MS	F (DFn, DFd)	P value
Interaction	285.1	2	142.6	F (2, 14) = 0.7626	P = 0.4849
Time	1997	2	998.4	F (2, 14) = 5.340	P = 0.0189
GluCl subunit	361.1	1	361.1	F (1, 7) = 1.968	P = 0.2034
Subjects (matching)	1284	7	183.5	F (7, 14) = 0.9813	P = 0.4818
Residual	2617	14	187.0		
Number of missing values	0				

Cp4 – Figure 10B

Two-way RM ANOVA	Matching: Stacked				
Alpha	0.05				
Source of Variation	% of total variation	P value	P value summary	Significant?	
Interaction	1.293	0.9212	ns	No	
Time	66.93	< 0.0001	****	Yes	
GluCl subunit	0.5907	0.3165	ns	No	
Subjects (matching)	4.726	0.0391	*	Yes	
ANOVA table	SS	DF	MS	F (DFn, DFd)	P value
Interaction	9095	11	826.8	F (11, 99) = 0.4638	P = 0.9212
Time	470887	11	42808	F (11, 99) = 24.01	P < 0.0001
GluCl subunit	4156	1	4156	F (1, 9) = 1.125	P = 0.3165
Subjects (matching)	33254	9	3695	F (9, 99) = 2.073	P = 0.0391
Residual	176485	99	1783		
Number of missing values	0				

Cp4 – Figure 10C

Two-way RM ANOVA	Matching: Stacked				
Alpha	0.05				
Source of Variation	% of total variation	P value	P value summary	Significant?	
Interaction	1.805	0.2743	ns	No	
Time	75.53	< 0.0001	****	Yes	
GluCl subunit	1.353	0.3165	ns	No	
Subjects (matching)	10.82	0.5593	ns	No	
ANOVA table	SS	DF	MS	F (DFn, DFd)	P value
Interaction	33285	1	33285	F (1, 9) = 1.355	P = 0.2743
Time	1.393e+006	1	1.393e+006	F (1, 9) = 56.71	P < 0.0001
GluCl subunit	24938	1	24938	F (1, 9) = 1.125	P = 0.3165
Subjects (matching)	199525	9	22169	F (9, 9) = 0.9028	P = 0.5593
Residual	221003	9	24556		
Number of missing values	0				

Chapter 5 ANOVA results

Cp5 – Figure 5f

Two-way ANOVA	Ordinary				
Alpha	0.05				
Source of Variation	% of total variation	P value	P value summary	Significant?	
Interaction	2.333	0.1569	ns	No	
Time	63.55	< 0.0001	****	Yes	
genotype	1.867	< 0.0001	****	Yes	
ANOVA table	SS	DF	MS	F (DFn, DFd)	P value
Interaction	426367	23	18538	F (23, 432) = 1.306	P = 0.1569
Time	1.161e+007	23	504952	F (23, 432) = 35.58	P < 0.0001
genotype	341252	1	341252	F (1, 432) = 24.05	P < 0.0001
Residual	6.131e+006	432	14192		

Cp5 – Figure 5j

Two-way ANOVA	Ordinary				
Alpha	0.05				
Source of Variation	% of total variation	P value	P value summary	Significant?	
Interaction	0.08641	0.9925	ns	No	
Force	1.840	0.5731	ns	No	
Genotype	10.88	0.0008	***	Yes	
ANOVA table	SS	DF	MS	F (DFn, DFd)	P value
Interaction	3.958	3	1.319	F (3, 95) = 0.03142	P = 0.9925
Force	84.27	3	28.09	F (3, 95) = 0.6691	P = 0.5731
Genotype	498.4	1	498.4	F (1, 95) = 11.87	P = 0.0008
Residual	3988	95	41.98		

Cp5 – Figure 5k

Two-way ANOVA	Ordinary				
Alpha	0.05				
Source of Variation	% of total variation	P value	P value summary	Significant?	
Interaction	2.053	0.4708	ns	No	
Force	14.55	0.0009	***	Yes	
Genotype	5.011	0.0144	*	Yes	
ANOVA table	SS	DF	MS	F (DFn, DFd)	P value
Interaction	1647	3	548.9	F (3, 96) = 0.8483	P = 0.4708
Force	11667	3	3889	F (3, 96) = 6.010	P = 0.0009
Genotype	4019	1	4019	F (1, 96) = 6.212	P = 0.0144
Residual	62118	96	647.1		

Cp5 – Figure 6f

Two-way ANOVA	Ordinary				
Alpha	0.05				
Source of Variation	% of total variation	P value	P value summary	Significant?	
Interaction	1.032	0.7613	ns	No	
force	38.39	< 0.0001	****	Yes	
drug	3.626	0.0470	*	Yes	
ANOVA table	SS	DF	MS	F (DFn, DFd)	P value
Interaction	2.609	3	0.8698	F (3, 64) = 0.3890	P = 0.7613
force	97.05	3	32.35	F (3, 64) = 14.47	P < 0.0001
drug	9.168	1	9.168	F (1, 64) = 4.101	P = 0.0470
Residual	143.1	64	2.236		